DESIGN OF APTAMER-FUNCTIONALIZED SUBSTRATES: TOWARDS BREAST CANCER STEM CELL ISOLATION AND DETECTION

Aliya Bekmurzayeva

A thesis submitted in partial fulfilment of the requirement of
Nazarbayev University for the degree of
Doctor of Philosophy in Science, Engineering and Technology

August 2020

ABSTRACT

Cancer relapse and metastasis remain one of the main problems in treatment of breast cancer (BC). A small subset from bulk tumor cells, called breast cancer stem cells (BCSCs), is found to be responsible for cancer initiation, recurrence, metastasis and resistance to therapy. Therefore, specifically detecting these cells is an important task in BC diagnosis and management. The main goal of this thesis was to develop aptamer-functionalized substrates which in the future could be used for BCSC isolation and detection. To achieve this objective, the project has been divided into three tasks as will be discussed below.

Given small number of available specific ligands against BCSC and their importance in BC, one of the tasks of this thesis was to select and characterize new single stranded DNA aptamers against BCSC. Fluorescently activated cell sorting was utilized to enrich oligonucleotides bound to cells while imaging flow cytometry was used to study their binding. Two of the selected aptamers showed increased binding to target cells than to control cells; however, their binding affinity was not fully studied. They are one of the few ligands reported to date to bind BCSC and were selected against well characterized BCSC derived from a triple-negative breast cancer.

Another task of this work was to functionalize stainless steel (SS) wire with aptamers specific to BCSC in order to alleviate the problem of "fishing out" such rare events as BCSC. For this, the wire electropolishing conditions were determined. In order to attach ligand, silanization by electrodeposition was optimized thus determining the most suitable applied potential (–0.8 V), pH of the solution (pH 5 and 5.5) and heat treatment temperature after electrodeposition (130°C). The silanized surface was then immobilized with commercially available CD44 aptamers (marker of BCSC) after being activated by a crosslinker to build a functionalized surface. This wire was able to capture the target cells in an *in vitro* test. The wires were analyzed by such surface characterization methods as atomic force microscopy (AFM), cyclic voltammetry (CV), scanning electron microscopy (SEM) and fluorescence microscopy.

In addition, using the same surface chemistry as in functionalized SS wire, another platform – fiber Bragg grating (FBG) sensor has been explored with a well-studied ligand-analyte pair (thrombin and thrombin-binding aptamer). For this, FBG was made

sensitive to the surrounding refractive index (RI) by chemical etching and calibrated in solutions with known RI before being functionalized with aptamers. Then the sensor demonstrated increased Bragg wavelength shift when tested in different thrombin concentrations.

In conclusion, the main goal of this thesis – developing aptamer-functionalized substrates with a perspective application in BCSC isolation and detection – was achieved, although each task of the project was completed with different level of success. Binding of aptamers selected against BCSC could not be fully studied. However, they are one of the few reported aptamers against an important subtype of BC. Besides, only a small fraction of aptamer candidates were characterized and better binders could still be revealed. Wires functionalized with CD44 aptamers, after further study, have a potential to be used for *in vivo* capture of target cells in the blood flow, since their small size allows the insertion as a standard guidewire in biomedical devices. For fabricated EGBF biosensor, selective detection of clinically relevant concentration of thrombin has been demonstrated. The used functionalization method allows a facile fabrication of the sensor not requiring thin film fabrication.

РЕФЕРАТ (ABSTRACT IN KAZAKH)

Сүт безінің қатерлі ісігін (СБҚІ) емдеудің негізгі мәселелерінің бірі қатерлі ісіктің қайта оралуы мен метастаз болып табылады. Қатерлі ісік жасушаларының ішінде СБҚІ-нің бағаналы жасушалары (СБҚІБЖ) деп аталатын жасушалардың бір бөлігі ғана аурудың басталуы, қайталануы, метастаздың және терапияға төзімділіктің пайда болуының себебі болып есептеледі. Сондықтан бұл жасушаларды нақты анықтау СБҚІ диагнозы мен оны басқарудағы маңызды міндет болып табылады. Бұл диссертациялық жұмыстың негізгі мақсаты болашақта СБҚІБЖ-ны оқшаулау және анықтау үшін қолданылуы мүмкін аптамермен қапталған субстраттар жасау болды. Осы мақсатқа жету үшін жоба төменде талқыланатын үш міндетке бөлінді.

СБҚІБЖ-ға өзіне тән қол жетімді лигандтардың аздығы және олардың СБҚІ-дегі маңыздылығын ескере отырып, бұл тезистің бірінші міндеті СБҚІБЖ-ға қарсы жаңа бір тізбекті ДНҚ аптамерлерін таңдау және сипаттау болды. Флуоресцентті активтендірілген жасушаларды сұрыптау тәсілі жасушалармен байланысқан олигонуклеотидтерді байыту үшін қолданылды, ал бейнелі ағын цитометрия олардың жасушалармен жабысуын зерттеу үшін қолданылды. Бөліп алынған аптамерлердің екеуін СБҚІБЖ-ға жабысуын толығымен зерттеу мүмкін болмады,. Дегенмен, бұл аптамерлер СБҚІБЖ-ға жабысатын лигандтардың бірден бірі және олар үш маркері көрінбейтін СБҚІ-ден алынған СБҚІБЖ-ға қарсы бөлініп алынған болатын.

Бұл жұмыстың тағы бір міндеті СБҚІБЖ сияқты сирек кездесетін жаушаларды «аулау» мәселесін жеңілдету үшін СБҚІБЖ-ға тән аптамерлері бар болат сымын функцияландыру болды. Бұл үшін сымды электрлік жолмен жылтырату шарттары анықталды. Лигандты бекіту үшін электродты силанизация жағдайлары оңтайландырылды, осылайша ең қолайлы қолданылатын потенциал (-0,8 В), ерітіндінің pH-ы (pH 5 және 5.5) және силанизациялағаннан кейін жоғары температурамен өңдеу температурасы (130°C) анықталды. Силанизацияланған сымның бетін одан әрі функционаландыру үшін глютаральдегидпен өңделіп, CD44 аптамерлерімен (СБҚІБЖ маркері) иммобилизацияланды. Бұл сым *in vitro* сынағында мақсатты жасушаларды өзіне жабыстыра алды. Осылайша функцияландырылған сымдар атомдық күш микроскопиясы (АФМ), циклдік

вольтамметрия (ЦВ), сканерлеуші электронды микроскопия (СЭМ) және флуоресценциялық микроскопия сияқты сипаттамалық әдістермен талданды.

Сонымен қатар, функционалды болат сымындағыдай химиялық реакцияларды қолдана отырып, тағы бір платформа – талшықты Брэгг торы (ТБГ) сенсорында жақсы зерттелген лиганд-аналит жұбы (тромбин және тромбинге байланысатын аптамер) зерттелді. Аптамерлерді жабыстырмас бұрын ТБГ қоршаған айналадағы сыну көрсеткішіне (СК) сезімтал болу үшін қышқылмен өңделіп, СК белгілі ерітінділерінде калибрленді. Осылайша әзірленге сенсор әр түрлі тромбин концентрациясында сыналған кезде, Брэгг толқын ұзындығының жоғарылауын көрсетті.

Қорытындылай келе, бұл тезистің негізгі мақсаты – СБҚІБЖ-ны оқшаулау мен анықтауда келешекте қолданыла алатын аптамермен функционаландырылған субстрат жасауға – қол жеткізілді, дегенмен жобаның әр тапсырмасы әр түрлі деңгейде орындалды. СБҚІБЖ-ға қарсы таңдалған аптамерлер әдебиетте көрсетілген аптамерлерге қарағанда жасушалармен байланысу қабілеті төмендігі көрсетілді. Алайда, олар СБҚІ ауруының маңызды түріне қарсы таңдап алынған аптамерлердің бірден бірі болып табылады. Сонымен қатар, таңдап алынған аптамерге үміткерлердің ішінен олардыі аз бөлігі ғана сипатталды және әлі де жасушаларға жақсырақ байланыса алатындары табылуы мүмкін. Қан ағымындағы мақсатты жасушаларды ұстау үшін CD44 аптамерімен жұмыс істейтін сымдарды қолдануға болады, өйткені олардың кішкентай мөлшері олардың биомедициналық құрылғыларға стандартты нұсқаулыққа сәйкес кіргізілуіне мүмкіндік береді. Ал жасалған ТБГ биосенсоры тромбиннің клиникалық тұрғыдан сәйкес концентрациясын селективті анықтай алатындығы көрсетілді. ТБГ биосенсорын жасауда қолданылған функционалдандыру әдісі жұқа қабатты дайындауды қажет етпейтін сенсорды оңай құрастыруға мүмкіндік береді.

Table of Contents

LIST OF TABLES

LIST OF FIGURES

Figure 2.8 An overview of functionalizing optical fiber surface with bioreceptors
Ab – antibody; c-oligo – carboxylated oligo; DIC – diisopropyl carbodiimide; DSS - dextran sulfate sodium; EDC – 1-ethyl-3(3-dimethylaminopropyl)-carbodiimide; GA – glutaraldehyde; GMBS - N-succinimidyl 4-maleimidobutyrate; N-oligo – aminated olig; NHS - N-hydroxysulfosuccinimide; PAA – polyacrylic acid; P-oligo – phosphorylated oligo; PEI – polyethylene imine; S-protein – thiolated protein; SulfoSMCC - sulfosuccinimidyl 4-(N-maleimidomethyl)cyclohexane-1-carboxylate; NB: Blocking step not shown. a) (299); b) (286); c) (304); d) (278, 302, 303); e) (305); f) (306); g) (298).

Figure 3.1. A schematic overview of *in vitro* selection of aptamers and their characterization.

Figure 3.2. Analysis of PCR products of cycle 7 on 10% polyacrylamide gel using 25 bp DNA ladder as a DNA marker.

Figure 3.3. Using FACS for selection of aptamers against BCSC: results for round 5 of *in vitro* selection of DNA aptamers is shown. A) Dot plots of side scatter area versus forward scatter area; B) Dot plots of forward scatter height versus width; C) Dot plot of side scatter versus fluorochrome intensity of cy5-oligonucleotides; D) Populations of cells

Figure 3.4. Results of next-generation sequencing of a random region for product of round 5 of selection: relative frequency of nucleotides in each of a position is shown. Statistics is shown for 715,560 sequences from which 693,414 are unique ones.

Figure 3.5. Secondary structures (predicted on *Mfold)* of aptamer candidates: structures for full length (left) and random region only (right) are displayed. Structures with the lowest free energy with loops similar/conserved for both lengths are shown in red brackets.

Figure 4.7. AFM micrographs of wire before (A, B, C) and after electropolishing (D, E, F). A and B: 5 μm × 5 μm; B and D: profiles of lines shown on A and D respectively; C and F: 3D images of A and D respectively. The figure was published as part of the paper (30) (MDPI Open Access License).

Figure 4.8. AFM images of APTES electrodeposition on sonicated SS wires under different potentials (10 μm × 10 μm and their corresponding 3D images). The figure was published as part of the paper (30) (MDPI Open Access License).

Figure 4.9. AFM images of SS after electrodeposition of APTES under different potential. From top to bottom: 2.5μm×2.5μm (for -0.6V 5μm×5μm); 1μm×1μm; 3D image of 1μm×1μm. rms shown for 1μm×1μm. Samples at -0.8V are discussed further. The figure was published as part of the paper (30) (MDPI Open Access License).

Figure 4.10. Cyclic voltammograms of electropolished SS electrode (Elpol) and silanized with APTES using different applied potentials (HT): −1.2; 0.8 and −0.6 V; CV done in PBS pH 7.4 containing 0.10 M KCl and 1.0 mM $[Fe(CN)^{6}]^{3-/4-}$ with a scan rate of 50 mV/s. Potential vs. RE (3 M NaCl).

Figure 4.11. AFM micrographs of electropolished SS wires after electrodeposition of APTES at the applied potential of −0.8 V for 30 min in solutions with pH values of 6; 5.5; 5 and 4. For each pH value, 1 μm × 1 μm images, their 3D images and profiles along the lines are shown. The figure was published as part of the paper (30) (MDPI Open Access License).

Figure 4.12. FITC analysis of the control (Elpol-electropolished) and silanized samples (HT) (electrodeposition at the applied potential of −0.8 V for 30 min) as visualized by fluorescence microscopy. The figure was published as part of the paper (30) (MDPI Open Access License).

Figure 5.4. Spectra of the FBG prior etching and after etching the FBG using hydrofluoric acid. The graphic shows spectra observed on the FBG interrogator. The figure published as part of the paper (31) (MDPI Open Access License).

Figure 5.5. Results of calibration of the EFBG using sucrose dissolved in water (1.5; 3.1; 6.2; 12.5; 25.0 and 50.0% w/v) which have different RI and the corresponding wavelength shift (1.5% set at 0). Sensitivity (17.4 nm/RIU) is estimated using linear regression. The figure published as part of the paper (31) (MDPI Open Access License).

Figure 5.6. High-resolution AFM topographical images of etched glass surface before after functionalization in air: 2D (left column) and 3D (right column). A) Etched surface (not functionalized); B) Etched + silanized (APTES); C) Etched + APTES + crosslinker (Glutaraldehyde). Scanning sizes: XY 1.5 μm x 1.5 μm; average height: -200 to +200 nm. The figure published as part of the paper (31) (MDPI Open Access License).

Figure 5.7. Dynamic of Bragg wavelength through the fabrication and functionalization of the EFBG thrombin biosensor. Graphic shows the estimated Bragg wavelength after each fabrication step (before thrombin detection). The figure published as part of the paper (31) (MDPI Open Access License).

Figure 5.8. Bragg wavelength shift observed during incubation of EFBG functionalized with thrombin-binding aptamer with thrombin. Results for 70 min detection of thrombin at different concentrations 10 nM to 80 nM is shown. The figure published as part of the paper (31) (MDPI Open Access License).

Figure 5.9. Results of the response of EFBG functionalized with thrombin-binding aptamer to thrombin: (a) Bragg wavelength shift observed for different thrombin concentrations after 10, 20, 30, and 40 min (b) detection accuracy (estimated as the standard deviation of the wavelength recorded over one-minute exposure). The figure published as part of the paper (31) (MDPI Open Access License).

Figure 5.10. (A) Reflection spectra of TFBG during etching; (B) Spectral change of the ETFBG (d ¼ 94 μm) in calibration solutions (sucrose); inset: zoom of the analyzed modes. Published as part of (32) (Elsevier Permission: Personal use of work by Authors).

Figure 5.11. (A) Reflection spectra of ETFBG during the detection of the analyte (thrombin 2.5 nM, 10 nM, 20 nM and 40 nM). (B) Results of analyte measurement (wavelength shift as a function of the thrombin concentration) for the 3 most sensitive modes. Error bar range: -0.44 to +0.45 pm. Published as part of (32) (Elsevier Permission: Personal use of work by Authors).

LIST OF ABBREVIATIONS

ALDH1	Aldehyde dehydrogenase 1
AFM	Atomic force microscopy
APTES	(3-aminopropyl)triethoxysilane
BB	Binding buffer
BC	Breast cancer
BCSC	Breast cancer stem cells
BSA	Bovine serum albumin
ca.	*lat*. circa; meaning "around, about, roughly
CRediT	Contributor Roles Taxonomy
CSC	Cancer stem cells
CTC	Circulating tumour cells
CV	Cyclic voltammetry
DNA	Deoxyribonucleic acid
EMT	Epithelial to mesenchymal transition
EpCAM	Epithelial cell adhesion molecule
et al.	*lat*. et alii; meaning "and others"
EFBG	Etched fiber Bragg grating
ETFBG	Etched tilted fiber Bragg grating
FACS	Fluorescence-activated cell sorting
FBG	Fiber Bragg grating
FDA	US Food and Drug Administration
FITC	Fluorescein isothiocyanate
GA	Glutaraldehyde
LOD	Limit of detection

NGS	Next-generation sequencing
NOD/SCID mice	Mice with non-obese diabetic/severe combined immunodeficiency
nt	Nucleotides (unit of length for single-stranded nucleic acids)
PBS	Phosphate-buffered saline
pH	*lat*. Potentia Hydrogenii meaning “potential of hydrogen”
RIU	Refractive index unit
rms	root mean square (roughness)
SELEX	Systematic evolution of ligands by exponential enrichment
SEM	Scanning electron microscope
SCA	Silane coupling agents
SS	Stainless steel
TBA	Thrombin-binding aptamer
TFBG	Tilted fiber Bragg grating
TN	Triple negative (breast cancer negative for expression of estrogen and progesterone receptors and lacking amplification of human epidermal growth factor receptor 2 gene)
v/v	volume to volume %
w/v	weight to volume %

AUTHORS DECLARATION

I declare that the research contained in this thesis, unless otherwise formally indicated within the text, is the original work of the author. The thesis has not been previously submitted to this or any other university for a degree and does not incorporate any material already submitted for a degree.

ACKNOWLEDGEMENT

I thank my main supervisor Dr. Damira Kanayeva for introducing me to biosensors, giving me the opportunity to be trained on aptamer selection and characterization and her thoughtful advice throughout this project. I also thank my co-supervisor Dr. Daniele Tosi for giving me chance to continue working on my thesis while being in his project, for his guidance in developing optical fiber biosensor and not being tired in explaining how scientific community operates. Both Damira and Daniele always believed in me as a scientist and made continuous encouragements for the completion of this thesis and this was a true blessing for me. I thank them for their patience and enthusiasm throughout the project.

I am also thankful to my external supervisor Dr. Helena S. Azevedo, in whose laboratory at Queen Mary University of London, I started surface modification of SS, for her critical view on experimental setup and result analysis; and for her help in writing review and research papers. I am also thankful to my external supervisor Dr. Wynter J. Duncanson (Boston University) who taught us principles of biomedical engineering at Nazarbayev University; and gave good insights on the project and was very helpful in improving my writing skills.

I wish to recognize the help from Dr. Sarah Shigdar from Deakin University (Australia) who helped me with experiments related to selection and characterization of aptamers. Also Dr. Enrico Marsili from Nazarbayev University who gave expert advice on electrochemical analysis used in this work. His advice was immensely useful for my thesis and a research paper.

I extend my gratitude to our collaborators at “National Laboratory Astana” and Nazarbayev University. Namely, to Yeldar Baiken, without whom it would have been impossible to select and characterize aptamers using FACS; and Dr. Natalie Barteneva and Zarina Sautbayeva for their help in using imaging flow cytometry. I am also thankful to people who taught me cell culturing, these are Aizada Chinybayeva, Damel Mektepbayeva and Sultan Mussakhan. Thank you to all the members of Core Facility of Nazarbayev University, namely, Rakhima Shamenova, Laura Khamkhash for teaching me how to operate on SEM and AFM. My gratitude also goes to Dr. Kanat Dukenbayev who was the first to show that my samples can be analyzed on AFM and gave some very

good insights. Thank you to all researchers and fellow PhD students who helped with equipment or consumables at different times of this project: Ainash Akmanova, Bakhytzhan Baptayev, Balnur Zhaisanbayeva, Aigerim Negmatova, Zhandos Tauanov, Sholpan Kauanova, Alzhan Baimenov.

Above all, this thesis was financially funded by State target program (Grant number 0111PK00364) from Science Committee of the Ministry of Education and Science (MES) of the Republic of Kazakhstan; Grant from the British Council and Newton – Al-Farabi Partnership Program "Researcher Links" and "LIFESTART" project at Nazarbayev University.

Thank you to Dr. Luis Rojas for improving our PhD program and making us feel like a family; and for teaching assistants and managers of School of Engineering and Digital Sciences in helping run this program, especially to Makpal Shomenova.

Most importantly, I thank the many past and present members of Laboratory of biosensors and bioinstruments for their aid in various aspects of the research process, but most importantly for their support and daily cheer-ups: Takhmina Ayupova (cell culturing), Madina Shaimerdenova (partner in building EFBG biosensor), Marzhan Sypabekova (improving optical fiber biosensor), Zhannat Ashikbayeva (chemical calculations), Madina Jelbuldina (principles of optical fiber), Sanzhar Korganbayev and Dr. Carlo Molardi (data analysis), Ildar Bekniyazov and Aida Amantayeva (electrochemistry).

Finally, I would like to express my gratitude to God for His Mercy and without whom my pursue of doctoral degree would not have been possible. I would like to thank my beloved parents, my elder sisters Botakoz and Saule, and friends (Aiida Syzdyk, Madina Akhmedova, Dinara Almetova, Moldir Kaiynbayeva, Zeinaf Muradova, Aiman Yedigeyeva, Madina Akan) for their continuous encouragement, patience and belief in me.

CHAPTER 1. INTRODUCTION

1.1. Background and Motivation

1.1.1. Breast cancer stem cells in breast cancer disease

BC is the most common cancer in women worldwide (1) with over six hundred thousand estimated deaths in 2018 (2). Despite the progress in treatment and prognosis, cancer recurrence and resistance to therapy remain the biggest problem in BC treatment (3). Moreover, metastasis is the main reason of death for patients with BC. Numerous studies suggest that only a small subset of cells is responsible for increased resistance to therapy and drive tumor growth and development. These cells are called cancer stem cells (CSC). They are a subset of tumor cells which have characteristics like normal stem cells: self-renewal and multi-lineage differentiation (4, 5). CSC are a source of both tumor propagation and heterogeneity in cancer cells (4, 5).

Range of methods for detection and isolation of these cells have been developed over the years as shown in **Table 1.1**. These methods utilize mostly one or more characteristics of CSC such as surface biomarkers, enzymatic activity, size, intracellular molecules, drug-exclusion ability, tumorigenicity in mice models. While offering many advantages, each of them has some drawbacks as low specificity and sensitivity, need in expensive equipment or trained personnel. Moreover, none of these methods detect CSC from blood directly. The presence of these cells in the blood gives an opportunity to use blood in diagnosis of BC (6). So far, analyzing BCSC has been done indirectly, i.e. not deriving them from the blood. One of the standard methods is forming human tumors in animal models, then analyzing their surface marker expressions using flow cytometry to find the cell population able to form tumors based on surface marker expression (7). Another methods are directly deriving the cells *in vitro* as mammospheres (without initial animal experiments) (8) or by isolating them from mature BC cell lines (9). Novel technologies for BCSC isolation from the bloodstream would allow the elimination of them from the bloodstream, therefore lowering the risk of developing risk of metastasis (10).

CSC characteristics	Method	Advantages	Disadvantages
Drug exclusion 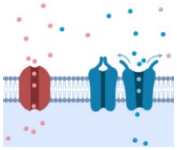	**Side population assay**	• Entails no specific cell markers	• Low specificity • Lack of purity • Not entire stem cell cohort • Costly
Enzymatic activity 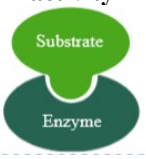	**Aldehyde dehydrogenase (ALDH) assay**	• Stability (compared to surface markers)	• Low specificity
Increased tumorigenicity in xenograft models 	**Xenotransplantation into NOD/SCID mice**	• Immature stem cells • Detection on a single-cell level • Widely accepted	• Time consuming • Expensive • Host factors • Potential to be biased
Surface markers, size, intracellular molecules 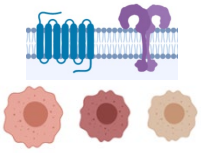	**Flow cytometry assisted cell sorting (FACS)**	• Multiparameter separation • Quantification	• High cost • Low viability of recovered cells • Trained personnel • Cell suspension solution • Possible cell activation
Surface markers 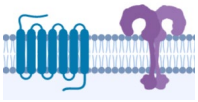	**Magnetic-assisted cell sorting (MACS)**	• Fast and easy	• Monoparameter separation • Cell suspension solutions
	Immuno-cytochemistry	Relatively inexpensive Very specific	• Cross reactivity • Background • Qualitative only
	Immuno-histochemistry	Inexpensive Highly specific	• Limited to tissue sample • Trained personnel
Resistance to drugs 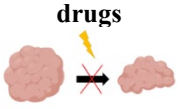	**Therapy resistance assay**	Fast and simple	• Low specificity, sensitivity

Table 1.1. Advantages and disadvantages of currently used methods of cancer stem cell isolation and analysis.

Table: Based on (3, 11); NOD/SCID mice – mice with non-obese diabetic/severe combined immunodeficiency

1.1.2. Aptamer as an advantageous ligand against BCSC

Given the importance of BCSC in BC recurrence, metastasis and resistance to therapy and also lack of synthetic binders, there is a need in discovering new ligands against them (12). One of such ligand candidates could be aptamers. Aptamers are single stranded oligonucleotides (DNA or RNA) or peptides that specifically bind to a broad range of targets. They are selected *in vitro* by systematic evolution of ligands by exponential enrichment (SELEX) (13, 14). Aptamers have qualities that can overcome some disadvantages of antibodies. For example, selection is done *in vitro* thus alleviating the use of animals during the selection process compared to antibodies; and their properties can be changed on demand: aptamers that can bind their targets in non-physiological conditions can be selected. SELEX has many modifications (15). One of them is cell-SELEX where aptamers against whole cells are selected. The main strengths of this method are: no need in prior knowledge of target molecule on cell surface; possibility to isolate aptamers against several molecules at once; biomarker discovery possibility; molecules are in their native state (16, 17). Recently RNA aptamers against epithelial cell adhesion molecule (EpCAM) – a CSC biomarker – were selected which specifically bind to breast, colorectal and gastric cancer cells that express this biomarker (18). Furthermore, aptamers against mouse embryonic stem cells were also selected (19). Therefore, one could assume that cell-based SELEX might be appropriate for the selection of aptamers against BCSC, by coupling with negative selection against differentiated cells.

Numerous studies in cancer biology rely on established cell cultures as models. For CSC, using a well characterized cells rather than isolating from patients seems to be more rational. This is due to difficulties associated with isolation of these cells described in **Table 1.1**. In this project BCSC from Celprogen were selected as target cells. Apart from having more than one surface biomarker associated with CSC (CD133, CD44, SSEA3/4, Oct4), they show enzymatic activities (Aldehyde dehydrogenase 1 (ALDH1) and telomerase) and tumorogenicity (<1000 cells). It has been shown that $CD44^{+}/CD24^{-/low}$ alone as a marker is not enough and should be used with ALDH activity since cells with both of these characteristics have higher metastatic ability and are more malignant (20). Moreover, using cell lines in CSC studies can be regarded as valid especially when self-renewing ability is shown *in vivo* (21).

1.1.3. Existing platforms for *in vivo* isolation of rare cells

Such important biomarkers in cancer as circulating tumor cells (CTC) as CSC, are rare events in the blood. One of the firstly reported devices for isolation of CTC that overcomes the issue of processing large blood volume was developed by Gilupi GMBH (www.gilupi.de). Their CellCollector™ is based on a medical guidewire made of SS covered with gold, hydrogel and EpCAM antibodies to capture CTC. It enables further downstream analysis of captured cells including immunofluorescence analysis, mutation analysis, fluorescence *in situ* hybridization, *ex vivo* cell culturing and other methods. CellCollector™ has shown a superior performance compared with CellSearch™ (a device cleared by Federal Drug Administration of the United States (FDA) for CTC detection) (22). Other fabricated devices for isolating rare cells from the blood stream include a system where magnetic nanoparticles are used for assisting capture and detection of CTC (23) and a "cytosensor" based on functionalized needle. All of these works, however, rely on the detection of CTC by EpCAM antibodies. EpCAM can be reduced in its expression during epithelial-to-mesenchymal transition which is associated with dissemination of tumor cells (24). Thus, there is a need in finding more specific markers and/or use combination of methods to isolate CSC from tumors (25).

1.2. Objectives and novelty of Thesis

In this project, it has been hypothesized that it is possible to develop aptamer-functionalized substrates which would bring us closer to isolation and detection of BCSC. To test this prediction, the hypotheses was divided into sub-hypotheses i) it is possible to select and characterize novel DNA aptamers against BCSC; ii) it is possible to functionalize SS wires with aptamers binding to BCSC and capture them; iii) it is possible to functionalize optical fiber with model aptamers to develop a biosensor. In this regard, research objective of this thesis was to develop aptamer-functionalized substrates which in the future could be used for BCSC isolation and detection. To achieve this objective, it has been divided into the following tasks:

1. Select and characterize DNA aptamers against BCSC;
2. Functionalize SS wire with aptamers specific to BCSC and capture them;

3. Functionalize optical fiber sensor with model aptamers for biosensor fabrication as a future platform.

One of the tasks of this project was to select novel ligands (aptamers) against breast CSC, with their intrinsic advantageous properties over antibodies. Literature review showed that certain aptamers against proteins overexpressed in BCSC have been already isolated. However, their selection was performed by aiming at specific biomarkers such as CD44 (26), ABCG2 protein (27), CD133 (28) which were either used as purified proteins or were expressed recombinantly. Targets on selected aptamers could be several when whole cell-SELEX approach is used (16), as is in our case, thus aptamers against multiple targets could possibly be selected.

Another novelty of this project is developing a substrate based on SS guidewire for its capability to analyze large blood volume and aptamers specific to BCSC to capture them. To the best of our knowledge, Gilupi hasn't developed CellCollector™ to capture cancer cells with stem-cell like properties nor they have used aptamers as bioprobes. If shown to be successful, this would be the first metal wire coated with bioprobes for BCSC isolation (rather than EpCAM-based detection method).

Optical fiber has been studied as a future platform for biosensor development using a well-characterized ligand-analyte model. The sensor is based on an etched fiber Bragg grating sensor functionalized using the same surface chemistry as SS wire.

1.3. Structure of Thesis

Together with Introduction and Conclusion, this Thesis is divided into five chapters each organized as a research article having the following sections: Abstract, Introduction, Materials and Methods, Results and Discussion; Conclusion.

In Chapter 2, a review of literature pertaining Thesis topic is presented. Namely, the chapter is divided into six parts: BC; BCSC; Aptamer selection and their advantages; Surface modification of SS for biomedical applications; Optical fibers and their functionalization; Characterization of functionalized surfaces.

In Chapter 3, we present a study done on *in vitro* selection of DNA aptamers against BCSC using SELEX. The process and the results of selection using fluorescence activated cell sorting (FACS) and sequencing of the final products are reported. In

addition, characterization of the selected aptamers using imaging flow cytometry is presented.

In Chapter 4, work done towards surface modification of SS as a platform for detection of BCSC is described. This chapter describes functionalization of SS wire with 3-aminopropyl)triethoxysilane (APTES), crosslinker and ligands against BCSC marker and its characterization by different techniques.

Finally, in Chapter 5, we present additional opportunities for building a sensing platform for BCSC using the same surface chemistry as in SS. This is done by reporting a work on the fabrication of optical fiber biosensor using a well-recognised thrombin and thrombin binding aptamer as a model system. Sensor's operation descriptions and experimental realization are presented in detail in this chapter.

Thesis is then commenced with Limitations, Future perspectives and Overall conclusion sections which shows limitations of the work, proposes possible future directions as well as gives an overall conclusion of the work described in the above chapters.

1.4. Role of collaborators

Damira Kanayeva, Helena Azevedo, and Wynter Duncanson helped in critically reviewing and editing an article on surface modification of SS (29) which is partially included in Chapter 2 of this thesis. My contribution to this paper was in searching for relevant articles related to the topic, systematically organizing relevant studies, original draft preparation, and writing the final paper after the review of co-authors and journal reviewers.

In an article on functionalization of SS (30), conceptualization was done and resource were obtained by Aliya Bekmurzayeva and Damira Kanayeva; methodology developed by Aliya Bekmurzayeva, Enrico Marsili and Kanat Dukenbayev; validation and investigation was performed by Aliya Bekmurzayeva; writing—original draft preparation was done by Aliya Bekmurzayeva; writing—review and editing by all authors; visualization by Aliya Bekmurzayeva and Helena S. Azevedo; the work was supervised by Enrico Marsili, Helena S. Azevedo, Daniele Tosi and Damira Kanayeva; funding acquisition, by Aliya Bekmurzayeva, Daniele Tosi and Damira Kanayeva.

For an article on etched fiber Bragg grating (EFBG) biosensor (31), conceptualization belongs to Aliya Bekmurzayeva, Madina Shaimerdenova, and Daniele Tosi. Design of methodology was done by Aliya Bekmurzayeva, Kanat Dukenbayev, Madina Shaimerdenova, and Daniele Tosi. Software-related works were performed by Carlo Molardi and Daniele Tosi. Experiments were performed and results validated by Aliya Bekmurzayeva, Madina Shaimerdenova, Kanat Dukenbayev, Takhmina Ayupova and Marzhan Sypabekova. Original manuscript was written by Aliya Bekmurzayeva, Kanat Dukenbayev and Ildar Bekniyazov; while reviewing and editing was done by Aliya Bekmurzayeva, Carlo Molardi and Daniele Tosi. The overall work was supervised, and funding acquired by Daniele Tosi.

For an article on etched tilted fiber Bragg grating (ETFBG) (32) Conceptualization belongs to Marzhan Sypabekova and Daniele Tosi; Investigation was performed by Marzhan Sypabekova, Alvaro Gonzalez-Vila, Aliya Bekmurzayeva, Takhmina Ayupova and Madina Shaimerdenova. Formal analysis was performed by Marzhan Sypabekova, Sanzhar Korganbayev and Daniele Tosi; Data curation and Software related tasks were done by Sanzhar Korganbayev; Methodology was developed by Marzhan Sypabekova and Alvaro Gonzalez-Vila. Validation done by Marzhan Sypabekova. Writing - original draft was done by Marzhan Sypabekova; Writing - review & editing performed by Marzhan Sypabekova, Alvaro Gonzalez-Vila, Christophe Caucheteur and Daniele Tosi. Project administration was performed by Aliya Bekmurzayeva, Takhmina Ayupova and Madina Shaimerdenova. The overall work was supervised by Luca Vangelista, Christophe Caucheteur and Daniele Tosi; Funding acquired by Daniele Tosi.

1.5. Funding

1. State target program (Grant number 0111PK00364) from Science Committee of the Ministry of Education and Science (MES) of the Republic of Kazakhstan;

2. PhD program state grant to Nazarbayev University from MES of the Republic of Kazakhstan;

3. Grant from the British Council and Newton – Al-Farabi Partnership Programme: Researcher Links Travel Grant (Grant number 216423762) for 6 months to Queen Mary University of London;
4. ORAU programme at Nazarbayev University. LIFESTART project (Lab-in-a-fiber for smart thermo-haptic treatment of tumors).

1.6. Thesis outputs

The following works are the output of this thesis:

Research articles:

1. A. Bekmurzayeva, K. Dukenbayev, H.S. Azevedo, E. Marsili, D. Tosi, D. Kanayeva. Optimizing Silanization to Functionalize Stainless Steel Wire: Towards Breast Cancer Stem Cell Isolation. *Materials* (*MDPI*) 2020, 13(17). (SiteScore 3.5; Impact factor 3.057; Q2 in Material sciences (misc.)) (30)
2. A. Bekmurzayeva, K. Dukenbayev, M. Shaimerdenova, I. Bekniyazov, T. Ayupova, M. Sypabekova, C. Molardi, D. Tosi. Etched Fiber Bragg Grating Biosensor Functionalized with Aptamers for Detection of Thrombin. *Sensors* 2018, 18(12). (SiteScore 3.72; Impact factor 3.031; Q2 in Medicine (misc.), Analytical chemistry, Electric and electronic engineering) (31).
3. M. Sypabekova, S. Korganbayev, A. González-Vila, C. Caucheteur, M. Shaimerdenova, T. Ayupova, A. Bekmurzayeva, L. Vangelista, D. Tosi. Functionalized etched tilted fiber Bragg grating aptasensor for label-free protein detection. *Biosensors and bioelectronics* 2019, 149(15), 111765. (SiteScore 8.95; Impact factor 9.518; Q1 in Biomedical Engineering, Electrochemistry, Medicine (misc.)) (32).

Review article:

1. A. Bekmurzayeva, W.J. Duncanson, H.S. Azevedo, D. Kanayeva, Surface modification of stainless steel for biomedical applications: Revisiting a century-old material, *Materials Science & Engineering C-Materials for Biological Applications* 2018, 93, 1073-1089. (SiteScore 5.07; Impact factor 4.959; Q1 in Material science (misc.)) (29).

Conference papers/posters:

1. A. Bekmurzayeva, Y. Baiken, D. Kanayeva. Selection and characterisation of an aptamer against breast cancer stem cells. Abstract in *World Congress on Biosensors* 2018. Miami, USA. June 12-15, 2018

2. A. Bekmurzayeva, M. Shaimerdenova, D. Tosi: Fabrication and interrogation of refractive index based on Etched Fiber Bragg Grating (EFBG). *40th Annual International Conference of the IEEE Engineering in Medicine and Biology Society* (EMBC). Honolulu, Hawaii, USA. July 17-21, 2018. https://doi.org/10.1109/EMBC.2018.8513240

3. M. Shaimerdenova, A. Bekmurzayeva, T. Ayupova, M. Sypabekova, S. Korganbayev, K. Dukenbayev, C. Molardi, D. Tosi: Detection of various Thrombin concentrations using etched fiber Bragg gratings functionalized with DNA aptamer. Proceedings Volume 10820, Optics in Health Care and Biomedical Optics VIII; 108200O Event: *SPIE/COS Photonics Asia*, Beijing, China. October 11-13, 2018. https://doi.org/10.1117/12.2502457

4. M. Shaimerdenova, A. Bekmurzayeva, M. Sypabekova, Y. Abukhanov, D. Tosi. Detection of tilted fiber Bragg grating fiber-optic sensors with short-term KLT: Towards low-cost biosensors. Proceedings Volume 10820, Optics in Health Care and Biomedical Optics VIII; 108203A. Event: *SPIE/COS Photonics Asia*, Beijing, China. October 11-13, 2018. https://doi.org/10.1117/12.2502468.

CHAPTER 2. LITERATURE REVIEW

This chapter presents literature review on topics relevant for the Thesis. It begins with a review of BC, its classification and diagnosis. Then it discusses BCSC and aptamers. This chapter also introduces SS and optical fiber as platforms used in biomedicine and their surface modification techniques and methods of surface analysis.

Part of this Chapter (namely, subsection 2.4) was published as part of a review article in Materials Science & Engineering C-Materials for Biological Applications Journal (Elsevier) (29). My contribution to this paper was as follows: searching for relevant articles related to the topic, systematically organizing relevant studies, original draft preparation, and writing the final paper after the review of co-authors and journal reviewers.

2.1. Breast cancer

2.1.1. Breast cancer burden

BC is the most common cancer in women in the world (33) comprising almost 30% of all cancer cases with approximately a million cases annually (34). It accounted for 1.7 million new cases in 2012 (35) and more than 2 million new cases in 2018 (2) (**Figure 2.1**). BC incidence is in rise in all countries except few developed countries (35). For the majority of countries (154 out of 185), BC is the most frequently diagnosed cancer type (2). Australia/New Zealand, Western Europe, Northern Europe, Northern America Southern Europe have the highest incidence rates of this disease (in descending order) (2).

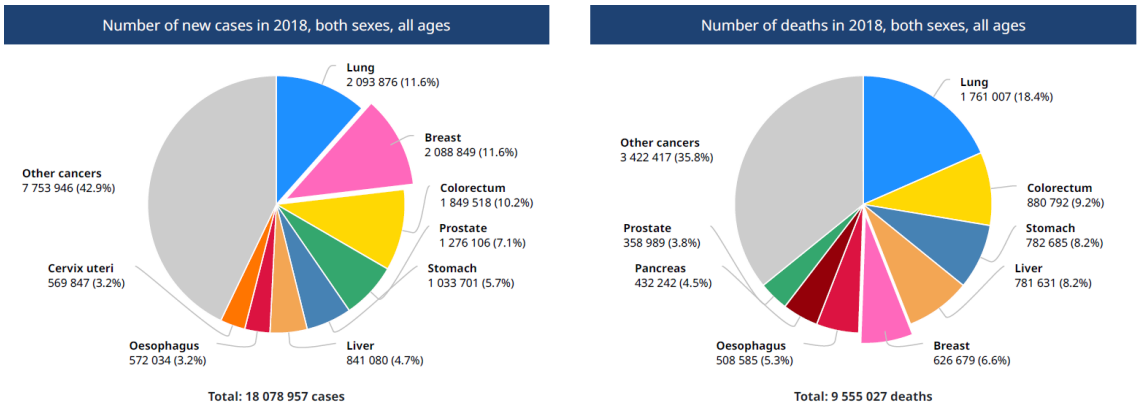

Figure 2.1. Number of new cases (incidence) and deaths (mortality) for breast cancer in 2018: data for both sexes and all ages. Source: International Agency for Research on Cancer (World Health Organization); GLOBOCAN.

According to GLOBOCAN 2018 (Global Cancer Observatory; published by the International Agency for Research on Cancer) the estimated deaths due to BC is more than a 660,000 people making it the fifth in the mortality ranking (**Figure 2.1**) (2). Among females, BC is the most death-causing cancer type worldwide (2). In Kazakhstan, BC is the most prevalent form of cancer among women (36), with every fifth case accounting to BC (37). Annually, ca. 4,600 new cases and 1,300 deaths occur due to BC in Kazakhstan (37). For more than hundred countries worldwide, BC is the leading cause of cancer-related deaths; exceptions are countries where lung cancer (Australia, New Zealand, Northern Europe, Northern America) or cervical cancer (many sub-Saharan countries) are the number one causes (2). Mortality is decreasing in many high-income countries but is rising in low- and middle-income countries (35). For approximately 90% of patients the initial treatment turns out effective leading to clinical remission (12). However, BC has high incidence of recurrence and treatment failure (38). Risk of recurrence is still high after about 5 years for these patients; and recurrent cancer is usually resistant to conventional therapies leading to poor survival rates of women with recurrent BC (12).

2.1.2. Classification of breast cancer

Morphologically and genetically, BC is a heterogeneous disease (38) which displays different histological, clinical and molecular phenotypes (39). Survival (disease-free and overall), patient outcome, treatment to therapy, prognosis vary in different subtypes of BC (40). Several subtypes of BC are known based on histological characteristics and molecular profiles. Classification of BC subtypes according to phenotypic characterization is shown in **Table 2.1.** Luminal A-like subtype is characterized by the expression of such biomarkers as estrogen receptor (ER), progesterone receptor (PR), and negative human epidermal growth factor receptor 2 (HER2) and clearly low Ki-67 (protein encoded by MKI67 gene) making it ER^+, PR^+, $HER2^-$ and $Ki\text{-}67^{low}$; while Luminal B-like is ER^+, $PR^{+/-}$, $HER2^{+/-}$ and $Ki\text{-}67^{high}$. HER2-like subtype of BC is characterized by the absence of ER, PR and presence of HER2 (ER^-, PR^-, $HER2^+$); TN subtype is negative to three receptors (ER^-, PR^-, $HER2^-$); while basal-like BC is characterized by ER^-, PR^-, $CK5^+$ (cytokeratin), $CK6^+$, $CK14^+$, $CK17^+$, $EGFR^+$; Claudin-low subtype has a low expression of Claudin 3, 4, 7 and e-cadherin and is also negative to three receptors as TN subtype; normal-like BC does not have clear phenotype (no homogenous identification) (41, 42). Luminal A subtype represents approximately 50-60% of all cases and has good prognosis and low relapse rates; while Luminal B subtype is 15-20% and has higher recurrence rate and lower survival rates than Luminal A (43). In general, luminal subtypes have a better prognosis and respond to endocrine therapy (44). HER2-like BC has a poor prognosis but responds well to chemotherapy with anti-HER2 agents such as monoclonal antibodies (44). TN BC also accounts to 15-20% of all BC cases but does not have an FDA-approved targeted treatment (45).

Breast cancer subtype	ER	PR	HER2	Ki-67	CK5 CK6/ CK14/ CK17/ EGFR	Claudin 3,4,7/ e-cadherin
Luminal A-like	+	+	-	**clearly low**		
Luminal B-like	+	+/-	+/-	**clearly high**		
HER2-overexpressed	-	-	+			
Triple-negative	-	-	-			
Basal-like	-	-			+	
Claudin-low	-	-	-			**low**
Normal-like	**without homogenous identification**					

Table 2.1. Classification of BC subtypes according to phenotypic characterization. Table based on (40, 42). Main phenotypes are shown for each subtype. "+" means expressing/overexpressing; "-" means no expression. ER –estrogen receptor; PR – progesterone receptor; HER2 – human epidermal growth factor receptor 2; Ki-67 - protein encoded by MKI67 gene; CK – cytokeratin.

2.1.3. Diagnosis of BC

BC is usually detected in one of the two ways: screening program or a symptom as pain or palpable mass in breast (46). Diagnosis of BC include such methods as magnetic resonance imaging (MRI), mammography, molecular breast imaging, breast biopsy, HER-2/neu detection assay, blood-based assays (serum biomarkers, cells, nucleic acids, autoantibodies) (33).

In mammography, breast is imaged using low doses of X-ray (47). While remaining a standard tool for BC screening, its performance depends on the density of breast tissue (48). Thus sensitivity of mammography decreases in cases of dense/heterogeneously dense breast tissues (33, 48). Full-field digital mammography when X-rays are converted into mammographical pictures of the breast, can be used to alleviate the effect of experience of the radiologists which affect accuracy and sensitivity of mammography as a diagnostic tool (49). Current screening includes physical examination and mammography which however has not enough sensitivity and

specificity. Thus sensitivity of 54-77% were reported for mammography depending on the type of procedure performed (34). Breast biopsy with concurrent histopathological and immunohistochemical analysis is considered a gold standard tool. However, this is an invasive procedure which can also be fatal in some cases (34). Ultrasound has been used as a complimentary tool for BC diagnosis. However, it increases false-positive results since benign tumors are detected mostly and requires further biopsy (50). MRI is considered to be more sensitive than mammography especially in cases of dense breast tissues because MRI detects malignancy depending on increased vascularity of BC (48). Although MRI can be used to avoid unnecessary biopsies by providing more evidence than other imaging techniques (51), its disadvantages include high cost of the test, limited availability and false positive rate of MRI (52). Positron emission tomography with computer tomography (PET/CT) is a powerful tool for determining presence of BC, its stages, recurrence and response to therapy depending on the radiopharmaceutical used (53). However, the technique is very expensive and cannot be used to find lesions of less than 1 cm in size (54); and it is shown to be not beneficial for patients with early stage disease (at least in case when fluorodeoxyglucose is used) (55).

Early diagnosis of BC is considered to be the most important strategy to reduce mortality and improve survival rate at present (33). Early diagnosis also entails alleviation of treatment as seen by smaller surgeries and reduced use of chemo- or radiotherapy agents (34). Convenient and accurate identification methods of women potentially having this disease have to be developed in order to detect breast carcinoma early (34). Mortality due to BC was reduced in Europe because of BC screening: by 25-31% for patients invited to screening and by 38-48% for women screened in between 1990 and 2010 (56).

Alternative ways of diagnosis are being studied to improve early detection of the disease because widely used methods are relatively complex, hard to access and have high cost (34). Moreover, they cause discomfort and pain to patients while being not sufficiently accurate. Improving methods of diagnosis or combining them, developing novel more effective, comfortable and non-invasive tools is underway (33). By using molecular diagnostic tools with conventional methods of diagnostics (ultrasound and MRI), it could be possible to tackle the issue of overdiagnosis of BC by these techniques (33). Learning more about the association of sonographic characteristics and molecular

markers and developing novel contrast agents could improve the performance of ultrasound as a molecular diagnostic tool (50). In PET/CT, developing radiopharmaceuticals with improved specificity to differentiate processes occurring during BC could enable improving early diagnosis of BC and developing personalized therapy (53).

BC biomarkers can be used as useful tools in BC diagnosis. They can be grouped into prognostic, therapeutic, and diagnostic biomarkers. Diagnostic biomarkers include such glycoproteins as HER2 and carcinoembryonic antigen (CEA), genes as BRCA1, micro RNAs as miR-21, miR-155 and miR-222 (57). A number of molecular tests for BC diagnosis and treatment are available (41). Since there is no panel of biomarkers which is considered to be the most appropriate and genetic profiling (to test multiple genes at once) is expensive and not available in many clinics, immunohistochemical analysis of such receptors a ER, PR and HER2 are more commonly used (40). After testing for the presence of the three main biomarkers (ER, PR and HER2) and clinical results such as stage of BC, tumor grade, lymph node involvement specific recommendations for further treatment and additional testing are given (41). In addition to the three common biomarkers and clinical results mentioned above, the following biomarkers identified in tumor tissue or serum have a potential to be used to determine severity of BC: urokinase-type plasminogen activator, plasminogen activator inhibitor 1, CA15-3, CA 27.29, CEA, Ki67, cyclin E, cathepsin D, and CTC (41). To be included in mass screening, biomarkers must be detected from biological fluid in a minimally invasive procedure and must be present in a sufficient level there (58).

2.2. Breast cancer stem cells (BCSC)

2.2.1. Characteristics and role of BCSC in BC

One of the hypothesis that explains relapse and recurrence of BCSC is a “Cancer stem cell” hypothesis (59). CSC are a subpopulation in cancer cells which (as normal stem cells) have ability to self-renew and differentiate. Thus they are both a source of tumor propagation and heterogeneity in cancer cells (4, 5). Despite its name being CSC, they are not necessarily derived from normal stem cells. The term is based on its following characteristics: tumor initiation in immunocompromised mice, tumor formation in

secondary mice (i.e. self-renewal) and forming bulk of tumor (i.e. differentiate into non-self renewing cells) (60). Characteristics of BCSC are shown in **Figure 2.2**. and will be discussed in detail later. While some researchers find CSC more appropriate to a term "tumor-initiating cell" (TIC) because the latter does not show its capability to differentiate (5), others regard TIC as a more convenient term given CSC's ability to initiate cancer in model organisms and being a less confusing term than CSC (60).

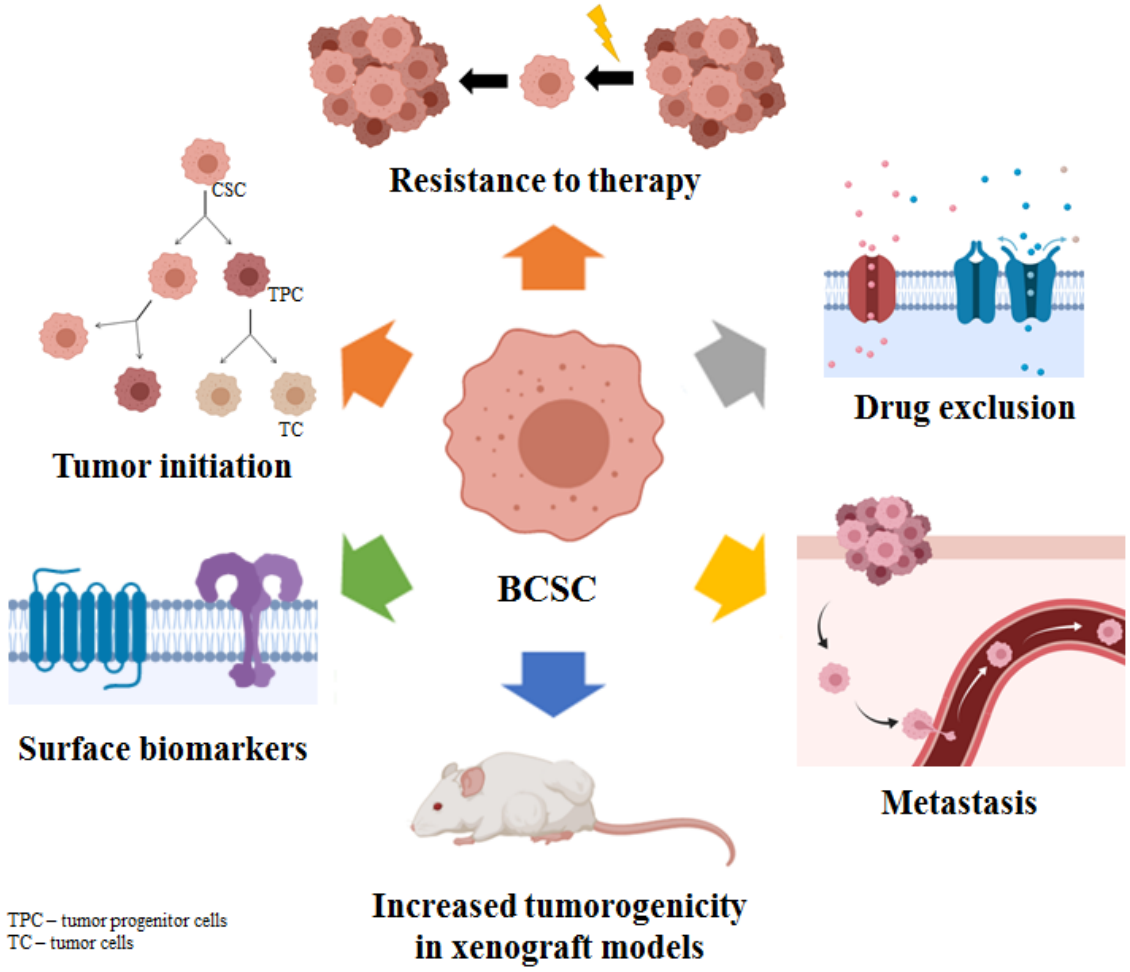

Figure 2.2. Characteristics of breast cancer stem cells. Figure drawn using BioRender platform.

In the middle of nineteenth century R. Virchow suggested a possible relationship between tissue teratocarcinomas and fetus. In 1994, cancer cells with stem-cell like properties in acute myeloid leukemia patients were first identified (4). Their existence in solid cancers was debated (60) until it was firstly discovered in BC by Al-Hajj (7) in 2003

where a subpopulation of tumor cells had the ability to form tumors in NOD/SCID mice. To date, they have been identified in many human cancer types including breast, brain, colorectal, head and neck, liver, ovarian, prostate, skin (4). These isolated BCSC had such surface markers as $CD44^{+}/CD24^{-/low}$ and few hundred of these cells were capable of initiating tumor in NOD/SCID mice (compared to tens of thousands of cells with other phenotype) (7). Later, cells with tumor initiating properties were also isolated from BC lesions and cell lines (MCF7 cells) also had $CD44^{+}/CD24^{-}$ with additional $Cx43^{-}$ (8). The number of cells with $CD44^{+}/CD24^{-}$ phenotype were able to form tumors in immunocompromised mice was found to be as low as 1000 as opposed to million cells in control cells (MCF7 cell line). They were also shown to express putative stem cell marker Oct-4 (8). When different BC cell lines were examined, five out of thirteen of them had cells characterized as $CD44^{+}/CD24^{-}$. These cells had higher expression of genes involved in cancer invasion (9). BCSC are able to form mammospheres which were identified to be early progenitor cells or stem cells capable of differentiation into mammary epithelial cells (61). Later clinical studies showed that cells remaining after endocrine and chemotherapy (i.e. tumor initiating cells or CSC) had characteristics of both mesenchymal and epithelial cells. For this, two types of methods for selecting cells with tumor initiating abilities were utilized, namely mammosphere formation and FACS by $CD44^{+}/CD24^{-}$. Among other subtypes of BC studied, they were more enriched in claudin-low subtype which has many genes associated with epithelial to mesenchymal transition (EMT). Gene expression profiling of selected cells was compared with control cells before and after treatments (endocrine and chemotherapy) and revealed to gene signatures related to $CD44^{+}/CD24^{-}$/mammosphere forming cells and claudin-low subtype (59).

Apart from $CD44^{+}/CD24^{-}$, a number of other BCSC related biomarkers were discovered for BCSC. Aldehyde dehydrogenase 1 is an enzyme involved in metabolism of substances important for maintenance and differentiation of normal stem cells and CSC (62). Other cell surface markers expressed in BCSC are ABCG2 (ATP-binding cassette G2) which is involved in drug efflux, CD10 (overexpressed in other tumors), EpCAM, epithelial surface antigen (ESA), CD133 (also expressed in other CSC), CXCR4 (metastasis; present in mammospheres), CD29 (cell adhesion and metastasis), CD49f (candidate stem cell marker), estrogen (expressed in many types of mammary cells: BC,

progenitor, BCSC) (63). Among studied phenotypes ($CD44^+/CD24^{-/low}$, ALDH1+ and $ALDH1^+CD44^+/CD24^{-/low}$), cells with a $ALDH1^+CD44^+/CD24^{-/low}$ phenotype had superior self-renewal, proliferation and invasion abilities (64). Further investigation of the roles these cells play in cancer biology, revealed that $CD44^+/CD24^-$ are more important in tumorigenesis (proved by xenotransplantation in mice) and cell proliferation (mammosphere assay); while cells with $CD44^+/CD24^-$ are crucial for cell migration and metastasis (65). Putting together the results of several studies, it was concluded that combination of well selected biomarkers can be beneficial in selecting more BCSC. This combination being $CD44^+/CD24^{-/low}$ phenotypes within cells with $EpCAM^+/CD49f^+$ (66). Novel molecular links connecting normal stem cells with BCSC are also being discovered (67). It is noteworthy mentioning that molecular subtypes of BC vary in terms of phenotype and frequency of BCSC. This could be one of the explanations of the observed difference in relapse, metastasis, and response to therapy among different subtypes of this disease. The following association have been revealed: BCSC with $CD44^+/CD24^-$ are more present in claudin-low and basal-like BC; ALDH-1 expressing BCSC predominantly found in HER2 type while luminal BC (both A and B) have cells with more of non-BCSC phenotype (more differentiated cells) with lower number of cells with $CD44^+/CD24^-$ and ALDH1 phenotypes (68).

BCSC are shown to be resistant to chemo- and radiotherapy and metastasis. BCSC are much more enriched in BC cell lines and human tissues which are chemo- and radioresistant (69). A large number of studies demonstrated the enrichment of BCSC after chemo- or radiotherapy which suggest their association in recurrence and resistance to these conventional treatment methods (68). Different chemotherapeutic agents showed to enrich different subpopulations of tumorigenic cells with stem-cell like properties in a number of studies (70). This is attributed to a number of properties that these cells possess. Thus they have an increased DNA repair capability (62). ALDH inhibitor suppressed the growth of BCSC *in vitro* and inhibited metastasis of these cells to the lung in mice (71). One of the drug efflux proteins which is important in building chemoresistance, ABCG2 (BC resistance protein), is overexpressed in some BCSC (69). According to CSC theory of cancer, BCSC are the main initiators and drivers of tumor growth. BCSC have increased ability to move and invade, overexpress genes involved in

metastasis. Their role in initiating metastasis has been well documented by many studies where BCSC caused metastasis (70). Li *et al* (65) studied expression of cellular markers in various cell lines and investigated their role in cancer biology both *in vitro* and *in vivo*. They showed that high ratio of $CD44^{+}/CD24^{-}$ was more indicative of tumor proliferation and tumorigenesis, while high ration of $ALDH1^{+}$ is associated with cell migration and metastasis.

2.2.2. Isolation and purification of CSC

Isolation and purification of CSC is based on one or more of their characteristics and include the following (72): sphere formation in cultures, membrane efflux, surface markers, enzymatic activity, tumor initiating ability in immunocompromised mice. Thus CSC ability to exclude drug is used in labeling with Hoechst dye which has low specificity, lack of purity and does not label the entire stem cell cohort. Specific enzymatic activity of CSC is used in Aldehyde dehydrogenase assay and FACS and is more stable compared to surface markers but has low specificity. A gold standard test of proving that cells are CSC is xenotransplantation into NOD/SCID mice, which is able to detect a single immature stem cell with increased tumorogenicity. However, this method is not time- and cost-effective and host factors might affect its performance (11). Moreover, these animals do not have the same growth factor/cytokine signals as humans and they lack immune cells (60). Magnetic nanoparticles covered with antibodies against surface markers specific to CSC are used in magnetic-assisted cell sorting which is a fast and easy method of separation of these cells. FACS, which uses specific surface markers and enzymatic activity, offers an efficient multi-parametric separation. However it has high cost, requires trained technicians, might have low viability of sorted cells (11).

CTC are cells with tumor initiating abilities found in blood circulation. CTC are more extensively studied in BC than in other cancers. CTC count in metastatic BC has a strong clinical evidence as a prognostic biomarker to study dynamics of the disease (73). Relationship of CSC with CTC is not always straightforward. CTC are shed from tumors and can be found in blood. These cells offer to be a good candidate to serve as a “liquid biopsy”. However the main drawback is their rarity in the blood: ranging from 0 to 10000 CTC per ml. Strong correlation of finding CTC in 7.5 ml of blood with progression free

and overall survival of patients with breast, colon and prostate cancer (74). A small portion of these CTC are thought to be circulating CSC (6)

The importance of CSC isolated from CTC in patients with BC is increasingly reported. Isolation of cells with mesenchymal properties and BCSC-like properties was found to be more relevant for the prediction of BC than counting CTC in blood alone (75). It has been shown that in EMT and CSC are directly linked and that EMT is responsible for generation of CSC in BC (76). Theodoropoulos *et al* (77) isolated cells with stem cell-like properties from cytokeratin-positive CTC of patients with metastatic BC. By analyzing CTC from BC by molecular assays and imaging techniques, it was possible to show that CTC express such CSC-like markers as CD44, ALDH1 and lack of CD24 (78). A number of other studies also isolated CSC from CTC of metastatic BC patients and other markers were revealed: CD47 (involved in inhibition of phagocytosis and cancer evasion) and MET (involved in activation of migration and invasion). These cells isolated from primary human luminal BC CTC were cells with tumor initiating properties and expressed $EPCAM^{+}CD44^{+}CD47^{+}MET^{+}$ (i.e. similar to BCSC) (79). While the bulk CTC from which these cells were isolated had a low efficiency in initiating tumor in xenograft model, enriched cells were more efficient. These cells were associated with lower overall survival and more metastatic sites in animal model used. Another research studied cells for their expression of EMT transcriptional factors and CSC-like properties in patients with metastatic HER^{2+} BC (80). They demonstrated that CTC which undergone EMT are present in those people which were CTC-negative using CellSearch™ system. Although there was no association of EMT gene expression with CSC like properties, their other findings support Cheffer's theory of metastatic cascade which states that CTC are plastic cells and can develop both to stem- and non-stem cell populations. Another study also revealed a population of cells having EMT (fibronectin and vimentin) and CSC-like (ALDH1) properties among CTC. Thus this study focused on detection of cells from CTC not based on commonly used EpCAM marker (81). All these studies suggest that using CTC with CSC characteristics rather than CTC alone is more relevant for BC in terms of its development, progression and outcomes; further large-scale clinical trials are needed to confirm their role in disease prognosis and prognosis (76). Multiparametric flow cytometry (staining cells with CD45 (to eliminate

leukocytes), EpCAM, CD44, CD24, CK-8, CK-18, CK-19 antibodies) revealed that cells with stem cell-like properties were more present in patients with stages III and IV than with I and II thus suggesting their possible role in early detection of BC as a guide to therapy and a prognostic tool (82).

Compared to CSC, detection and isolation of CTC have been studied more to develop different assays including portable ones. CTC isolation and enrichment methods include such approaches density-gradient centrifugation, immunomagnetic separation (antibodies on magnetic nanoparticles), microfluidic platforms and filtration devices (78). Many of antibody-based tests are based on surface markers, especially EpCAM. CTC Chip technology is microfluidic platform coated with EpCAM antibodies using unprocessed peripheral blood. It was specifically designed to have controlled conditions (laminar flow through microposts) where cells would encounter antibodies that capture them (83). Using fluorescently labeled EpCAM and HER2 antibodies and integrating optical fibers in the microfluidic system, Pedrol *et al* designed a device for BC detection of blood (84). However, due to EMT where carcinoma cells acquire characteristics of mesenchymal cells (e.g. motility, lack of cell polarity and ability to invade), expression of epithelial markers such as EpCAM can be downregulated (73). Although most of BC subtypes were efficiently isolated using EpCAM (85). In order to test their clinical use, it is important to have quality control, standardized CTC detection and characterization methodologies (78). BC CTC detection and molecular characterization include imaging-based approaches (using labeled antibodies against cell surface markers) and molecular assays to detect nucleic acids (78) CellSearch™ is based on EpCAM antibodies which is designed to sample CTC in 7.5 ml of blood; it is the only test approved by FDA for CTC quantification (86). Using CellSearch™ to detect CTC in metastatic BC patients allowed classifying patients ino risk groups (87). Presence of five or more CTC in the blood (7.5 ml is drawn, and cells analyzed using CellSpotter™) of patients diagnosed with metastatic BC before initiating any therapy is associated with short overall and progress-free survival. Moreover, presence of the cells in 3-4 weeks after therapy initiation and during restaging is also correlated with prognosis (88). However, images obtained from CellSearch™ can be interpreted subjectively and no further analysis of cells is possible (89). First *in vivo* device for CTC isolation that is aimed to overcome the issue of blood

volume was developed by Gilupi GMBH (www.gilupi.de). Their CellCollector™ device is based on a medical guidewire. A guidewire is a device widely used in medicine to facilitate the delivery of catheters, stents and other interventional devices for diagnostic and therapeutic purposes. CellCollector™ guidewire is covered with EpCAM antibodies to capture CTC and enables their further downstream analysis such as immunofluorescence analysis, mutation analysis, fluorescence *in situ* hybridization, *ex vivo* cell culturing. Surface of SS is covered with gold and hydrogel for covalent immobilization of antibodies. CellCollector™ has been compared with FDA approved CellSearch™ and showed higher sensitivity for BC: 74% compared to 12%, and high precision (linear regression, r^2 = 0.96) (22). Furthermore, Gilupi™ provides customized CellCollector™ functionalized with an antibody of interest. To the best of our knowledge, Gilupi™ hasn't developed CellCollector™ against CSC yet (but they are planning to do so) and they use only antibodies as bioprobes. Real-time PCR is another assay which can be used to amplify cytokeratin genes from breast CTC. However, this requires preliminary enrichment of CTC and RNA extraction which on their own have drawbacks (90).

One of our assumptions is that using BCSC as target cells and BC cells and breast epithelial cells as control cells during selection of bioreceptors, one is able to find molecules which bind to cell surface biomolecules that are different from non-CSC. These aptamers then potentially can be used to isolate BCSC from the blood stream by using guidewire similar to Gilupi™. The lack of an effective molecular contrast agents to be used in early diagnosis, cell migration tracking and monitoring treatment of BC is the major bottleneck in detection of BC in early stages (91). As stated above, BCSC are characterized by such phenotype as $CD24^{-}/CD44^{+}$, however this means the need in more than one antibody to select for these cells. Moreover, antibodies have inherent disadvantages as detection agents (12). Molecules able to specifically and sensitively detect biomarkers on pathogenic cells is very important for diagnosis of diseases (92). These new molecular probes could be aptamers. Selecting new aptamers targeting BCSC could be a promising instrument to better understand the biology of BCSC; moreover these new ligands could be used as probes in imaging and diagnostics, cargo molecule during therapy (12).

2.3. Aptamers

2.3.1. Aptamers: selection and advantages

Aptamers (from Latin "*aptus*" – fit (93)) are short single-stranded oligonucleotides (both DNA and RNA) or peptides that are selected *in vitro* to bind their target with high affinity and specificity (13, 14, 94). Short RNA molecules were first selected in 1990 by Tuerk and Gold to bind bacteriophage T4 DNA polymerase from a pool of molecules (95). They termed the process of selection SELEX. Independently, another group of scientists almost at the same time published similar process of selection of specific RNA molecules against organic dyes (Cibacron Blue and Reactive Blue 4) and called these molecules aptamers (96). This way, both new ligands and the method of their selection were introduced.

Since their first selection, aptamers not only of RNA origin but also of DNA and peptide nature were selected against a range of targets. To date aptamers have been selected against targets that include metal ions (97), small organic/inorganic molecules (ATP (98), cocaine (99), amino acids (100, 101)), a variety of proteins (proteins secreted by bacteria (94, 102, 103), clinically important proteins (104-106)), peptides (107), polysaccharides (108), viruses and virus particles (109, 110), whole cells (16, 18, 111, 112), and even tissues (15, 113). They bind their target with high affinity: often with a dissociation constant ranging from nanomolar to picomolar range (114). Aptamers fold into certain structures such as pseudoknots, hairpins and quadruplex (113). They are capable of binding to target molecules with high selectivity (14). In fact, they can distinguish between closely related compounds such as theophylline and caffeine (15). In case of proteins, epitopes targeted by the selected aptamers, can be a structured epitope and even a denatured peptide (113).

SELEX procedure is characterized by the repetition of several steps. It includes three main stages: incubation of a random library with the target; separation of bound aptamers from unbound ones; amplification of bound sequences using PCR (113). For selection of DNA aptamers, random ssDNA library synthesized to have a central randomized region flanked with known sequences of primers from both sides is used (115). The length of random region widely used ranges from 20 to 60 nucleotides (nt). The known sequences are necessary for the amplification of oligonucleotides for further steps (113). Library with a random region of 40 nt theoretically should contain 1.2×10^{24}

individual sequences (4^{40}). In reality, this number is limited by the synthesis itself. Initial library is incubated with the target of choice. For instance, solid-phase DNA synthesis with a synthesis scale of 1 μmole will result in 10^{14}-10^{15} individual sequences (93). Methods of partition of bound sequences from unbound ones are different: nitrocellulose membrane (111), biotin/streptavidin affinity, FACS (116), capillary electrophoresis (117), centrifugation and others. After separation, bound species are amplified with PCR and ssDNA is generated using different methods including denaturing polyacrylamide gels, assymetric PCR, lambda exonuclease digestion, magnetic affinity columns (118). These sequences are then subjected to another round of selection until high-binding aptamers are enriched.

Although the basic principles of SELEX did not change (119), different modifications of SELEX are known (15) including SELEX with libraries based on genomic sequences (genomic SELEX), free of fixed sequences (tailored SELEX), using several targets (toggle SELEX for aptamers with broad specificity) and etc. (113). In some cases library with modified nucleotides can be used to select aptamers against certain classes of target (hydrophobic targets), to increase their resistance to nucleases or to (93). Recent advancements in SELEX include use of bioinformatics tools such as Apta-LoopEnc. It is a nucleic acid encoding strategy developed to find aptamers with superior performance among aptamer candidates and assist in the design and optimization of new sequences in SELEX (120). Automated SELEX and single-round selection (using capillary electrophoresis) are also available (119). One of the variations of SELEX is *in situ* tissue slide-based SELEX (121). Another type of SELEX combines cell-SELEX with 3D culture systems that mimic tissue environment *in vitro*. Aptamers selected this way considered to have a similar response *in vivo* (122).

Aptamers have qualities that can overcome some disadvantages of antibodies. For example, aptamers are synthesized *in vitro* from a library that contains large numbers of random sequences. This alleviates use of animals during the selection process compared to antibodies (102). Their properties can be changed on demand: aptamers that can bind their targets in harsh environments (different pH and temperatures) can be selected. Aptamers can be selected against non-immunogenic or toxic targets (93). Production of selected aptamers is done by chemical synthesis and thus they have less batch to batch

variation and are more pure (114). Furthermore, they can be massively synthesized once selected in a reproducible way (123). Aptamer synthesis is more cost-effective than production of antibodies. Aptamers made from nucleic acids are more stable than antibodies and they can be kept in ambient temperatures. In addition, they are smaller in size and their affinities are not affected by labelling (124-126). Different modifications during their production are used for increased stability, bioavailability and immobilization in diagnostic assays (114).

2.3.2. Aptamers against cells (Cell-SELEX)

A wide variety of aptamers have been generated by SELEX, mostly targeting highly purified molecules (127). On the contrary, recent development of cell-based SELEX procedures enables the isolation of aptamers against cell surface molecules of unknown identity or proteins inappropriate for purification in fully active conformations The main advantages of using cell-SELEX are as follows: aptamers specific to target cells can be selected without prior knowledge of molecular changes associated with a particular type of cancer, there is no need in purification of the target protein, cell surface proteins are in their native structure, aptamers can be selected against post-translationally modified proteins. Moreover, there is a possibility of discovering a new biomarker associated with cancer (128, 129).

Because of the abovementioned properties aptamers are used in areas that include functional studies of proteins, therapeutics, diagnostics and biosensing (14, 113, 123). Numerous research suggests that by selecting internalized surface markers on cancer cells it is possible to select aptamers which are able to target cancer cells and use them as a delivery agents (130). Aptamers targeting cells have a potential to be used as efficient probes for cell isolation and imaging *in vivo*. Aptamers are being selected for use in biosensing mainly (in addition to be selected against almost any target) because they can be selected and used under any pre-defined conditions and they can be easily immobilized to obtain a custom-made surface. Coupling the change in shape of aptamers upon binding to the target with different signalling mechanisms can be utilized in the event of molecular recognition (125). Human pluripotent stem cells with more than 97% purity were obtained from a cell mixture (~20% of target cells) using aptamer-based assay (131).

Aptamers were also used as a probe to rapidly and effectively isolate adult mesenchymal stem cells from porcine bone marrow in FACS (132). Another aptamer has also a promising use as a FACS reagent in isolating cells (c-kit-positive) from bone marrow cells (133). To elucidate the eligibility of using antibody-based therapy against CD30 positive lymphoma, aptamers (first RNA-based and later DNA based) against this biomarker were used in an *in vivo* setting to image tumor tissues (134). They were able to bind tumors expressing CD-30 and not bind to CD30-negative tumor tissues. Aptamers against gliosarcoma cells were successfully used to stain tissues (135) and liver cancer cells from tissues (136).

2.3.3. Aptamers against cancer cells

To date a range of aptamers have been selected against a number of cancer cells including brain, gastric, kidney, ovarian, cervical and BC cells as shown in **Table 2.2**. Together with anti-tumor effect, some selected aptamers can increase sensitivity to therapy. U2 aptamer against EGFRvIII overexpressing glioblastoma cells improved sensitivity to radiotherapy of cells *in vitro* (137). One fluorescently labeled aptamer was shown to successfully stain frozen xenograft tissues; and able to distinguish various liver carcinoma subtypes (138). Some selected aptamers were even used in *in vivo* settings. Thus glioblastoma cells with high expression of EGFRvIII were imaged with the selected aptamer in mice (139). Radio-labeled aptamers were able to cross blood-brain barrier. Another aptamer was able to recognize its target in a complex mixture of normal bone marrow aspirates (140). Capillary column was immobilized with aptamers to capture liver CTC with 70% capturing efficiency (141).

Performing SELEX against cancer cells requires taking into consideration more factors than when selecting aptamers against proteins. The use of control cells during selection is important to select aptamers which can differentiate target cells from closely related cells (139). Cells used as controls in counter selection include normal cells or low- or non-metastatic cancer cells (135, 136, 142, 143), cells not expressing a protein of interest (133, 139, 144) or cells from another cancer type (145, 146). Dissociation constants of aptamer-cell complexes are usually determined using FACS where dependency of intensity of specific binding on concentration of aptamers is calculated

(143, 147, 148). In some cases, aptamers bound to cells are quantified by qPCR and dissociation constant is calculated by non-linear regression analysis (149). Increasing the stringency of selection can be done in a number of ways as shown in **Table 2.3**. They can be grouped into several groups: conditions related to cells (number of target and control cells) (133, 150), DNA (139, 143), washes (146, 150, 151), incubation of oligonucleotides with cells (139, 143, 150) and blocking agents (139, 146, 150). Usually library is incubated with cells either at 4°C or 37°C. Cooler temperature is used to reduce metabolism of the cells to avoid fluctuation in cell surface marker representation. However, this has a risk of selecting aptamers that would bind only at this temperature and not in physiological conditions; to avoid this 37°C can be used but the incubation time should be minimized (116). Moreover, aptamers enriched at physiological conditions can be lost by possible endocytosis (143). Interestingly though, some studies (135, 140, 143, 151, 152) showed that binding of the selected aptamers was not affected by the temperature of 37°C even when the selection was done at 4°C.

Aptamer (random region length, Kd)	**Target cell (cell line)**	**# of rounds**	**Negative control/counter selection used**	**Reference**
Brain cancer				
40 nt 3.37-16.78nM	Glioblastoma cells (U87MG) with EGFRvIII overexpression	11	U87MG– starting from the fourth round	(139)
45 nt 21-97 nM	Gliosarcoma cells (K308)	16	Normal human brain astroglia cell line (SVGp12) – starting from the third round	(135)
Lung cancer				
35 nt 97-157 nM	Small cell lung cancer (NCI-H69)	25	Non-small cell lung cancer (NCIH661)	(145)
Leukemia/lymphoma				
52 nt 0.8-229 nM	T cell acute lymphoblastic leukemia (CCRF-CEM)	20	B cell line from human Burkitt's lymphoma (Ramos)	(146)
45 nt 4.5-256 nM	Acute myeloid leukemia cells (HL60)	15	Acute myeloid leukemia cells (NB4)	(140)
49 nt	Burkitt's lymphoma B cells ($CD19^{+}$)	10	Leukemic T cell lymphoblasts	(116)
29 nt 12.21 nM	Lymphoblastoma overexpressing murine	6	Lymphoblastoma (BJAB) – from round 2	(133)

Aptamer (random region length, Kd)	Target cell (cell line)	# of rounds	Negative control/counter selection used	Reference
	c-kit receptor (BJAB-c-kit)			
49 nt 49.6nM	Burkitt lymphoma B cells	10 Using FACS	NS	(153)
Liver cancer				
45 nt 4.51-157	Mouse liver hepatoma (BNL 1ME A.7R.1)	20	Normal mouse liver cells (BNL CL2)	(136)
25 nt 64-349nM	Human hepatoma cell (HepG2)	19	Normal liver cells (THLE-2) from the third round	(151)
50 nt 19-450 nM	Human hepatoma (HepG2)	12	Human normal hepatocyte cells	(154)
1.47-16.44 NS	Liver carcinoma cells (SMMC-7721)	13	(HepG2)-from fourth round	(155)
40 nt 167.3-369.7nM	HCCLM9 (high metastatic properties)	10	MHCC97L (low metastatic properties)	(142)
Gastric cancer				
52 nt	Gastric cancer cells (AGS)	12	Human normal gastric epithelial cells (GES-1)	(156)
40 nt 5.22-73.90 nM	Gastric cancer cells (HGC-27)	19	Human normal gastric epithelial cells (GES-1)	(157)
Ovarian/Cervical cancer				
40 nt 0.25-132nM	Ovarian cancer cells (TOV-21G and CAOV-3)	22	Cervical cancer cells (HeLa)	(158)
20 nt 365.3-505.7nM	Ovarian cancer cells (CAOV-3)	15	Nonmalignant ovarian epithelial (HOSE 6-3)	(159)
52 nt	Human papillomavirus-transformed HeLa cervical carcinoma cells	18	Non-tumorigenic revertants of HeLa cells	(160)
Kidney cancer				
40 nt 26.6-107.7 nM	Renal cell carcinoma cells (786-)	12	Embryonic kidney cells (293T)	(150)
Colorectal				
40 nt 5.9-138.2nM	Metastatic colorectal cancer cells (LoVo)	14	Non-metastatic colorectal carcinoma cells (SW480)	(147)
45 nt 8.1 nM	Metastatic colorectal cancer cells (LoVo)	22	Non-metastatic cells (HCT-8)	(143)
Breast cancer				
40 nt NS	Breast cancer cell line (MCF-10TA1)	NS	Non-cancer cell line (MCF-10AT1)	(161)

Aptamer (random region length, Kd)	Target cell (cell line)	# of rounds	Negative control/counter selection used	Reference
45 nt 2.6-108 nM	Metastatic breast cancer cells (MDA-MB-231 cell line)	15	Normal breast epithelium cells (MCF-10A)	(162)
45 nt 19.36-30.49nM	Mammospheres from MCF7 cells	13	Normal epithelium cells (MCF-10A) and MCF-7 cells treated with Salinomycin	(163)
NS	Human HER2-overexpressing breast cancer cells (SK-BR3)	16	Human HER2 negative breast cancer cells (MDA-MB468)	(144)
40 nt 94.6nM	Human HER2-overexpressing breast cancer cells (SK-BR3)	20	Human HER2 negative breast cancer cells (MDA-MB231)	(149)
60 nt	Baby hamster kidney (BHK) cells expressing ABCG2 (transfected cell line)	15	BHK cells	(27)
60 nt	BCSC from MCF-7 and MDA-MB-231, by Aldefluorassay kit	15	MCF-7 cells	(27)
40 nt ND	13 samples of postoperative breast tumor tissues from different patients	11	Benign tumor tissue, adjacent healthy tissues, breast tissues from mastopathy patients, and also tissues of other types of malignant tumors	(58)

Table 2.2. Some examples of aptamers selected against cancer cells and conditions used to select them. NS – not specified

Condition type	How changed
Number of cells	Number of target cells decrease (133, 150)
	Number of control cells (150)
Oligonucleotides	Volume decrease (139, 143)
Washes after incubating target cells with oligonucleotides	Number increase (139, 146)
	Volume increase (146, 151)
	Time increase (146, 150, 151)
Incubation of oligonucleotides with cells	Time with target cells decrease (139, 143, 150)
	Time with control cells increase (135)
Blocking agents	Genomic DNA increase (146)
	FBS increase (146, 150)
	Salmon sperm DNA Increased (139)

Table 2.3. Conditions used to increase the stringency of selection during SELEX

2.3.4. Aptamers against breast cancer cells and their application

A number of aptamers were selected against BC cells and are presented in **Table 2.4**. The length of random region for the used libraries ranges from to 45 nt in a total of 10-16 rounds of SELEX. While some of these aptamers were selected against protein biomarkers relevant in BC such as CA 15-3 protein (115) or amplified in BC 1 (AIB1) oncogene (164) and were not tested on BC cells; the majority of studies used cancer cells as targets during selection and showed binding of the selected aptamers with BC cells.

#	Target in selection	Shown to bind cells/tissues	[Name] and sequence of the random region, 5'-3'; Dissociation constant if determined in nM in brackets	Reference
1	Breast tumor antigen CA 15-3 protein	No	GAAGTGAATATGACAGATCACAACT (45.47 ± 3.415) TACTGCATGCAGACCACATCAACTT (67.1 ± 3.289) CATACAATCAATCACCAGTGCGGTG (81.56 ± 4.198)	(115)
2	Amplified in breast cancer 1 (AIB1) oncogene	No	GGGATGCGAAGTTCCGCGGTCGAGT ATATGATACATCCAT (47.83 ± 4.99)	(164)
3	HER2 overexpressing cells	Human breast cancer cells overexpressing HER2 (SK-BR3)	NS	(165)
4	HER2 overexpressing cells	Human breast cancer cells overexpressing HER2 (SK-BR3)	[S6*] TGGATGGGGAGATCCGTTGAGTAAG CGGGCGTGTCTCTCTGCCGCCTTGCT ATGGGG** (94.6 nM)	(149)
5	HER2 extracellular domain	Human breast cancer cells overexpressing HER2 (SK-BR3)	[HB5] TGCACTTGTCATTTTGTATATGTATT TGGTTTTTGGCTCT (316 nM)	(166)
6	HER3 protein (oligomeric state of the extracellular domains)	MCF7 cells	[A6] AGAACAAUCGCAUAGGCCGCAAGG UUAGUUUCGUUGUCCGCCCGGUGC A [A18] ACGAGUAUAGCCCACAUGGCACGA CAGGGACGUUUCAUGUGCACAGUU G [A19] AGAUCAGGACAGAGCGCACAGGUG CCAUCCUGGUCUAACGCCCUCGAUG	(167)

#	Target in selection	Shown to bind cells/tissues	[Name] and sequence of the random region, 5'-3'; Dissociation constant if determined in nM in brackets	Reference
			[A23] GAGGGGCGAGGACGCCGAGUAUAG CCCCUAGAGGUGGAUGUUUCACGG U [A30] CAGCGAAAGUUGCGUAUGGGUCAC AUCGCAGGCACAUGUCAUCUGGGC G [A37] UUGAGAGGUCGUGCCAACUCUCAA GGUUGUCUUUCCUCUCCGCUCUGU G	
7	CD44 protein (GST-tagged recombinant)	CD44 expressing breast cancer cells (MDA-MB-231, MCF7, and T47D)	[Apt1] CAUCUGGAUUUGCGCGUGCCAGAA UAAAGA GUAUAACGUGUGAAU (81.3 ± 30.6 nM) [Apt2] GGAGUAUGCGCUUGGCCGUAAUAA UGUCGA GGCUGCCCAGGUUGU [Apt3] GGAGUACGACUUGGCUGUGUUCUU UCGGUGC UUCUGCGUAGGCCG	(26)
8	Exon v10 of CD44	CD44 expressed on HCC38 cells	[Apt#4 (full length)] GGGAGACAAGAATAAACGCAA CTC CCA GCC CCT CAC GTC AGC CCG C TTCGACAGGAGGCTCACAACAGGC [Apt#7 (full length)] GGGAGACAAGAATAAACGCAA CCG CGA ACC CCC CCC CTT AAT GTC A TTCGACAGGAGGCTCACAACAGGC	(168)
9	CD44 protein hyaluronic acid binding domain (recombinant)	CD44 expressing cells ovarian cancer cells - (SKOV3, IGROV, and A2780)	Thioaptamers [TA1] CCAAGGCCTGCAAGGGGAACCAAG GACACG [TA2] CCAAGGCATGCAAGGGAACCAAGG ACACAG [TA3] TGCAGATGCAAGGTAACCATATCCA AAGCA [TA4] CGTATGCAAGGTGAAAGCAGCACAC CAATA [TA5] GCGGCAGTAGTTGATCCCGAAGCGT TACGA [TA6] TTGGGACGGTGTTAAACGAAAGGGG ACGAC	(169)

#	Target in selection	Shown to bind cells/tissues	[Name] and sequence of the random region, 5'-3'; Dissociation constant if determined in nM in brackets	Reference
10	$ALDH^+$ breast cancer cells from breast cancer cell lines (MCF-7, MDA-MB-231 or breast specimens)	Mammospheres	[BCS/A35] ACGCTCGGATGCCACTACAGATCGC CCCTCACCTCATGGACGTGCTGGTG AC	(27)
11	ABCG2 expressing BHK cells	ABCG2 expressing BHK cells, mammospheres	[ABCG2/A12] ACGCTCGGATGCCACTACAGGCCCA CCCTCATGGACGTGCTGGTGAC	(27)
12	Existing aptamers against CD44	MCF7, mammospheres from MCF7	[Truncated from TA1] CCAAGGCCTGCAAGGGAACCAAGG [Truncated from TA6] GGACGGTGTTAAACGAAAGGGGAC GACC	(170)
13	Mammospheres from MCF7 cells	Mammospheres from MCF7 cells	[MS01] CTAAGCTAGTCTTTTCCGATATTTTG TTCGTGTTGTTTTTTTTTG [MS02] TATGGCTCACGCATCGCGTTTTCTTT CTAGTTTGTTCTTTGTTTT [MS03] GCATGGGGTTTCGGCGTTTCGTCTAT CTTGTTTCTGTTAGCGTCT (19.36 ± 6.28) [MS04] TTGCGCCCATTAATGTTGTAGTCTTT TGTCTCTCGGTTTTTTGGA [MS05] TTCTGATGCTTACCGGTCGTTTTCTT TTTCTTACTTACTTACTCTCTGT (30.49 ± 5.720)	(163)
14	Metastatic breast cancer cells (MDA-MB-231 cell line)	Cells: MDA-MB-231 Tissues: yes	TCAGTCGTCCCTTTATGCTTGGTGCT CACCGTCTGAATTTCTTCA (2.6 ± 1.2) TAATCCCTTGTGTTTGACGTTCGAAG ATTATTTCTATCTTTTAG (3 ± 1.7) CAATTGTGGTTCTTACCCTATCCCTT GTGTTTGGCGTTCGTTGC (15 ± 4) GCGTGAGTCTTTTGCGGTGGCTCGG GTTCGAATATCTACGACCTT (19 ± 5) AAGTAGTTTTCCTTCTAACCTAAGAA CCCGCGGCAGTTTAATGTA (44 ± 8) TAGTAAGAATCTGTTTCTGGTCCTAG TCTTGCTTGTGTTTCCT (108 ± 32)	(162)
15	MCF7 (human mammary gland adenocarcinoma)	H460 (large cell lung cancer)	[MCF7-2] GGGCACGGCATTGATTTGCTGCCTT ATTGGTGTTGGTGGGGGG [MCF7-10] CCAGGGGAGAAGCTTAGGGGGGAT GAGGAGAATTGGGGTTTTG	(92)

#	Target in selection	Shown to bind cells/tissues	[Name] and sequence of the random region, 5'-3'; Dissociation constant if determined in nM in brackets	Refer ence
			[MCF7-11] GGACGCTACATCTAGACCGCAGGGG CTGGGGTGGGGTTACCTG [MCF7-12] CGGGGGGAGCGGATGTCTGGGAAA ACCGCGGGGTGCCCTCCGA Others are not shown	

Table 2.4. Conditions and results of SELEX used to select aptamers for breast cancer diagnosis

NS - not specified
* - sequence for one aptamer is shown
**- DNA sequences are shown; but originally selected RNA aptamers

Aptamers (both RNA and DNA) were selected against HER2 protein using cells overexpressing this protein in three independent studies. HER2 is found in approximately 20-30% of BC and is associated with a more aggressive form of the disease with high recurrence rate and low overall survival rate (166). While Liu *et al* used extracellular domain peptide of HER2 (166), two other studies used a cell line well-known to have overexpression of HER2 (149, 165); all of these studies tested binding of resulting in aptamers with HER2 overexpressing cells (SK-BR3). The target of these aptamers being HER2 was confirmed either by incubating with HER2 extracellular domain peptide (166), showing lower affinity towards HER2-negative BC cells (MDA-MB-231; HER2 expression analyzed by Western blot (149) or mRNA expression (165); by comparing cells transfected and not transfected with HER2 gene (NIH-3T3 cells) (149) or by knocking down HER2 expression in the original cell line (149).

Some biomarkers targeted for aptamer selection for BC studies are CSC biomarkers. Biomarkers associated with stemness of cancer cells can be either in cytoplasm, nucleus or on the cell surface; the latter one is of interest because it is easy to target them and they can be used for "receptor mediated targeting" (170). CD44 is a protein associated with cell proliferation, migration, angiogenesis; it is also a receptor for major component of extracellular matrix – hyaluronan (26). Different forms of CD44 protein (whole protein (26), v10 exon (168), hyaluronic acid binding domain(169)) were used during selection with a later evidence of binding to CD44-expressing cells. Palaniyandi *et al* (27) selected two types of aptamers: aptamers binding to BCSC derived

from MCF7 cells and against ATP binding cassette (ABC) transporter group G number 2 (ABCG2) expressed in baby hamster kidney cells. Other studies did not use a particular biomarker in mind but rather used metastatic BC cells for potential use in for earlier diagnosis and treatment of metastatic BC (162). Mammospheres from BC cells to target cells which are key players in cancer recurrence and metastasis (163). These cells had a $CD44^{+}/CD24^{-/low}$ phenotype. Some aptamers were generated *in silico* by truncating existing aptamers (170). Binding efficiency of some aptamers was modulated when they were truncated.

Aptamers selected against BC cells due to their inherent advantages over antibodies have potential application in therapeutics and diagnosis of BC. Often these selected aptamers are somehow modified to reach the effectiveness. Thus study by Mahlknecht *et al* (171) used a multimerized version of the originally selected aptamer and it showed a superior antitumor effect by targeting cancer biomarkers (ErbB-2/HER2) compared to monoclonal antibodies against the same marker. This modified aptamer was effective in reducing the cell growth both *in vitro* and in a xenograft model. Employing two aptamers binding to BC cells, Wang *et al* (172) developed a colorimetric assay with a limit of detection (LOD) of 10 cells/ml. In another study, MCF-7 cells were quantified by two different assays (photoluminescence and square-wave voltammetric assay) using two aptamers binding separate markers on the cell surface. Cells were firstly isolated with magnetic beads covered with MUC1 aptamer and then detected with quantum-dot bound second nucleolin-binding aptamer (AS1411). This assay had a lower LOD compared to photoluminescence (85 versus 201 cells/ml) (173). Aptamer BC-15 originally selected against BC tissue but then shown to bind to a range of other cancer types was shown to be effective as a probe to isolate CTC from blood of patients with pancreatic cancer (174). This study is important in showing that the identification efficacy using aptamers was similar to that of anti-cytokeratin method, an established method of CTC identification but which has disadvantages of being lost during EMT. Only a fraction of aptamers were used in actual clinical samples. Thus Zamay *et al* a selected an aptamer using tissue specimens from surgery (tissue suspensions used in SELEX) (58). Other aptamers were selected taking into account the drawbacks of the existing antibodies, such as fast

developing resistance to Trastuzumab which is used in treatment of HER2 subtype BC (166).

2.4. Surface modification of stainless steel for biomedical applications

2.4.1. Stainless steel as a biomaterial

Due to their excellent mechanical properties such as high strength-toughness, fatigue resistance and inertness, metals have been used in various biomedical applications for a century (175, 176). Among these metals, three most extensively used ones in biomedical engineering are SS, titanium (Ti), and cobalt-chromium-molybdenum (CoCrMo); this is mostly because of their biocompatibility and mechanical properties (176, 177). SS is an iron-based alloy with at least 12% chromium which allows it to resist rust formation in unpolluted atmosphere (178). Most implants used in cardiovascular, orthopedics, dentistry, craniofacial surgery, and otorhinology applications are made of SS (176). Some permanent (artificial joints) implants and many temporary implants (plates, medullary nails, screws, pins, sutures and steel threads and networks used in fixing fractures) are made of SS (179). Compared to Ti and CoCrMo, SS has a lower cost (180) and its demand is also still high in developing countries (181, 182). Particularly in case of orthopedic implants, SS is a most cost-effective choice because of its lower cost, availability, ease of manufacturing, and reasonable corrosion resistance (183).

When introduced in human body or other biological environment, metals are affected by protein adsorption, biofilm formation, and corrosion. Moreover, in spite of its wide application as a biomaterial and its general good biocompatibility (180), SS does not have inherent biofunctional properties: blood compatibility, osteoconductivity, and bioactivity (176). Unmodified SS surface has hydrophobic properties (e.g. has high contact angle of 86.32±4.5˚ (184)) and hydrophobic surfaces tend to attract the adsorption of proteins. Earlier studies have shown the susceptibility of SS for biofilm formation and protein adsorption (185). It is believed that adsorption of organic molecules such as proteins on the surface leads to biofilm formation, which in turn can lead to corrosion or itself be a source of bacterial contamination (186). Therefore, many surface modification techniques target these surface properties to improve their application in biomedicine.

2.4.2. Surface modification of SS for improved corrosion resistance

Corrosion resistance is an important characteristic of metallic biomaterials. More than 90% of all retrieved SS implants (which failed) occurred due to corrosion attack, by pitting or crevice corrosion (187). Different physical and chemical techniques have been used to increase the corrosion resistance of SS. Chemical composition and the presence of surface oxide layers on SS play an important role in their corrosion resistance. 316L SS is not susceptible to intergranular corrosion due to its low carbon content. It is protected against corrosion by a spontaneously formed oxide layer; this layer enhances properties of metals including increased corrosion resistance and inertness in biological fluids, passivation, improved wear, and adhesion characteristics (188, 189). Different acid treatment methods (Piranha (184, 185, 190-192), sulfochromic acid (193, 194) and nitric acid (195)) have been widely used to obtain SS surface rich in hydroxyl groups. Physical methods of improving corrosion resistance include plasma immersion ion implantation and deposition of TiO film (196), closed field unbalanced magnetron sputtering of Ti-Cu coating (197), radio frequency magnetron sputtering on nanostructured Zr_2CN (198), direct current and radio frequency glow discharge of trimethylsilane (199); while chemical techniques comprise of electropolishing and acid dipping (181), electrodeposition of polyaniline-graphene oxide (200), plasma assisted vapor deposition of TiN coating (201), sol-gel spin coating of polypyrrole-strontium hydroxyapatite (202).

2.4.3. Adding functional groups to SS

Native oxide layers on the SS surface were used for introduction of new functionalities (including biomolecules) in several studies. However, coupling biomolecules on a metal stent is not straightforward due to the need of incorporating linker molecules (203). Typically, ad-layer of functional groups, such as amines, carboxyls, or quinones is required on metal surface (204). Different functional groups on SS have been introduced either by silanization or coating with dopamine or via self-assembled monolayers (SAMs). In addition, biological activity such as release of drugs, capturing specific analytes (e.g. cells), could be required. For this, SS has to have an active compound (for example, drug or antibody). To introduce the above mentioned desired properties without sacrificing important bulk characteristics (205), SS surface is modified through various

coatings and biofunctionalization methods. Among these materials is dopamine which was initially discovered in marine mussles and possesses catechol and amine groups. Polydopamine films were formed on different surfaces including metals and semiconductors (206). On SS, dopamine was copolymerized with hexamethylendiamine to obtain a surface rich in amine groups by simple dipping. Heparin was tethered by its carboxyl groups on the surface (207). In another study, surface with increased hydrophilicity and corrosion resistance was obtained when polydopamine-coated SS was used to graft 2-hydroxyethylmethacrylate (by irradiation with ^{60}Co-γ-rays). (208). All in all, functionalization with dopamine is an easy way of producing SS with amine/quinone groups for further attachment of molecules. Nevertheless, because dopamine produces only amine/catechol on the surface only limited chemical linkers/molecules (e.g. carboxyl groups) can be grafted on these surfaces (**Figure 2.3**).

ADVANTAGES		DISADVANTAGES
• easily used	**Dopamine**	• limited functional groups (amine/catechol only)
• hydrophilic • antifouling • non-toxic • non-immunogenic • homo- and bifunctional available (or can be synthesized)	**PEG**	• non-reactive with SS • need additional groups to make reactive with SS
• ease of modification • range of terminal groups	**SAM (aliphatic acids, alkylthiols)**	• less stable • additional techniques for an efficient attachment (electrodeposition, glow plasma discharge)
• SS-reactive • many functional groups available • can generate surface containing more than one SCA type • bifunctional SCAs are available	**SCA**	• additional techniques for an efficient silanization • different SCAs might have different surface reactivity

Figure 2.3. Linkers commonly used for surface modification of SS and their advantages and disadvantages.

Silane-coupling agents (SCA) are silicon-based linkers which are often used to link organic and inorganic materials; they have a general formula of $R'(CH_2)_nSi(OR)_3$, where R′ being an organofunctional group and R is a hydrolysable alkoxy group (209). Once mixed with water/ethanol, this alkoxy groups are converted to silanol groups (SiOH). Silanol groups then form hydrogen bonds with surface hydroxyl groups and the

excess of silanol groups form siloxane network (Si-O-Si). It was shown to be chemically stable and exhibits resistance to corrosion (210).

Depending on SCA type, SS with different functional groups can be obtained and these are showed in **Figure 2.4**. Usually SCA binds to SS with their methoxy or ethoxy groups and their functional groups can be different depending on intended use. After modification, SS can be turned into non-reactive for antifouling purposes (mPEG-IPTS (184, 211) and hexamethyldisilane (191)), or various groups: amine, carboxyl, epoxide and thiol can be tethered on the surface. After Silanization the surfaces were used for attaching different molecules. This includes grafting poly(ethylene glycol)methacrylate for reducing protein adsorption (212); ionic liquids (213) and N-halamine (214) for improving antibacterial properties of the surface, or antibodies to capture cells (205); various polymers for reducing protein adsorption (215). Different SCA types can vary by their hydrolysis rate: it was shown that compared to ethoxy groups, methoxy groups had higher hydrolysis rate and can react directly with a metal during an incomplete hydrolysis (216).

SS surface have been pretreated using various strategies in order to make it more suitable for silanization; most of the times by increasing the density of surface oxides. One of such methods includes heating at high temperatures prior silanization. Thus Ni-free SS was oxidized in air at 800 K (217) and 316L SS heated at 500°C (218) before being successfully silanized with APTES. Another strategy is deposition of metal oxides on the surface. Aluminum oxide layer was deposited before silanization and grafting phospholipids (219) and tantalum oxide deposited for collagen immobilization (195). Both of these oxide layers improved Silanization of the surfaces. Electrochemical passivation was also a choice of pre-treatment before silanization with SCA or silanized polymer (215, 216, 220). The composition of the surface also had an impact on SCA attachment: Fe oxides were better for attachment of APTES than Cr oxides (217).

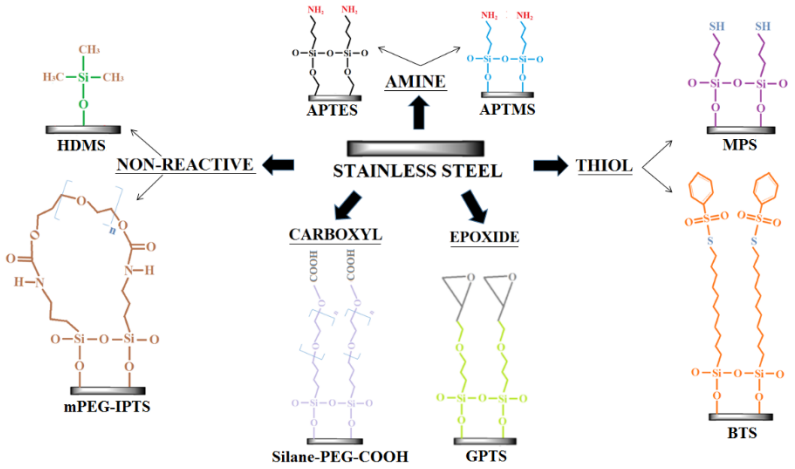

Figure 2.4. Silanization of SS using different SCA to generate various functional groups. APTES – (3-aminopropyl)triethoxysilane (217); APTMS – (3-aminopropyl) trimethoxysilane (216, 221); BTS – S-(11-trichlorosilylundecanyl)-benzene-thiosulfonate (205); GPTS – glycidoxypropyltrimethoxysilane (214, 215); HDMS – hexadimethylsilane (191); mPEG-IPTS (methyl-polyethylene glycol - 3 - isocyanato-propyltriethoxysilane (184, 211); MPS – (3-mercapto-propyl)trimethoxysilane (212, 213, 221); Silane-PEG-COOH (220). Published as part of (29) (Elsevier Permission: Personal use of work by Authors).

It is also possible to use more than one SCA on one surface thus opening the way to multifunctional surfaces. Vuori *et al.* (221) studied synergetic effect of two SCA: APTMS (3-aminopropyl)trimethoxysilane) (used for passivation) and (3-mercaptopropyl) trimethoxysilane (MPS) (for thiol groups). These molecules were co-adsorbed on the surface after hydroxylation by electrochemical treatment. The study found that MPS was dispersed in APTMS and with the increasing concentrations of MPS its uptake on the surface did not increase linearly. The difference in their surface properties could be due to difference in their intrinsic (hydrolysis and condensation rates). Therefore, it is important to consider the properties of different SCA used together for modification of one surface.

Molecules lacking silane group can be synthesized to have one: methoxy-PEG (MW 2000) synthesized using IPTS (3-isocyanatopropyltriethoxysilane) was grafted on the acid treated surface (184) resulting in lowered fibrinogen adsorption and platelet activation and adhesion as well as enhanced adherence and proliferation of HUVECs. A simpler approach would be using commercially available bifunctional PEG with silane

one side and readily available functional group on another side as demonstrated by Hynninen *et al.* (220).

PEG is widely used for surface modification of different materials including SS. PEG is applied for its antifouling properties such as lowering protein adsorption and also for attaching other molecules on the surface. PEG is hydrophilic, non-toxic, non-immunogenic and flexible (222). Direct coupling of PEG on SS not easy due to the relatively low concentration of surface oxides on SS (223), therefore, SS has first been silanized and then grafted with PEG (212), (215). Another way is attaching silane group on PEG as discussed above. Also PEG was attached on aminated surface prepared by physical adsorption of polyethylene imine (PEI) with further bifunctional PEG (aldehyde group and methoxy-group) this surface (223).

Another set of molecules used for surface modification of SS are SAMs made of different acids which served as linkers to attach molecules of interest. For instance, dodecylphosphonic and phosphoundecanoic acid which are phosphonic acids were attached on SS forming methyl- and carboxyl-terminated SAMs as a result (224). In another study surface was enriched with hydroxyl- and carboxyl groups consisting of nanofunctional alkanethiol SAMs of 11-mercaptoundecanoic acid and 11-mercapto-1-undecanol.

2.4.4. Assisted deposition of molecules/ions on SS

Electrochemical methods and plasma deposition have been studied to deposit different molecules on SS. These methods allow functionalization the surface with molecules otherwise difficult to obtain or result in more reproducible results.

SAMs can be attached on SS using plasma or electrochemical methods. One of the first examples of potential assisted SAM formation on SS was performed by Shustak *et al.* (225). Six polymers were deposited on SS by glow discharge plasma polymerization to add functionalities to SS. This study is important as a platform for developing coronary stents with covalently coupled bioactive agents (191). Alkanethiol SAMs with carboxyl and hydroxyl groups were prepared on SS surface using glow plasma discharge method (226).

Electrodeposition of molecules on SS for added functionality is also a well-known method. Okner *et al.* (222) synthesized PEG-diIPTS, a silanized PEG, and performed a one-step sol-gel electrodeposition. When negative potential is applied, the pH of the electrode surface changes and catalyzes the condensation of precursor (which must first be hydrolyzed). The study found that thickness of the film depended on the time of exposure and potential applied. Electrodeposited surface was shown to be hydrophilic, mostly smooth and uniform. Another study showed electrodeposition of mercaptoundecanoic acid for producing SS coupons with carboxyl group; after activation with n-hydroxysuccinimide and 1-ethyl-3-(3-dimethylaminopropyl] carbodiimide, fibronectin was covalently linked (227).

Mild deposition of biomolecules otherwise difficult to achieve was possible by using plasma methods. It was used not only to increase surface oxides and also modifying SS with new functional groups (228). Plasma enhanced chemical vapor deposition (229) rendered SS with carboxylic groups; and was used for direct biofunctionalization when extracellular matrix protein (tropoelastin) was covalently linked on acetylene-polymerized SS (230).

Figure 2.5 gives a summary of different methods to functionalize SS surface depending on the molecule of interest. To attach molecules with carboxyl groups (e.g. heparin for blood compatibility or enzymes for reducing biofilm formation), one might consider coating SS with PEI or dopamine by physiosorption as a simple method which usually do not require specialized equipment. To obtain more stable coatings (but might require specialized equipment for improved results) silanization or coating with allylamine can be chosen. Molecules with free hydroxyl groups can be tethered on surface to readily-made SAMs composed of aliphatic acids (but stability can be an issue); another approach for these molecules is synthesizing their silanized form first; but synthesis can be time-consuming despite reduceing overall steps in functionalization) (222). In order to attach molecules with amine groups, SS can be enriched with ester groups via trisuccinimidyl citrate (231), or carboxyl groups.

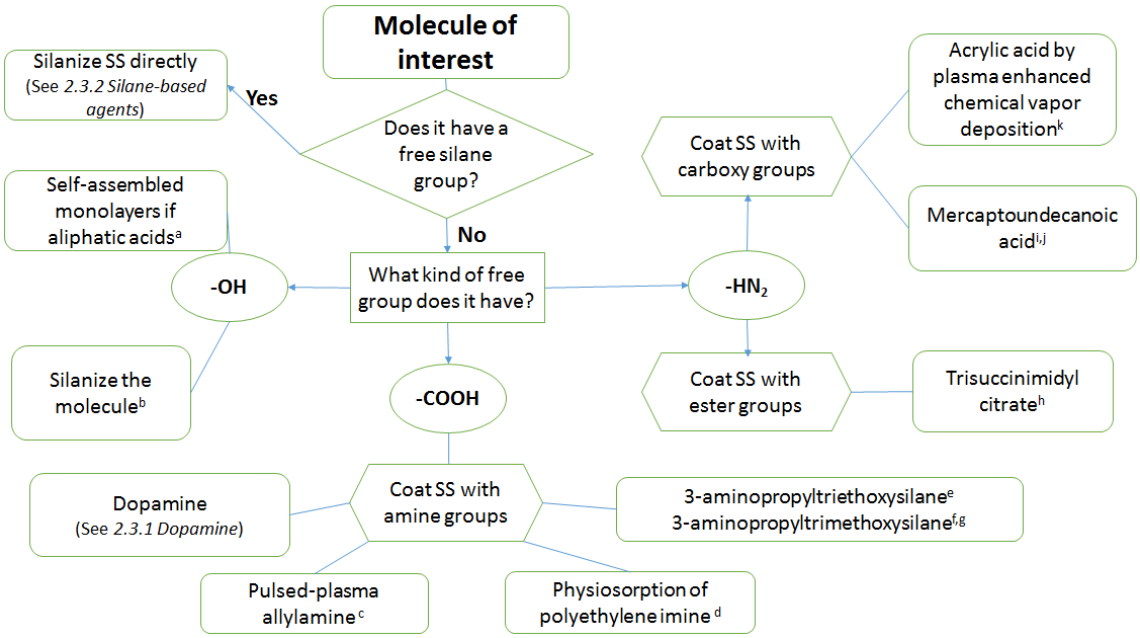

Figure 2.5. A summary of different methods to functionalize SS surface depending on the molecule of interest. a) (224)*;* b) (222)*;* c) (228)*;* d) (232)*;* e) (217) f) (216)*;* g) (221)*;* h) (231)*;* i) (227)*;* j) (226)*;* k) (229). Published as part of (29) (Elsevier Permission: Personal use of work by Authors).

2.4.5. Applications of modified SS in biomedicine

Many dental prostheses, orthopedic fixation plates, vascular stents and guidewires used in biomedicine are made of SS. Studies on biofunctionalization of SS for combating infection and tackling restenosis, improving osseointegration and blood compatibility are ongoing.

Implants developing biofilms remain a serious problem which can be reduced by surface modification. Two surface modification approaches are most common in antibacterial surface production: passive and active surface modification. While passive surface modification includes modifying the surface properties (especially hydrophobicity) with molecules lacking antimicrobial properties *per se*, but which have an effect on bacterial adhesion reducing it. In active modification biological molecules with a specific interaction (233) with biofilm are used. These include such agents as antibiotics (vancomycin and gentamicin (233)), peptides (such as magainin I and nisin (194)), enzymes (such as trypsin, lysozyme (232), (185)), and ions and ionic liquids (such

as Cu and Ti (197), Si, N^+, O^+ and SiF_3 (234, 235)). In these studies plasma-based methods were used for antibacterial ion species. Antibacterial enzymes and peptides were grafted on the surface.

In orthopedics SS, is mostly used as temporary implants or cemented implants due to poor wear and corrosion resistance of SS relative to Ti and CoCrMo alloys (236). To improve its osseointegration properties different methods have been tried. Coating SS with ceramic coating (hydroxyapatite) and modification to change surface topography are the main ones. Coating SS with hydroxyapatite showed to improve corrosion resistance and their ability to interact with surrounding tissues including bone. Hydroxyapatite was used both unmodified and in combination with other moieties. Nanoparticles made of hydroxyapatite incorporated with Zn and coated with chitosan (237), a bilayer consisting of polypyrrole (as a protective and adherent interface) with salicylate (nonsteroidal anti-inflammatory drug) and strontium hydroxyapatite (to render porosity) electrodeposited on SS (238), Mg and Sr substituted porous hydroxyapatite/poly(3,4-ethylenedioxythiophene) (239) are some of the examples of hydroxyapatite use. Other strategies include passively adsorbed fibronectin on SS screws for improved osseointegration (240). Hybrid organic–inorganic coating (consisting of silicon alkoxide, silicon alkyl alkoxide and colloidal silica) was studied by Omar *et al* (182) where they functionalized SS with 45S5 Bioglass® and the same bioglass with Sr as a partial substitute to Ca. The coating formed a protective layer against media attack and the release of corrosion products.

For blood-contacting devices blood compatibility is of utmost importance (241) and SS surface has also been modified to improve its blood compatibility. For this, heparin, an anticoagulation molecule with an anti-inflammatory effect ,(175)) has been studied the most. Heparin has been coated on SS by simple electrostatic assembly of multiple layers with PEI (242); a more stable coating of heparin was achieved when it was copolymerized with hexamethylendiamine (207); or as a hydrogel (chemically synthesized dopamine/tyramine linked to 4-arm poly(propylene glycol)-co-poly(ethylene glycol)) (243). Alternative methods of improving blood compatibility of SS together with more conventional methods are being studied including one of the components in traditional Chinese medicine (also found in citruses) (244), attaching alginic acid after

silanization (218) or immobilizing hyaluronan via combination of plasma reactor and electrospray (245).

Surface of SS has been functionalized for tackling restenosis. Restenosis occurs when endovascular stents (designed to enlarge vessels and prevent stenosis) cause blood clotting and thrombosis and growth of endothelial cells on stent surfaces leading to the recurrence of stenosis (246). Having SS stents which favour the growth of endothelial progenitor cells (EPC) and disfavor platelet adhesion could be a solution to the problem. For this, SS has been modified with various cell capturing agents such as vascular endothelial-cadherin (CD144), CD34 antibodies (247), EPC aptamers (248), peptide nanofibers (249). Another strategy is designing drug-eluting stents, and different strategies has been employed to functionalize stents made of SS used as drug-eluting stents. These include release of the drug from stent depending on the number of chitosan/heparin layers forms on the surface (250), using magnetic nanoparticles which can be turned on and off (251), or by changing the physiochemical properties of liposomes to which drug was attached (229). Commercially available SS stents functionalized for re-endothelialization and drug-elution include Genous™, Taxus®, JACTAX®, Excel™, BuMA™ stents.

2.4.6. Applications of modified SS in capturing cancer cells for potential use *in vivo*

A number of assays have been developed for capturing CTC since they are promising cancer biomarkers including various chips (micropost, microfilter, microcrescent, microvortex, microspiral, microsieve and etc) (252). Some of the assays are intended to be used *in vivo*. One of the early reports on using metal wires for capturing CTC from blood is a work by Saucedo-Zeni *et al.* (253) discussed earlier. After being captured, cells were treated with fluorescently labeled anti-EpCAM antibodies and CD45 antibodies (for ruling out leukocytes) and also exposed to various post-capture treatments such as immunostaining and observing under fluorescent microscope (254), determining mutations in certain genes using NGS (255), or chip-based digital PCR (256), DNA fluorescent-in-situ-hybridization (257). In some studies using Gilupi guidewire, a decrease in CTC count was observed after treatment (surgery) and more CTC were found in later stages of disease (254). Thus, Gilupi device could be useful for monitoring

treatment responses. Post-capture procedures could be beneficial in determining therapy targets and studying mechanism of resistance. It is argued that, although simply drawing blood is easier than placing guidewire for half an hour, cancer patients usually go through unpleasant and time consuming procedures (MRI, CT, biopsies) which may result in infection or bleeding (256). Applying guidewire in clinical settings might improve early diagnosis, prognosis and therapy of cancer patients (at least in the studied cancer types). Furthermore, capturing CTC using this device and further molecular characterization of the cells could make us closer to personalized medicine (258, 259).

Type of Gilupi device	**Patients (number, cancer type)**	**Analysis after capturing**	**Results**	**Ref.**
NS	30 with BC	ICH staining with EpCAM or CD45 antibodies	• Good biocompatibility • No side effects • Higher cell capture than CellSearch™	(260)*
NS	42 with stage I-IV BC	ICH staining with EpCAM and CD45 antibodies	• Global sensitivity 89.7 % vs. 19% with CellSearch™ • sensitivity for early and non-early stage BC was 91,7 % and 82,3 %, respectively • CTC detection rate >4 times higher than CellSearch™	(258)*
CellCollector®	380 with NSCLC, BC, PC and CRC	ICH staining with EpCAM and/or CD45 antibodies	• No side effects • Similar sensitivity for early and late stage cancer patients • Cell detection rate 79.2% vs. 16.7% CellSearch™ • Specificity 84% (79.5% for CellSearch™)	(259)*
CellCollector®	18 lung cancer patients (with different stages)	NS	• Difference between CTC occurrence before and after surgery • Correlation between CTC enumeration and clinical lack of recurrence.	(261)*

Type of Gilupi device	Patients (number, cancer type)	Analysis after capturing	Results	Ref.
Detektor CANCER01 (DC01)	48 NSCLC patients (stages I-IIIB) and 12 non-cancer patients	ICH staining with EpCAM and/or CD45 antibodies	• Sensitivity 94% (similar for early and late stage NSCLC patients) vs. 5.8% (CellSearch™) • 100% specificity for DC01	(262)*
NS	48 NSCLC patients (stages IA to IIIB) and 12 non-cancer patients	ICH staining with EpCAM and CD45 antibodies	• No side effects • Sensitivity 94% (similar for early and late stage NSCLC patients) • No CTC in non-cancer patients	(263)*
CellCollector®	25 NSCLC patients (stages IA to IIIB)	Mutations in KRAS and EGFR genes	• Pre-surgical isolation rate was 79%, post-operative rate was 72% • EGFR and KRAS mutations could be detected in all patients • Cell detection rate 72%	(255)*
NS	16 metastasized -PC (PCa-m), 24 local PC, 19 men with benign prostate hypertrophy and 21 women	ICH staining with EpCAM and CD45 antibodies	• No side effects • sensitivity of 82% in PCa-m; 68% in PCa-l patients • 80 % specificity	(264)
CellCollector®	43 PC patients (different stages) and 11 control	ICH staining with EpCAM and CD45 antibodies; EGFR and PSMA genes	• CTC counts of 4.6; 16.8 and 26.8 for localized, locally advanced and metastatic PC, respectively • 5 CTCs had a mortality risk • EGFR and PSMA 42.8% and 14.3% respectively	(265)

Type of Gilupi device	Patients (number, cancer type)	Analysis after capturing	Results	Ref.
CellCollector®	50 lung cancer patients different stages (mostly NSCLC)	ICH staining with EpCAM and CD45 antibodies; mutations in the KRAS and EGFR genes	• CTC isolation 58% vs 27% for CellSearch™ • Treatment response during therapy associated with significant decrease in CTC number • mutations relevant for treatment decisions could be detected in CTCs captured	(256)
CellCollector®	127 metastatic BC; 63 benign breast tumor	HER2 testing and gene sequencing	• Sensitivity 74.8% • Specificity 100%	(266)
CellCollector®	22 SCCHN patients	EGFR expression	• Much higher detection rate for advanced stage than that in early stages • Detection rate before treatment 72.7% and 46.7% after surgery	(254)
CellCollector®	108 high-risk PC patients and 36 healthy volunteers	14 genes (EMT, epithelial and stem cell-like)	• High heterogeneity in gene expression in the captured CTCs for each patient	(267)
CellCollector®	NSCLC	ICH staining with EpCAM antibodies; chromosomal translocation of the ALK gene (DNA FISH)	• Method combining immunofluorescence staining and DNA FISH	(257)
CellCollector®	73 PC pateints (tumor stage ≥2c)	ICH staining with EpCAM and CD45 antibodies; Real-time quantitative PCR	• EMT genes (at least one) in 43.8%; increased after therapy • Epithelial markers (at least one) in 29.5%; decrease after therapy • Stem cell like markers (at least one) in 14.3%; present only before treatment	(267)

Type of Gilupi device	Patients (number, cancer type)	Analysis after capturing	Results	Ref.
			• The combination of with downstream RNA analysis is highly promising	

Table 2.5. Application of different Gilupi functionalized and nanostructured guidewires covered with EpCAM antibodies in detecting CTC from different cancer patients. Time of exposure in blood was 30 min for all.

* - conference paper
CRC – colorectal cancer
ICH - Immunocytochemical
NS – not shown
NSCLC – non-small cell lung cancer
PC – prostate cancer
SCCHN - squamous cell carcinoma of head and neck

An improved surface of guidewire for CTC capturing was engineered using layer-by-layer method (268). The resulted surface consisted of several layers each serving its purpose: protective layer (dividing metal from solution), protein resistant layer (for reduction of non-specific binding) and EpCAM antibody layer (for capturing CTC). According to *in vitro* experiments, compared to leukocytes, the enrichment factor of 3000 was achieved for CTC. Isolated cells showed high purity (>90%) and could be further used for genetic analysis. In another interesting work, in addition to the wire functionalized with antibodies, magnetic nanoparticles were used (23). In a porcine model, it was possible to label and capture CTC in just ten seconds. The demonstrated capture efficiency of this device was much higher (10-80 times) than if the 5 ml blood sample would have been used; while enrichment was 500-5000 times higher than CellCollector®.

All of the above works on CTC capture do not actually quantify the cells but are more of capturing devices which can be used for further analysis (gene sequencing, fluorescent staining); very few studies focused on developing system able to quantify CTC from the blood. One of this kind of work was done by Weng *et al.* (269) who fabricated a needle-like biosensor, a so called "cytosensor". After being silanized and covered with EpCAM antibodies, the ability of the functionalized needle to capture CTC

was studied in an *in vitro* setting mimicking human circulation system. A wide detection range (10^2 to $^{106)}$ was achieved for this biosensor. By using an electrochemical method of CV, detectable signal was demonstrated for a concentration of cells of 21 cells/ml.

In conclusion, SS remains an important biomaterial despite the emergence of new metal alloys. Surface modified SS, such as stents, are commercially available and used for anti-restenosis. Plenty of ongoing research aims to overcome inherent flaws of SS (as a foreign material) and meet its new application needs through surface modification techniques. Promising and emerging applications of SS could be in using it as a substrate in sorption of target analytes as a new substrate for a jacket-free stir bar (270) and diagnostic substrate in faradic impedimetric immunosensor (271) or as a guidewire to improve detection of rare cancer cells (253).

2.5. Optical fiber biosensors and their functionalization

2.5.1. Optical fibers

The working principle of optical fiber biosensors is based on transmission of the light through an optical fiber (usually made of either silica glass or plastic) to the analysis site (272). Optical fiber (shown in **Figure 2.6**) consists of a narrow cylinder called a core which is doped with elements such as Ge to increase its refractive index (RI) (having guided field; 2-10 μm in diameter), a cladding that surrounds the core (having exponentially decaying evanescent field; 125 μm in diameter) and a buffer coating (protective coating). Since the core has a RI n_1 which is higher than the RI of the core (n_2), the light that entered the core stays inside the material because of total internal reflection and is therefore transmitted forward (273, 274).

Using optical fiber as a transducer offers such advantages as having low LOD, low cost, chemical inertness, wide range of surface modification techniques that can be applied and the potential to be used for remote sensing (273, 275). Moreover, they have a possibility of being miniaturized, used in *in vivo* applications and being multiplexed to detect several analytes simultaneously and are immune to electric or magnetic interference (272, 276).

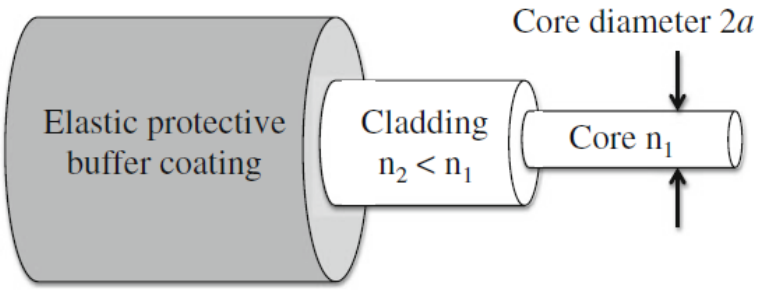

Figure 2.6. A schematic diagram of an optical fiber showing the position of the core (diameter 2a), cladding and jacket. Source: (277) (Springer Nature license).

2.5.2. Fiber Bragg grating (FBG) biosensors

One way of using optical fiber as an intrinsic sensor is to inscribe a grating onto fiber as a simple intrinsic sensing element which is sensitive to RI (275) These types of sensors have been recently considered as a useful tool in medical and environmental diagnostics (278). Fiber Bragg grating (FBG) is an intrinsic fiber element inside a short segment of an optical fiver that has a certain range of reflected and transmitted wavelengths of light. This is achieved by periodic modulation of the RI inside the core by illuminating it with ultrviolet light to build grating structure. As light enters the core of the fiber and travels through FBG structure, the wavelength is selectively reflected by Bragg gratings (279).

Due to the small size of silica fibers, high sensitivity, biocompatibility and non-toxicity, FBG act as promising devices for biomedical application. They also have fast response and high spatial resolution and are highly inert to electromagnetic interference that confers them with distinguishing advantages. More importantly, they bring no harm for the patient in terms of the fact that there is no immune reaction from the host immune system. They also can be used *in vivo* for repeated or continuous measurements. Independence from electromagnetic field makes FBG a perfect candidate for clinical use (279). Optical grating sensors have such advantages as high sensitivity, possibility for multiplexing, small size, light weight, multi-modal sensing capability and low fabrication cost (278, 280, 281).

Sensitivity to surrounding chemical and biological molecules is one of the key characteristics of optical biosensor fabrication. There have been several studies on investigation of the changes of surrounding-medium RI and its effect on FBG response

(282-285). RI is an estimation of the speed of light that travels through the material. The measurement is performed by surrounding the waveguide of the sensor by the samples of different refractive indices. When the measurand initiates its action, the Bragg wavelength starts to shift depending on the changes of refractive indices of bioanalytes.

Several types of optical FBG biosensors are known relying on different principles of operation: long-period gratings (LPG), etched FBG (EFBG), tilted FBG (TFBG), microstructured FBGs (mFBG), photonic crystal fibers (PCF) (sometimes regarded as a subtype of mFBG), LPG in PCF, LPG and TFBG in SPR (286, 287). Sketches and coupling mechanisms of these FBGs is shown in **Figure 2.7**.

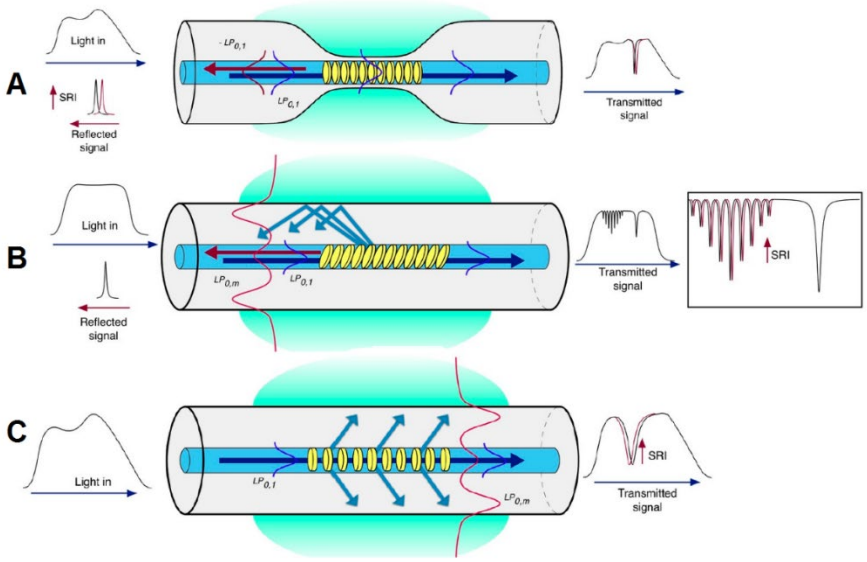

Figure 2.7 Sketches and coupling mechanisms of an etched fiber Bragg grating (A); tilted fiber Bragg grating (B) and long period grating (C). SRI – surrounding refractive index. Source: (288) (MDPI Open Access License).

2.5.3. EFBG biosensors

FBG sensors are one type of optical sensors which are called evanescent wave sensors. One of the ways of using optical fiber as an evanescent wave sensor, is to remove its cladding to allow the evanescent field of the propagating mode to interact with the surrounding medium or analyte (281). In case of standard optical fibers, effective refractive index of the fundamental mode is almost independent of the surrounding RI (289). When the cladding is removed, the RI of the cladding will be replaced by the RI of the surrounding media (290). In FBG sensors, change of RI in surrounding media is

transduced into change of reflected wavelength which can be easily measured (278). For FBG with etched cladding higher order modes are larger than fundamental modes (275). The interaction between an analyte of interest and ligand (which is immobilized on EFBG) changes the RI on the surface and thus Bragg wavelength is shifted and grating reflectivity is changed. This way, concentration of the analyte can be measured by analyzing FBG spectral changes (in transmission or reflection) (291).

Cladding of the fiber can be reduced in a number of ways including mechanical polishing (producing D-shaped fibers) and chemical etching (281). Static etching is the most common method among chemical etching (292). Disadvantages of chemical etching include its dependence on etching solution and the environment and most importantly the difficulty in determining etching time (292). Hydrofluoric acid (HF) is widely used for etching optical fibers. Ko *et al* used less toxic HF-free solution based on NH_4F and $(NH_4)_2SO_4$ (293). Another etchant used to collapse the cladding is buffer oxide etch with or without surfactant which consist of 0.5-10% HF, 40-70% water, 30-50% ammonium fluoride, 0.5-10% surfactant (294).

Controlling etching only by time is insufficient because temperature and etching solution composition influence it (290). Therefore, a number of studies used spectrometer to monitor chemical etching. Tao *et al* used Ocean Optics HR4000 spectrometer to collect light intensity during etching which was then plotted as a function of etching time (292). Light intensity stays stable when only cladding is etched but then starts to drop when the core is affected. Another study plotted Bragg wavelength as a function of time (281) and used an optical spectral analyzer (ANDO, AQ6317B with a resolution 10pm). To simplify the etching process, a low cost monitoring system consisting of LED and PIN silicon photodiode was used to online monitoring the etching process which is not affected by the temperature and etchant density (HF) (290).

Fiber is etched in a conical manner when acid-etched. This conical shape etching of the fiber could possibly be explained by the gradient in the concentration of the solution. In one study, the gradient of HF formed was thought to be causing the conical shaped fiber tip: fiber region etched slower had a filament-like shape while the region in a stronger solution had a trapezoid shape (292). The slight increase in light intensity

during etching was observed when filament was fully etched and a trapezoid shape is achieved (292).

For multimode fibers, etching of a tip in the bulk etchant was modeled (295) and etch rates of cladding and the core and core diameter were crucial in determining the shape of the tip. They also concluded that the shape of the fiber in meniscus region (immiscible organic solvent) during etching is not dependent on the temperature and composition of the etching solution. Dip in the middle of the peak was observed was associated with the introduction of a phase-shift to the grating due to uneven etching (281). Protective tubing and an optical fiber mount were used in one study to address an issue of uniformity of FBG etching because surface irregularities can change the final spectral characteristics of an EFBG. The mounting of fibers was shown to be affecting the spectra obtained during etching (281). Oleic acid was used in manufacturing tapered OF to protect the fiber and the environment during HF etching (292).

FBG sensors with different functionalities were successfully used to detect different molecules including BSA (296), peanut agglutinin (294), NaCl (297) and DNA (278). Protein attached to an EFBG with DNA as a sensing element puts strain on fiber and changes RI of the surface and thus red shift (0.141 nm) occurs (296). Moreover, when the concentration of protein is increased (from 50 μg/ml to 300 μg/ml) decrease of the reflected power is observed.

2.5.4. Functionalization of optical fiber surface

In order to develop a biosensor based on optical fiber, it is necessary to attach a bioreceptor on the glass surface which will bind the analyte of interest. Number of immobilization methods of receptors on fiber optic biosensors were utilized: adsorption, electrostatic self-assembly, cross-linking by multifunctional reagent, covalent attachment and biotin-avidin linkage (298). In case of cladding-etched FBG sensors, the glass is the most commonly silanized before attaching a molecule. One of the silanization molecules widely used is APTES. Chen *et al* functionalized optical fiber with a covalently immobilized phosphorylated oligonucleotides via EDC-mediated reaction after silanization with APTES. This fiber was then used to detect hybridization of DNA (286).

In another study, antibodies were immobilized on fiber after silanization it with MPS, a silane-coupling agent with a thiol group at the end (299).

In case of plasmonic FBG, gold substrate is covered with molecules directly in one of the approaches: physical immobilization or covalent immobilization. Physical adsorption has such advantages as being fast and easy but on the other hand less stable and less reproducible. Covalently linked molecules are usually more stable, reproducible and have more coverage. There are two types of covalent linking: one-step and two-step receptor immobilization (300). In some instances, molecules to be coated are first thiolated as was the case when biotinylated thiols were covered on a gold coated FBG (301). In other one-step approaches, an existing thiol-reacting group is utilized. Two-step approach include the use of bifunctional SAMs which are able to react both with surface and the ligand (300).

One of the first steps of functionalization of fiber is its pretreatment to get a hydroxylated surface for further modification. A variety of methods such as Piranha (H_2SO_4:H_2O_2), HCl, methanol/HCl, H_2SO_4 are used both with and without heating the solution. Due to its nature, OF are usually silanized with SCA. APTES is a most commonly SCA used for fiber functionalization. Details of silanization with APTES varies widely starting from its final concentration (0.2-10% in acetone, ethanol, propanol, toluene or water), incubation time (10 min to overnight) and presence or absence of heat treatment for condensation. In any case, aminated surface is obtained. Other SCA utilized for bioreceptor binding on the surface include APTMS which also yields aminated surface, GOPS – glycidyloxypropyl-trimethoxysilane yielding epoxide surface and MPS rendering the surface with thiol groups.

After silanization, either groups on the surface or on the bioreceptor need to be activated using crosslinkers as can be seen from **Figure 2.8**. For example, one terminal of glutaraldehyde forms amino bond with APTES and the second terminal is available for immobilizing amine-terminated oligonucleotide (for DNA hybridization or aptamers against various molecules) (278, 302, 303). One study compared three ways of attaching bovine serum albumin (BSA) protein on TFBG surface (298). In ionic bondings only method self-assembled layer of alternating polyethylene imine and dextran sulfate sodium are formed; to which negatively charged bioreceptor (BSA) (by putting into

buffer with appropriate pH) are absorbed. Second method included the same layer but used strong interaction between extravidin and biotin by electrostatically attaching extravidin on the surface and then attaching biotinylated BSA. The third way of immobilization combined covalent attachment of polyacrylic acid layer onto silanazed surface with an avidin-biotin linkage. Improved biological activity of Bioreceptor and lower LOD of analyte (anti-BSA) was obtained for the second and third methods. Another study compared different methods of immobilization of DNA on glass surface and the best performance was observed for immobilizing amine-modified DNA on aldehyde surface (304).

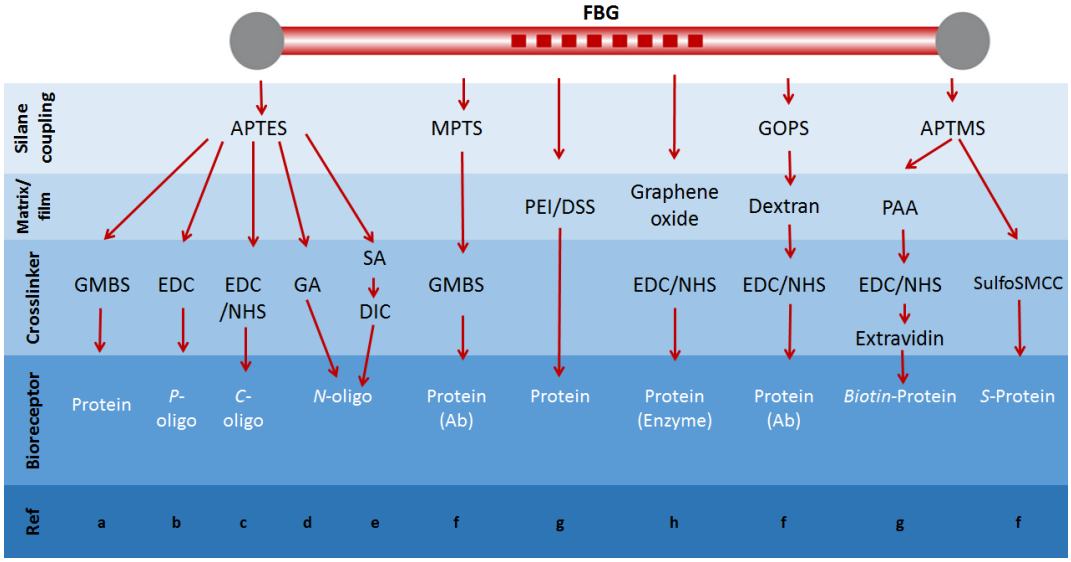

Figure 2.8 An overview of functionalizing optical fiber surface with bioreceptors Ab – antibody; c-oligo – carboxylated oligo; DIC – diisopropyl carbodiimide; DSS - dextran sulfate sodium; EDC – 1-ethyl-3(3-dimethylaminopropyl)-carbodiimide; GA – glutaraldehyde; GMBS - N-succinimidyl 4-maleimidobutyrate; N-oligo – aminated olig; NHS - *N*-hydroxysulfosuccinimide; PAA – polyacrylic acid; P-oligo – phosphorylated oligo; PEI – polyethylene imine; S-protein – thiolated protein; SulfoSMCC - sulfosuccinimidyl 4-(N-maleimidomethyl)cyclohexane-1-carboxylate; NB: Blocking step not shown. a) (299);b) (286); c) (304); d) (278, 302, 303); e) (305); f) (306); g) (298).

Blocking the surface after the bioreceptor is attached is an important step to reduce non-specific binding. For this purpose such compounds as ethanolamine (after APTES-PDITC (307)), $NaBH_4$ (after incubating DNA with aldehyde surface (after APTES-gluteraldehyde (308) and APTES-PCC (304)), BSA have been used.

2.6. Characterization of functionalized surfaces

Once functionalized, the surface has to be analyzed to confirm that each step of modification was done successfully. There are a number of methods for surface analysis including contact angle measurement, AFM, SEM, EDS, Auger Electron Spectroscopy (AES), X-ray photoelectron spectroscopy (XPS), Secondary ion mass spectrometry (SIMS) and Fourier Transform Infrared Spectroscopy (FTIR). These methods are based on different principles and have various sensitivity, operation interphase (air, liquid, aqueous, vacuum), spatial resolution, depth of surface that can be analyzed and chemical composition information they can give (elements, compounds, isotopes) (188). All of these techniques in combination or separately were used in different studies to analyze functionalized SS or optical fiber. Methods which were available for our use and were used (or attempted to be used) for surface analysis of SS and OF will be discussed below.

2.6.1. Surface characterization of functionalized SS

SS modified for different biomedical applications have been studied using a number of techniques. Studying SS modified with APTES is shown in **Table 2.5**.

AFM has been widely used for surface morphology analysis of functionalized SS. Chitosan and lysozyme layers on SS were studied and root mean surface roughness values (R_a) of the surfaces after each modification step were compared showing a successful increase with each layer (185). Several layers of chondroitin 6-sulfate/heparin for developing a drug eluting stent were also confirmed by AFM (250). AFM allows to analyze the surface of very thin metal layers as was demonstrated by sampling 0.406 mm nickel titanium orthodontic wire (309). SS surfaces functionalized with APTES and then with gold nanoparticles were studied with AFM to confirm successful electrodeposition of the nanoparticles (271).

	(310)	(311)	(271)	(218)	(217)
SS Substrate	304 SS 1×5cm coupon Bright anneal state Die-cut	316L SS 1.2×1.2×0.1cm 0.25um SiC paper polished Diamond paste until mirror polished	Medical 316 Rod 0.03 mm Emery paper (1000 grade), alumina slurry polished	316L 10×10×0.1 mm^3 pieces	Ni-free SS
Surface characterization methods	• LEEIXS • XPS • FTIR	• XPS • FTIR • Bromphenol assay (Enzymatic assay)	• Electrochemical measurement • CV • SEM • AFM	• XPS	• XPS • AFM
Use of silanized surface	Studying silanization; appl. LEEIXS	Lysozyme immobilization for antibiofilm	+GNP for impedimetric biosensor	Studying immobilization of alginic acid	Studying HT

Table 2.5. Analyzing SS modified with APTES used for different biomedical applications.

CV – cyclic voltammetry
FTIR - Fourier Transform Infrared Spectroscopy
GNP – gold nanoparticles
HT – heat treatment
LEEIXS – low energy electron induced X ray spectrometry
XPS – X-ray spectroscopy

SEM is another popular technique to study modified SS surface. It was used for morphology analysis of SS after different surface treatments as polishing (wet-grinding followed with chemical mechanical polishing), blasting (using aluminum oxide) and coating with hydroxyapatite (177). Rough estimation of the coating thickness was also possible with SEM. Using an EDS feature of SEM, elemental distribution on the surface was also demonstrated in this study. In another study, SEM was used to compare modified surfaces (grafted with dopamine, chitosan and lysozyme) with unmodified for their ability to inhibit bacterial growth (185).

FTIR is a powerful technique to study the presence of chemical groups on the surface. Silicone rubber coated SS was characterized with FTIR in attenuated total reflection (ATR) mode (312). The presence of such bonds as Si–C, Si–O–Si, C–H and Si–CH_3 was determined. (204, 222, 226, 312, 313). SS used in our project is in the form

of wire to resemble guidewire that is inserted into cubital vein. This makes some of the techniques such as FTIR not feasible. SS analyzed by FTIR used samples which were large enough to be held on the ATR holder: SS plates (1×10×20 mm), disks (1 mm thickness and 14 mm diameter), stents (L 12 mm, surface area 48mm^2, closed diameter 1.8 mm (222).

Hydrophilicity of the modified SS surface can be analyzed by measuring contact angle (θ) of the surface using different liquids. Contact angle values towards distilled water on differently modified SS surfaces was compared by Huang *et al* (250). Contact angle increased after gold sputtering and then decreased with subsequent steps of modification: thiolization with dimercaptosuccinic acid, chitosan, heparin. Samples used in this study were sheets of SS (with unspecified size). Other studies used contact angle measurement for studying hydrophilicity of 10 mm × 10 mm × 1 mm sheets with different surface roughness (314), silanized and polymer grafted 10 mm × 15 mm × 1 mm (width × length × thickness) SS samples (215), 10 mm × 10 mm × 1 mm coupons silanized and coated with nanocoatings for improved corrosion resistance (199). However, our sample is too thin to hold liquid which is measured, and this method was also omitted. Other techniques used in case of functionalized SS include XPS (silane layer, antibody analysis on SS (194, 199, 205, 232, 234) and XRD (234). However, XPS technique was not available for our disposal and could not be used.

Analyzing modified surfaces of thin metal samples is not as common as the analysis of flattened metal samples perhaps probably due to their limited applicability and difficulties associated with their use for surface analysis; these methods are summarized in **Table 2.6**.

Metal wire (composition, size)	**Purpose of wire**	**Method of characterization**	**Application of the method**	**Reference**
NiTi 0.406 mm	Sorptive extraction	SEM	Surface morphology (500X)	(309)
		EDS	Elemental analysis	
		Raman spectroscopy	Elemental analysis	

Metal wire (composition, size)	Purpose of wire	Method of characterization	Application of the method	Reference
		AFM	Surface morphology	
		3D optical profilometer	Surface morphology	
$Fe_{77.5}B_{15}Si_{7.5}$ Diameter 120 µm, length 33 mm	Humidity sensor	SEM	Surface morphology	(315)
		EDS	Elemental analysis	
SS stent Length 15- mm, Diameter 2- mm	Cell capture for re-endo-thelialisation	SEM	Surface morphology	(316)
		EDS	Elemental analysis	
		Fluorescent microscopy	Imaging captured cells	
SS 316L 0.5 mm	General biomedical application	Anodic polarization	Corrosion resistance	(189)
		SEM	Surface morphology	
		EDS	Composition of oxide film	
		AES	Surface composition	
		XPS	Chemical composition of oxide films	
		TEM	Characterization of oxide film	
SS 304 180 µm coated with Pd	Solid-phase microextraction	SEM	Surface morphology	(317)
		EDS	Composition of Pd coating	
SS wire 3 cm	Sorptive extraction	SEM	Surface morphology	(318)
		FTIR	Composition of polymer coating	
SS 316 Diameter 0.03mm		SEM	Surface morphology	
		CV	Charge-transfer resistance	

Metal wire (composition, size)	Purpose of wire	Method of characterization	Application of the method	Reference
	Impedimetric immunosensors	EIS	Electrolyte solution resistance, charge transfer resistance	(271)
		AFM	Surface morphology	

Table 2.6. Surface analysis techniques used to study different modified metal wires used in biomedical applications.

In some cases, it is possible to confirm successful surface modification by analyzing the bioactivity of the surface: enzymatic activity if the enzyme is the active compound being immobilized as in (232), utilizing antibodies against biological molecules immobilized on the surface in an essay similar to ELISA (enzyme-linked immunosorbent assay) (231, 232), adding chromogenic substrate of the immobilized enzyme directly (203) or increase of certain minerals in simulated body fluid (*in vitro* bioactivity) (319). Fluorescence microscopy analysis is also feasible to study surfaces after modification. Thus FITC analysis was used to confirm the polymer grafting on the surfaces given the formation of chemical bond between FITC and aminated surface (215). Adsorption of fluorescently labeled proteins (which have affinity towards the immobilized entity or to study non-specific binding) and their visualization under microscope is also an option (220).

Electrochemical analysis of the functionalized surface can be performed in different formats: electrochemical impedance spectroscopy (EIS) (182, 239), CV, potentiodynamic polarization (PDP) (182, 239). EIS studies (usually by Nyquist plots) can be done in different solutions such as Ringer's solution and resistance of the surface before and after modification could serve as an evidence of formation of layer (239). Different polarization parameters (corrosion potential, breakdown potential and repassivation potential) could also be obtained using PDP to study formation of passive film on SS (239). Integrity of sol-gel hybrid film on SS after immersing into SBF was studied by Omar *et al* (182). PDP analysis of uncoated and forsterite coated SS samples in simulated body fluid were performed (319).

Thin metal wires (not only SS), according to literature, can be modified and used for different biomedical applications: sorptive extraction of different chemicals, humidity sensor, biosensor and capturing cells for re-endothelization. Different methods used to study the surface of modified wires are shown in **Table 2.6**. These methods include SEM/EDS, AFM, FTIR, Raman spectroscopy, TEM, electrochemical methods, profilometer and fluorescent microscopy. Apart from methods explained above, application of TEM is an interesting approach where thin oxide layers formed on SS wire were first stripped from the surface with a solution, filtered and cleaned for a further study on TEM (189).

2.6.2. Surface analysis of functionalized optical fiber

Analysis of optical fiber surface functionalized for biosensing purposes includes the use of SEM/EDS, AFM, FTIR, XRD, thermogravimetric analysis (320). Functionalized glass substrates (not optical fiber) were also studied with other techniques include XPS analysis and contact angle measurement (321). But most common method used, is the analysis of spectral characteristics during functionalization. Functionalization steps of dual-peak LPG (cleaning, silanization and oligonucleotide attachment) were monitored and wavelength shift during the steps were compared with one another. Immobilization of DNA resulted in a bigger blue shift than when than silanization (with APTES) (286). When EFBG was silanized with APTES and 3-aminopropyl-monoethoxydimethyl-silane (APDMS), it was observed that silanization of the surface occurs in the first 15 min as was observed with optical spectrum analyzer (OSA). As opposed to APDMS, APTES did not form a monolayer but formed a seven chained polymer film on the fiber. Immobilization of probe DNA on the surface is also confirmed by monitoring wavelength shift during hybridization with a complimentary DNA (278). In another study, an increase of Bragg wavelength with each successive step of functionalization is observed: silanization with APTES, crosslinking with glutaraldehyde (GA). They also observed most of the change takes place in the first 10 min when shift of wavelength with time is measured (275).

SEM was used to study the stability of gold layer of SPR-optical fiver with preliminary silanization of the surface after thermal and chemical treatments (322).

SEM/EDS was also used to demonstrate successful functionalization of fiber surface. EDS analysis demonstrated increased content of oxygen on the modified surface compared to unmodified ones and the ratio of silicon to oxygen was also indicative of silanization of the surface (320). Two dimensional coatings of graphene oxide on EFBG were analyzed with SEM (323). EFBG coated with graphene oxide and antibodies was also demonstrated with SEM (324).

AFM is very useful in determining nanoscale changes on the modified surface (300). An increased surface roughness was observed on FBG biosensor based on tapered fiber-optic interferometer which was treated with APTES, GA, HER2 antibodies and also when analyte (HER2) was detected (325). It has also been used to study self-assembled monolayer of thiols and antibodies on the surface of plasmonic grating sensors (326).

Other methods used for studying the surface of modified optical fiber include different dye assays and FTIR. Similar as in FITC use for SS analysis, acridin orange can be used to study silanization of the fiber. After incubating with the dye and rinsing it off, samples can be inspected using microplate fluorimeter at different time points and fluorescence intensity compared (320). Similarly, samples could be excited at 488 nm and emission observed (at 514 nm) under fluorescent microscope. Streptavidin conjugated with fluorophore (such as QD) can be used to study biotinylated fiber surfaces (327). FTIR in ATR mode as a sensitive tool to study surface chemistry was used to confirm silanization of the glass surface (microstructured optical fiber) (328).

CHAPTER 3. SELECTION AND CHARACTERIZATION OF DNA APTAMERS AGAINST BREAST CANCER STEM CELLS

3.1. Abstract

BCSC are a small population of cells in the bulk tumor which play an important role in initiation, recurrence and metastasis of BC. Therefore, finding new molecules that specifically bind BCSC is important for diagnosis, treatment and prognosis of this disease. The aim of the current study was to select and characterize aptamers that bind BCSC. For this, well-characterized cells with a number of biomarkers and characteristics pertaining to BCSC were chosen as a target. Despite the availability of different aptamers relevant for BC diagnosis, most of them either target protein biomarkers or were selected against a particular cell-surface biomarker. In this work, FACS was used to sort oligonucleotides bound to well characterized BCSC without a particular marker in mind; most importantly preliminary analysis showed that some sequences bind to target cells more than to normal breast epithelial cells. Moreover, target cells used for aptamer selection were originally derived from TN breast tissues. Binding of selected aptamer candidates to cells was studied using IFC which combines the capabilities of both flow cytometry and fluorescent microscopy. IFC is an emerging tool to characterize binding of aptamers to cells and this work could be an important for other researchers in learning how to apply this tool for aptamer characterization in the future studies.

This Chapter is part of a manuscript yet to be submitted to a journal for review. My contribution to the manuscript (according to Contributor Roles Taxonomy (CRediT)) is as follows: conceptualization (formulation of research goals and aims), designing methodology for *in vitro* selection, validation, investigation (performing experiments and data collection), original draft preparation, and writing (review and editing).

3.2. Introduction

BC is the most common malignancy in women worldwide with a rising incidence (329). High rate of tumor recurrence after treatment of this disease is associated with the presence of CSC and inability of conventional therapies to eradicate them (12). The investigation of CSC received an enormous attention in the last decade. CSC are a rare

subpopulation of tumor cells that have distinct stem like properties that can initiate tumor, promote invasive growth and dissemination to distant organs. Conventional chemo- or radiotherapy may efficiently kill the bulk of differentiated drug sensitive BC cells, but not the resistant self-renewable BCSC (330). Thus, targeting and detecting these cells is crucial in cancer therapy, diagnosis and prognosis (128). A key challenge in detection of CSC is the lack or scarcity of ligands against BCSC. Given a limited number of cell-surface and intracellular markers of BCSC and the instability of antibodies that target these markers, it is important to identify new molecules that bind them (12).

Herein, we report selection of aptamers against cells with BCSC characteristics. For this, ssDNA library was first incubated with BCSC and fluorescently activated cell sorting was used to enrich live cells with bound oligonucleotides; these ssDNA molecules were then separated from cells and amplified; after PCR, products were turned into ssDNA using lambda exonuclease digestion, thus completing one round of selection. Oligonucleotides from selected rounds were subsequently sequenced and grouped into families with next-generation sequencing and bioinformatics analysis. Sequences of selected aptamer candidates were synthesized and used in IFC to analyze their binding to cells. The overall scheme of the selection and characterization of DNA aptamers against BCSC is displayed in **Figure 3.1**.

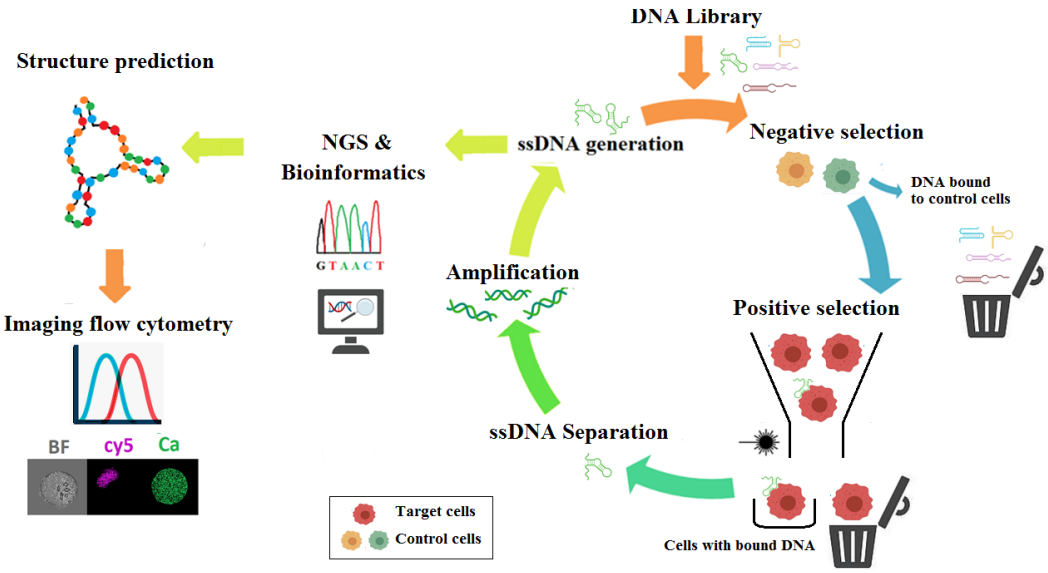

Figure 3.1. A schematic overview of *in vitro* selection of aptamers and their characterization.

3.3. Materials and Methods

3.3.1. DNA library and primers

To initiate a selection process, a random DNA library consisting of single-stranded 81-mer with a central random region consisting of 45 nt was synthesized (Lumiprobe). Random region was flanked by primer regions with known sequences for PCR amplification as shown in **Table 3.1**. Forward primer labeled with cy-5 (Sigma Aldrich) was used for obtaining fluorescently labeled sequences for use in FACS, phosphorylated reverse primer was used for obtaining ssDNA from dsDNA by lambda exonuclease (New England Biosciences) digestion.

Oligonucleotide	Sequence, 5'-3'	Manufacturer
Random library	cy5-ATCCAGAGTGACGCAGCA-45N-TGGACACGGTGGCTTAGT	Lumiprobe, Russia
Forward primer	cy5-ATCCAGAGTGACGCAGCA	Lumiprobe, Russia
Reverse primer	Phos-ACTAAGCCACCGTGTCCA	Sigma Aldrich, Germany

Table 3.1. Nucleotide sequences of the random library and primers used in the SELEX procedure (16).

3.3.2. Cells, media, extracellular matrix

To select new ligands (aptamers) against BCSC, well characterized human BCSC (Celprogen; Cat.no 36102-29) were chosen as target cells. They were grown on human BCSC extracellular matrix (ECM) (Celprogen; Cat.no E36102-29) in human BCSC complete media with serum (Celprogen; Cat.no M36102-29PS). Two types of cells, namely, human breast epithelial primary cell culture (Celprogen; Cat.no 36056-01) and human BC cells (Cat.no 77002-07) were used as control cells in negative selection procedure. These cells were grown on human breast epithelial cell culture ECM (Celprogen; Cat.no E36056-01) in human breast epithelial cell culture complete media with serum (Celprogen; Cat.no M36056-01S) and on human BC cell ECM (Celprogen; Cat.no E77002-07) in human BC cell complete media with serum (Celprogen; Cat.no M77002-07) respectively. Cells were grown in a humidified incubator with 5% CO_2 at

37°C (ThermoFisher, 3121). Characteristics of cells used for selection are shown in **Table 3.2**.

Cells	Use during selection (round)	Characteristics
Breast cancer stem cells	Target (all rounds)	**Source**: Human Breast Cancer tissue (Triple Negative: ER, PR and HER2 Negative) **Positive Markers**: CD133, CD44, SSEA3/4, Oct4, Tumorigenicity (<1000 cells), Alkaline Phosphatase, Aldehyde Dehydrogenase, Telomerase
Breast epithelial cells	Control (7 and 10)	**Source**: Breast Tissue **Positive Markers**: ESA, Nestin, CD49f, Keratin, ER, c-kit, endothelin-1, EGFR, heparin sulfate, PR
Breast cancer cells	Control (3 and 9)	**Source**: Human Breast Cancer tissue. **Positive Markers**: KGF, HGF, Cdx-1, Cdx-2, Oct 4, HNF-1B (TCF-2), ESA, Telomerase, CA15-3, CA27.29, $HER2^-$, $Progesterone^-$, $Estrogen^-$ & Ephrine $B4^+$

Table 3.2. Characteristics of cells from Celprogen used during the selection of aptamers

EGFR – epidermal growth factor receptor; ER – Estrogen receptor; ESA – epithelial surface antigen; HER2 – human epidermal growth factor receptor 2; HGF – hepatocyte growth factor; KGF – keratinocyte growth factor; PR – Progesterone receptor.

3.3.3. Buffers and other reagents

Dulbecco's modified PBS (DPBS), glucose, PBS tablets, tRNA from yeast were purchased from Sigma Aldrich. EDTA, Calcein violet AM salmon sperm DNA, BSA and $MgCl_2$ were purchased from ThermoFisher Scientific. Lambda exonuclease was obtained from New England Biolabs. Buffers were prepared according to Sefah *et al* (16)**.** To prepare washing buffer (WB), 4.5 g of glucose, 5 ml of 1 M $MgCl_2$ were added to 1l of DPBS. For binding buffer (BB), 100 mg tRNA and 1 g BSA were added to WB. Salmon sperm DNA was added just before incubation of cells with DNA during selection in a concentration of 1 mg/ml.

3.3.4. *In vitro* selection of aptamers using FACS

Aptamer candidates against BCSC were selected using the SELEX method based on (16) with some modifications. A well characterized human BCSC cell line (**Table 3.2**) was

utilized as a target for aptamer enrichment. Two other cell lines, human BC cells and human breast epithelial cells (BEC), served as the negative controls to ensure that selected of DNA entities would not bind surface molecules present on these cells. All cells were grown on their particular media and extracellular matrix to ensure their properties are retained.

Cells grown until reaching about 90% confluency were washed with DPBS and then dissociated from plate using PBS/EDTA (2.5mM) for about 5 min. Dissociated cells were washed with WB twice and resuspended in BB. Cells were counted and their viability assessed using hemocytometer. After filtering cells through 70 μm strainer, 2×10^6 cells were incubated with 10 nmol of DNA (for the first cycle of SELEX). Prior incubation with cells, DNA library was denatured at 95°C for 5 min in a block heater (Stuart; SBH130D) followed by cooling on ice. To reduce non-specific binding of DNA to cells, together with BSA present in BB, salmon sperm DNA (final concentration of 1mg/ml) was added and the mixture of cell-DNA was incubated on ice for 60 min on a multipurpose rotator (Thermo scientific). To distinguish live cells from dead during cell sorting, calcein violet AM was used according to the manufacturer's instructions. After incubation, sample was washed with BB and was sorted using BD FACSAria™ cell sorter (BD) equipped with 355, 405, 488, 561, 640 nm lasers. Flow cytometer laser lines of Violet 405 and Red 640 nm and channels APC (excitation/emission same as for cy5) and BV421 (excitation/emission same as for Calcein violet AM) were used in this study. In order to get a better overview, pulses were shown in a logarithmic scale. The following plots were taken: side scatter (SSC) versus forward scatter (FSC), FSC width (FSC-W) versus FSC height (FSC-H) and fluorescent intensities of both dyes. Cells with higher intensity for both of the dyes were gated and sorted. Sorted cells were collected in dH_2O and ssDNA was recovered from the cells by heat/elution/denaturation: heating sample for 5 min at 95°C and centrifuging at 16100g for 5 min with a further precipitation of DNA as described below. In order to increase the stringency of enrichment process, certain parameters of incubation were modified: number of cells used each cycle (decreased from 2×10^6 cells to 3.5×10^5 cells), amount of DNA used (lowered from 10 nmol to 700 pmol), washing after incubation (gradual rise from 1 to 4), incubation time decreased (from 60 min to 30 min) as shown in **Table 3.3**. Control cells were used during negative

selection four times during the third, seventh, ninth and tenth rounds of SELEX. For this, control cell lines were firstly incubated with ssDNA and then the supernatant containing unbound DNAs was collected and used for the positive selection against BCSC.

Round #	Target cells	ssDNA (pmol)	Incubation time (min)	Number of washes after incubation	Negative control used during selection
1	2.0×10^6	10000	60	1	-
2	1.5×10^6	2800			-
3	1.0×10^6	2468	50		Breast cancer cells (227 500 cells; 50 min)
4	5.1×10^5	2000		2	-
5	4.4×10^5	1214	40		-
6	4.0×10^5	1142			-
7	3.9×10^5	1130		3	Breast epithelial cells (200 000 cells; 40 min)
8	3.5×10^5	707	30		-
9	3.5×10^5	700		4	Breast cancer cells (400 000 cells;30 min)
10	3.5×10^5	700			Breast epithelial cells (400 000 cells; 30 min)

Table 3.3. Parameters of *in vitro* selection of DNA aptamers against BCSC using FACS

3.3.5. DNA precipitation and amplification

After *in vitro* selection and lambda exonuclease digestion, DNA was precipitated using ethanol/sodium acetate. After adding one tenth volume of sodium acetate (pH 5.2-5.6) to DNA sample with a final concentration of 0.3 M, 2.5 volumes of cold 95% ethanol was added. After overnight incubation at -80^{0}C, DNA was centrifuged for 30 min at 13200g

and the obtained pellet was washed twice with ethanol. After being dried and resuspended in dH2O, DNA was further amplified or used in *in vitro* selection.

Singe-stranded DNA was amplified with PCR in order to increase its amount with the following thermocycling conditions: initial denaturation at 95ºC for 15s and final extension at 72ºC for 30s; and 9 cycles of denaturation at 95ºC for 30s; annealing at 56.3ºC for 30s and extension at 72ºC for 30s in a Eppendorf thermocycler Gradient. Phosphorylated reverse primers were used in PCR to get dsDNA suitable for further ssDNA preparation. If there was insufficient DNA, another 9-cycle PCR was performed to obtain more DNA. Non-denaturing 10-12% polyacrylamide gel (PAGE) electrophoresis at 200V for 20-30 min after binding with SYBR Green 1 (Invitrogen, USA) was used to analyze amplified PCR. Lambda exonuclease (New England Biolabs, USA) (5 units of per 50 µl reaction) was utilized to get ssDNA by digestion of PCR products. Products of digestion were precipitated as above and used for the next round of SELEX.

3.3.6. Next-generation sequencing and secondary structure prediction

After completion of round 10 of *in vitro* selection, initial library, SELEX products from rounds 5 and 9 (round 10 products could not be amplified) were prepared for NGS and bioinformatics analysis. For this, they were PCR amplified by adding indexes to the selection primer sequences truncated from the 5'-end as shown in **Table 3.4**. After amplification using these primers, samples were analyzed on 10% PAGE and purified using MiniElute PCR Purification Kit (Qiagen) and further shipped to Germany to perform NGS on our samples in Translational Oncology at the University Medical Center of the Johannes Gutenberg University Mainz on Illumina NGS and bioinformatics analysis (performed by AptaIT).

DNA sample	Forward primer, 5'-3'	Reverse primer, 5'-3'
DNA library	GGC TAC GAC GCA GCA	GGC TAC CCG TGT CCA
Round 5 DNA	CTT GTA GAC GCA GCA	CTT GTA CCG TGT CCA
Round 9 DNA	AGT CAA GAC GCA GCA	AGT CAA CCG TGT CCA

Table 3.4. Sequences of primers used for sequencing (NGS) of DNA samples

Secondary structures of the sequences were predicted using *Mfold* (http://unafold.rna.albany.edu/?q=mfold/DNA-Folding-Form) both using default settings and with the following conditions: 1mM Mg^{2+} at 4°C temperature to imitate selection conditions.

3.3.7. Imaging flow cytometry analysis

The binding of aptamer candidates from rounds 5 and 9 with target cells (grown in T75 flask) as well as control cells was studied. For this, aptamers were denatured at 95ºC and then cooled on ice. Cells were washed with WB three times, dissociated from the flask using PBS/EDTA (2.5 mM) and filtered through cell strainer (70µm). Then they were incubated with aptamers (250 nM final concentration in BB) on ice for 30 min in the dark with addition of salmon sperm DNA and calcein violet AM. After incubation cells were washed twice with WB and resuspended in 60 µl BB before being analyzed on ImageStream.

Cell images were acquired on 4-lasers Imagestream X Mark II system (EMD Millipore) as described before (331). At least 10,000 events were collected with 40× or 60× magnification. A 405 nm laser was used to excite calcein violet and 640 nm laser to excite aptamers. For double stained cells (calcein violet and aptamers) single-stained controls were used to compensate fluorescence between channel images on a pixel-to-pixel basis. Analysis was done using IDEAS software package (EMD Millipore). Gating on bivariate plot of cell area versus aspect ratio was first used to isolate a single-cell population, and gating on calcein violet-positive cells to exclude dead cells from consideration. Statistical data analysis was performed with Prism 7.0 software using

student t-test, one-way or two-way ANOVA as indicated. A value of $p < 0.05$ is considered to be statistically significant

3.4. Results and Discussion

3.4.1. *In vitro* selection of aptamers using FACS

CSC are a minor population of tumor cells which are able to initiate tumor upon transplantation (332). They play an important role in cancer relapse and metastasis in BC. Detecting and targeting these cells could be one of the promising strategies in diagnosis and treatment of this disease and thus discovering new ligands against them is important. Previously, a number of aptamers have been selected with the aim of BC diagnosis as described in Section 2.3.4. In this study, an attempt was made to select novel aptamers against BCSC. To select aptamers, commercially available cells from Celprogen Inc. were chosen due to their well characterized features relevant for CSC in BC. In order to exclude the oligonucleotides that could bind to BC cells and breast epithelial cells, these cells (also from the same manufacturer) were used in negative selection procedure. Performing counter-selection procedures is considered to enhance selectivity of aptamers (145). The nature of control cells used in a study depends on the objective of the aptamers. For instance, some studies used normal cells to select aptamers against cancer cells (136, 151, 162), or different cancer cell type to select for very specific aptamers (116, 140, 145, 146), non-metastatic or low metastatic cancer cells to enrich ligands against metastatic cells (142, 147), cells with no expression of a target biomarker to select aptamers specifically binding one target on the cell (144, 149). Some studies used counter selection starting from the third round (135) or the fourth round (139, 151) or several times throughout selection (rounds 3 and 8 (333); rounds 3, 5, 7, 9 and 12 (152)). In this study, control cells were used in rounds 3, 7, 9 and 10 and two control cells were used alternately. The cells used as targets in this work were used for studying expressed genes (334) biomolecular characterization of exosomes secreted from the cells (335), studying Notch-1 signaling (336), expression and targeting ALDH1 and Notch-1 (337).

DNA library and primers sequences were taken from Sefah *et al* (140) in order to ensure high PCR amplification efficiency. Despite using efficient set of library-primers

in this work, it was shown that using 25 and 30 cycles of amplification leads to accumulation of nonspecific bands thus it was decided to use 9 cycles of PCR and then use these products for another 9-cycled reaction. This way, it was possible to get a band of correct size (ca. 80 base pair in length as the initial library) as shown in **Figure 3.2.** Increasing the number of PCR cycles, despite yielding more DNA, is one of the main factors affecting specificity of the obtained bands (the correct size of the product with no non-specific sequences). This is thought to occur due to the depletion of primers with more number of cycles and product annealing with the template producing non-specific sequences (338).

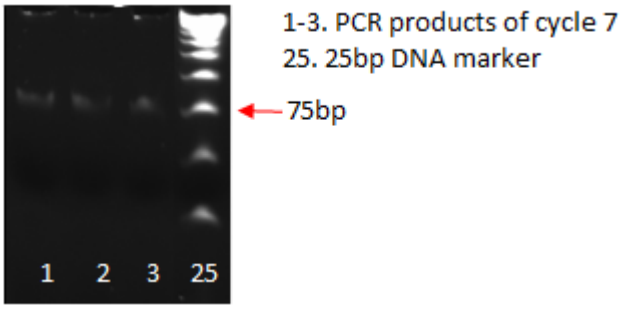

Figure 3.2 - Analysis of PCR products of cycle 7 on 10% polyacrylamide gel using 25 base pair DNA ladder as a DNA marker.

To ensure the selection of specific and high affinity ligands during SELEX, it is important to apply stringency during selection (16). Various strategies are employed during the selection of specific aptamers (alone or in combination). In this work, the amount of DNA used for incubation with cells was decreased with each round. In order not to loose DNA and have a good recovery of DNA, the difference in the amounts of DNA was less obvious towards the last cycles. When target molecules are complex as cells, it is also important to consider other point. One of them being the stability of surface proteins on the cells during cell dissociation (16). Commonly used agents for cell dissociation such as trypsin or some non-enzymatic cell dissociation solutions can damage molecules expressed on cell surface; thus it might be more preferential to perform SELEX directly on cells grown on dishes (16). However, the volume of DNA used in this case has to be increased and DNA could non-specifically bind to culture dish. Trypsin can be used when it is know that the target antigen is highly expressed and/or to get a

faster dissociation of the cells (339). In our study, since SELEX is done without a specific target in mind but rather taking cells with target characteristics, trypsin was not used. Instead, PBS/EDTA with 2.5mM EDTA (or 0.073% w/v) was found to be optimal for dissociation of BCSC and control cells.

Separation of target bound DNA from unbound ones is one of the most important steps in selection. Using FACS as a separating tool in SELEX (as opposed to centrifugation) offers more reliability during enrichment, allows targeting specific population of cells (e.g. live/dead), simultaneous monitoring of enrichment and less number of selection cycles (16, 116, 153). FACS has been used for aptamer selection for a decade; with a study by Raddatz *et al* in 2008 (153) probably being one of the first applications. Later, Mayer *et al* in 2010 (116) published a fully described protocol for the application of FACS in SELEX. Since that time FACS has been successfully exploited in two main categories: as a method of separation of cell-bound aptamers (16, 153) and for studying enrichment of aptamers during the enrichment process and their binding affinity towards target cells and other cells in specificity studies (18, 28, 136, 139, 143, 146, 148, 151).

In FACS-SELEX, side scatter area versus forward scatter area (SSC-A vs FSC-A), forward scatter width versus height (FSC-W vs FSC-H) and dot plot of side scatter versus fluorochrome intensity of cy5-oligonucleotides for round 5 are shown in **Figure 3.3**. SSC-A vs FSC-A was performed in order to eliminate cell debris from the analysis, while FSC-W vs FSC-H served for exclusion of cell doublets. Unstained sample cells, cells incubated with the initial DNA library labeled with cy5 as well as cells incubated with a dye that distinguishes between dead and live cells were used in FACS. Unstained cells were used in order to eliminate autofluorescence from the cells. Dead cells are known to be non-specifically bind DNA and thus need to be eliminated from the analysis (16). To further enhance this, together with SSC-A vs FSC-A, Calcein violet AM was used as a live/dead cell discriminator in this study to verify position of live cells. It is a cell permeable fluorescent dye which is hydrolyzed by intracellular esterases to produce fluorescent product. This dye was chosen due to several reasons: it is not a DNA-intercalating dye and should not bind to oligonucleotides used; its excitation/emission

spectra does not overlap with the one of cy5. Cells showing high intensity of both cy5 and Calcein were sorted and DNA was extracted and amplified as described above.

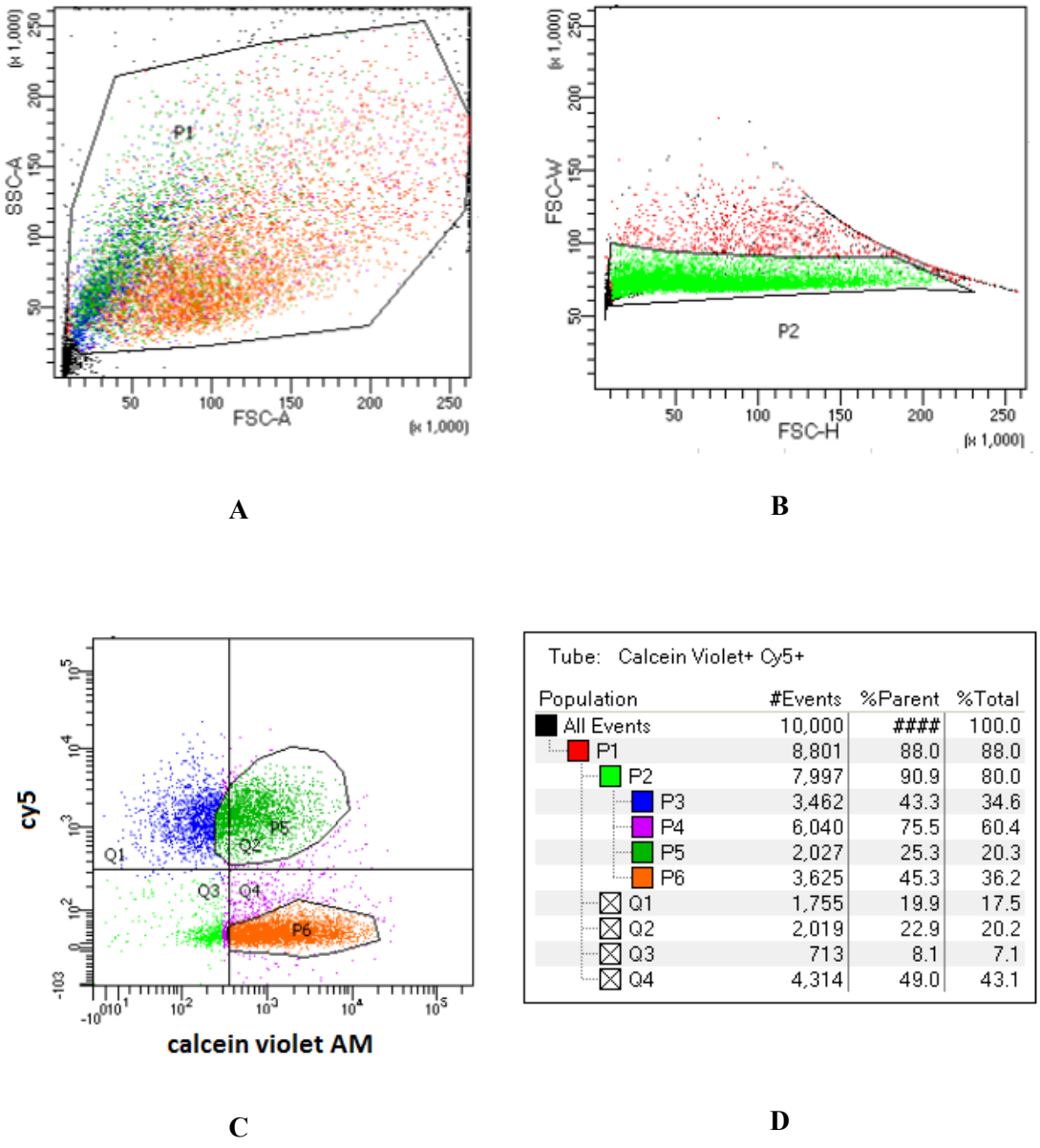

A **B**

C **D**

Figure 3.3. Using FACS for selection of aptamers against BCSC: results for round 5 of *in vitro* selection of DNA aptamers is shown. A) Dot plots of side scatter area versus forward scatter area; B) Dot plots of forward scatter height versus width; C) Dot plot of side scatter versus fluorochrome intensity of cy5-oligonucleotides; D) Populations of cells

3.4.2. NGS of aptamers and secondary structure prediction

In order to know the sequences of the aptamers and study the enrichment of sequences, NGS was performed for initial library and DNA from rounds 5 and 9 and results are shown in **Figure 3.4**. NGS enables to sequence a lot more sequences than traditional Sanger method in a shorter period of time and monitor the population dynamics occurring during the selection process (340, 341). Sequences of rounds 5 and 9 were grouped into several families according to a sequence similarity. Secondary structures of aptamer candidates were predicted and those sequences which had 2D structures with low free energy and were predicted to form a similar loop structure in both full- and shortened (random region only) leading to spontaneous folding (122) (as seen in **Figure 3.5**) were selected for further binding analysis with cells (**Table 3.5**). From round 5 aptamer candidates 5.1 and 5.8 were chosen; and for round 9, aptamer candidates 9.11 and 9.12 were chosen. Aptamer candidate 5.1 was a representative of the most frequently observed family present 24 times (total number of members 5 in a family). While aptamer candidate 5.8 was a representative of a family present 5 times (total number of members 1 in a family). The length of some candidates were revealed to be less than 45 nt long and this could be possibly explained by the fact that the length of random region in the initial library was mostly 45 nt with a small amount of shorter oligonucleotides present (44, 46, 43, 42, 41 and 40 in the order of abundancy respectively). Interestingly, some sequences actually comprised of a forward primer and/or reverse primer binding site showing an enrichment of DNA comprised of primers. The sequence of aptamer candidate 5.1 comprised of a reverse primer binding site followed by forward primer, 7 nt (random) and another reverse primer binding site. A sequence with two reverse primer binding sites was also selected by Tolle *et al* (342). However, they did not analyze the binding affinity of the selected product with the target. The length of PCR products observed during the selection process was of correct size in PAGE (**Figure 3.2**) so it was not possible to predict the formation of parasitic sequences without performing sequencing. The sequence of aptamer candidate 5.8 did not contain such parasitic regions. Other sequences had more Ts than other nucleotides present. Our aptamer candidates were found to be rich in thymine (as seen in **Figure 3.3**) which also can be explained by the T-rich initial library. Aptamer candidates rich in thymine were also identified in other studies and were

found to bind specifically to its target (139). In the future, to avoid the enrichment of T-rich sequences during selection, it is advisable to use optimized DNA libraries which has a balanced distribution of four nucleotides in the random region. This will allow to reach a maximum diversity of the initial pool and hence increase target-binding capacity of the candidates. Having an initial library with an optimized/unbiased distribution of four nucleotides in the random region allows starting the selection procedure optimally by increasing the sequence space and potentially allowing selection of aptamers with better affinity to their targets (343).

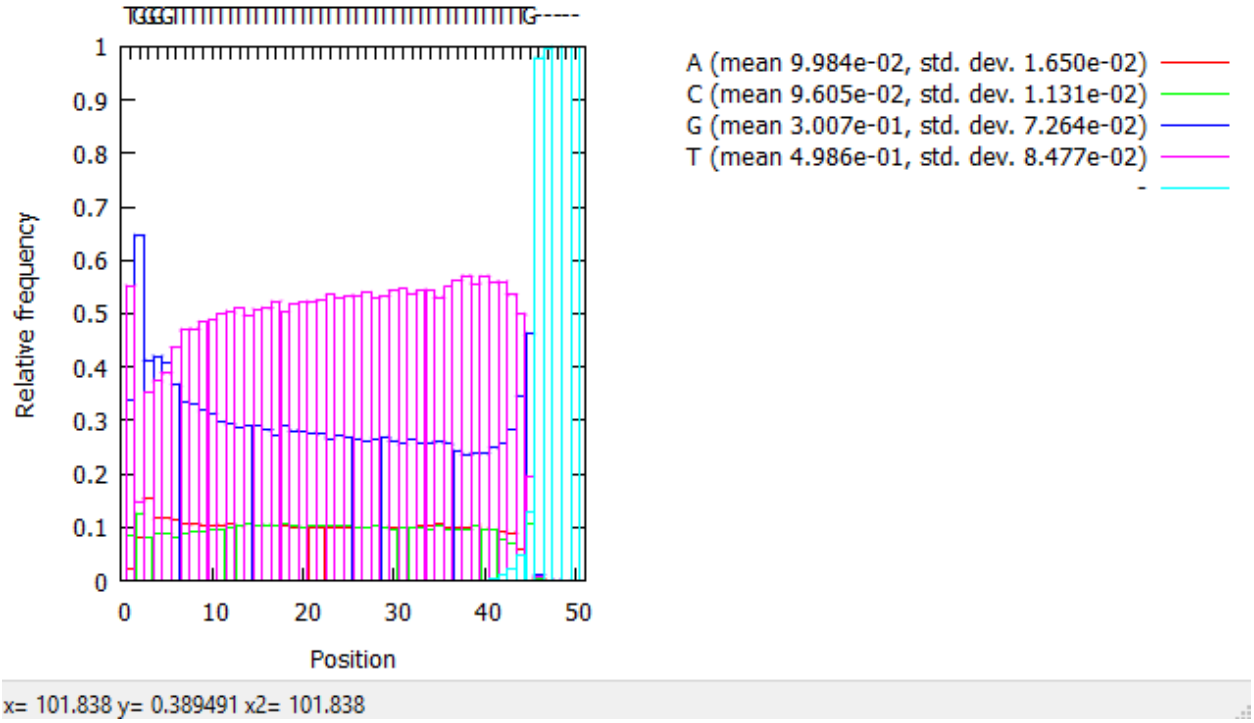

Figure 3.4. Results of next-generation sequencing of a random region for product of round 5 of selection: relative frequency of nucleotides in each of a position in the oligo is shown. Statistics is shown for 715560 sequences from which 693414 are unique ones.

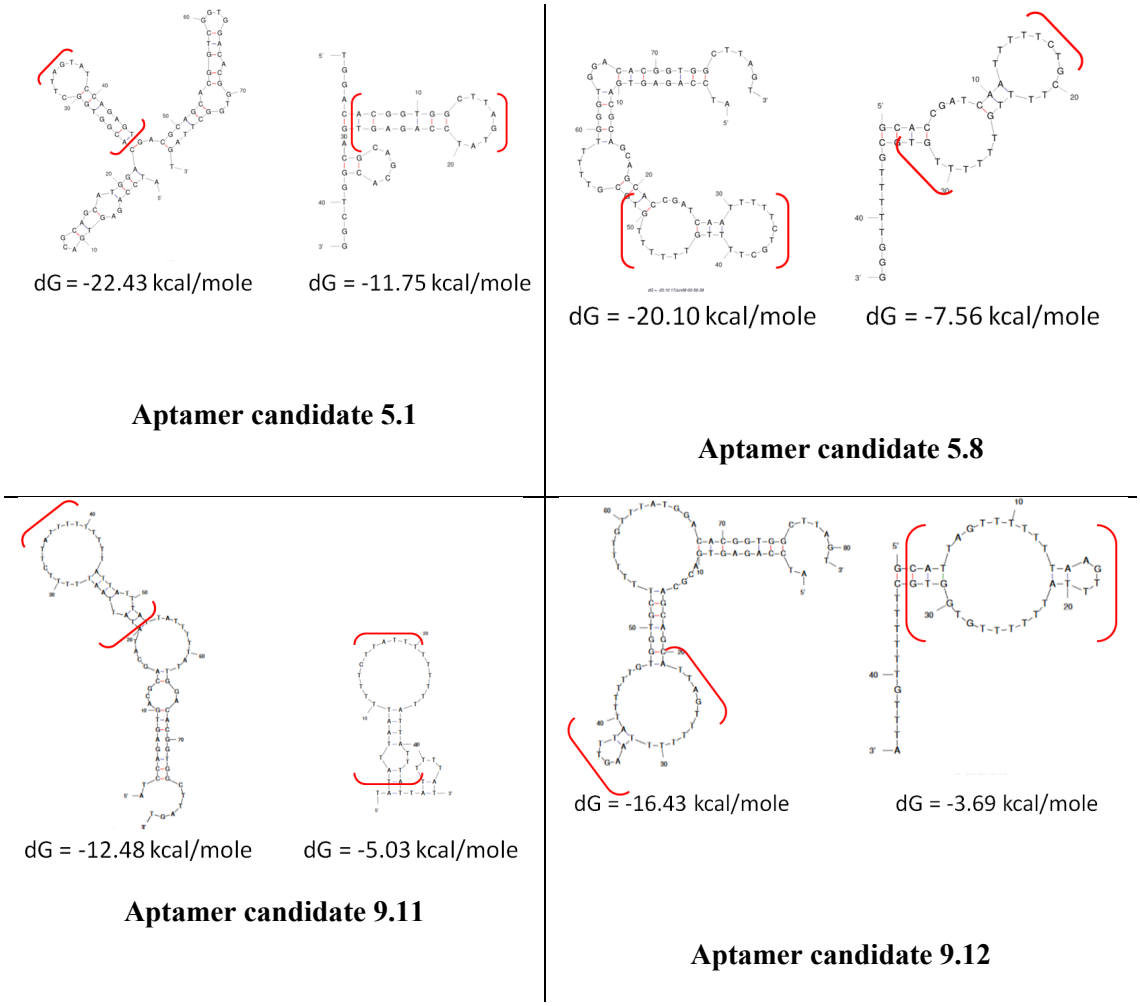

Figure 3.5. Secondary structures (predicted on *Mfold)* of aptamer candidates: structures for full length (left) and random region only (right) are displayed. Structures with the lowest free energy with loops similar/conserved for both lengths are shown in red brackets.

Oligo name	Sequence 5'-3'	Repeats*	Length nt	MW g/mole
5.1	TGGACACGGTGGCTTAGTATCC AGAGTGACGCAGCACGGTCGG	17	43	13349.7
5.8	GCACCGATCAATTTTTCTGCTTT TGTTTTTTGTGCGTTTTTGGG	5	44	13503.7
9.11	TATATTAATTTTTCTTATTTTTT TTTATTATTTATTATTTTTAT	17	44	13397.8
9.12	GCATTAGTTTTTTTAAGTTTATT TTTTGTGGTGCTTTTTTGTTTA	21	45	13851.0

Table 3.5. Aptamer candidates selected against breast cancer stem cells using FACS-SELEX

*- times of this sequence among all the tested clones

3.4.3. Imaging flow cytometry (IFC)

Both FACS and confocal microscopy are widely used methods for characterizing binding of the selected aptamers with cells as exemplified by numerous studies in the field (18, 129, 135, 136, 333). IFC analysis is a powerful tool which combines speed and statistical capabilities of flow cytometry with imaging features of microscopy (344). Since every particle which passes through the flow cell is automatically recorded, this eliminates a potential bias from an operator's side during analysis (344). Moreover, resulting images and their representative graphs are linked thus empowering an operator to perform a single-cell-based analysis at the click of a button (345). Given its capabilities, IFC can study cells for its morphology (size and shape), expression of different antigens, localization of the signal and its intensity (346).

While there are examples of using IFC such as localization of antigens in cells (346), studying cell-cell interactions (347), analyzing cell morphology change during maturation (348), intracellular parasite quantification (349), studying cells/structures with inherent fluorescence (phytoplankton (344)), the application of IFC in aptamer characterization is limited or even non-existent to the best of our knowledge. The use of aptamers in IFC was highlighted in the work by Nascimento *et al* (339) where sample preparation for imaging cytometry is considered identical to flow cytometry (except that in IFC cells being plated on slides). However, workflow or data analysis regarding the use of IFC for aptamer studies are not considered according to literature review. IFC system (ImageStream) used in this study is able to analyze several hundreds of thousands

objects in several parameters at the same time combining this with fluorescent microscopy imaging (350). After preparing aptamers and cells, incubating them together with Calcein violet, gating on focused events was done to select single cells from cell clumps and doublets (**Figure 3.6**). FCS gradient root mean squared histogram was used to gate in-focus single cells. Calcein violet AM aspect ratio histogram was used to remove dead cells and an overlay of histograms of cells stained with aptamers *vs*. controls. As can be seen from the figure, there is a slight shift in intensity of aptamer binding to target cells compared to control cells (breast epithelial cells). The binding of the selected aptamers has to be studied in detail using different concentrations of cy5-labelled aptamers in order to determine dissociation constant. According to **Figure 3.7** some aptamers are seen as a spot on the cells while others are internalized. Aptamers binding to spot on cells (not fully covering) and binding only to a fraction of cells is not a surprising phenomenon. Taking into account the principle behind SELEX, any molecular differences between the target cells and control cells might lead to an enrichment of aptamers which will bind to either all target cells or only a fraction of them (146). Similar to Palaniyandi *et al* (27) we also performed selection on ice but interestingly aptamers were shown to be internalized too. Aptamers with internalizing properties are promising tools for developing an effective drug delivery system in cancer therapy (28). **Figure 3.7A** shows live cells with high intensity on cy-5 channel (aptamer staining) and confirmed by imaging; **Figure 3.7B** shows those not confirmed with imaging and excluded from the study. Binding of only a fraction of the selected aptamer candidates was performed and analyzing other sequences might reveal better binders.

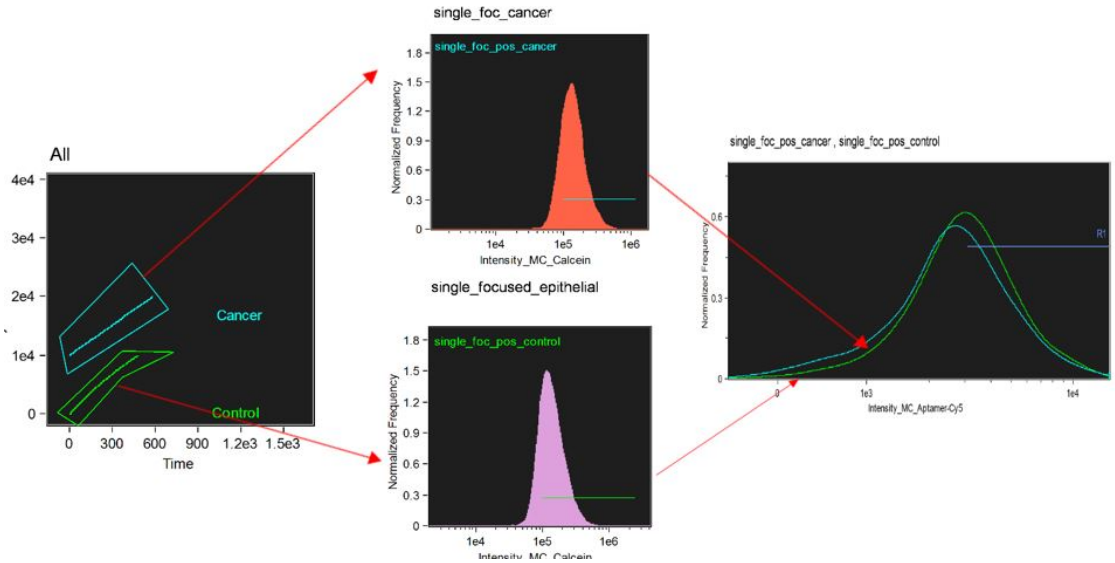

Figure 3.6. A scheme of gating for IFC analysis of aptamer binding to cell targets. (**A)** Cell lines gating; (**B, C**) Single focusing gating; (**D**) Overlay of cell lines (control and BSCS).

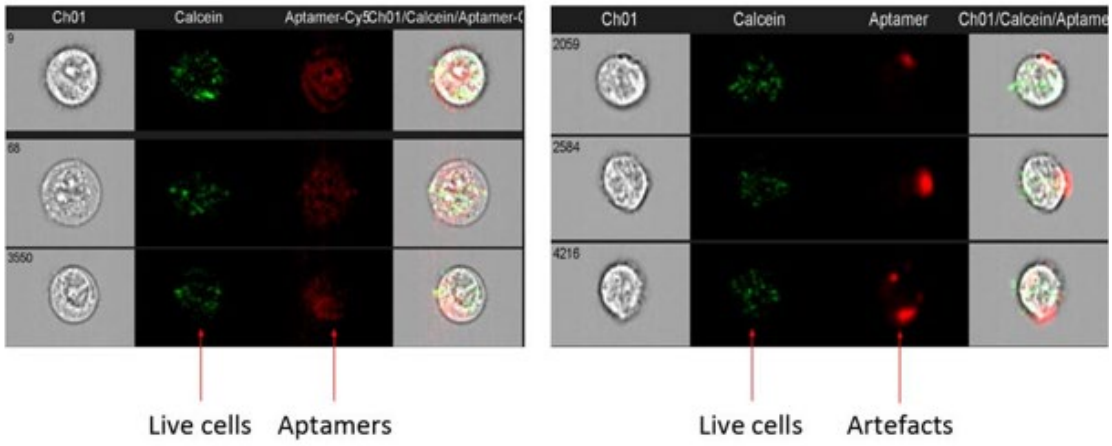

A **B**

Figure 3.7. (**A**) A gallery of BSCS cells stained with Calcein AM Violet; (**B**) A gallery of artefact staining with aptamers visualized by IFC. Ch01 – brightfield; Ch06 – calcein violet AM staining; Ch11 – cy-5. Magnification 60X.

3.5. Conclusion

BCSC play a major role in metastasis, relapse and recurrence of BC and therefore finding new ligands binding these cells is important in improving BC diagnosis and treatment. FACS-SELEX was employed to select aptamers against BCSC. DNA aptamers were selected against these cells using FACS-SELEX method and their binding was studied with IFC which showed that their higher affinity towards target cells than controls. Although, the binding of the selected sequences was not fully studied, to the best of our knowledge, this would be the thirdly reported synthetic ligands that were selected against BCSC (and not regular BC cells) and without the prior knowledge of its target (i.e. not aiming at binding to a certain marker). Moreover, cells used here have more described CSC-characteristics than the two reported works ((12) and (163)) and were originally derived from BC. This study is one of the first examples of using IFC in analyzing aptamer binding to cells. IFC is an emerging tool for analyzing aptamers raised against cells and a workflow for using this technique is given in this work. We believe that both fundamental and diagnostic (including therapeutic) studies will benefit from selection of new aptamers against BCSC and that IFC will be used more for aptamer-cell interaction analysis in the future.

CHAPTER 4. FUNCTIONALIZATION AND CHARACTERIZATION OF STAINLESS STEEL: TOWARDS DEVELOPING MEDICAL GUIDEWIRE TO DETECT BREAST CANCER STEM CELLS

4.1. Abstract

SS is a widely used metal in biomedicine including guidewires and stents; and could be used as a substrate to capture such small events in blood as BCSC after successful functionalization. Silanization is one of the widely used first steps in functionalization of SS before adding biomolecule on the surface. Before silanization of SS, a pre-treatment of the surface by electropolishing found to be important. Electropolishing distance and time were determined for a given electropolishing solution. Electropolishing also provides better substrates for surface analysis using AFM compared to non-electropolished samples. For silanization, parameters of electrodeposition such as applied potential, pH of the solution and heat treatment were explored. After silanization, SS was modified with crosslinker and CD44 aptamers which are against BCSC marker molecules. Together with AFM, SEM/EDS, CV could be used to study modified SS to overcome challenges associated with small size of the samples. The functionalized wire was shown to capture target cells compared to control wire.

This Chapter is part of an article published in Materials journal (MDPI) (30). My contribution to the manuscript (according to CRediT) is as follows: conceptualization (formulation of research goals and aims), designing methodology for functionalization of SS, validation, investigation (performing experiments on SS surface modification, characterization and data collection), original draft preparation, and writing the manuscript.

4.2. Introduction

The aim of this work was to functionalize SS wire with bioprobes with an ultimate goal of capturing BCSC. For this, wires were silanized with APTES and treated with GA before immobilizing bioprobes (DNA aptamers against CD44 protein) on the surface. Commercially available bioprobes (CD44 aptamers) were used for wire functionalization because characterization of aptamer candidates we selected took longer time than planned and could not be used when starting experiments on functionalization of wire.

The overviews of SS functionalization and surface analysis are shown in **Figure 4.1** and **Figures 4.2** respectively. Surface after functionalization was studied by fluorescent microscope, SEM/EDS, CV and AFM.

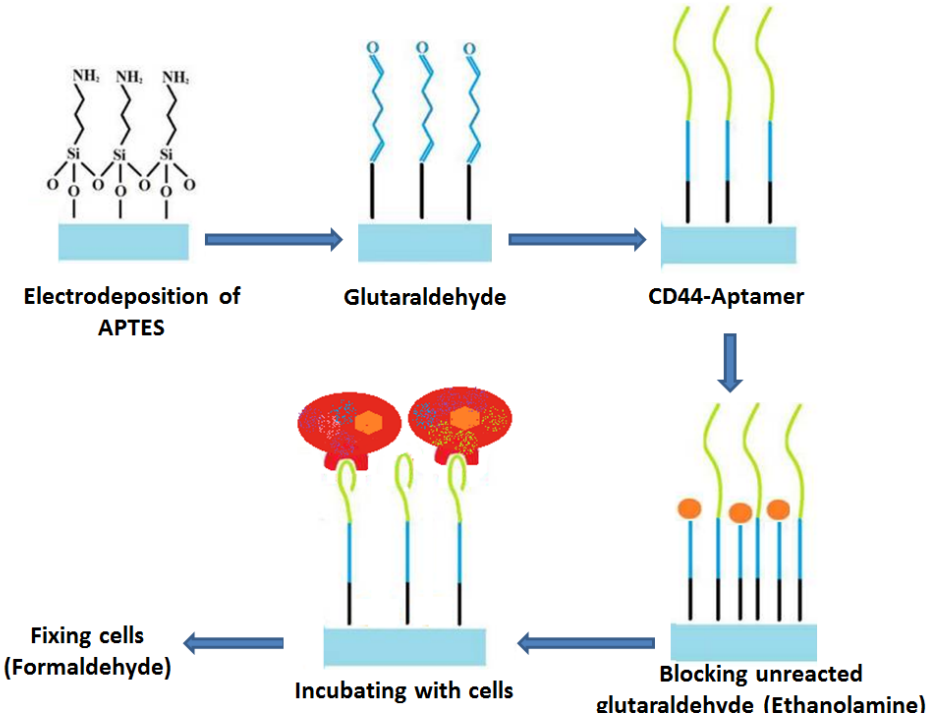

Figure 4.1. The overview of functionalization of stainless steel wire to isolate breast cancer stem cells.

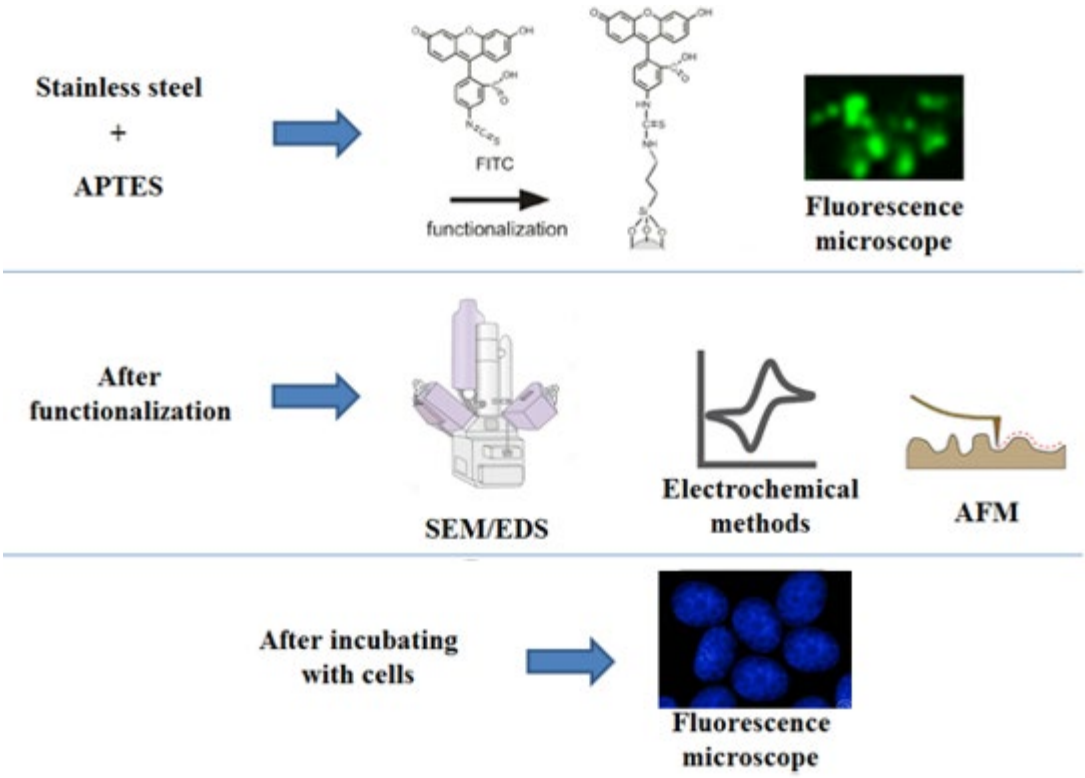

Figure 4.2. The overview of analysis of functionalization of stainless steel to isolate breast cancer stem cells.

4.3. Materials and Methods

4.3.1. Pretreatment of SS

Two pretreatment methods were used before silanization of the surface: sonicated (Sample: *Sonic*) and sonicated=>electropolished (Sample: *Elpol*). SS wires (316L SS from CrazyWire company) were cut (approximately 7-8 cm) forming a hook one side (for handling and better connection during electrodeposition) and washed with soap water. Then they were sonicated according to (351), briefly sonicated in water, acetone and ethanol for 10 min each with additional sonication in water. In electropolishing, flat SS wires were used as a counter electrode and reaction was performed under constant temperature (75-80°C) while keeping distance between electrodes constant (15 mm). Electropolishing solution was prepared according to (352) and consisted of 11 M H_3PO_4 and 4.5 M H_2SO_4. Potential of 1.8 was applied with PalmSens4 potentiostat (PalmSens BV). After electropolishing samples were washed in acetone and then sonicated in acetone and water for 5 min each.

4.3.2. Silanization of SS

Electrodeposition according to (353) (with modifications: nitrogen flow after electrodeposition, HT for 1 hour at 130°C, rinse in water for 2 min) (271)**.** Three electrode system consisting of platinum electrode (counter electrode (CE)), silver electrode (quasi-reference electrode (RE)) and working electrode (*Sonic* or *Elpol*) (**Figure 4.3**) using IM6 electrochemical station (Zahner elektrik). Silver electrode was coated with Ag/AgCl ink and heated at 70°C for 20 min in oven. Electrodeposition solution contained 0.02 M APTES (Sigma Aldrich, Germany) to which different volumes of 0.1 M HCl and ethanol were added (to get pH 4-6) for a final volume of 131 mL. The solution was hydrolyzed for 1 hour before being deposited. Constant negative potential (–0.6; –0.8; –1.0 or –1.2V vs silver electrode) was applied to samples for 30 min (353) then dried under N_2 flow and heat treated (Sample: *HT*) for 1 hour at either 70ºC or 130ºC in oven. After heat treatment (HT), samples were rinsed in water for 2 min to remove physiosorbed molecules (271) and cut for further analyses.

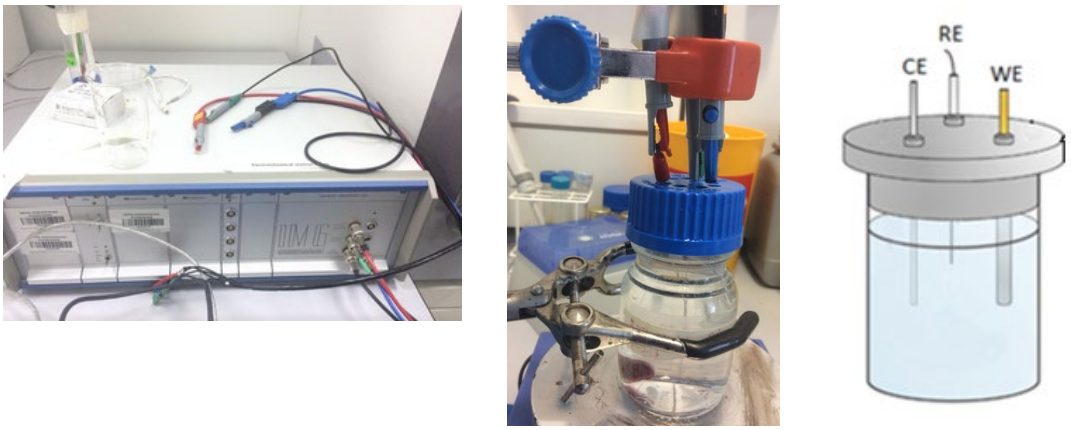

A **B** **C**

Figure 4.3. Setup used for electrochemical deposition of APTES on SS wires: electrochemical station (A); three electrodes in electrodeposition solution (B); schematic view of three electrode system (C). CE – counter electrode (platinum); WE – working electrode (SS samples); RE – quasireference electrode (silver).

4.3.3. Cyclic voltammetry

CV was performed in PBS (pH 7.4) containing 0.1 M KCl and 1mM $K_3[Fe(CN)_6]/K_4[Fe(CN)_6]$ with potential set from –0.6 V to 0.7 V and a scan rate of 50 mV/s. Three electrode system consisting of platinum electrode (CE), silver/silver chloride electrode reference electrode (RE) (3 M NaCl) (Zimmer and Peacock) and working electrode (*sample of interest*) used. Eight cycles were performed and the last one used for comparison.

4.3.4. Scanning electron microscopy (SEM) and Energy-dispersive X-ray spectroscopy (EDS) analysis

The samples were analyzed on one of the two SEM: FeSEM Auriga (ZEISS; Crossbeam 540) or JSM-IT200 (JEOL). Samples were attached onto carbon tape (Agar scientific G3348N) before analysis.

4.3.5. FITC analysis

HT samples were reacted with 125 µg/ml FITC in sodium carbonate/bicarbonate (pH 9.2) buffer for 2 h in the dark and washed with ethanol for 5 min and dried. Samples were then attached on glass slides and visualized on FLoid™ cell imaging station.

4.3.6. Immobilizing ligands

HT samples were further incubated with 5% GA solution in PBS for 1 h, washed with PBS and dried under nitrogen flow (Samples: *HT-GA*). To immobilize aptamers, amine-modified aptamers (2.5 µM) in binding buffer (50 mM Tris-HCl and 20 mM $MgCl_2$, pH 7.4) for 1 hour at 37°C and rinsed with BB dried under nitrogen flow (Samples: *HT-GA-Apt*). Amine-modified CD44-aptamers with the following sequence 5'-AmC6F]-CCAAGGCCTGCAAGGGAACCAAGG-3' (Sigma Aldrich, Germany) were used for immobilization. They were originally selected by SELEX (169) and then truncated in an *in silico* study (170). Unreacted aldehyde groups on wires are blocked by ethanolamine (0.5 M) for 15 min. After blocking, aptamer functionalized samples (*HT-GA-Apt-Block)* are rinsed with washing buffer (BB with 0.1% Tween 20). Samples are used immediately

or stored at 4°C in BB. Electropolished wire (no APTES) was used in all functionalization steps and treated as control samples (sample: *Elpol-GA-Apt-Block* or control wire).

4.3.7. AFM

High-resolution topographical characterization of the surfaces was carried out using SmartSPM 1000 (AIST-NT Inc., Novato, CA, USA) in AC-Mode (non-contact mode). All measurements were performed with a scanning rate 0.7 Hz; scan range was 5µm×5µm (2.5µm×2.5µm or 1µm×1µm) in X-Y; and height Z was set automatically. Super sharp type "NSG30_SS" cantilever, with a tip radius curvature of up to 2 nm, force constant of 22–100 N/m, and resonance frequency of 240–440 kHz in air (Golden Silicon Probes; TipsNano) was used.

4.3.8. Testing the Functionalized SS Surface to Capture BCSC

To test the ability of the functionalized wires to capture cells, BCSC used during selection of aptamers were grown, dissociated and filtered as discussed in Section 3.3.2. Cells (5×10^5 cells/mL) were incubated with functionalized and control samples for 30 min and then fixed with 3.7% formaldehyde (Sigma Aldrich) for 15 min and stained with DAPI (4′,6-diamidino-2-phenylindole). Wires were then visualized on a fluorescence microscope (FLoid™ cell imaging station, Thermofisher).

4.4. Results and Discussion

4.4.1. Pretreatment of SS

In the literature, SS surfaces which were successfully silanized with APTES were first mechanically polished (SiC paper polished, diamond paste until mirror polished (311); emery paper, alumina slurry polished (271)); some samples were bright anneal state, die cut (310) or surface finish (218) as shown in **Table 2.5** (Chapter 2). However, mechanical polishing was not possible to achieve given the small size of our wire. Apart from polishing, surfaces were also differently pretreated before incubation with APTES for increased surface hydroxyls and/or to get a smoother surface: treated in sulfochromic bath; electropolished or heat treated (HT). While sulfochromic bath (the combination of

sulfochromic and sulfuric acids) is harmful for both people and environment; and also not available in our facilities; other two methods need special pieces of equipment. HT offers an easier method; when this was tried for our samples, it indeed increased the surface oxides however failed to produce silanized surfaces (at least when HT samples were used for dip-coating as in (218) not electrodeposition as in later experiments). Hence, one of the available options was using electropolishing before silanization.

In this work, SS wires were electropolished under constant potential using phosphoric and sulfuric acid. Most of the reported studies on electropolishing SS have used SEM and or AFM for surface characterization (354). We also have used these two methods. SEM images of both wire (**Figure 4.4**) and a cathode (**Figure 4.5**) before and after electropolishing suggests successful polishing of the surface and dissolution of the particles to cathode respectively. Residual roughness features from manufacturing process (stripes) diminished due to electropolishing for 300 s; the overall diameter of the wire decreased from 162.5 to 140.1 μm as seen from **Figure 4.4**.

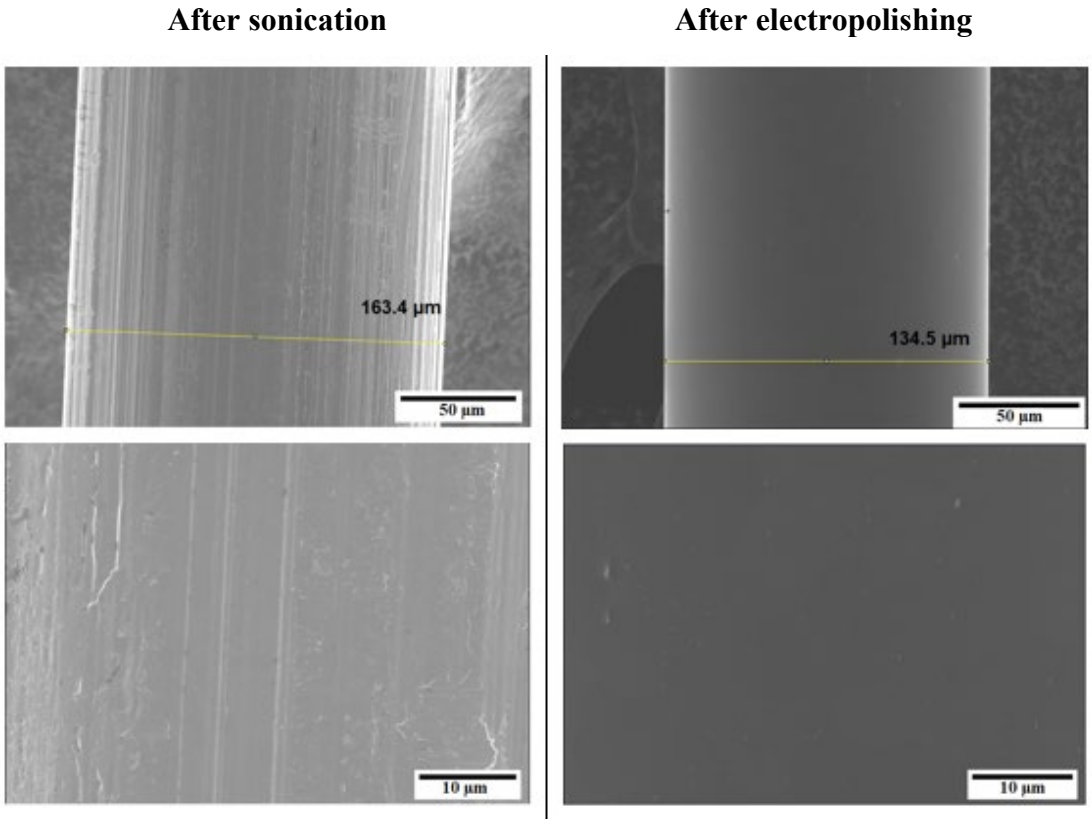

Figure 4.4. Scanning electron micrographs of wire before (**left**) and after electropolishing (**right**) (magnifications 500X and 2000X). The figure was published as part of the paper (30) (MDPI Open Access License).

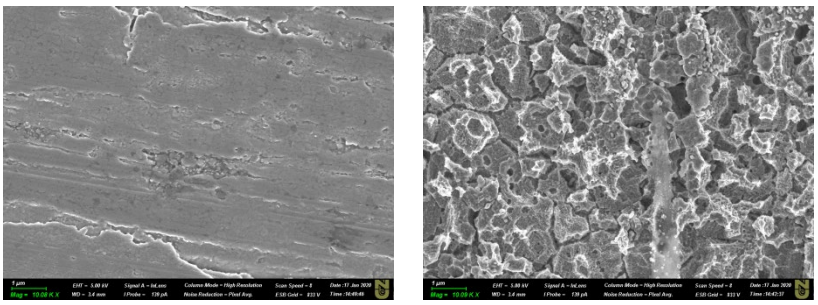

A **B**

Figure 4.5. Scanning electron micrographs of SS flattened wire before (**A**) and after being used as a cathode in electropolishing of six samples (**B**) (magnification 10k×).

Electropolished samples for 100 and 200s still have stripes from the manufacturing process (**Figure 4.6**). When all electropolished wires (100-300 s) were

visualized using secondary electrodes (SE) in SEM, no identifiable grain boundaries after electropolishing can be seen (**Figure 4.6**) similar to results obtained by (355). Also wire polished with closer distance to cathode (10 mm instead of 15 mm) leading to the surface covered with small holes formed possibly due to gas formation and pitting of the metal (results not shown).

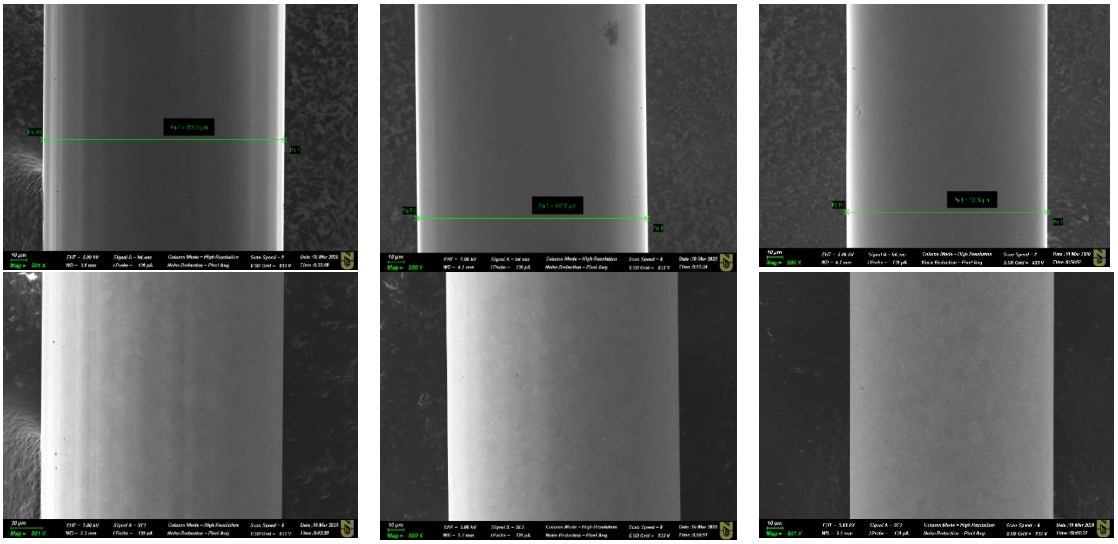

100 s **200 s** **300 s**

Figure 4.6 Scanning electron micrographs of wire after electropolishing for 100, 200 and 300 s (magnifications 500× and 2000×; Images using two detectors shown: InLens (upper) and Secondary electrode (lower)).

Studying samples after electropolishing with AFM further support the results of SEM of a successful electropolishing as seen from **Figure 4.7**. Large unevenness of the surface was levelled out by polishing. Stripes present on sonicated samples disappear and it becomes smoother.

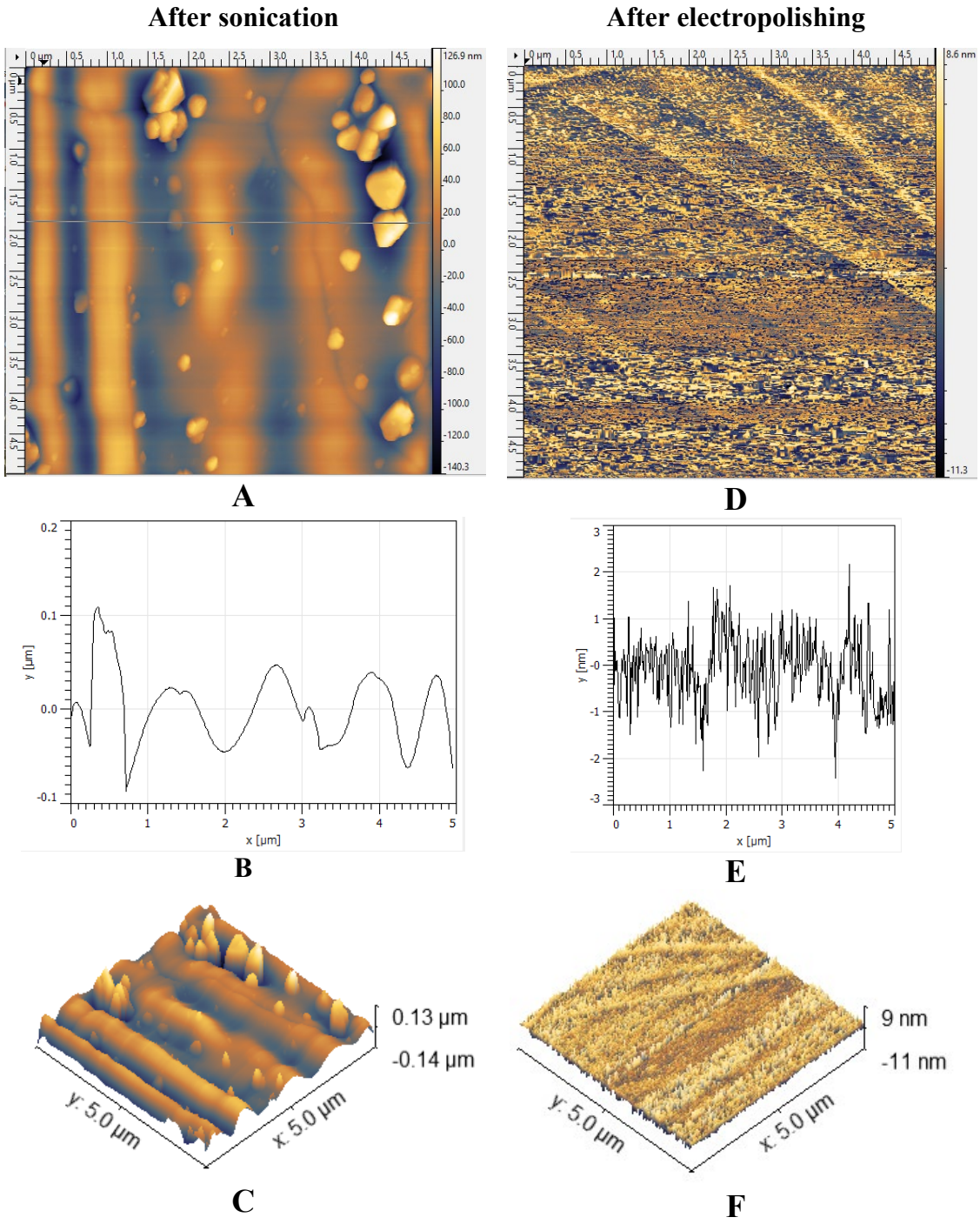

Figure 4.7. AFM micrographs of wire before (**A, B, C**) and after electropolishing (**D, E, F**). A and B: 5 µm × 5 µm; **B** and **D**: profiles of lines shown on **A** and **D,** respectively; **C** and **F**: 3D images of **A** and **D,** respectively. The figure was published as part of the paper (30) (MDPI Open Access License).

4.4.2. Electrodeposition of APTES: general considerations

Silanization of SS for further attaching biomolecules is a widely used method. Our first attempts of dip-coating SS with APTES were not successful. One of the alternatives was of attaching silane molecule on the surface is using electrodeposition. During electrodeposition of silane, applied negative potential causes the formation of hydroxyl ions which catalyze the binding of silane on surface (356). Electrodeposition of silane-coupling agents offers a more uniform coating (357), possibility of controlling thickness and coating geometrically complex shapes (353). During 3-electrode electrodeposition of APTES on SS, we used quasireference electrode (QRE). The use of QRE in nonaqueous solutions instead of RE is justified by the difficulty in finding an appropriate RE that will not contaminate the test solution. It is expected that in experiments where no essential bulk solution change occurs, the potential of QRE will also not change (358). Moreover, the porous frit of RE can be clogged by silane causing increased and irreproducible junction potentials (356). However, the potential of QRE will vary from experiment to experiment but especially in various electrolytes. The silane film formation *per se* will not be affected but variability in film thickness can occur (356). Several works on electrodepositing silane on metals (SS, gold, aluminum) or other electrode (glass carbon electrode) in nonaqueous solutions also report the use of QRE (353, 356, 359).

4.4.3. Electrodeposition of APTES: Applied Potential

AFM images of APTES electrodeposition on sonicated SS wires under different potentials are shown in **Figure 4.8**. The intrinsic surface roughness of sonicated sample does not allow properly analyze the surface using AFM after silanization (adding another reason to electropolish the surface before treatment). Therefore, the rest of samples describe here are electropolished ones. It is important to state, that finding a suitable method for surface characterization was important since some methods failed to produce good results either due to thin nature of our samples (FTIR, contact cangle measurement) or need to be further optimized (Raman spectroscopy).

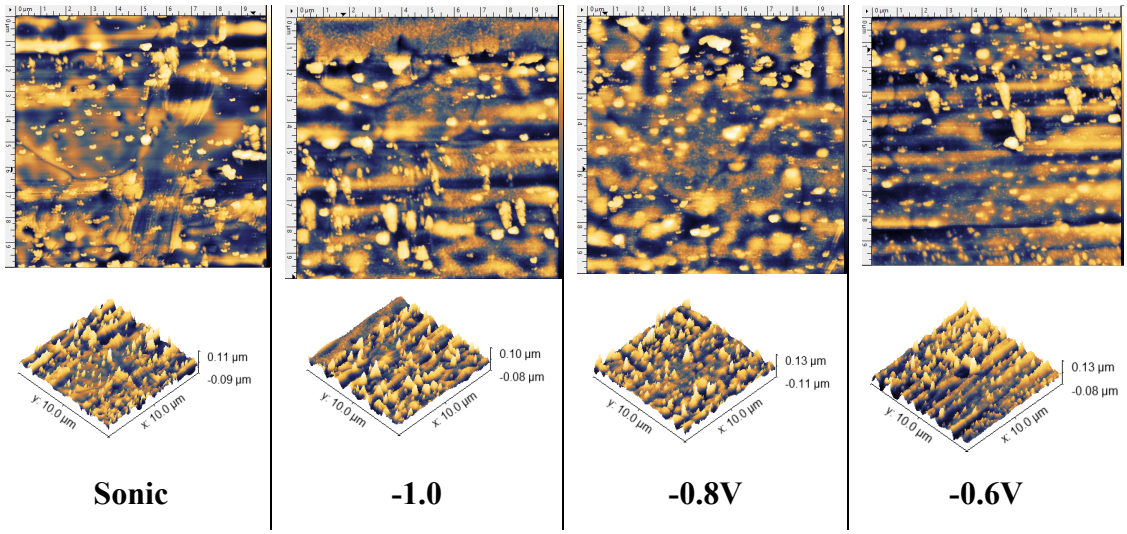

Figure 4.8. AFM images of APTES electrodeposition on sonicated SS wires under different potentials (10 µm × 10 µm and their corresponding 3D images). The figure was published as part of the paper (30) (MDPI Open Access License).

APTES electrodeposition on electropolished SS wires and their AFM images under different potentials (–0.6; –0.8; –1.0 and –1.2 V) were also studied **(Figure 4.9)**. Stabilized current density was observed for all potentials in the beginning except for –0.8 V where it first decreases and stability reached over time. Several papers also report a stabilized current density over time of electrodeposition: PEG400diIPTS on SS (222); copper coating on SS (360); cobalt on gold electrode (361), polyaniline on indium tin oxide (362) etc. Roughness of the surface increases as the potential becomes more negative from –0.6 to –1.2V **(Figure 4.9)** as shown by the increase in the root mean square roughness (rms) of the surfaces. Increase of the film thickness with more negative potentials was also reported by (353) (but for two silane-coupling agents used together) with more negative potentials; at –1.2 V irregular films are formed probably due to massive hydrogen evolution. Potential –0.8 V further studied in more details because of two reasons. Firstly, it produced more uniform surfaces with correct height of the particles as will be discussed further**.** Secondly, during electrodeposition at –0.8 V the chronamperometry graphs were decreasing and then stabilizing as in (222) (silanized poly-ethylene glycol on SS; although our graph not sharply decreasing) rather than being stable from the beginning.

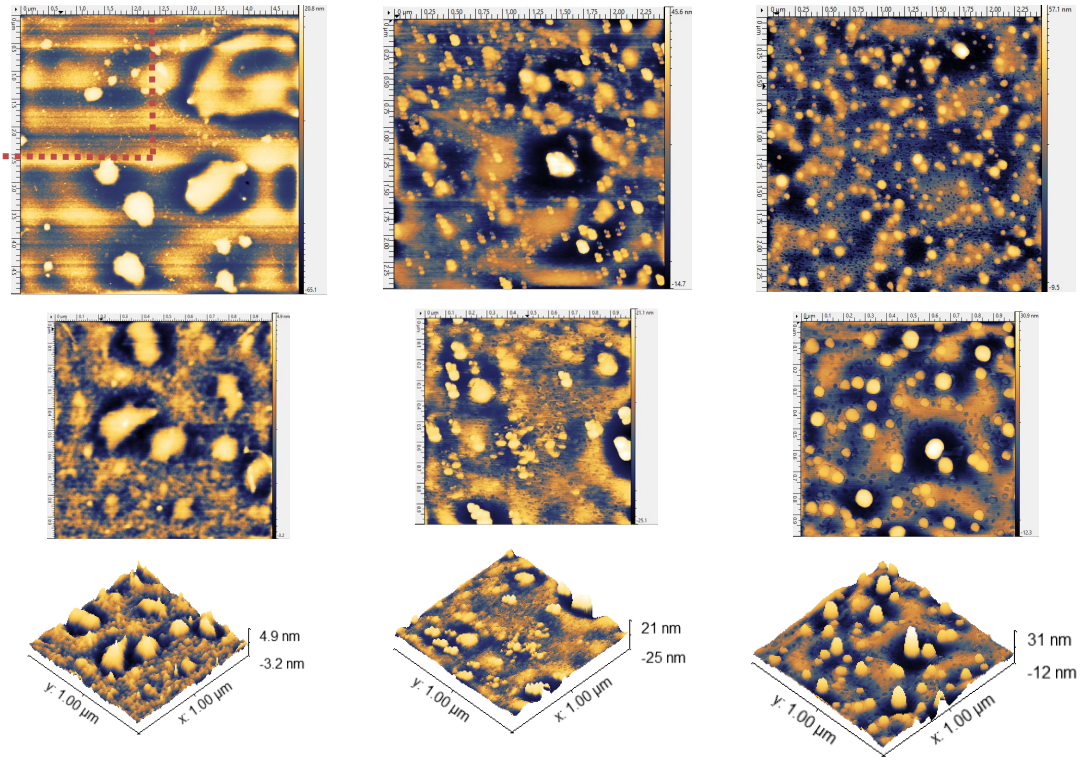

-0.6V

rms 721 pm

-1.0V

rms 2.4 nm

-1.2V

rms 3.6 nm

Figure 4.9. AFM images of SS after electrodeposition of APTES under different potential. From top to bottom: 2.5µm×2.5µm (for –0.6 V 5 µm × 5 µm); 1µm×1µm; 3D image of 1 µm × 1 µm. rms shown for 1 µm × 1 µm. Samples at -0.8 V are discussed further. The figure was published as part of the paper (30) (MDPI Open Access License).

To interpret AFM results of silanized surfaces, it was necessary first to decide what comprises the correctly silanized surfaces according to the literature results. Reported AFM results for surfaces silanized with APTES are different: value of 0.8 ± 0.1 nm was reported to be a good APTES film while higher than this value were polymerized APTES (363); Nevertheless, many studies report higher particle height with their further successful applications; these include 1.8 nm for APTES layer (364); less than 2 nm for a single APTES layer (365); and even ca. 14 nm (366). As reported by Howarter *et al* (367), particles of 1.5-2.9 nm correspond to 2-4 APTES layers when no

agglomerates or multi-island growth are present. Rms value of 9.6 ± 1.4 nm (368); rms of 3-4 nm (369) were also reported. Although some studies report roughening of the surface after APTES: rms of 0.69 nm increased from 0.51 nm (365). Increased roughness was attributed to multi-layer APTES but which was thin and stable (compared to other concentrations) and was successfully used for GA and antibody immobilization (365). Similarly, it was decided to consider APTES functional not only if the surface became smoother but also if it was uniformly covered and the range of particle size was 0.8-2 nm; and no or minimum of big sized particles (indicating polymerized APTES). Also, surfaces with particles with height of less than 0.7-0.8 nm were not considered silanized.

Another surface characterization technique which can be used for small diameter wires is CV. CV can show the changes in peak current and peak-to-peak separation after each modification step and this correlates with the electron transfer resistance of the surface due to the formation of film after surface modification. This indicates the formation of a non-conductive silanized layer on the surface (370). According to the literature, metals after silanization studied on CV most of the time block the electron transfer of redox couples in CV. Thus complete blocking was observed for SS stent covered PEGylated silane molecules compared to bare stent in CV (1 mM $Ru(NH_2)_6^{3+}$ in 0.1 M KCl) (222). Permeability of silane film (APTES plus tetraethoxysilane) electrodeposited on gold electrode also showed to decrease (5 mM $Ru(NH_2)_6^{3+}$) (371). APTES on SS when analyzed on CV (1 mM $[Fe(CN)^{6}]^{3-/4-}$ in phosphate buffer pH 5.0 with 0.1 M KCl) also lowered redox permeability (271). In case of bare SS electrodes studied in CV with redox couple, its shape is not a classical duck shape; but when SS was studied in PBS without redox couple a duck-shaped response was observed; in this case the control electrode (screen printed calomel electrode) was studied in PBS with redox couple (269). We used CV conditions as in (271) (buffer with 0.1 M KCl and 1mM redox couple; – 0.6 to 0.7 V) but with 0.01M PBS pH 7.4 (not pH 5.0 and 0.1 M) since it's widely used buffer for biological samples (to keep the functionality of aptamers/antibodies) and was used in several works to study silanized surfaces (372, 373)

The CV of wires silanized with APTES using different applied potentials is shown in **Figure 4.10**. The electron transfer resistance followed the following order: −1.2 V < Elpol < −0.6 V < −0.8 V, with −0.8 V producing the optimal silanized layer. The lower

electron transfer resistance at −1.2 V is likely due to a less uniform coverage of the surface and formation of larger particles, as shown on AFM (**Figure 4.9**). The samples silanized at −0.8 V showed the highest concentration of Si, C, and O in the EDS analysis and were further functionalized with aptamers. Sample −0.8 V which had more complete blockage of electron transfer between redox couple and electron surface in CV (green line vs. blue **Figure 4.10**) also had higher increase in Si and C and additional O in EDS analysis. These samples had an extra hook and more AgCl ink on Ag electrode during electrodeposition as compared to previous samples. Also, their chronoamperometry graphs were lower than other −0.8 V samples.

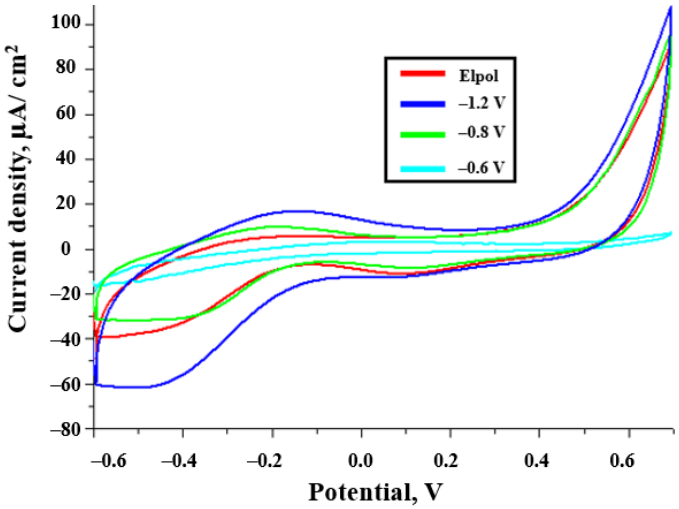

Figure 4.10. Cyclic voltammograms of electropolished SS electrode (Elpol) and silanized with APTES using different applied potentials (HT): −1.2; −0.8 and −0.6 V; CV done in PBS pH 7.4 containing 0.10 M KCl and 1.0 mM $[Fe(CN)^6]^{3-/4-}$ with a scan rate of 50 mV/s. Potential vs. RE (3 M NaCl).The figure was published as part of the paper (30) (MDPI Open Access License).

4.4.4. Electrodeposition of APTES: pH of the Solution

Apart from applied potential, the pH of the solution is an important factor for electrodeposition since it affects hydrolysis and condensation of APTES. Before being immobilized on metal, APTES solution has to be hydrolyzed to form silanol (Si-OH)

groups. However after hydrolysis, condensation can take place where it is polymerized and precipitated (374). It was reported by (375) that at pH 7 hydrolysis rate is minimal and at pH 4.3 condensation is minimum for APTES; where condensation is a base-catalyzed reaction. Minimizing silane concentration also minimizes its condensation (374).

In this work, we tried APTES solution with different pH values (measured by pH paper). AFM results of surfaces electrodeposited at –0.8 V using solutions with different pH values (pH 4–6) are shown in **Figure 4.11**. All surfaces silanized with various solutions are seen as covered on AFM. They have particles with 0.8-1.0 nm in height. However, at pH 4 and pH 6, higher particles (>6 and >10 nm respectively) and in case of pH 5.5 some particles with 4 nm size were formed. The most uniform surfaces are formed at pH 5.

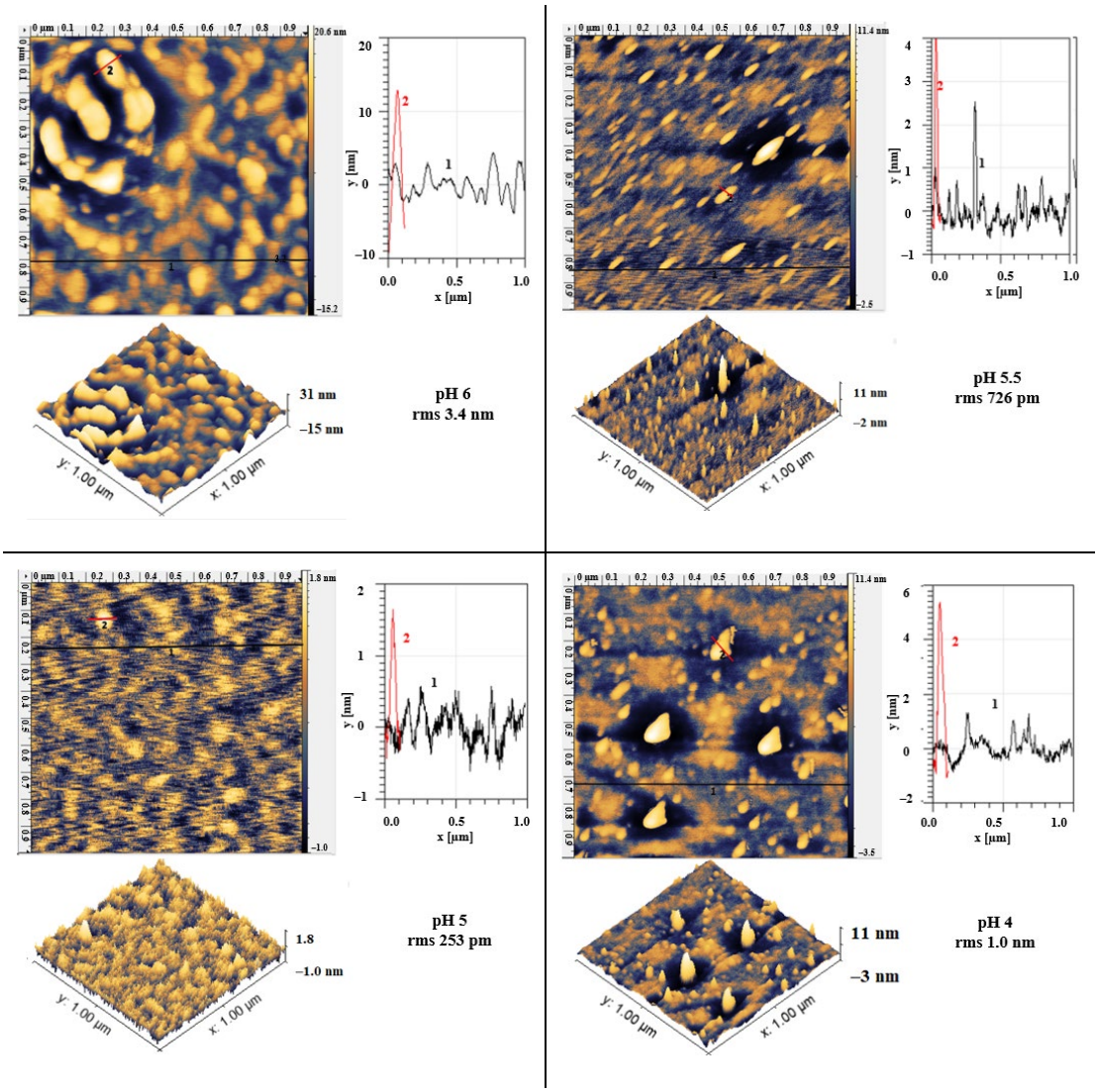

Figure 4.11. AFM micrographs of electropolished SS wires after electrodeposition of APTES at the applied potential of −0.8 V for 30 min in solutions with pH values of 6; 5.5; 5 and 4. For each pH value, 1 µm × 1 µm images, their 3D images and profiles along the lines are shown. The figure was published as part of the paper (30) (MDPI Open Access License).

Additionally to AFM, the presence of APTES on the surface was also studied FITC analysis, where samples are incubated with FITC. FITC is a fluorescent dye having N=C=S functional group which reacts with amine and thiol groups (376). FITC analysis is a fast qualitative method to show the surface has been silanized by APTES since it reacts with amine groups of APTES. In FITC analysis, two samples were used and the

results are seen in **Figure 4.12**. The control sample (Elpol + FITC) had lower signal intensity (autofluorescence) than the silanized samples (HT + FITC). Similarly, FITC analysis was used for qualitative analysis of various surfaces after silanization with APTES, including silicon oxide (376), poly(dimethylsiloxane) (377), nanoparticles (378), and titanium (379).

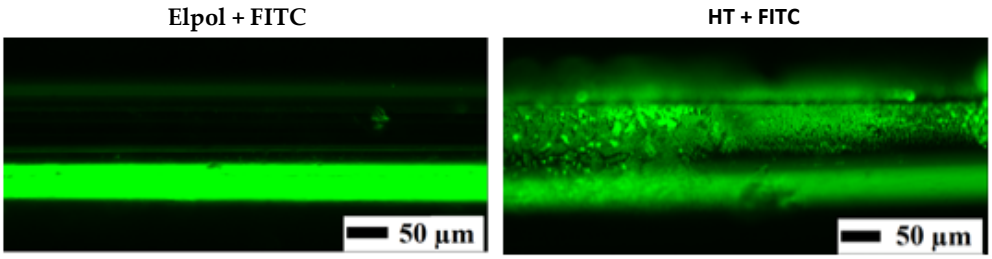

Figure 4.12. FITC analysis of the control (Elpol-electropolished) and silanized samples (HT) (electrodeposition at the applied potential of −0.8 V for 30 min) as visualized by fluorescence microscopy. The figure was published as part of the paper (30) (MDPI Open Access License).

SEM/EDS were also attempted for surface characterization of silanized wires. Observing silanized wires using SEM did not reveal much information. According to the literature, when surfaces (SS or other metals) silanized with APTES are visualized on SEM they are either smooth (353) or have some aggregates (particle size not reported but estimated to be 10-60 nm) (271, 380). For those that have aggregates, surfaces before silanization are not given and thus difficult to make a definite conclusion using SEM data. As opposed to SEM, EDS seems a more useful tool to study silanization. On EDS, the presence of APTES on nanoparticles was proven by the increase of C and Si in (381); more C, N, O and Si on nanopore (382); more C, O and Si on metal surface (383); more C resulting from the APTES hydrocarbon chain when on SiO nanoparticles (384). For silanized samples that also showed blocking in CV, an increase of Si (from to 0.70 to 0.83 at. %) when compared to Elpol was observed. For some samples, increased content of C (from 0 to 13.70 at. %) and O (from 0 to 3.77 at. %) was also observed.

4.4.5. Electrodeposition of APTES: heat treatment

Heat treatment after silanization is another important parameter to consider since it affects the covalent bond forming between APTES molecule and the surface. Two heat treatment temperatures (70 °C (269) and 130 °C (271)) were tested for HT after electrodeposition (**Figure 4.13A,B**) taken as the lowest and the highest reported in the literature. Analyzing the samples with AFM revealed that at higher temperature (130 °C) a more uniform layer of APTES was formed. At 70 °C, some larger particles (up to 4.5 nm) were seen. Additionally, FITC analysis of these samples showed that at 130 °C the surface had a more uniform and higher intensity signal for FITC than that of 70 °C (**Figure 4.13C,D**).

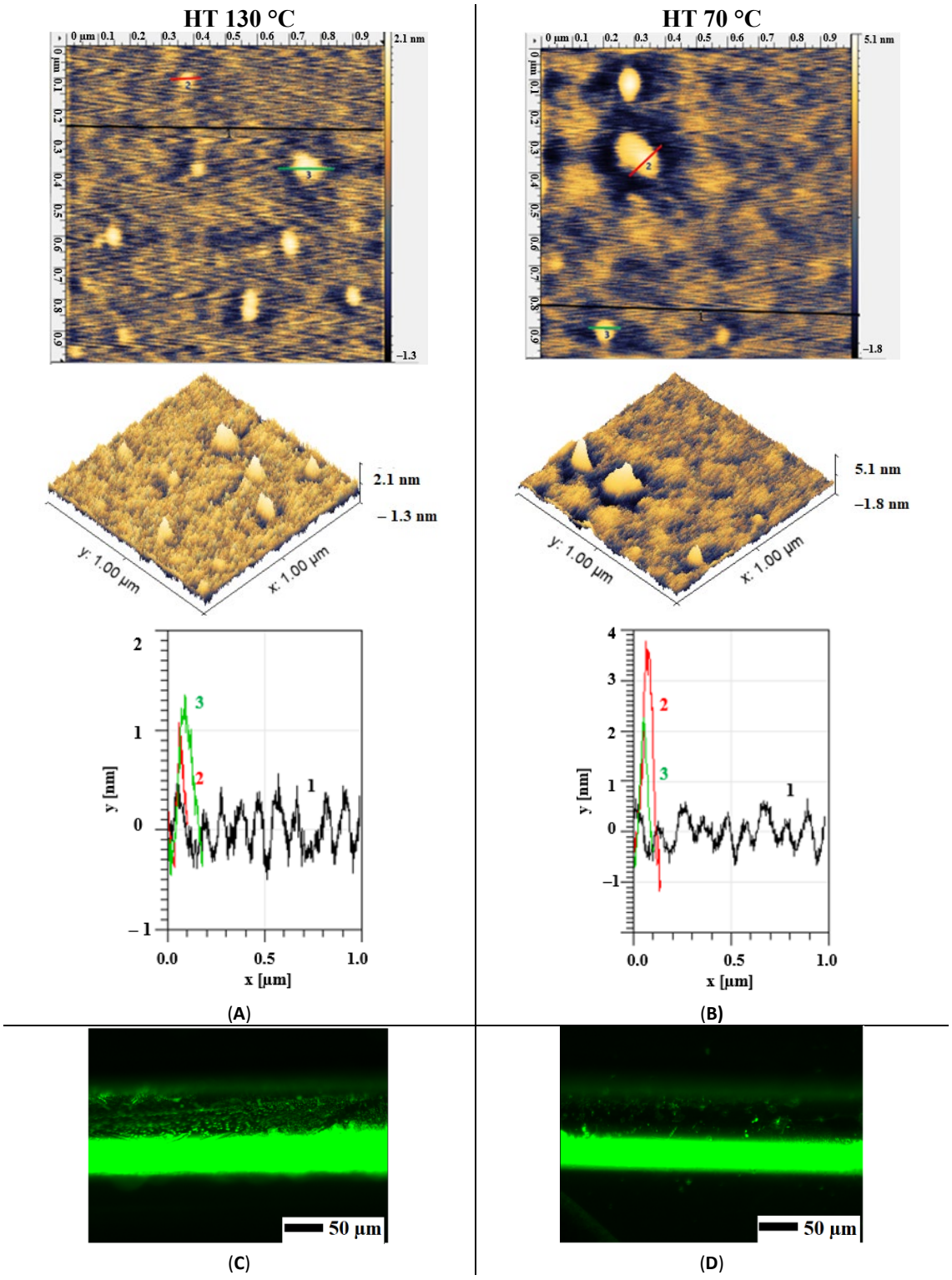

Figure 4.13. AFM micrographs (A,B) and FITC analysis (C,D) of SS wire at two different heat treatment temperatures (130 °C and 70 °C) after electrodeposition of APTES using −0.8 V vs. QRE. The figure was published as part of the paper (30) (MDPI Open Access License).

4.4.6. Immobilizing aptamers

In order to immobilize ligands on silanized surface, first it has to be crosslinked; in our case we used GA whose aldehyde groups (-CHO) can be used to form imines for further immobilization (325). After treating with GA, it is expected that the surface either retains the same rms: same rms as silanized surface (0.18 nm) (385); becomes smoother: smoother layer was formed after GA on cellulose membrane (from rms 0.830 µm to 0.524 µm) (386), smoother after GA on APTES (rms from 0.69 to 0.51 nm) (365). Although fewer studies report roughening of the surface (6.952 ± 2.555 nm) after incubating with GA resulting in evenly distributed nano-ridges (387). In this work, we also observed lowering surface rms (**Figure 4.14**). Surface roughness decrease after GA (rms) was from 0.1 to 2 nm across the samples.

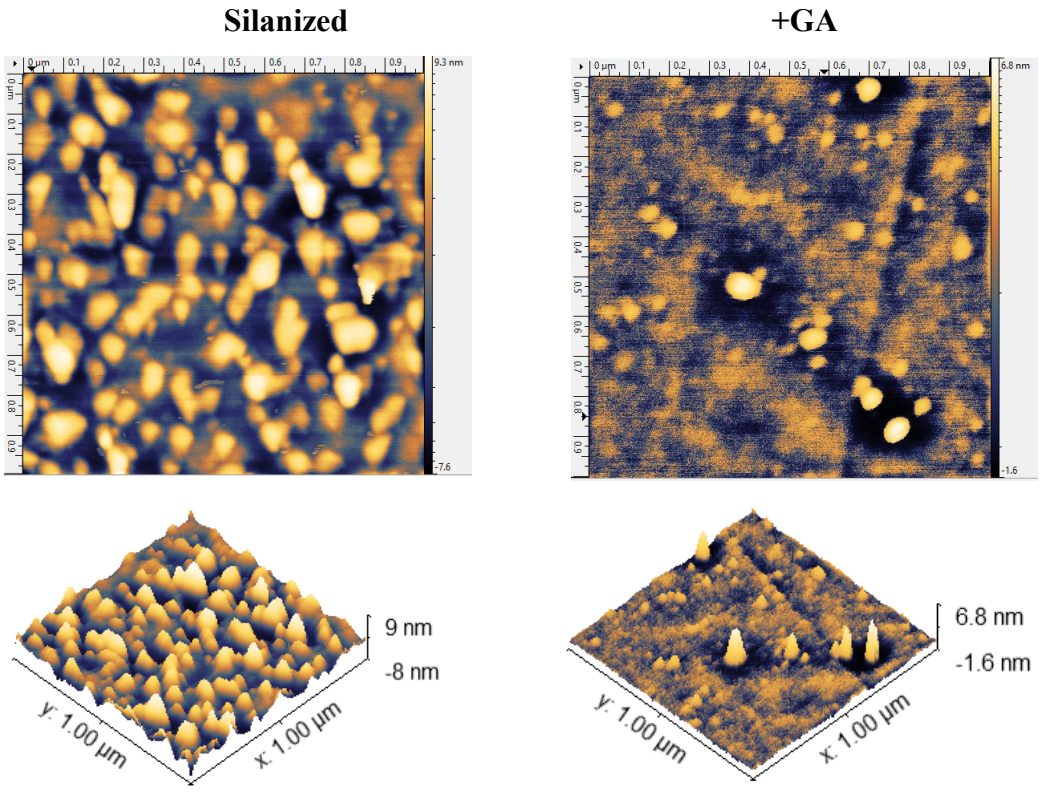

Figure 4.14. AFM images of silanized SS before and after treatment with GA. The figure was published as part of the paper (30) (MDPI Open Access License).

After incubation with GA, the samples were also analyzed using CV. Binding of GA on silanized wires was confirmed by CV where after GA, treatment of the HT sample lowered the peak current and increased the peak-to-peak separation (**Figure 4.15**). In the literature, when treated with GA, the electrode's (organoclay nanogold composite modified) (388) had lowered peak current and increased peak to peak separation. This was attributed to the insulating film of GA forming on the surface. Negatively charged GA had electrostatic repulsion with redox couple.

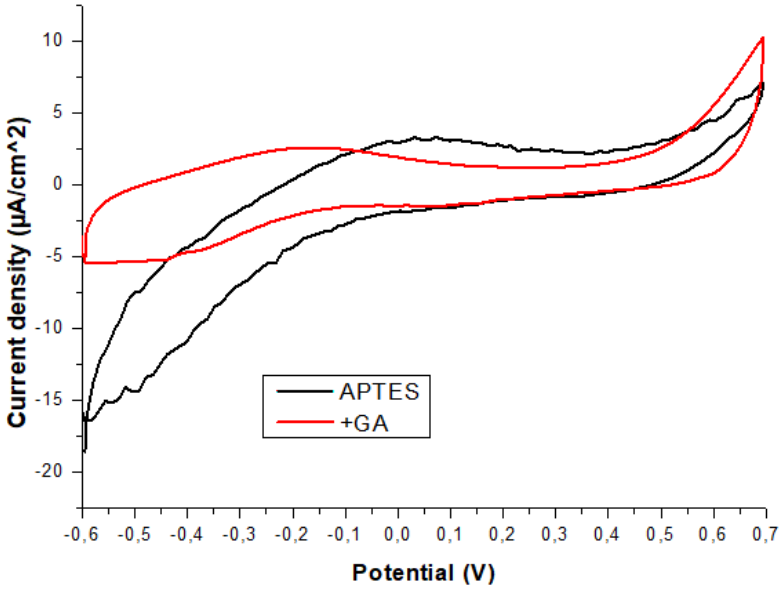

Figure 4.15. Cyclic voltammograms of silanized SS electrode after treatment with GA.

Silanization with APTES introduces amine groups and successive GA binding allows attaching either amine-modified aptamers. Commercially available aptamers were used instead of aptamers we selected (Chapter 3) since their binding with the target cells was not superior to other reported aptamers and binding analysis has not been done fully. CD44 aptamers were chosen as ligands for functionalization of SS wire since CD44 is an important BCSC marker and it is expressed in the target cells from Celprogen. CD44 protein is one of the firstly discovered and well-known markers of BCSC (389). Together with other two markers (absence of CD24 and presence of ALDH1), CD44 is present on cells with the highest progenitor abilities within the breast tumor cells (66).

In AFM, aptamer-treated surfaces showed smoother (mean roughness Ra from 1.46 for bare to 1.36 nm) (390) or rougher (1.79 nm for bare to 2.53 nm for aptamer)

(391) surfaces in two different studies. We also observed a range of different results: smoother, rougher or similar in surface topography **(Figure 4.16**) but all of them showed that surface was modified after GA.

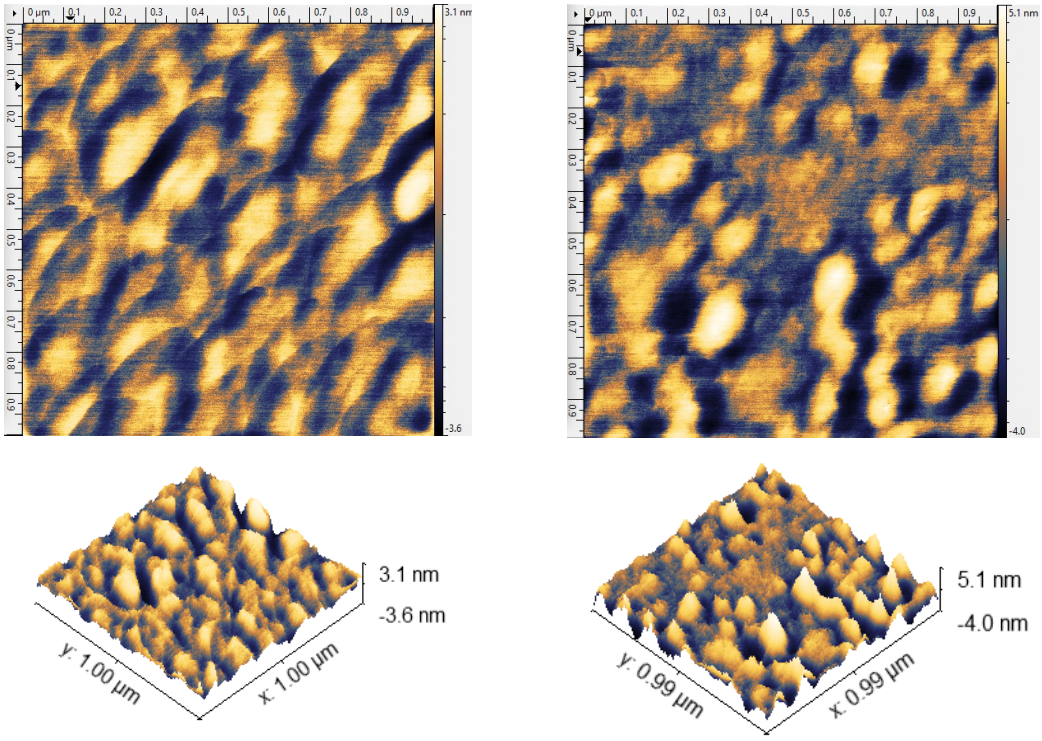

rms 604 pm rms 939 pm

Figure 4.16. AFM images of cross-linked SS (APTES+GA) before and after treatment with Aptamers. The figure was published as part of the paper (30) (MDPI Open Access License).

Studying aptamers on electrode with CV by Arya *et al* (390) showed lowering of peak current; while (392) reported slight increase of current compared to GA surface; and lowered peak current and peak to peak separation (393). In this work, aptamer treated surface also had lowered current (**Figure 4.17**) suggesting blocking of electron transfer between redox couple and the surface by aptamer layer.

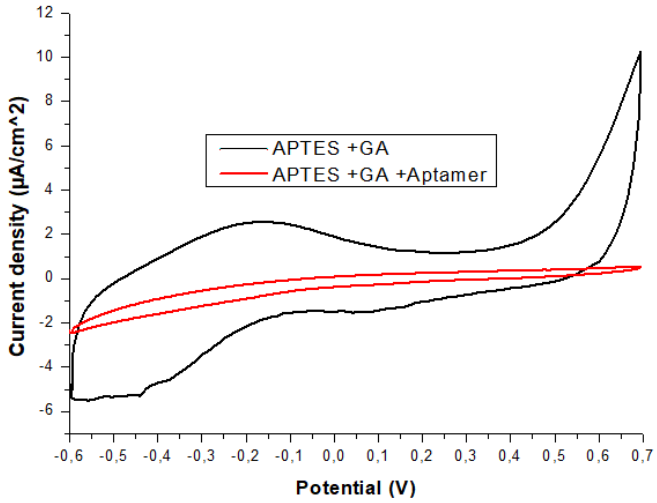

Figure 4.17. Cyclic voltammograms of silanized SS with crosslinker (APTES+GA) treated with aptamers (APTES+GA+Apt).

After attaching ligands, unreacted GA sites after treatment with the ligands were blocked with ethanolamine. Unfortunately, not many results could be found on ethanolamine (both CV and AFM) in the literature. Lowering of peak current and increasing of peak to peak separation in CV after blocking ITO/glass with ethanolamine (linked with fullerene) was reported (370). In AFM, after blocking ITO/ZnO with ethanolmine, rms increased slightly from 1.86 to 1.96 nm (394). However, our results showed a dramatic increase in peak current. AFM images of samples after blocking show the presence of big structures. Washing with higher concentration of Tween-20 (0.1 instead of 0.05%) seem to help reduce the structures. Some works observed that 1 M ethanolamine formed white opaque surface which was hard to wash without deteriorating the performance of the surface; ethanolamine concentration with optimal biosensor performance was 0.5 M (395). Blocking after aptamers resulted in various results in AFM in our work: same rms, increased and lowered. Given the results obtained on CV and AFM with 1M ethanolamine, its concentration was lowered to 0.5 M, Tween-20 concentration during washing was increased and samples were washed with BB before being tested with the cells.

4.4.7. Testing the Surface to Capture Cells

BCSC were chosen as target cells given their importance in BC diagnosis. These were well-characterized cells from patients with TN BC with a number of biomarkers and characteristics pertaining to BCSC as discussed in **Table 3.2**. **Figure 4.18** shows the results of fluorescence imaging of the fully functionalized and control wires after incubation with the cells. Cells (blue-stained nucleus) are captured more on functionalized wires than on control. The importance of this test lies in showing that a biocompatible material as SS wire (which can be inserted as standard guidewire) can capture target cells crucial in BC disease. In order to be fully used, a number of additional experiments are required: testing the wire in blood-mimicking flow system, using other cells not expressing CD44 proteins, testing using different BCSC concentrations.

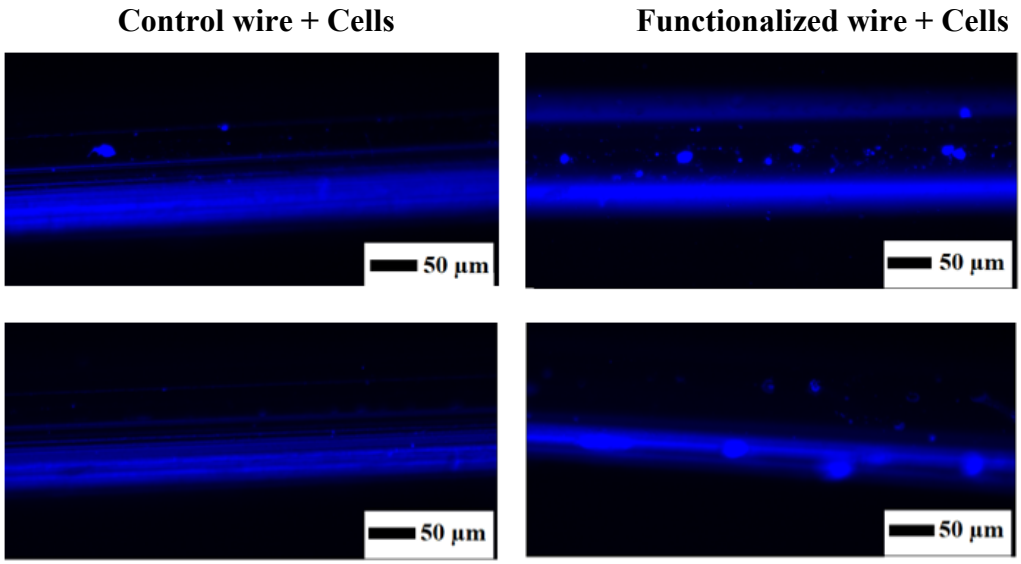

Figure 4.18. Ability of functionalized wires to capture BCSC by fluorescent microscopy. Images of control (left) and functionalized (right) wires after DAPI staining. Different areas of the same sample are shown. The figure was published as part of the paper (30) (MDPI Open Access License).

4.4.8. Conclusion

Electropolishing conditions for SS were determined including distance between anode and cathode, applied potential and time. Electropolishing resulted in a smooth surface which was also found to be important for characterization using AFM. For silanization of

SS, applying –0.8V in electrodeposition is better than other applied potentials (–0.6; –1.0 and –1.2V) and with increased applied potential surface roughness (rms) is increased and coverage is less even. Heat treatment after electrodeposition at 130°C give superior surface coverage compared to 70°C as demonstrated by AFM and FITC analysis. GA and aptamers were bound on the silanized surface according to AFM and CV. Electrodeposition, in terms of surface coverage, was better at pH 5 and 5.5 than at 4 and 6. Functionalized wire was able to capture BCSC as opposed to control wire when visualized on fluorescence microscope.

Small diameter wires, given their ability to fit standard catheter and being covered with aptamers against BCSC biomarker could be important in diagnostics. After further assessment, they could be used *in vivo* to capture such rare cancerous cells as BCSC by processing a large volume of blood. Performance of functionalized surfaces (including sensitivity and stability) depend on such factors as the orientation of ligands, surface density and analyte-binding efficiency of the ligands after their immobilization (396). The future works could focus on optimizing aptamer immobilization by studying such parameters as immobilization buffer, aptamer concentration, linker length. Moreover, it was shown that using bivalent aptamers for multimerization enhances the avidity of aptamers (397). Similarly, obtaining wires densely populated with aptamers with active sites is important to obtain functional surface with high affinity. In order to increase its avidity, a bivalent aptamer consisting of CD44 aptamers and another aptamer against BCSC markers such as CD133 could be constructed and immobilized.

CHAPTER 5. FUNCTIONALIZATION AND CHARACTERIZATION OF OPTICAL FIBER BIOSENSOR: USING A WELL-KNOWN LIGAND-ANALYTE SYSTEM

5.1. Abstract

This chapter describes a biosensor based on an EFBG and ETFBG for thrombin detection. Using a widely used model system in biosensor development, namely thrombin and thrombin-binding aptamer (TBA), the surface of optical fiber sensor was modified to explore the possibility of developing a biosensor. Although it is still far from the ultimate aim – sensing cells using OF biosensors, the work described in this chapter is important because it is a first optical fiber biosensor based on EFBG for thrombin detection. The sensing system itself consists of an FBG/TFBG which is made sensitive to surrounding RI via chemical etching. The achieved RI sensitivity of the EFBG was 17.4 nm/RIU (refractive index unit) and up to 23.38 nm/RIU for ETFBG. For selective detection of the analyte, the surface of EFBG was treated with APTES and GA before immobilizing TBA. The performance of the biosensor was investigated with thrombin concentration. Despite numerous examples of thrombin biosensors based on optical fiber grating sensors (e.g. LPG, TFBG), this biosensor offers a fast fabrication process requiring only chemical etching with further functionalization where no gold sputtering or chemical vapor deposition equipment is required. Moreover, both EFBG and ETFBG have more possibilities in being multiplexed.

The results reported herein were published as a research paper in Sensors (MDPI) Journal (31). Putting in terms of CRediT, my contribution to the above published paper is as follows: conceptualization (formulation of research goals and aims), designing methodology, validation, investigation (performing experiments and data collection), original draft preparation, and writing (review and editing). Part of the results were also published in Biosensors and Bioelectronics (Elsevier) (32) where my contribution was in developing silanization protocol, investigation and project administration.

5.2. Introduction

Thrombin is a protein which plays an important role in both pathological and normal blood coagulation with a normal concentration ranging from nanomolar to low

micromolar (398). Besides coagulation, its level can be increased during extra- and intravascular activation of blood coagulation by tumor cells (399). Thrombin is also involved in such diseases as atherosclerosis, thromboembolic disease, cancer and inflammatory disease (400, 401), and therefore detecting thrombin in blood is important both for research and clinical applications (402). Due to its clinical importance, there is a wide range of works aimed to detect thrombin and most of them are based on aptamers (398).

First thrombin binding aptamer (TBA) was described in a work by Bock *et al.* (104) who selected aptamers against human α-thrombin. Among the selected aptamer candidates, one particular aptamer consisting of 29 nt and a dissociation constant (K_D) of 100 nM, was widely used in the upcoming studies. In another study Tasset *et al.* (105) selected a 15-mer aptamer against thrombin with a K_D shown to be 0.5 nM, 200 times lower than 29-mer. When binding with the protein, both of these aptamers formed a G-quadruplex with the target with a difference in binding site: 15-mer binds heparin binding site of thrombin while 29-mer binds fibrinogen-binding site (403). G-quadruplex are stabilized by four Guanine (G) bases forming planar structure by Hogsten hydrogen bonding. Aptamers containing G-quadruplexes in their structures have such advantages as thermodynamic and chemical stability, no immunogenicity and nuclease resistance (404).

TBA-thrombin pair is a very widely used system to explore new biosensor possibilities. Using these two aptamers, numerous thrombin biosensors have been fabricated and they use aptamers coupled to different transduction schemes. such as chemiluminescence (405), electrochemiluminescence (406), electrochemistry (407), surface plasmon resonance (SPR) (408) and optical fiber gratings (409).

Shevchenko *et al.* (408) developed a thrombin biosensor using TFBG which was coated by a 50 nm gold layer. A thiolated, 15-mer TBA was attached on its surface by absorption. It was possible to distinguish thrombin from other control proteins (BSA, pepsin, human serum). Later, Han *et al.* (410) fabricated a modified version of thrombin biosensor based on TFBG. Here, fiber surface was coated with gold and then with SAMs of 11-mercaptoundecanoic acid and thrombin aptamers. After adding analyte (thrombin), a second TBA attached to gold nanoparticle was applied. As a result of this sandwich

type assay, there was an increase in transmission intensity change compared to a single aptamer format, thus improving the sensitivity of thrombin detection. A minimal cross-sensitivity to the outside temperature was observed for this biosensor. Moreover, the obtained K_D values were in a well agreement with those reported in the literature. Another study (300) focused on developing thrombin biosensor combining SPR effect with TFBG-based approach in a one sensor; it was able to detect small shifts due to analyte binding with high accuracy.

Two types of optical fiber biosensors were compared in their ability to detect thrombin (10 to 100 nM): LPG and plasmonic (SPR) (411). Compared to LPG biosensor, SPR biosensor showed higher sensitivity probably due to its higher sensitivity to RI and insensitivity to thermal variations. A work by Arghir *et al.* (322) studied an improved fiber functionalization method. The fiber was coated with APTMS to provide thiol groups before gold coating. When compared to reference fiber without silanization, the silanized fiber showed an improvement in gold adhesion; moreover, the superior chemical and mechanical stability as well as usability of the sensor were reported.

EFBG (or cladding-etched FBG) have also been recently investigated to measure RI (412). When ligand is immobilized on the EFBG surface and it interacts with the analyte, RI of the surface changes. This leads to a shift of Bragg wavelength and a change in grating reflectivity. Thus by analyzing FBG spectral changes (in transmission or reflection)the analyte concentration can be measured (291). EFBG fabrication using chemical etchants is a straghtforward and fast; the etchant itself (usually HF) is available and can remove the cladding from the fiber in a controlled way in short period of time. Another was of EFBG fabrication is through the use of laser micromachining station is not usually available in common laboratories and is less practical (413). Having less sensitivity to the change of the outer RI compared to TFBG, LPG or SPR-assisted LPG and FBG, EFBG has their own advantages. They are more simple in tuning their sensitivity to RI (414). TFBG and LPG work in a transmission mode, while EFBG measures reflection and does not need a polarization control (415). An additional step of fabricating a broadband mirror on the cleaved tip (often as a thin film) is required to them to work in reflection (300). Multiple resonance peaks of LPG limited its multiplexing capabilities; its broad line-width at full-width at half maximum also puts some limitations

on its measurement accuracy (416). Studies on improving the gold adhesion for plasmonic optical fiber sensors are being researched (322) but this still does not alleviate the need in special equipment to deposit gold (322) or the use of gold nanoparticles (417). Alternatively, the glass surface of EFBG can be silanized with different silane-coupling agents producing different functional groups for further immobilization of bioreceptors without the need of deposition of gold layer. Due to these advantages of EFBG sensors, we aimed at using it as a platform for biosensor development. In this chapter, we report an EFBG-based biosensor based on a grating which operates in the third optical window. TBA and thrombin were selected as a ligand-analyte system due to its well-characterized nature and high affinity of the ligand towards the analyte.

5.3. Materials and Methods

5.3.1. Materials

For EFBG, single-mode pure silica fibers (SMF-28C, 10/125 μm core/cladding diameter) were purchased from Technica S.A. They had inscribed Bragg gratings (1.0 cm length, >90% reflectivity, ~1550 nm central wavelength) in their sensing region. TFBG photo-inscription was made as described in (32). The following reagents used in this chapter were purchased from Sigma Aldrich: oleic acid, APTES, GA, phosphate buffered saline (PBS), thrombin protein, sulfuric acid. Sucrose, acetone, sodium dodecyl sulfate (SDS), BSA, Tris-HCl, KCl, $MgCl_2$, NaCl were from ThermoFisher Scientific. TBA with amine modification on its 5'-end (5'-AmC6FTTTTT-AGTCCGTGGTAGGGCAGGTTGGGGTGACT-3') was synthesized by Sigma Aldrich. Buffers used for experiments are shown in **Table 5.1**.

Buffer name	Used in step	Composition	Reference
Sodium citrate buffer	Resuspension of stock thrombin protein	100 mM sodium citrate, 100 mM citric acid	*
Affinity buffer	Sensor-aptamer + thrombin	50 mM Tris-HCl pH 7.4, 250 mM NaCl, 5 mM $MgCl_2$	(105)
Measurement buffer	Regeneration	10 mM Tris-HCl pH 7.4, 100 mM KCl	(411)

Table 5.1. Buffers used for fabrication of EFBG biosensor for thrombin detection

* - manufacturer's recommendation

5.3.2. Setup

Figure 5.1 shows the setup used for the development and interrogation of the thrombin biosensor. An FBG sensor was attached to a stick (which is resistant to solutions used during functionalization such as HF, Piranha solution) and was calibrated and treated as mentioned further. The peak wavelength shift and the reflection spectra of FBG during calibration, functionalization and analysis were measured using a si255 optical sensing interrogator (Micron Optics Inc.). Having a resolution, of 8 pm over 160 nm bandwidth (20,000 points for wavelength grid), it is able to distinguish area of 8 pm between two detected signals. Interrogator has eight physically separated channels which allow obtaining signal from eight different sensors at a time. The light source of this interrogator system consists of a wide-range swept wavelength laser; it can scan a range of wavelength from 1460 to 1620 nm. EFBG spectra throughout fabrication and functionalization steps, as well as during real-time detection of analyte have been detected by the instrument. The interrogator performs the spectral measurement of the reflection spectra of each grating; A signal processing technique (described in (418)) named the centroid demodulation of the spectrum was used to estimate the Bragg wavelength from the EFBG spectra. This technique allows achieving a LOD of ~0.2 pm.

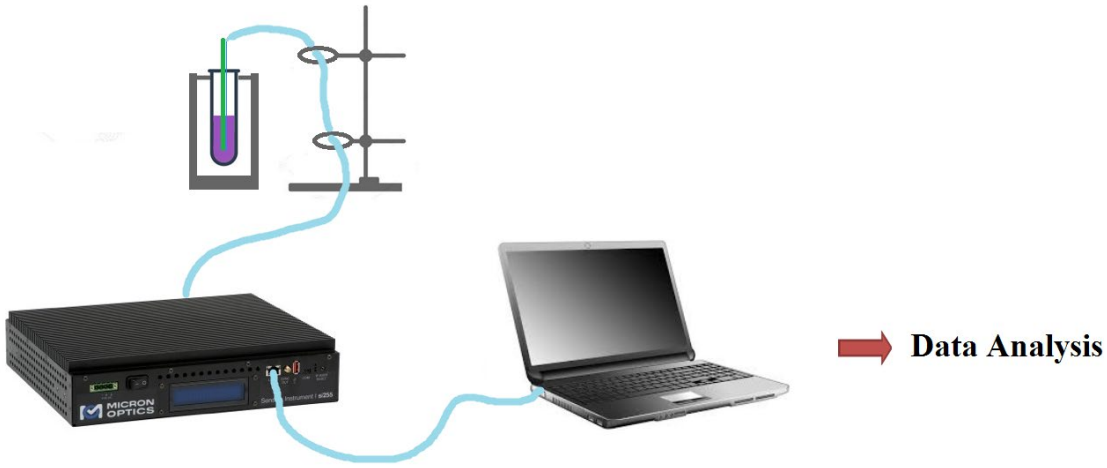

Figure 5.1. Setup used for developing a thrombin EFBG biosensor: EFBG was attached to a plastic stick (shown in green) and connected to optical sensing interrogator for data acquisition during measurements before data analysis.

For ETFBG, its peak wavelength shift and the reflection spectra of the ETFBG were measured on Optical Backscatter Reflectometer (OBR 4600, Luna Inc.). This OBR has a resolution of 8 pm, and operates in a wavelength window from 1530 to 1616.4 nm with an operating in distributed sensing mode at a speed of 3 Hz.

5.3.3. Etching and calibration

The buffer coating surrounding the FBG was stripped with stripper and the layer protecting the active sensing area was removed using acetone. To ensure that etching occurs in the tip and protect the fiber from mechanical damages, the sensor was attached to a plastic stick (diameter about 4 cm; length 20 cm). The grating area of the sensor was then etched in an HF solution (48% concentration) topped with oleic acid (for protection of the etched fiber and the environment (292)) in a fume hood (Waldner Secuflow airflow controller) at room temperature (25°C). After etching, EFBG was calibrated in solutions with different RI: sucrose in water (1.5; 3.1; 6.2; 12.5; 25.0 and 50.0% weight/volume (w/v)). In our studies, we used calibrated solutions of sucrose with estimated refractive indices according to (419). In total several FBG sensors were etched and calibrated. TFBG was also etched in HF and calibrated in sucrose solutions with known RI.

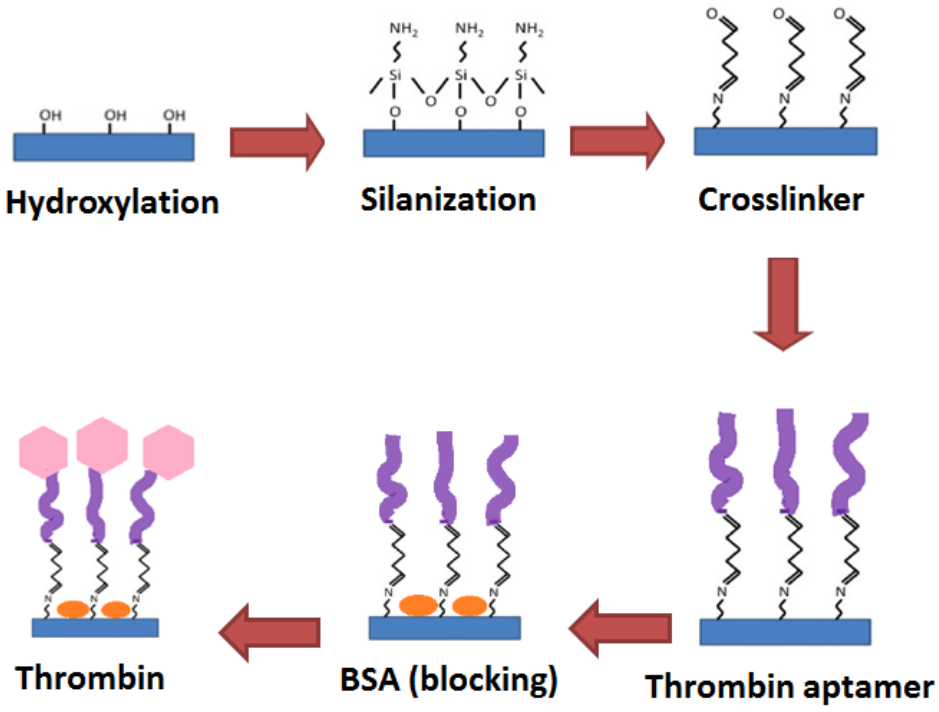

Figure 5.2. Schematic overview of thrombin biosensor based on etched FBG.

5.3.4. Silanization of FBG sensors

Schematic overview of thrombin biosensor based on etched FBG is sketched in **Figure 5.2**. EFBG was immersed into Piranha solution containing H_2SO_4:H_2O_2 (3:1 ration; v/v) in order to clean the surface and increase its hydrophilicity before functionalization. After treatment with Piranha, it was silanized with APTES (1% in absolute ethanol) for 30 min and then rinsed with ethanol. To catalyze the reaction between silica and the SCA, sensor was heat treated at 110°C for 30 min and incubated in 25% GA in PBS for 1 hour (420) and washed in water (421). Immediately after treating with the cross-linker, sensor was treated with aminated thrombin aptamers for 4 hours. To wash away the unbound aptamers, the surface was washed with 0.2% sodium dodecyl sulfate in PBS. In order to reduce non-specific binding, it was blocked with 1% BSA in PBS for 30 min. In order to test the performance of biosensor, EFBG with immobilized aptamers was incubated with thrombin protein in different concentrations (10, 20, 40, 80 nM in affinity buffer) for 2 hours each. ETFBG was silanized and cross-linked similar to EFBG as above and then

incubated with aminated aptamers for at least two hours. After functionalization, it was used to measure thrombin in different concentrations (0.625 to 40 nM in PBS) for 15 min.

5.3.5. AFM analysis of the functionalized surface

Topography of the surface was studied using AFM as described in Section 4.3.7 with the following modifications: scan range 1500 nm in X-Y with scanning rate 0.2 Hz.

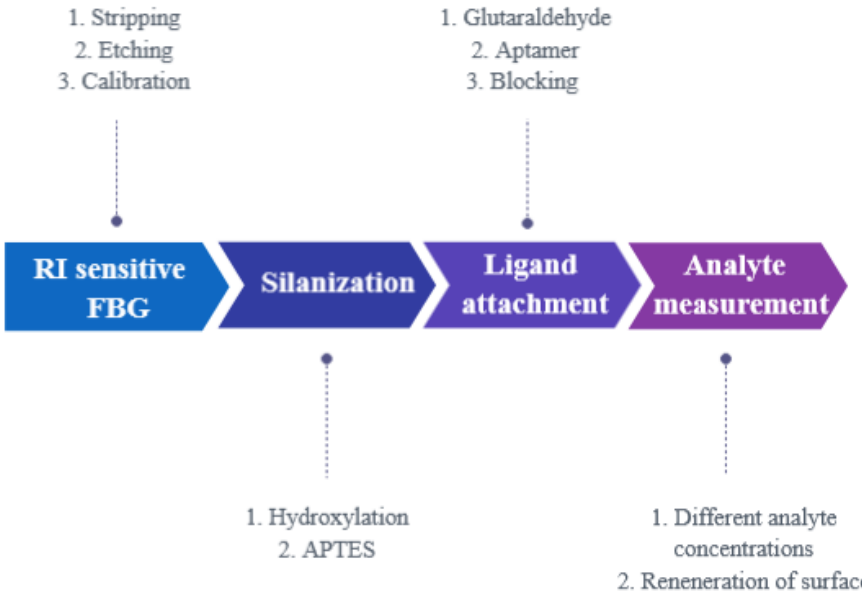

Figure 5.3. Overview of developing biosensor based on etched FBG

5.4. Results

EFBG biosensor was fabricated according to a schematic shown in **Figure 5.3**. In order to remove the cladding and make the FBG sensitive to the surrounding RI, it was immersed in a solution of HF at 48%, maintained at room temperature in a fume hood. As a result of etching, diameter of cladding is reduced progressively and sensitivity starts to appear. **Figure 5.4**. shows a shift of a Bragg wavelength from the original FBG (1549.98 nm), after the grating has been etched to a diameter of approximately 25 μm. Etching results in a change of both wavelength and a reduction of FBG peak: wavelength shift of -2.1 nm and 11.6 dB reduction. This corresponds to the evanescent wave effect of the etched sensor, resulting in this extra attenuation on both the forward and backward waves.

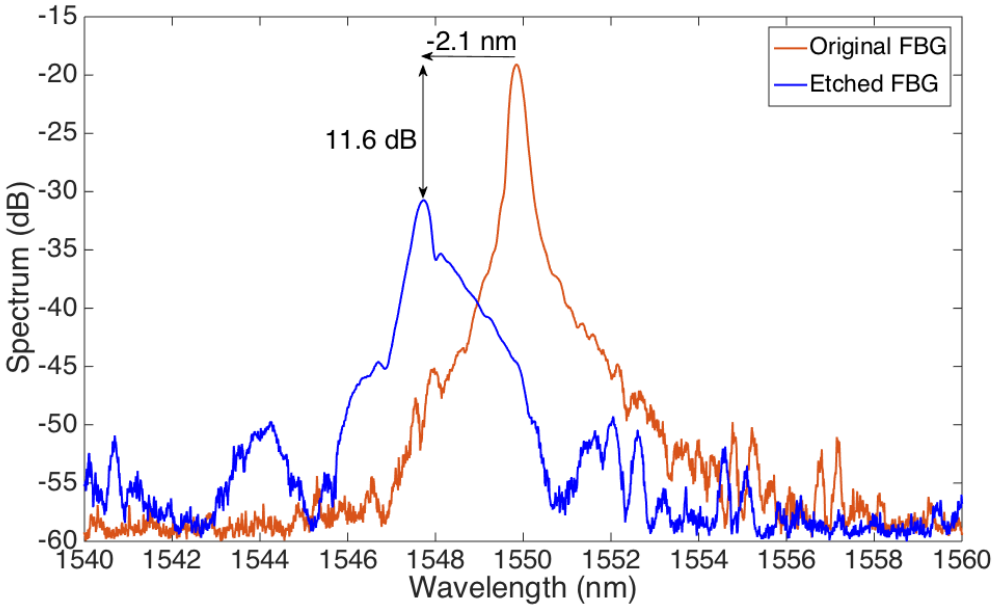

Figure 5.4. Spectra of the FBG prior etching and after etching the FBG using hydrofluoric acid. The graphic shows spectra observed on the FBG interrogator. The figure published as part of the paper (31) (MDPI Open Access License).

EFBG was then calibrated for determining its sensitivity to RI using a method previously used in (415). This was done by immersing it into water/sucrose solutions (1.6%, 3.1%, 6.3%, 12.5%, 25.0%) with different RI; the RI change is ~1.85×10-3 RIU for each 1% of sucrose, for such values of RI. As seen in **Figure 5.5**, when the RI increases, the wavelength shifts towards the longest values. As a result, an estimated sensitivity of 17.4 nm/RIU and linearity coefficient 0.993 is obtained.

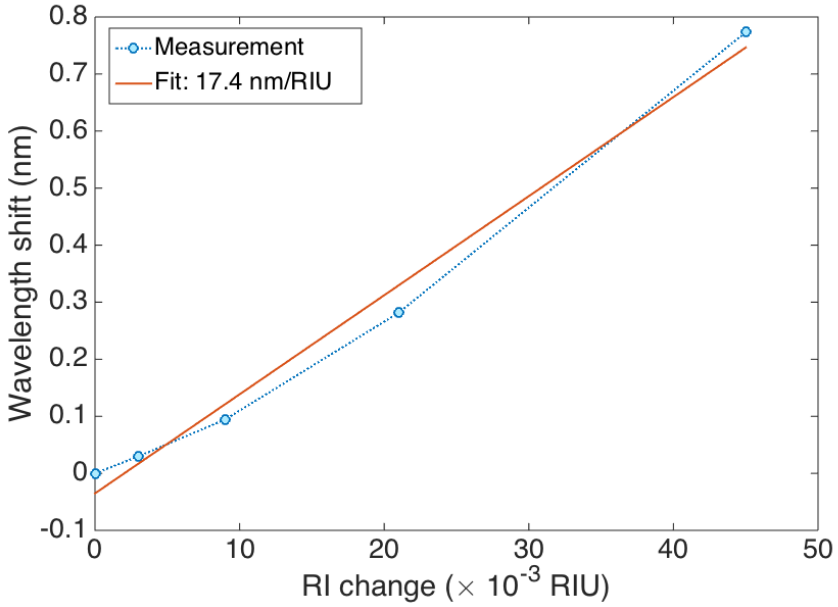

Figure 5.5. Results of calibration of the EFBG using sucrose dissolved in water (1.5; 3.1; 6.2; 12.5; 25.0 and 50.0% w/v) which have different RI and the corresponding wavelength shift (1.5% set at 0). Sensitivity (17.4 nm/RIU) is estimated using linear regression. The figure published as part of the paper (31) (MDPI Open Access License).

In order to confirm surface modification, the surfaces of control samples which were treated the same way as sensors, were studied on AFM using a super-sharp cantilever. **Figure 5.6**. shows high-resolution AFM topographical images of control etched glass optical fiber surfaces without treatment, treated with APTES and GA. An increased roughness of the surface with the larger particles can be seen from the figure.

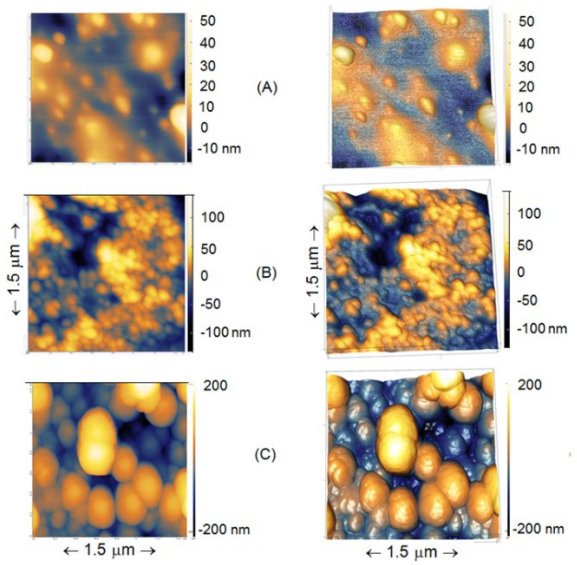

Figure 5.6. High-resolution AFM topographical images of etched glass surface before after functionalization in air: 2D (left column) and 3D (right column). A) Etched surface (not functionalized); B) Etched + silanized (APTES); C) Etched + APTES + crosslinker (GA). Scanning sizes: XY 1.5 µm x 1.5 µm; average height: -200 to +200 nm. The figure published as part of the paper (31) (MDPI Open Access License).

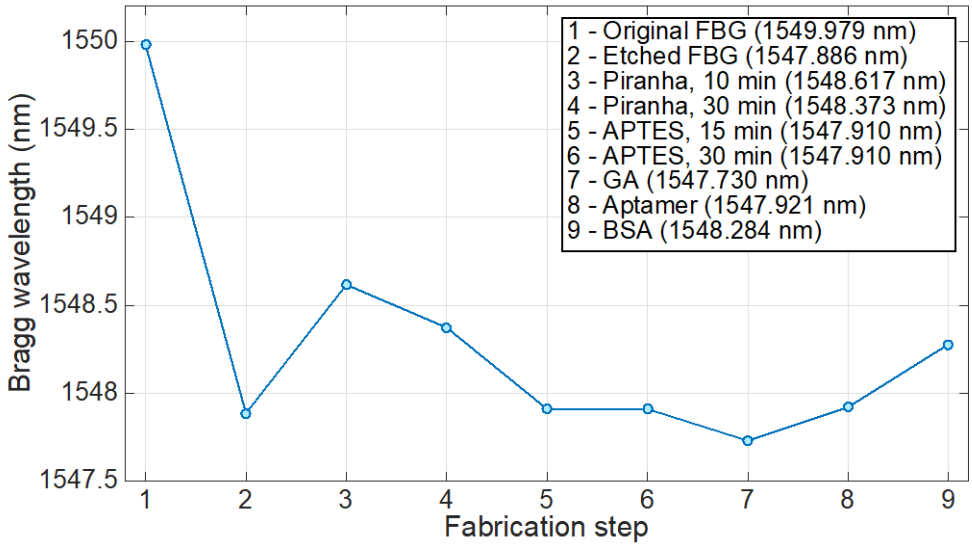

Figure 5.7. Dynamic of Bragg wavelength through the fabrication and functionalization of the EFBG thrombin biosensor. Graphic shows the estimated Bragg wavelength after each fabrication step (before thrombin detection). The figure published as part of the paper (31) (MDPI Open Access License).

Figure 5.7 shows dynamic of Bragg wavelength through the fabrication and functionalization of the EFBG thrombin biosensor. Graphic shows the estimated Bragg wavelength after each fabrication step (before thrombin detection). The results of the main measurements, i.e. Bragg wavelength shift observed during incubation of EFBG functionalized with TBA with thrombin is shown in **Figure 5.8**. Results for 70 min detection of thrombin at different concentrations 10 nM to 80 nM is shown to different concentrations of thrombin as exposure time progresses. At the first moment of exposure all measurements have been initialized by setting the time to zero, and the wavelength is tracked with a 10 s sampling rate. Thrombin is washed out from sensor using measurement buffer after each measurement. During the initial several minutes, deviation of the Bragg wavelength progressively from the initial position, (few picometers) which probably occurs due to instrument drift or binding-rebinding of thrombin on the sensor surface. So, in the beginning of the measurement, we observe that sensor has not reached the regime and the wavelength appears to float. But then after some time (ca. 20 min onwards), the response at different concentrations appear to stabilize. During the rest of the measurement, the Bragg wavelength appears to remain quite stable. Given the time required for clinical testing, 20 min can be considered as sufficient time (407).

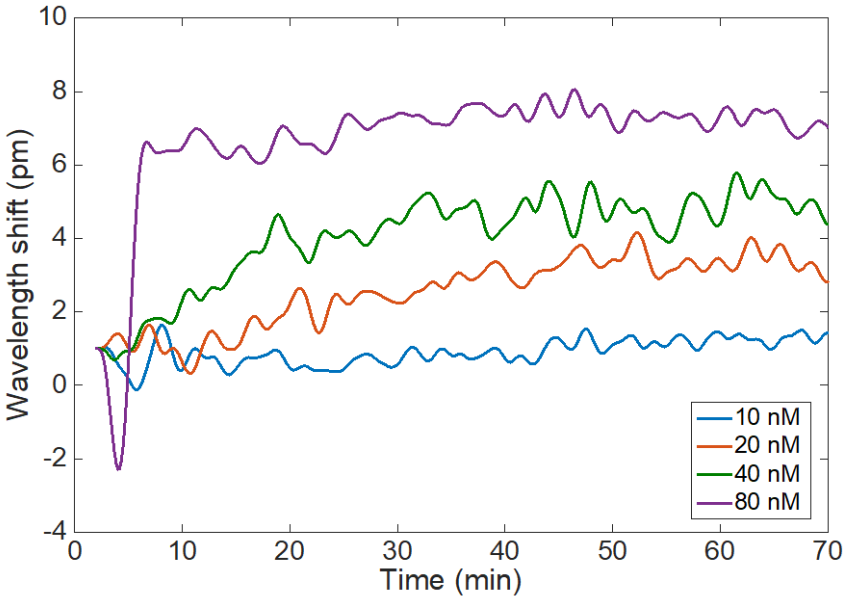

Figure 5.8. Bragg wavelength shift observed during incubation of EFBG functionalized with thrombin-binding aptamer with thrombin. Results for 70 min detection of thrombin at different concentrations 10 nM to 80 nM is shown. The figure published as part of the paper (31) (MDPI Open Access License).

The results of Bragg wavelength shift observed during incubation of functionalized sensor with thrombin (**Figure 5.8**) have been further analyzed for the evaluation of the sensor response over time and to evaluate the uncertainty. **Figure 5.9a** shows a plot of Bragg wavelength shift recorded over one minute against different thrombin concentrations. When the thrombin is measured at 10 nM, it is difficult to distinguish the wavelength shift change over time but then this is improved at higher concentrations of thrombin. Moreover, at constant thrombin concentrations, accuracy of the sensor was estimated as the standard deviation of the Bragg wavelength change recorded over one minute (**Figure 5.9b**). We can clearly see an improved accuracy of measurement. For most of the measurements, a range of 0.05 to 0.3 pm the Bragg wavelength deviation is observed. This is the same value estimated for the Bragg wavelength detection on the interrogator (0.2 pm).

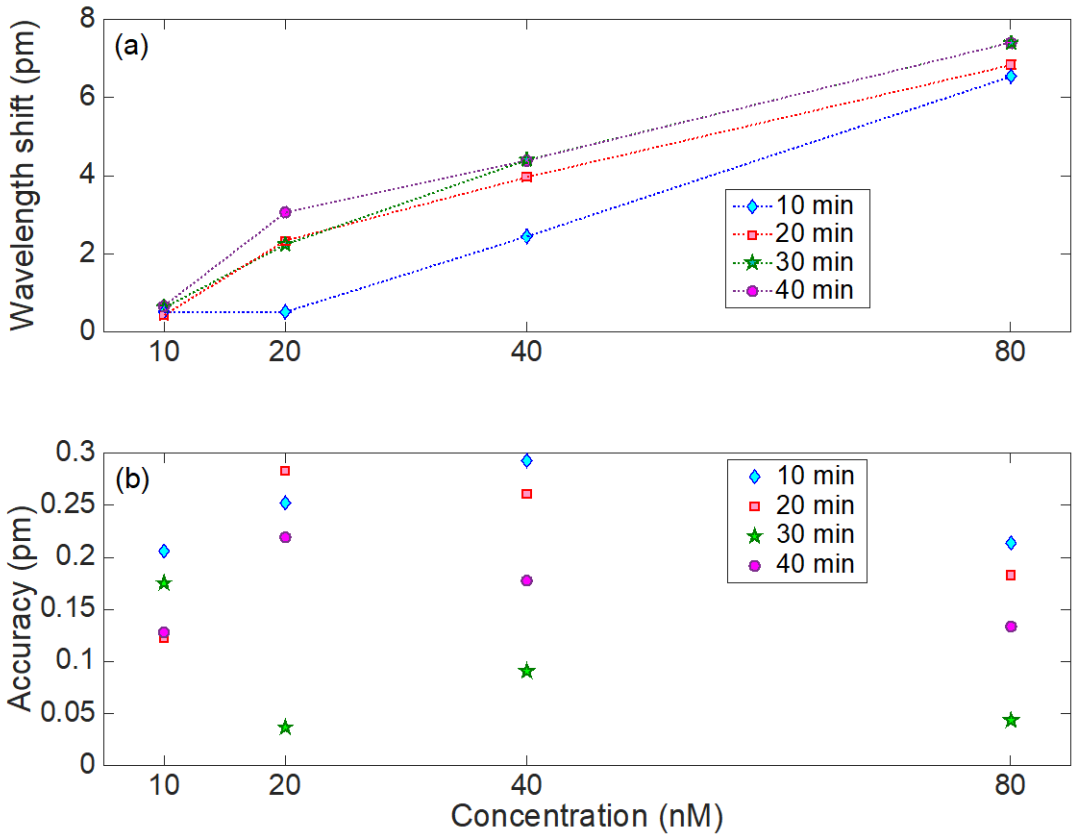

Figure 5.9. Results of the response of EFBG functionalized with thrombin-binding aptamer to thrombin: (a) Bragg wavelength shift observed for different thrombin concentrations after 10, 20, 30, and 40 min (b) detection accuracy (estimated as the standard deviation of the wavelength recorded over one-minute exposure). The figure published as part of the paper (31) (MDPI Open Access License).

When TFBG was etched (**Figure 5.10 A**), the overall diameter was decreased from 125 to 13 µm with a characteristic spectral evolution. An overall increase in bandwidth occurs as the etching progresses because of mode escaping to the surrounding media. Wavelength span between cladding modes increased as the diameter of fiber decreased. After etching, ETFBG with different diameters were immersed in calibration solutions with different RI (**Figure 5.10 B**), and spectral changes were analyzed (for modes 1568.5 and 1569.5 nm). With increased etching, the sensitivity to RI also increased: 23.38 nm/RIU for 13 µm and 1.25 nm/RIU for non-etched TFBG.

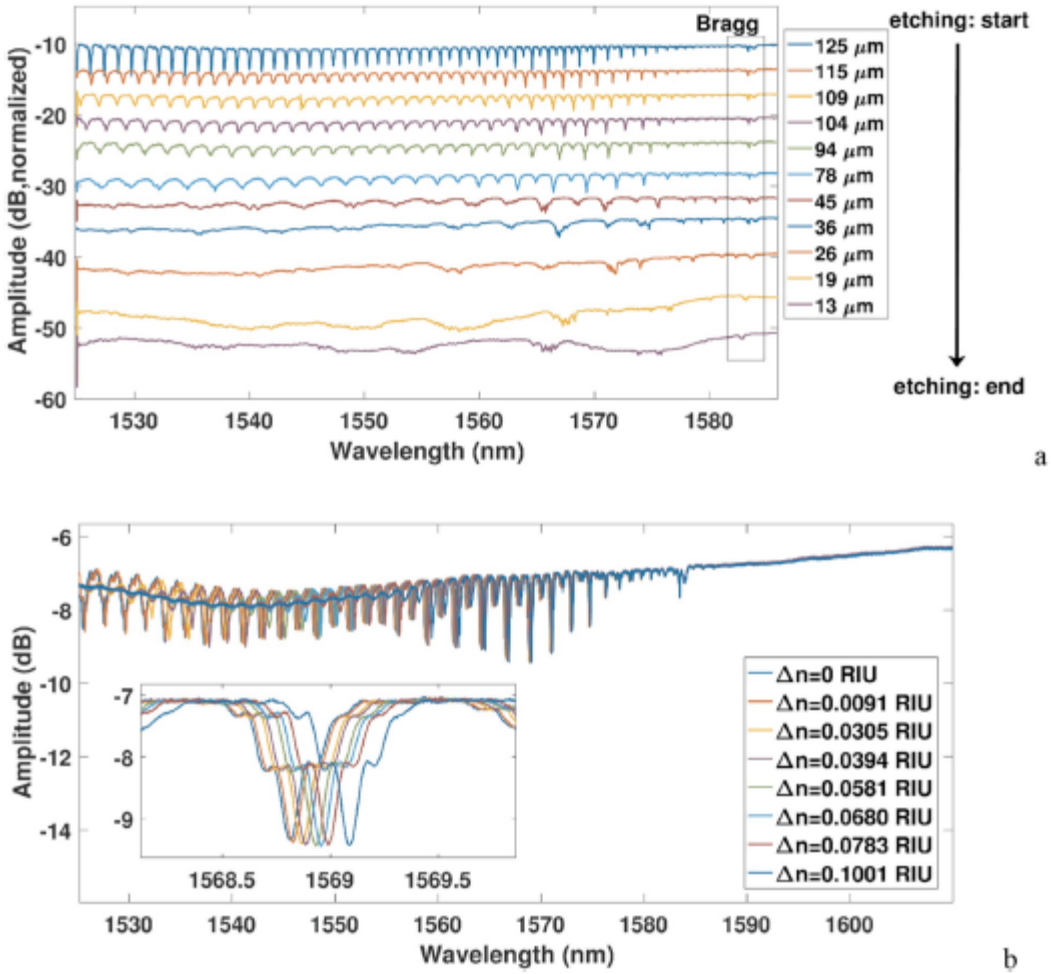

Figure 5.10. (**A**) Reflection spectra of TFBG during etching; (**B**) Spectral change of the ETFBG (d ¼ 94 μm) in calibration solutions (sucrose); inset: zoom of the analyzed modes. Published as part of (32) (Elsevier Permission: Personal use of work by Authors).

Results for thrombin detection by ETFBG (sensitivity to RI 2.53 nm/RIU and dimeter 94μm) are shown in **Figure 5.11**. The sensor was immersed in different thrombin concentrations (2.5-40 nM) and cladding modes between 1256 and 1529.1 nm were observed (**Figure 5.11A**). A red shift is observed as thrombin concentration is increased. When thrombin detection was analyzed on three modes in proximity of the leftmost part of the detection window (**Figure 5.11B**), surface sensiitivities of 2.3; 2.8 and 3.3 pm/nM were estimated. Theoretical LOD for two of the estimated modes was found to be 0.110 nM and 0.75 nM.

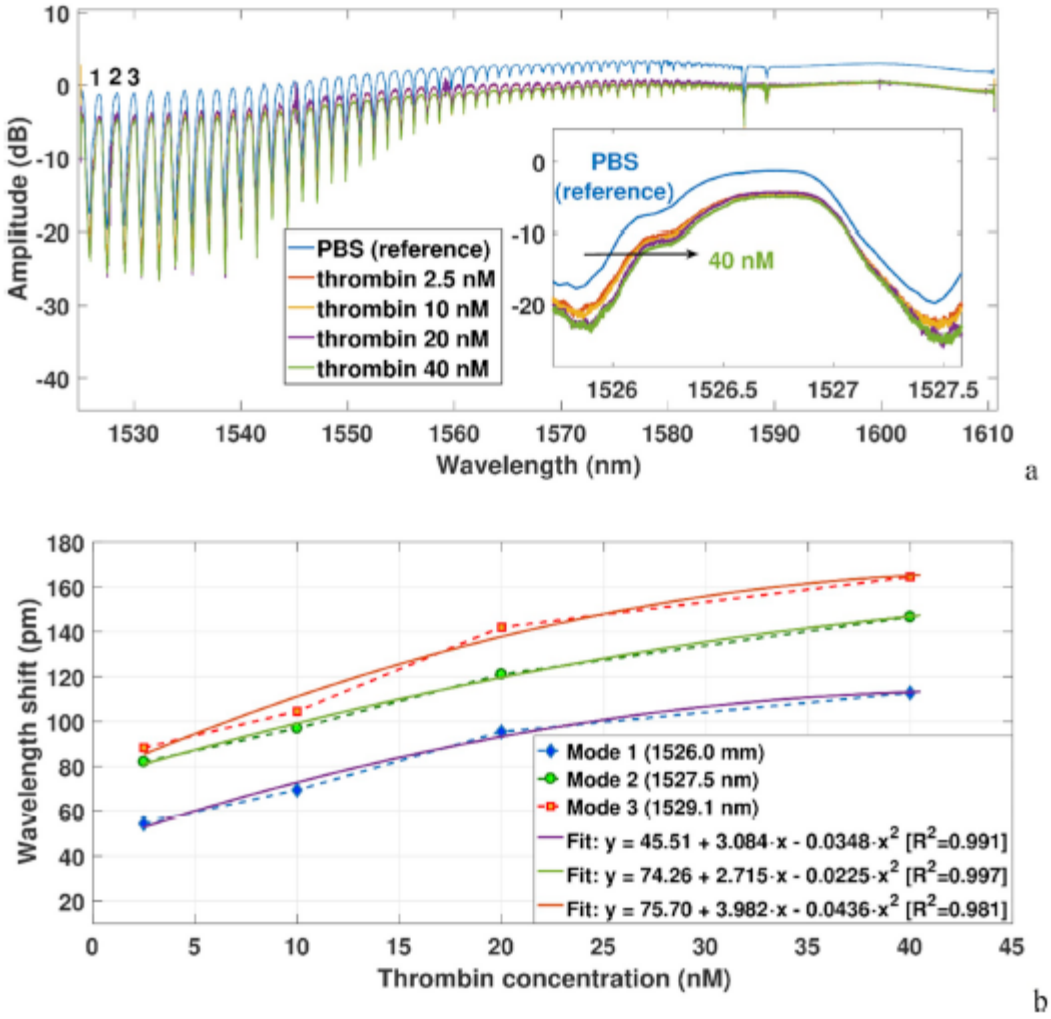

Figure 5.11. (**A**) Reflection spectra of ETFBG during the detection of the analyte (thrombin 2.5 nM, 10 nM, 20 nM and 40 nM). (**B**) Results of analyte measurement (wavelength shift as a function of the thrombin concentration) for the 3 most sensitive modes. Error bar range: -0.44 to þ0.45 pm. Published as part of (32) (Elsevier Permission: Personal use of work by Authors).

5.5. Discussion

In order to make FBG sensitive to RI for its further use as a sensor, its cladding has to be depleted so that the interaction of the evanescent wave field of the propagating mode and surrounding medium or analyte can occur (281). While there are different ways of removing cladding, chemical etching using HF is one of the advantageous methods due to its simplicity and wide use (292). Just in few minutes HF can etch a diaphragm with a

fast operating rate (422). When the grating is being etched, its spectrum is monitored in order to track the wavelength shift due to the change of sensitivity of the EFBG to external refractive index. By linearizing the relationship of fiber diameter from time as observed under microscope, it has been estimated that an etching rate of approximately (3.7 ± 0.5) μm/min was achieved; this was estimated on a control.

When the fiber diameter is decreased (from 125 μm to 25 μm) a shift in Bragg wavelength of 2.1 nm is measured. This shift happens both due to a nearby temperature increment of the chemical response as well as due to diminish of the cladding thickness (414). A quick diminish of Bragg wavelength was seen after fiber diameter comes to 20 μm since of an expanding interaction between HF and essential guided mode of the fiber (289). With a longer etching process a thinner cladding of a fiber is achieved and as a result the largest sensitivity is obtained as observed in (423). However, with a longer etching process evanescent field is also increasingly arise leading to multi-modality of sensor. Multimodal FBG spectrum is significantly enlarged and has a different from an original shape of spectrum. The obtained FBG spectrum can still be detected by the FBG interrogator, and the wavelength shift corresponds to the change of sensitivity to the surrounding RI. A larger diameter of the etched fiber gives a higher mechanical strength. As **Figure 5.4** demonstrates, etching FBG resulted in a sensor sensitive to the surrounding RI which suggests it is possible to be used as a biosensor. Similarly, ETFBG becomes more sensitive to RI of solutions and is superior to non-etched TFBG (1.25 nm/RIU). Etching TFBG affects the spectrum in calibration solutions by acting on the separation of cladding modes. The mode of interest was chosen according to its sensitivity and persistence (quantitative nm/RIU value at larger RI range; presence of the mode in interrogation window and never failing below cut-off).

In this work, TBA on the surface of two types of FBG (EFBG and TFBG) after etching was immobilized using APTES and GA. In one of the earlier studies, LPG sensor was also functionalized with APTES and then with GA for attachment of ligand to fabricate stable label-free biosensor for bacteria detection (424). Very often, the surface of optical fiber is hydroxylated before its functionalization and Piranha solution is one of the frequently used ones; it also cleans the surface. When etched fiber fiber sensor was treated with Piranha solution resulted in an increase of the wavelength in the beginning

with a slight decrease afterwards; an overall shift of approximately 0.5 nm was observed (**Figure 5.7**). To fabricate a biosensor a ligand specific to an analyte of interest has to be attached on optical fiber. One method of attaching a ligand on the surface of FBG is silanization. It was observed that immobilization of APTES is progressed more rapidly in the beginning and is stabilized after 15 min. For instance, a final shift of 0.46 nm occurred during its attachment. Saini *et al.* (278) observed a Bragg wavelength shift of 28 pm during attachment of 1% APTES on FBG which was also observed during the first 15 min of incubation.

AFM is a popular technique of analyzing the morphology of the modified surfaces. Control samples were treated in the same manner as FBG sensors and were analyzed using AFM. Results show that with each step of modification the surface morphology gets rougher (**Figure 5.6**) in the following order: etched < silanized < crosslinked thus confirming successful modification of the studied surfaces. These obtained results are similar to increased roughness demonstrated obtained by Sun *et al.* on FBG (325). Various thickness of APTES layers were reported in the literature: 0.7 nm (on Silicon wire) (420) or 1.8 nm. For some regions on the image it is clearly shown that the thickness of APTES, GA in our study was shown in a range of 1 -5 nm. Such a dissimilarity within the obtained thickness might be due to the number of layers shaped on the surface and for a few ranges on the etched fiber were non-homogenously conveyed APTES, GA particles all through the fiber surface.

After attaching TBA on the surface, its performance was tested by incubating in different thrombin concentrations. Usually, clinically relevant concentrations of biomarkers depend on the diseases. In case of blood coagulation disorders, thrombin concentration changes in a range from 1 to 500 nM and thus biosensors able to detect this range would be of clinical use (408). Concentrations of thrombin used in the work (10-80 nM) was similar to those used in this work by Coelho *et al* (411). For all measured concentrations of thrombin there was a propensity of increased output signal for functionalized biosensors. In the same work (411), they were able to detect 10 nM thrombin with a wavelength shift of 3.5 nm and a resolution of 0.54 nM. In spite of the fact that our biosensor has a lower performance, the EFBG strategy with silanization-based functionalization utilized in this research is appealing since it combines the

highlights of fiber optic biosensors with an effortless manufacture process. EFBG differs in term of its working principle than other grating-based technologies: a simple measurement of the Bragg wavelength in reflection. This feature has been is already integrated in most commercially available interrogators and thus does not require additional manufacturing steps. Compared to EFBG, TFBG and LPG with thin metal coating operate in transmission. This is not very practical for a sensing probe because light must be transmitted through the sensing region. A mirror has to be fabricated on the sensor tip to detect the transmission reflection spectrum; however, this fabrication requires an additional step. There are two main alternatives to grating sensors: tapers and SPR sensors based on optical fibers; however, they are also harder to manufacture. Sensors base on tapers are very fragile and its fabrication process results in a low throughput for narrow tapers. Typically, sensitivity of optical fiber sensors using SPR phenomena is in orders of magnitude sensitive (nm/RIU figure) higher than EFBG sensors. For its operation, SPR needs a polarization control and it operates in transmission and SPR signal detection is based on a large spectral hole. Single mode EFBG, on the other hand, has a small shift of a narrow spectrum which can be implemented using signal processing methods (418). Typical accuracy ranges are 0.1–1 pm for this method. As the previous figures demonstrate, detecting range at the tens of nM level, is compatible with many biosensors applications. The diminished sensitivity has moreover the result of bringing down the amount of evanescent power disseminated within the surrounding of the biosensor. Another advantage of the EFBG with regard to the other strategies is that EFBG's spectrum is in a narrow wavelength range, which permits a proficient use of the bandwidth and the plausibility to make sensing networks by stacking numerous sensors within the same fiber. Within the future, by utilizing different detecting regions, it will be conceivable to identify diverse analytes (other biomarkers) or utilizing controls (for temperature remuneration or other proteins) on the same fiber. Moreover, because EFBG sensors work in reflection mode, they are more compatible for building *in vivo* sensors compared to LPG and tilted FBG sensors which work in transmission.

Similarly, TFBG has been etched and silanized to produce thrombin biosensor with a maximum sensitivity of 3.3 pm/nM. Although the estimated theoretical LOD are one

magnitude lower than those reported for other grating sensors, these sensors also require thin film deposition with its added work as discussed above.

Using a similar surface modification method, it could be possible to immobilize aptamers against BCSC on optical fibers in order develop biosensor for their detection. Compared to a platform for their detection in vein, that having advantage of processing large volume of blood, is not actually a biosensor. TFBG coated with gold and them SAM with carboxylic acids was formed for immobilization of antibodies against EGFR (425). Detection range of the selective biosensor was from 2×10^6 to 5×10^6 cells/ml. EGFR-overexpressing human epidermoid carcinoma cells (A431) served as target cells while EGFR-negative uveal melanoma cells (OCM-1) were used as controls. Using optical vector analyzer, the binding of cells to functionalized OF was monitored and signal recorded. Optical fibers were used as transducer elements in label-free biosensors in different configurations. These biosensors were used for detection of various analytes: hydrogen peroxide (426), glucose (426), dopamine (427), DNA (275, 408), antibodies (428, 429) and other proteins (300, 323, 430-432), hemoglobin (433), virus (434, 435) and microbial cells (436-438). Developing a biosensor for *in vivo* sensing and also sensing cells – label-free

Possibility to detect cancer biomarker in tissues has been demonstrated by a plasmonic optical fiber biosensor (326). It was used to sense cytokeratin 17 in porous gel matrix and also in a preliminary test in a human lung tissue thus making a possibility to use optical fiber *in vivo* closer. Gold coated TFBG sensor with immobilized antibodies was used to detect cancer cells overexpressing EGFR membrane proteins (439). Compared to cancer cells control cells (with low expression of EGFR) showed a signal similar to those of background (growth media). In another study, human acute leukemia cell with difference in intracellular densities (separated by discontinuous sucrose gradient centrifugation) were detected using TFBG sensor (440). This was made possible by using a novel data analysis technique for differential polarimetric spectral transmission. It was possible to detect RI changes comparable with those detected using plasmonic TFBG without the need in precisely controlled gold layer. Moreover, LOD values obtained for detection of various analytes in case of EFBG are 0.5 nM (concanavalin A), 1.0 nM

(glucose) for EFBG and up to 8 pM (biotin) for TFBG (287). This shows that these platforms have promising applications in biosensing.

Apart from the above-mentioned studies, several works demonstrating the use of optical fiber sensors to study the response of cells attached to fiber to different analytes are known. One study showed successful monitoring of cell activation thus opening possibility for new tools in clinical diagnosis based on measuring cell functions in a real-time manner (441). Optical fibers forming high-density arrays loaded with cells can be used as sensing elements for studying the response of attached cells to different compounds (442). Photonic crystal fiber-based biosensors might be better suited for detecting cells or using them as sensing elements as demonstrated by several studies. Prostate cancer cells were detected using biosensor utilizing photonic-crystal and total internal reflection thus being an alternative to detecting prostate specific antigen which has issues as low specificity (443).

5.6. Conclusions

In this chapter, we report, to the best of our knowledge, a first biosensor for thrombin detection based on an etched standard EFBG. The fabrication process consisted of rendering FBG sensitive to surrounding RI. This was done by etching FBG which resulted in the sensitivity of the EFBG Bragg wavelength with respect to RI is 17.4 nm/RIU (when tested in different sucrose concentrations). For selective sensing of the analyte of interest, the fiber is functionalized by silanization with APTES and immobilizing thrombin binding aptamer. AFM measurements of the modified control surfaces (etched => etched + APTES => etched + APTES + GA) showed increased roughness suggesting successful modification of the surface. When the fabricated biosensor was exposed to different concentrations of thrombin (from 10 to 80 nM), different shift in Bragg wavelength for each concentration was observed: 0.5 (10 nM), 2 (20 nM), 4 (40 nM), 7 pm (80 nM) with standard deviation of 0.3 pm. Moreover, by using the same surface chemistry on other grating sensor, namely TFBG after etching, the overall performance of the sensor were improved: sensitivity to RI after etching and for thrombin detection. Thrombin concentrations used in this work were in the range of clinically relevant values. Although

performance of the biosensor is not as good (in terms of sensitivity) compared to other FBG-based biosensors, this can be compensated by the ease of fabrication, cost effectiveness and easier data analysis. Future work can be addressed to improve the fabrication process, and functionalizing other aptamers for use in other biosensing applications such as for detection of biomarkers associated with BCSC.

LIMITATIONS OF THE WORK AND FUTURE PERSPECTIVES

As all experimental studies, this work is also not free from its limitations. One of them, lies in the aptamers: a very small fraction of the selected aptamers were tested for their ability to bind target cells and hey do not have superior performance over already selected aptamers in the literature. Due to their performance, they could not be used for surface functionalization. Instead, aptamers available in the literature which bind to proteins on our target cells were sought and used in modification experiments. Also, after each step of modification, chemical groups on the surface could not be confirmed by such techniques as FTIR, X-ray photoelectron spectroscopy (XPS) or Raman spectroscopy. Attempts were made to use FTIR but failed due to thinness of our samples; while XPS is not available in our facilities. The application of Raman spectroscopy to our samples seems to require more optimizations and expert advice. Lack of these techniques was partially compensated by the use of combination of CV, AFM, EDS and FITC analysis. One important aspect requiring study for any device with potential use in human body is cytotoxicity. This was unfortunately not studied because it was out of scope of the study due time limit.

In the future, more binding analysis for other selected sequences is needed to find the better binders among them. Another interesting approach is analysing the affinity of the sequences from NGS to proteins present on the cells with available crystal structures (for instance CD44 or CD133) using virtual docking or *in silico* screening approach. This would allow analyzing more sequences and narrow down potential candidates before experimental analysis. In characterizing of modifies surfaces performing additional electrochemical impedance spectroscopy (EIS) for the samples at each functionalization step could be an additional prove of surface modification. In the literature, EIS has been used for characterizing SS in different works (199, 269, 271, 353, 444). Most importantly, the functionalized surfaces need to be evaluated for their isolation of the actual BCSC more thoroughly. For this, an *in vitro* model mimicking blood flow consisting of peristaltic pump and tube is planned to be used. Apart from fluorescent microscope, another way to study the surface with the cells are SEM, CV and EIS analysis as done by (269).

OVERALL CONCLUSION

BC remains the most common cancer type among women worldwide. Metastasis, relapse and recurrence of BC are thought to occur due to a small subset of cells called BCSC. Thus, both developing platforms for their detection and isolation and finding new ligands binding these cells are important in improving BC diagnosis and treatment. In this work, in order to find new ligands against BCSC, FACS-SELEX was employed. Binding of the aptamer candidates was studied with IFC which, to the best of our knowledge has not been used for aptamer characterization, showing more binding to the target cells than control cells. Despite having lower performance compared to commercially available aptamers, the selected sequences, to the best of our knowledge, would be the thirdly reported synthetic ligands against BCSC (and not regular BC cells). Furthermore, SELEX was performed without the prior knowledge of its target and target cells have more characteristics associated with CSC than other reported studies ((12), (163)). Target cells were derived from a patient with a TN BC which does not respond to hormonal therapies. Also, this study is one of the first examples of using IFC in analyzing aptamer binding to cells.

Another task of the thesis was functionalizing SS wire with bioprobes with an ultimate goal of capturing BCSC. Finding appropriate methods for silanization of SS and characterization of functionalized wires were the main bottleneck in this work. Earlier attempts of directly dip-coating SS were unsuccessful (at least with characterization methods used at that time). Electrodeposition of silane coating was the only available method thought suitable and available; and hence was attempted in this work. Non-pretreated samples (after sonication only) after electrodeposition were not distinguishable from one another on AFM due to intrinsic roughness of the pretreated samples. Electropolishing of the sample allowed the use of AFM as a characterization method. Electrodeposition temperature, pH of solution and applied potential have been determined for optimized silanization. FITC analysis after silanization has been evaluated. Also CV was found to be a suitable method for characterizing each functionalization step. After silanization, the surface was bound with crosslinker and aptamers. Optimized conditions of silanization (applied potential, solution pH, heat treatment temperature) for obtaining an aptamer-functionalized wire were determined in this work together with the use of

several surface characterization techniques suitable for small-sized and circular wires. These modified wires have potential applications for the *in vivo* capture of target cells in blood flow, since their small size allows their insertion as standard guidewires in biomedical devices.

Using similar chemistry for functionalizing SS, another platform based on an etched standard FBG for biosensor development was investigated. For this, FBG was fabricated to be sensitive to surrounding RI by wet-etching resulting in the sensitivity to the surrounding RI to be 17.4 nm/RIU when tested in different concentrations of sucrose. The fiber was then functionalized with APTES and GA for immobilizing thrombin binding aptamer. AFM measurement results of the modified control surfaces at each step of functionalization, suggest successful modification of the surface. The fabricated biosensor was tested to detect various concentrations of thrombin (10-80 nM) resulting in different shift in Bragg wavelength for each concentration ranging from 0.5-7 pm (±0.3 pm). Lower performance of the biosensor when compared to other FBG-based biosensors could be compensated by the relative ease and cost effectiveness of the fabrication process, as well as easier data analysis. In the future, by improving the fabrication process and functionalizing aptamers against other targets such as biomarkers associated with BCSC, biosensor for BC detection could also be fabricated.

In conclusion, the first sub-hypothesis of the work was proven to be true since the aptamers against BCSC have been selected. Selected aptamers were found to bind to target cells more than to control cells and their binding has to be further studied. Most importantly, there are plenty of uncharacterized aptamer candidates which could be better binders and this study is one of the first examples of using such an emerging and promising tool as IFC in the characterization of aptamers. Despite that in the second sub-hypothesis immobilized aptamers were from a commercial source (not selected aptamers), the overall aim of functionalizing SS wire with aptamers against BCSC has been achieved. The third sub-hypothesis was also proven to be true, because optical fiber sensor based on model aptamers was successfully built. As a result, the overall hypothesis of the work was proven to be true taking into account the future works as discussed above: characterization of other aptamer candidates, further *in vitro* studies of the functionalized

wires (blood mimicking flow system and exploring more sophisticated optical fiber based systems for building biosensor for BCSC detection.

REFERENCES

1. Gangopadhyay S, Nandy A, Hor P, Mukhopadhyay A. Breast Cancer Stem Cells: A Novel Therapeutic Target. Clinical Breast Cancer. 2013;13(1):7-15.

2. Bray F, Boerjomataram I, Siegel R, Torre L, Jemal A. Global Cancer Statistics 2018: GLOBOCAN Estimates of Incidence and Mortality Worldwide for 36 Cancers in 185 Countries. A Cancer Journal for clinicians. 2018;0:1-31.

3. Islam F, Gopalan V, Smith R, Lam A. Translational potential of cancer stem cells: A review of the detection of cancer stem cells and their roles in cancer recurrence and cancer treatment. Experimental Cell Research. 2015;335(1):135-47.

4. Ribatti D. Cancer stem cells and tumor angiogenesis. Cancer letters. 2012;321(1).

5. Sampieri K, Fodde R. Cancer stem cells and metastasis. Seminars in Cancer Biology. 2012;22(3):187-93.

6. Mirzaei A, Madjd Z, Kadijani AA, Alinaghi S, Akbari A, Tavoosidana G. Cancer Stem Cell's Potential Clinical Implications. Iranian Journal of Cancer Prevention. 2017;10(1).

7. Hajj M, WIcha M, Benito-Hernandez S, Morrison S, Clarke M. Prospective identification of tumorigenic breast cancer cells. Proc Natl Acad Sci USA. 2003:3983-8.

8. Ponti D, Costa A, Zaffaroni N, Pratesi G, Petrangolini G, Coradini D, et al. Isolation and in vitro propagation of tumorigenic breast cancer cells with stem/progenitor cell properties. Cancer Research. 2005;65(13):5506-11.

9. Sheridan C, Kishimoto H, Fuchs RK, Mehrotra S, Bhat-Nakshatri P, Turner CH, et al. CD44(+)/CD24(-) breast cancer cells exhibit enhanced invasive properties: an early step necessary for metastasis. Breast Cancer Research. 2006;8(5).

10. Chiotaki R, Polioudaki H, Theodoropoulos PA. Stem cell technology in breast cancer: current status and potential applications. Stem Cells and Cloning-Advances and Applications. 2016;9:17-29.

11. Moghbeli M, Moghbeli F, Forghanifard MM, Abbaszadegan MR. Cancer stem cell detection and isolation. Medical Oncology. 2014;31(9).

12. Chen LX, Long C, Tran KAM, Lee J. A Synthetic Binder of Breast Cancer Stem Cells. Chemistry-a European Journal. 2018;24(15):3694-8.

13. Joshi R, Janagama H, Dwivedi HP, Kumar TMAS, Jaykus L-A, Schefers J, et al. Selection, characterization, and application of DNA aptamers for the capture and detection of Salmonella enterica serovars. Molecular and Cellular Probes. 2009;23(1).
14. Khati M. The future of aptamers in medicine. Journal of Clinical Pathology. 2010;63(6).
15. Stoltenburg R, Reinemann C, Strehlitz B. SELEX-A (r)evolutionary method to generate high-affinity nucleic acid ligands. Biomolecular Engineering. 2007;24(4).
16. Sefah K, Shangguan D, Xiong X, O'Donoghue MB, Tan W. Development of DNA aptamers using Cell-SELEX. Nat Protocols. 2010;5(6):1169-85.
17. Wu X, Chen J, Wu M, Zhao JX. Aptamers: Active Targeting Ligands for Cancer Diagnosis and Therapy. Theranostics. 2015;5(4):322-44.
18. Shigdar S, Lin J, Yu Y, Pastuovic M, Wei M, Duan W. RNA aptamer against a cancer stem cell marker epithelial cell adhesion molecule. Cancer Science. 2011;102(5).
19. Iwagawa T, Ohuchi SP, Watanabe S, Nakamura Y. Selection of RNA aptamers against mouse embryonic stem cells. Biochimie. 2012;94(1).
20. Croker AK, Goodale D, Chu J, Postenka C, Hedley BD, Hess DA, et al. High aldehyde dehydrogenase and expression of cancer stem cell markers selects for breast cancer cells with enhanced malignant and metastatic ability. Journal of Cellular and Molecular Medicine. 2009;13(8B):2236-52.
21. Charafe-Jauffret E, Ginestier C, Birnbaum D. Breast cancer stem cells: tools and models to rely on. Bmc Cancer. 2009;9.
22. Nowaczyk P, Dlugaszewska S, Herold S, Krahn T, Mayer M, Morgenthaler N, et al., editors. A novel technology for in vivo isolation of circulating tumor cells in breast cancer patients. 9th European Breast Cancer Conference; 2014; Glasgow, UK.
23. Vermesh O, Aalipour A, Ge J, Saenz Y, Guo Y, Alam I, et al. An intravascular magnetic wire for the high-throughput retrieval of circulating tumour cells in vivo. Nature Biomedical Engieering. 2018;2:696-705.
24. Pantel K, Alix-Panabieres C. Circulating tumour cells in cancer patients: challenges and perspectives. Trends in Molecular Medicine. 2010;16(9):398-406.
25. Tirino V, Desiderio V, Paino F, Papaccio G, De Rosa M. Methods for cancer stem cell detection and isolation. Methods in molecular biology (Clifton, NJ). 2012;879.

26. Ababneh N, Alshaer W, Allozi O, Mahafzah A, El-Khateeb M, Hillaireau H, et al. In Vitro Selection of Modified RNA Aptamers Against CD44 Cancer Stem Cell Marker. Nucleic Acid Therapeutics. 2013;23(6):401-7.
27. Palaniyandi K, Pockaj B, Gendler S, Chang X-B. Human Breast Cancer Stem Cells Have Significantly Higher Rate of Clathrin-Independent and Caveolin-Independent Endocytosis than the Differentiated Breast Cancer Cells. Journal of Cancer Science Therapy. 2012;4(7):214-22.
28. Shigdar S, Qiao L, Zhou S-F, Xiang D, Wang T, Li Y, et al. RNA aptamers targeting cancer stem cell marker CD133. Cancer Letters. 2013;330(1):84-95.
29. Bekmurzayeva A, Duncanson WJ, Azevedo HS, Kanayeva D. Surface modification of stainless steel for biomedical applications: Revisiting a century-old material. Materials Science & Engineering C-Materials for Biological Applications. 2018;93:1073-89.
30. Bekmurzayeva A, Dukenbayev K, Azevedo S H, Marsili E, Tosi D, Kanayeva D. Optimizing silanization to functionalize stainless steel wire: towards breast cancer stem cell isolation. Materials. 2020;13(17).
31. Bekmurzayeva A, Dukenbayev K, Shaimerdenova M, Bekniyazov I, Ayupova T, Sypabekova M, et al. Etched Fiber Bragg Grating Biosensor Functionalized with Aptamers for Detection of Thrombin. Sensors. 2018;18(12).
32. Sypabekova M, Korganbayev S, Gonzalez-Vila A, Caucheteur C, Shaimerdenova M, Ayupova T, et al. Functionalized etched tilted fiber Bragg grating aptasensor for label-free protein detection. Biosensors & Bioelectronics. 2019;146.
33. Li J, Peng YL, Duan YX. Diagnosis of breast cancer based on breath analysis: An emerging method. Critical Reviews in Oncology Hematology. 2013;87(1):28-40.
34. Porto-Mascarenhas EC, Assad DX, Chardin H, Gozal D, Canto GD, Acevedo AC, et al. Salivary biomarkers in the diagnosis of breast cancer: A review. Critical Reviews in Oncology Hematology. 2017;110:62-73.
35. Coleman C. Early detection and screening for breast cancer. Seminars in Oncology Nursing. 2017;33(2):141-55.
36. Bektur C, Dushimova Z, Kaidarova D, Pennington MW. Epidemiology of breast cancer in Kazakhstan in 2014-2018. Value in Health. 2019;22:S90-S.

37. Igissinov N, Toguzbayeva A, Turdaliyeva B, Igissinova G, Bilyalova Z, Akpolatova G, et al. Breast Cancer in Megapolises of Kazakhstan: Epidemiological Assessment of Incidence and Mortality. Iranian Journal of Public Health. 2019;48(7):1257-64.
38. Stivarou T, Stellas D, Vartzi G, Thomaidou D, Patsavoudi E. Targeting highly expressed extracellular HSP90 in breast cancer stem cells inhibits tumor growth in vitro and in vivo. Cancer Biology & Therapy. 2016;17(8):799-812.
39. Rakha EA, Green AR. Molecular classification of breast cancer: what the pathologist needs to know. Pathology. 2017;49(2):111-9.
40. McCafferty M, Healy N, Kerin M. Breast cancer subtypes and molecular biomarkers. Diagnostic histopathology. 2009;15(10):485-9.
41. Berse B, Lynch JA. Molecular diagnostic testing in breast cancer. Seminars in Oncology Nursing. 2015;31(2):108-21.
42. Godone RLN, Leitao GM, Araujo NB, Castelletti CHM, Lima JL, Martins DBG. Clinical and molecular aspects of breast cancer: Targets and therapies. Biomedicine & Pharmacotherapy. 2018;106:14-34.
43. Yersal O, Barutca S. Biological subtypes of breast cancer: prognostic and therapeutic implications. World J Clin Oncology. 2014;5(3):412-24.
44. Nguyen NP, Almeida FS, Chi A, Nguyen LM, Cohen D, Karlsson U, et al. Molecular biology of breast cancer stem cells: Potential clinical applications. Cancer Treatment Reviews. 2010;36(6):485-91.
45. Hwang SY, Park S, Kwon Y. Recent therapeutic trends and promising targets in triple negative breast cancer. Pharmacology & Therapeutics. 2019;199:30-57.
46. McDonald ES, Clark AS, Tchou J, Zhang P, Freedman GM. Clinical Diagnosis and Management of Breast Cancer. Journal of Nuclear Medicine. 2016;57:9S-16S.
47. Raghavendra P, Pullaiah T. Biomedical imaging role in cellular and molecular diagnostics. Advances in cell and molecular diagnostics: Academic Press; 2018. p. 85-111.
48. Sabel M. Principles of breast cancer screening. Essentials of breast surgery: Mosby; 2009. p. 19-40.

49. Wolff A, Domchek S, Davidson N, Sacchini V, McCormic B. Cancer of breast. In: Niederhuber J, Armitage J, Kastan M, Doroshow J, Tepper J, editors. Abelott's Clinical Oncology. Fifth ed: Elsevier; 2014. p. 1630-92.
50. Guo RR, Lu GL, Qin BJ, Fei BW. Ultrasound imaging technologies for breast cancer detection and management: a review. Ultrasound in Medicine and Biology. 2018;44(1):37-70.
51. Leithner D, Wengert GJ, Helbich TH, Thakur S, Ochoa-Albiztegui RE, Morris EA, et al. Clinical role of breast MRI now and going forward. Clinical Radiology. 2018;73(8):700-14.
52. Redman A, Lowes S, Leaver A. Imaging techniques in breast cancer. Surgery (Oxford). 2016;34(1):8-18.
53. Vercher-Conejero JL, Pelegrí-Martinez L, Lopez-Aznar D, Cózar-Santiago MdP. Positron Emission Tomography in Breast Cancer. Diagnostics. 2015;5:61-83.
54. Papathanassiou D, Bruna-Muraille C, Liehn JC, Nguyen TD, Cure H. Positron Emission Tomography in oncology: Present and future of PET and PET/CT. Critical Reviews in Oncology Hematology. 2009;72(3):239-54.
55. Chakraborty D, Basu S, Ulaner GA, Alavi A, Kumar R. Diagnostic Role of Fluorodeoxyglucose PET in Breast Cancer A History to Current Application. Pet Clinics. 2018;13(3).
56. Cedolini C, Bertozzi S, Londero AP, Bernardi S, Seriau L, Concina S, et al. Type of Breast Cancer Diagnosis, Screening, and Survival. Clinical Breast Cancer. 2014;14(4):235-40.
57. Mittal S, Kaur H, Gautam N, Mantho A. Biosensors for breast cancer diagnosis: a review of bioreceptors, biotransducers and signal amplification strategies. Biosensors and biotransducers. 2016.
58. Zamay GS, Kolovskaya OS, Zamay TN, Glazyrin YE, Krat AV, Zubkova O, et al. Aptamers Selected to Postoperative Lung Adenocarcinoma Detect Circulating Tumor Cells in Human Blood. Molecular Therapy. 2015;23(9):1486-96.
59. Creighton CJ, Li X, Landis M, Dixon JM, Neumeister VM, Sjolund A, et al. Residual breast cancers after conventional therapy display mesenchymal as well as

tumor-initiating features. Proceedings of the National Academy of Sciences of the United States of America. 2009;106(33):13820-5.
60. McDermott SP, Wicha MS. Targeting breast cancer stem cells. Molecular Oncology. 2010;4(5):404-19.
61. Wicha M, Dontu G, Liu S, Mantle I. Stem cells in human breast development and cancer. Breast Cancer Research. 2005;7:S8-S.
62. Cojoc M, Mabert K, Muders MH, Dubrovska A. A role for cancer stem cells in therapy resistance: Cellular and molecular mechanisms. Seminars in Cancer Biology. 2015;31:16-27.
63. Morrison BJ, Schmidt CW, Lakhani SR, Reynolds BA, Lopez JA. Breast cancer stem cells: implications for therapy of breast cancer. Breast Cancer Research. 2008;10(4).
64. Shao J, Fan W, Ma BA, Wu YP. Breast cancer stem cells expressing different stem cell markers exhibit distinct biological characteristics. Molecular Medicine Reports. 2016;14(6):4991-8.
65. Li WZ, Ma HL, Zhang J, Zhu L, Wang C, Yang YL. Unraveling the roles of CD44/CD24 and ALDH1 as cancer stem cell markers in tumorigenesis and metastasis. Scientific Reports. 2017;7.
66. Mannello F. Understanding breast cancer stem cell heterogeneity: time to move on to a new research paradigm. Bmc Medicine. 2013;11.
67. Shimono Y, Zabala M, Cho RW, Lobo N, Dalerba P, Qian DL, et al. Downregulation of miRNA-200c Links Breast Cancer Stem Cells with Normal Stem Cells. Cell. 2009;138(3):592-603.
68. Lin CY, Barry-Holson KQ, Allison KH. Breast cancer stem cells: are we ready to go from bench to bedside? Histopathology. 2016;68(1):119-37.
69. Bai XP, Ni J, Beretov J, Graham P, Li Y. Cancer stem cell in breast cancer therapeutic resistance. Cancer Treatment Reviews. 2018;69:152-63.
70. Velasco-Velázquez M, Homsia N, Fuente L, Pestella R. Breast cancer stem cells. The International Journal of Biochemistry & Cell Biology. 2012;44:573-7.

71. Kim RJ, Park JR, Roh KJ, Choi AR, Kim SR, Kim PH, et al. High aldehyde dehydrogenase activity enhances stem cell features in breast cancer cells by activating hypoxia-inducible factor-2 alpha. Cancer Letters. 2013;333(1):18-31.
72. Mannelli G, Gallo O. Cancer stem cells hypothesis and stem cells in head and neck cancers. Cancer Treatment Reviews. 2012;38(5).
73. Bidard FC, Proudhon C, Pierga JY. Circulating tumor cells in breast cancer. Molecular Oncology. 2016;10(3):418-30.
74. Dalum G, Holland L, Terstappen L. Metastasis and circulating tumor cells. The Journal of the International Federation of Clinical Chemistry and Laboratory Medicine. 2012;23(3).
75. Barriere G, Riouallon A, Renaudie J, Tartary M, Rigaud M. Mesenchymal Characterization: Alternative to Simple CTC Detection in Two Clinical Trials. Anticancer Research. 2012;32(8):3363-9.
76. Kamal M, Razaq W, Leslie M, Adhikari S, Tanaka T. Circulating tumor cells in breast cancer: a potential liquid biopsy. In: Van Pham P, editor. Breast Cancer - From Biology to Medicine: InTech Open; 2017.
77. Theodoropoulos PA, Polioudaki H, Agelaki S, Kallergi G, Saridaki Z, Mavroudis D, et al. Circulating tumor cells with a putative stem cell phenotype in peripheral blood of patients with breast cancer. Cancer Letters. 2010;288(1):99-106.
78. Lianidou ES, Markou A. Circulating Tumor Cells in Breast Cancer: Detection Systems, Molecular Characterization, and Future Challenges. Clinical Chemistry. 2011;57(9):1242-55.
79. Baccelli I, Schneeweiss A, Riethdorf S, Stenzinger A, Schillert A, Vogel V, et al. Identification of a population of blood circulating tumor cells from breast cancer patients that initiates metastasis in a xenograft assay. Nature Biotechnology. 2013;31(6):539-U143.
80. Giordano A, Gao H, Anfossi S, Cohen E, Mego M, Lee BN, et al. Epithelial-Mesenchymal Transition and Stem Cell Markers in Patients with HER2-Positive Metastatic Breast Cancer. Molecular Cancer Therapeutics. 2012;11(11):2526-34.

81. Raimondi C, Gradilone A, Naso G, Vincenzi B, Petracca A, Nicolazzo C, et al. Epithelial-mesenchymal transition and stemness features in circulating tumor cells from breast cancer patients. Breast Cancer Research and Treatment. 2011;130(2):449-55.
82. Hu Y, Zheng Je, Huang S. Detection of circulating tumor cells and circulating tumor cells in breast cancer by flow cytometry. In: Xu K, editor. Tumor metastasis: InTech Open; 2017.
83. Nagrath S, Sequist LV, Maheswaran S, Bell DW, Irimia D, Ulkus L, et al. Isolation of rare circulating tumour cells in cancer patients by microchip technology. Nature. 2007;450(7173):1235-U10.
84. Pedrol E, Garcia-Algar M, Massons J, Nazarenus M, Guerrini L, Martinez J, et al. Optofluidic device for the quantification of circulating tumor cells in breast cancer. Scientific Reports. 2017;7.
85. Ring AE, Zabaglo L, Ormerod MG, Smith IE, Dowsett M. Detection of circulating epithelial cells in the blood of patients with breast cancer: comparison of three techniques. British Journal of Cancer. 2005;92(5):906-12.
86. Andree KC, van Dalum G, Terstappen L. Challenges in circulating tumor cell detection by the CellSearch system. Molecular Oncology. 2016;10(3):395-407.
87. Cristofanilli M, Budd GT, Ellis MJ, Stopeck A, Matera J, Miller MC, et al. Circulating tumor cells, disease progression, and survival in metastatic breast cancer. N Engl J Med. 2004;351(8):781-91.
88. Cristofanilli M, Hayes DF, Budd GT, Ellis MJ, Stopeck A, Reuben JM, et al. Circulating tumor cells: A novel prognostic factor for newly diagnosed metastatic breast cancer. Journal of Clinical Oncology. 2005;23(7):1420-30.
89. Man Y, Wang Q, Kemmner W. Currently Used Markers for CTC Isolation Advantages, Limitations and Impact on Cancer Prognosis. J Clinic Experiment Patholog. 2011;1(1):1-7.
90. Andergassen U, Kolbl AC, Hutter S, Friese K, Jeschke U. Detection of Circulating Tumour Cells from Blood of Breast Cancer Patients via RT-qPCR. Cancers. 2013;5(4):1212-20.

91. Zhu X, Yang J, Liu M, Wu Y, Shen Z, Li G. Sensitive detection of human breast cancer cells based on aptamer-cell-aptamer sandwich architecture. Analytica Chimica Acta. 2013;764:59-63.
92. Civit L, Taghdisi SM, Jonczyk A, Hassel SK, Grober C, Blank M, et al. Systematic evaluation of cell-SELEX enriched aptamers binding to breast cancer cells. Biochimie. 2018;145:53-62.
93. Jayasena SD. Aptamers: An emerging class of molecules that rival antibodies in diagnostics. Clinical Chemistry. 1999;45(9).
94. Bruno JG, Kiel JL. In vitro selection of DNA aptamers to anthrax spores with electrochemiluminescence detection. Biosensors & Bioelectronics. 1999;14(5).
95. Tuerk C, Gold L. Systematic evolution of ligands by exponential enrichment - RNA ligands to bacteriophage-T4 DNA-polymerase. Science. 1990;249(4968):505-10.
96. Ellington A, Szostak J. In vitro selection of RNA molecules that bind specific targets. Nature. 1990;346:818-22.
97. Qu H, Csordas AT, Wang JP, Oh SS, Eisenstein MS, Soh HT. Rapid and Label-Free Strategy to Isolate Aptamers for Metal Ions. Acs Nano. 2016;10(8):7558-65.
98. Xia T, Yuan JH, Fang XH. Conformational Dynamics of an ATP-Binding DNA Aptamer: A Single-Molecule Study. Journal of Physical Chemistry B. 2013;117(48):14994-5003.
99. Stojanovic MN, de Prada P, Landry DW. Aptamer-based folding fluorescent sensor for cocaine. Journal of the American Chemical Society. 2001;123(21):4928-31.
100. Mannironi C, Scerch C, Fruscoloni P, Tocchini-Valentini GP. Molecular recognition of amino acids by RNA aptamers: The evolution into an L-tyrosine binder of a dopamine-binding RNA motif. Rna-a Publication of the Rna Society. 2000;6(4):520-7.
101. McKeague M, Foster A, Miguel Y, Giamberardino A, Verdin C, Chan JYS, et al. Development of a DNA aptamer for direct and selective homocysteine detection in human serum. Rsc Advances. 2013;3(46):24415-22.
102. Qin L, Zheng R, Ma Z, Feng Y, Liu Z, Yang H, et al. The selection and application of ssDNA aptamers against MPT64 protein in Mycobacterium tuberculosis. Clinical Chemistry and Laboratory Medicine. 2009;47(4):405-11.

103.Sypabekova M, Bekmurzayeva A, Wang RH, Li YB, Nogues C, Kanayeva D. Selection, characterization, and application of DNA aptamers for detection of Mycobacterium tuberculosis secreted protein MPT64. Tuberculosis. 2017;104:70-8.
104.Bock LC, Griffin LC, Latham JA, Vermaas EH, Toole JJ. Selection of single-stranded-DNA molecules that bind and inhibit human thrombin. Nature. 1992;355(6360):564-6.
105.Tasset DM, Kubik MF, Steiner W. Oligonucleotide inhibitors of human thrombin that bind distinct epitopes. Journal of Molecular Biology. 1997;272(5):688-98.
106.Wang DL, Song YL, Zhu Z, Li XL, Zou Y, Yang HT, et al. Selection of DNA aptamers against epidermal growth factor receptor with high affinity and specificity. Biochemical and Biophysical Research Communications. 2014;453(4):681-5.
107.Xu W, Ellington AD. Anti-peptide aptamers recognize amino acid sequence and bind a protein epitope. Proceedings of the National Academy of Sciences of the United States of America. 1996;93(15):7475-80.
108.Sun W, Du LP, Li MY. Aptamer-Based Carbohydrate Recognition. Current Pharmaceutical Design. 2010;16(20):2269-78.
109.Boiziau C, Dausse E, Yurchenko L, Toulme JJ. DNA aptamers selected against the HIV-1 trans-activation-responsive RNA element form RNA-DNA kissing complexes. Journal of Biological Chemistry. 1999;274(18):12730-7.
110.Gopinath SCB, Misono TS, Kawasaki K, Mizuno T, Imai M, Odagiri T, et al. An RNA aptamer that distinguishes between closely related human influenza viruses and inhibits haemagglutinin-mediated membrane fusion. Journal of General Virology. 2006;87.
111.Vivekananda J, Kiel JL. Anti-Francisella tularensis DNA aptamers detect tularemia antigen from different subspecies by aptamer-linked immobilized sorbent assay. Laboratory Investigation. 2006;86(6).
112.Li H, Ding XH, Peng ZH, Deng L, Wang D, Chen H, et al. Aptamer selection for the detection of Escherichia coli K88. Canadian Journal of Microbiology. 2011;57(6):453-9.
113.Kulbachinskiy AV. Methods for selection of aptamers to protein targets. Biochemistry-Moscow. 2007;72(13).

114.Catuogno S, Esposito CL. Aptamer Cell-Based Selection: Overview and Advances. Biomedicines. 2017;5(3).
115.Agnihotri N, Dubey S, Bhide M. Design and Characterization of DNA Aptamer for Breast Tumor Marker by an Advantageous Method. International Journal of Innovative Research in Science, Engineering and Technology. 2014;3(10).
116.Mayer G, Ahmed M-SL, Dolf A, Endl E, Knolle PA, Famulok M. Fluorescence-activated cell sorting for aptamer SELEX with cell mixtures. Nature Protocols. 2010;5(12):1993-2004.
117.Mosing RK, Mendonsa SD, Bowser MT. Capillary electrophoresis-SELEX selection of aptamers with affinity for HIV-1 reverse transcriptase. Analytical Chemistry. 2005;77(19):6107-12.
118.Avci-Adali M, Paul A, Wilhelm N, Ziemer G, Wendel HP. Upgrading SELEX Technology by Using Lambda Exonuclease Digestion for Single-Stranded DNA Generation. Molecules. 2010;15(1):1-11.
119.Bunka DHJ, Stockley PG. Aptamers come of age - at last. Nature Reviews Microbiology. 2006;4(8):588-96.
120.Yang Q, Wang SP, Yu XL, Yang XH, Guo QP, Tang LJ, et al. A novel nucleic acid sequence encoding strategy for high-performance aptamer identification and the aid of sequence design and optimization. Chemometrics and Intelligent Laboratory Systems. 2017;170:32-7.
121.Li SH, Xu H, Ding HM, Huang YP, Cao XX, Yang G, et al. Identification of an aptamer targeting hnRNP A1 by tissue slide-based SELEX. Journal of Pathology. 2009;218(3):327-36.
122.Souza AG, Marangoni K, Fujimura PT, Alves PT, Silva MJ, Bastos VAF, et al. 3D Cell-SELEX: Development of RNA aptamers as molecular probes for PC-3 tumor cell line. Experimental Cell Research. 2016;341(2):147-56.
123.Zhou J, Battig MR, Wang Y. Aptamer-based molecular recognition for biosensor development. Analytical and Bioanalytical Chemistry. 2010;398(6):2471-80.
124.Musheev MU, Krylov SN. Selection of aptamers by systematic evolution of ligands by exponential enrichment: Addressing the polymerase chain reaction issue. Analytica Chimica Acta. 2006;564(1).

125.Navani NK, Li YF. Nucleic acid aptamers and enzymes as sensors. Current Opinion in Chemical Biology. 2006;10(3).
126.Han K, Liang Z, Zhou N. Design Strategies for Aptamer-Based Biosensors. Sensors. 2010;10(5).
127.Ohuchi S. Cell-SELEX technology. Biores Open Access. 2012;1(6):265-72.
128.Tu LC, Foltz G, Lin E, Hood L, Tian Q. Targeting Stem Cells-Clinical Implications for Cancer Therapy. Curr Stem Cell Res Ther. 2009;4(2):147-53.
129.Sefah K, Meng L, Lopez-Colon D, Jimenez E, Liu C, Tan W. DNA Aptamers as Molecular Probes for Colorectal Cancer Study. Plos One. 2010;5(12).
130.Orava EW, Cicmil N, Gariepy J. Delivering cargoes into cancer cells using DNA aptamers targeting internalized surface portals. Biochimica Et Biophysica Acta-Biomembranes. 2010;1798(12):2190-200.
131.Hou ZG, Meyer S, Propson NE, Nie J, Jiang P, Stewart R, et al. Characterization and target identification of a DNA aptamer that labels pluripotent stem cells. Cell Research. 2015;25(3):390-3.
132.Guo KT, Schafer R, Paul A, Gerber A, Ziemer G, Wendel HP. A new technique for the isolation and surface immobilization of mesenchymal stem cells from whole bone marrow using high-specific DNA aptamers. Stem Cells. 2006;24(10):2220-31.
133.Meyer S, Maufort JP, Nie J, Stewart R, McIntosh BE, Conti LR, et al. Development of an Efficient Targeted Cell-SELEX Procedure for DNA Aptamer Reagents. Plos One. 2013;8(8).
134.Zeng ZH, Parekh P, Li Z, Shi ZZ, Tung CH, Zu YL. Specific and Sensitive Tumor Imaging Using Biostable Oligonucleotide Aptamer Probes. Theranostics. 2014;4(9):945-52.
135.Wu QY, Wu L, Wang YZ, Zhu Z, Song YL, Tan YY, et al. Evolution of DNA aptamers for malignant brain tumor gliosarcoma cell recognition and clinical tissue imaging. Biosensors & Bioelectronics. 2016;80:1-8.
136.Shangguan D, Meng L, Cao ZC, Xiao Z, Fang X, Li Y, et al. Identification of liver cancer-specific aptamers using whole live cells. Analytical Chemistry. 2008;80(3):721-8.

137.Zhang XM, Peng L, Liang ZM, Kou ZW, Chen Y, Shi GW, et al. Effects of Aptamer to U87-EGFRvIII Cells on the Proliferation, Radiosensitivity, and Radiotherapy of Glioblastoma Cells. Molecular Therapy-Nucleic Acids. 2018;10:438-49.
138.Yang XH, Zhang XZ, Wang KM, Wang Q, Tan YY, Guo QP, et al. Whole cell-SELEX aptamers for fluorescence staining of frozen hepatocellular carcinoma tissues. Analytical Methods. 2014;6(10):3506-9.
139.Wu X, Liang H, Tan Y, Yuan C, Li S, Li X, et al. Cell-SELEX Aptamer for Highly Specific Radionuclide Molecular Imaging of Glioblastoma In Vivo. Plos One. 2014;9(3).
140.Sefah K, Tang ZW, Shangguan DH, Chen H, Lopez-Colon D, Li Y, et al. Molecular recognition of acute myeloid leukemia using aptamers. Leukemia. 2009;23(2):235-44.
141.Liu LK, Yang KG, Zhu XD, Liang Y, Chen YB, Fang F, et al. Aptamer-immobilized open tubular capillary column to capture circulating tumor cells for proteome analysis. Talanta. 2017;175:189-93.
142.Chen H, Yuan CH, Yang YF, Yin CQ, Guan Q, Wang FB, et al. Subtractive Cell-SELEX Selection of DNA Aptamers Binding Specifically and Selectively to Hepatocellular Carcinoma Cells with High Metastatic Potential. Biomed Research International. 2016.
143.Li WM, Bing T, Wei JY, Chen ZZ, Shangguan DH, Fang J. Cell-SELEX-based selection of aptamers that recognize distinct targets on metastatic colorectal cancer cells. Biomaterials. 2014;35(25):6998-7007.
144.Dastjerdi K, Tabar G, Valadan R. Enriched DNA pool for HER2-positive breast cancer cell line. Journal of Cellular Immunotherapy. 2015;1(1):13-5.
145.Chen HW, Medley CD, Sefah K, Shangguan D, Tang ZW, Meng L, et al. Molecular recognition of small-cell lung cancer cells using aptamers. Chemmedchem. 2008;3(6):991-1001.
146.Shangguan D, Li Y, Tang Z, Cao ZC, Chen HW, Mallikaratchy P, et al. Aptamers evolved from live cells as effective molecular probes for cancer study. Proceedings of the National Academy of Sciences of the United States of America. 2006;103(32).

147.Yuan BY, Jiang XC, Chen YY, Guo QP, Wang KM, Meng XX, et al. Metastatic cancer cell and tissue-specific fluorescence imaging using a new DNA aptamet developed by Cell-SELEX. Talanta. 2017;170:56-62.
148.Kim Y, Wu Q, Hamerlik P, Hitomi M, Sloan AE, Barnett GH, et al. Aptamer Identification of Brain Tumor-Initiating Cells. Cancer Research. 2013;73(15):4923-36.
149.Kang HS, Huh YM, Kim S, Lee D-k. Isolation of RNA Aptamers Targeting HER-2-overexpressing Breast Cancer Cells Using Cell-SELEX. Bulletin of the Korean Chemical Society. 2009;30(8):1827-31.
150.Wang JN, Zhang YJ, Chen Y, Hong SN, Sun Y, Sun N, et al. In vitro selection of DNA, aptamers against renal cell carcinoma using living cell-SELEX. Talanta. 2017;175:235-42.
151.Xu JH, Teng IT, Zhang LQ, Delgado S, Champanhac C, Cansiz S, et al. Molecular Recognition of Human Liver Cancer Cells Using DNA Aptamers Generated via Cell-SELEX. Plos One. 2015;10(5).
152.Liu J, Liu HX, Sefah K, Liu B, Pu Y, Van Simaeys D, et al. Selection of Aptamers Specific for Adipose Tissue. Plos One. 2012;7(5).
153.Raddatz M-SL, Dolf A, Endl E, Knolle P, Famulok M, Mayer G. Enrichment of cell-targeting and population-specific aptamers by fluorescence-activated cell sorting. Angewandte Chemie-International Edition. 2008;47(28):5190-3.
154.Ninomiya K, Kaneda K, Kawashima S, Miyachi Y, Ogino C, Shimizu N. Cell-SELEX based selection and characterization of DNA aptamer recognizing human hepatocarcinoma. Bioorganic & Medicinal Chemistry Letters. 2013;23(6):1797-802.
155.Yu XL, Yu RQ, Tang LJ, Guo QP, Zhang Y, Zhou Y, et al. Recognition of candidate aptamer sequences for human hepatocellular carcinoma in SELEX screening using structure-activity relationships. Chemometrics and Intelligent Laboratory Systems. 2014;136:10-4.
156.Cao HY, Yuan AH, Shi XS, Chen W, Miao Y. Evolution of a gastric carcinoma cell-specific DNA aptamer by live cell-SELEX. Oncology Reports. 2014;32(5):2054-60.

157.Zhang XJ, Zhang J, Ma YY, Pei XY, Liu QM, Lu B, et al. A cell-based single-stranded DNA aptamer specifically targets gastric cancer. International Journal of Biochemistry & Cell Biology. 2014;46:1-8.
158.Van Simaeys D, Lopez-Colon D, Sefah K, Sutphen R, Jimenez E, Tan W. Study of the Molecular Recognition of Aptamers Selected through Ovarian Cancer Cell-SELEX. Plos One. 2010;5(11).
159.Benedetto G, Hamp TJ, Wesselman PJ, Richardson C. Identification of Epithelial Ovarian Tumor-Specific Aptamers. Nucleic Acid Therapeutics. 2015;25(3):162-72.
160.Graham JC, Zarbl H. Use of Cell-SELEX to Generate DNA Aptamers as Molecular Probes of HPV-Associated Cervical Cancer Cells. Plos One. 2012;7(4).
161.Zhang K, Sefah K, Tang L, Zhao Z, Zhu G, Ye M, et al. A Novel Aptamer Developed for Breast Cancer Cell Internalization. Chemmedchem. 2012;7(1):79-84.
162.Li XL, Zhang WY, Liu L, Zhu Z, Ouyang GL, An Y, et al. In Vitro Selection of DNA Aptamers for Metastatic Breast Cancer Cell Recognition and Tissue Imaging. Analytical Chemistry. 2014;86(13):6596-603.
163.Lu M, Zhou L, Zheng XH, Quan Y, Wang XL, Zhou XN, et al. A novel molecular marker of breast cancer stem cells identified by cell-SELEX method. Cancer Biomarkers. 2015;15(2):163-70.
164.An Y, Wu J, Yang B, Zhu Z, Gao MX, Yu CD, et al. Selection and Application of DNA Aptamer Against Oncogene Amplified in Breast Cancer 1. Journal of Molecular Evolution. 2015;81(5-6):179-85.
165.Dastjerdi K, Tabar GH, Dehghani H, Haghparast A. Generation of an enriched pool of DNA aptamers for an HER2-overexpressing cell line selected by Cell SELEX. Biotechnology and Applied Biochemistry. 2011;58(4):226-30.
166.Liu Z, Duan J-H, Song Y-M, Ma J, Wang F-D, Lu X, et al. Novel HER2 Aptamer Selectively Delivers Cytotoxic Drug to HER2-positive Breast Cancer Cells in Vitro. Journal of Translational Medicine. 2012;10.
167.Chen CHB, Chernis GA, Hoang VQ, Landgraf R. Inhibition of heregulin signaling by an aptamer that preferentially binds to the oligomeric form of human epidermal growth factor receptor-3. Proceedings of the National Academy of Sciences of the United States of America. 2003;100(16):9226-31.

168.Iida J, Clancy R, Dorchak J, Somiari RI, Somiari S, Cutler ML, et al. DNA Aptamers against Exon v10 of CD44 Inhibit Breast Cancer Cell Migration. Plos One. 2014;9(2).
169.Somasunderam A, Thiviyanathan V, Tanaka T, Li X, Neerathilingam M, Lokesh GLR, et al. Combinatorial Selection of DNA Thioaptamers Targeted to the HA Binding Domain of Human CD44. Biochemistry. 2010;49(42):9106-12.
170.Subramanian N, Akilandeswari B, Bhutra A, Alameen M, Vetrivel U, Khetan V, et al. Targeting CD44, ABCG2 and CD133 markers using aptamers: in silico analysis of CD133 extracellular domain 2 and its aptamer. Rsc Advances. 2016;6(38):32115-23.
171.Mahlknecht G, Maron R, Mancini M, Schechter B, Sela M, Yarden Y. Aptamer to ErbB-2/HER2 enhances degradation of the target and inhibits tumorigenic growth. Proceedings of the National Academy of Sciences of the United States of America. 2013;110(20):8170-5.
172.Wang K, Fan DQ, Liu YQ, Wang EK. Highly sensitive and specific colorimetric detection of cancer cells via dual-aptamer target binding strategy. Biosensors & Bioelectronics. 2015;73:1-6.
173.Hua X, Zhou Z, Yuan L, Liu S. Selective collection and detection of MCF-7 breast cancer cells using aptamer-functionalized magnetic beads and quantum dots based nano-bio-probes. Analytica Chimica Acta. 2013;788:135-40.
174.Zhang JQ, Li SH, Liu F, Zhou LP, Shao NS, Zhao XH. SELEX Aptamer Used as a Probe to Detect Circulating Tumor Cells in Peripheral Blood of Pancreatic Cancer Patients. Plos One. 2015;10(3).
175.Xiao M, Chen YM, Biao MN, Zhang XD, Yang BC. Bio-functionalization of biomedical metals. Materials Science & Engineering C-Materials for Biological Applications. 2017;70:1057-70.
176.Hermawan H, Ramdan D, Djuansjah J. Metals for biomedical applications. In: Fazel-Rezai R, editor. Biomedical Engineering – From Theory to Applications. p. 411-30.
177.Zhang H, Han J, Sun Y, Huang Y, Zhou M. MC3T3-E1 cell response to stainless steel 316L with different surface treatments. Materials Science & Engineering C-Materials for Biological Applications. 2015;56:22-9.

178.Davis JR. Introduction to Stainless Steels. Alloy Digest Sourcebook: Stainless stees: ASM International; 2000. p. 584.
179.Virtanen S, Milosev I, Gomez-Barrena E, Trebse R, Salo J, Konttinen YT. Special modes of corrosion under physiological and simulated physiological conditions. Acta Biomaterialia. 2008;4(3):468-76.
180.Chen QZ, Thouas GA. Metallic implant biomaterials. Materials Science & Engineering R-Reports. 2015;87:1-57.
181.Latifi A, Imani M, Khorasani MT, Joupari MD. Electrochemical and chemical methods for improving surface characteristics of 316L stainless steel for biomedical applications. Surface & Coatings Technology. 2013;221:1-12.
182.Omar S, Repp F, Desimone PM, Weinkamer R, Wagermaier W, Cere S, et al. Sol-gel hybrid coatings with strontium-doped 45S5 glass particles for enhancing the performance of stainless steel implants: Electrochemical, bioactive and in vivo response. Journal of Non-Crystalline Solids. 2015;425:1-10.
183.Fathi MH, Zahrani EM, Zomorodian A. Novel fluorapatite/niobium composite coating for metallic human body implants. Materials Letters. 2009;63(13-14):1195-8.
184.Xiao YL, Zhao L, Shi YF, Liu N, Liu YL, Liu B, et al. Surface Modification of 316L Stainless Steel by Grafting Methoxy Poly(ethylene glycol) to Improve the Biocompatibility. Chemical Research in Chinese Universities. 2015;31(4):651-7.
185.Yuan S, Yin J, Jiang W, Liang B, Pehkonen SO, Choong C. Enhancing antibacterial activity of surface-grafted chitosan with immobilized lysozyme on bioinspired stainless steel substrates. Colloids and Surfaces B-Biointerfaces. 2013;106:11-21.
186.Medilanski E, Kaufmann K, Wick LY, Wanner O, Harms H. Influence of the surface topography of stainless steel on bacterial adhesion. Biofouling. 2002;18(3):193-203.
187.Manivasagam G, Dhinasekaram D, Rajamanicham A. Biomedical implants: Corrosion and its prevention - A review. Recent Patents on Corrosion Science. 2010:40-54.
188.Garcia A. Surface Modification of Biomaterials. In: Atala A, Lanza R, Thomson J, Nerem R, editors. Principles of Regenerative Medicine. 3. 2 ed2011.

189.Shih CC, Shih CM, Su YY, Su LHJ, Chang MS, Lin SJ. Effect of surface oxide properties on corrosion resistance of 316L stainless steel for biomedical applications. Corrosion Science. 2004;46(2):427-41.
190.Khalil F, Franzmann E, Ramcke J, Dakischew O, Lips KS, Reinhardt A, et al. Biomimetic PEG-catecholates for stabile antifouling coatings on metal surfaces: Applications on TiO2 and stainless steel. Colloids and Surfaces B-Biointerfaces. 2014;117:185-92.
191.Bayram C, Mizrak AK, Akturk S, Kursaklioglu H, Iyisoy A, Ifran A, et al. In vitro biocompatibility of plasma-aided surface-modified 316L stainless steel for intracoronary stents. Biomedical Materials. 2010;5(5).
192.Yang WJ, Cai T, Neoh K-G, Kang E-T, Dickinson GH, Teo SL-M, et al. Biomimetic Anchors for Antifouling and Antibacterial Polymer Brushes on Stainless Steel. Langmuir. 2011;27(11):7065-76.
193.Zhu Z, Xu G, An Y, He C. Construction of octadecyltrichlorosilane self-assembled monolayer on stainless steel 316L surface. Colloids and Surfaces a-Physicochemical and Engineering Aspects. 2014;457:408-13.
194.Hequet A, Humblot V, Berjeaud J-M, Pradier C-M. Optimized grafting of antimicrobial peptides on stainless steel surface and biofilm resistance tests. Colloids and Surfaces B-Biointerfaces. 2011;84(2):301-9.
195.Muller R, Abke J, Schnell E, Macionczyk F, Gbureck U, Mehrl R, et al. Surface engineering of stainless steel materials by covalent collagen immobilization to improve implant biocompatibility. Biomaterials. 2005;26(34):6962-72.
196.Xie D, Wan GJ, Maitz MF, Sun H, Huang N. Deformation and corrosion behaviors of Ti-O film deposited 316L stainless steel by plasma immersion ion implantation and deposition. Surface & Coatings Technology. 2013;214:117-23.
197.Jin X, Gao L, Liu E, Yu F, Shu X, Wang H. Microstructure, corrosion and tribological and antibacterial properties of Ti-Cu coated stainless steel. Journal of the Mechanical Behavior of Biomedical Materials. 2015;50:23-32.
198.Wang L, Zhao X, Ding MH, Zheng H, Zhang HS, Zhang B, et al. Surface modification of biomedical AISI 316L stainless steel with zirconium carbonitride coatings. Applied Surface Science. 2015;340:113-9.

199.Jones JE, Chen M, Yu QS. Corrosion resistance improvement for 316L stainless steel coronary artery stents by trimethylsilane plasma nanocoatings. Journal of Biomedical Materials Research Part B-Applied Biomaterials. 2014;102(7):1363-74.
200.Qiu CC, Liu DM, Jin K, Fang L, Xie GX, Robertson J. Electrochemical functionalization of 316 stainless steel with polyaniline-graphene oxide: Corrosion resistance study. Materials Chemistry and Physics. 2017;198:90-8.
201.Park J, Kim DJ, Kim YK, Lee KH, Lee H, Ahn S. Improvement of the biocompatibility and mechanical properties of surgical tools with TiN coating by PACVD. Thin Solid Films. 2003;435(1-2):102-7.
202.Salahinejad E, Hadianfard MJ, Macdonald DD, Mozafari M, Vashaee D, Tayebi L. A new double-layer sol-gel coating to improve the corrosion resistance of a medical-grade stainless steel in a simulated body fluid. Materials Letters. 2013;97:162-5.
203.Wise S, Praveesuda M, Waterhouse A, Santos M, Fillipe E, Hung J, et al. Immobilization of bioactive plasmin reduces the thrombogenicity of metal surfaces. Colloids and Surfaces B: Biointerfaces. 2015;136:944-54.
204.Liu Y, Luo R, Shen F, Tang L, Wang J, Huang N. Construction of mussel-inspired coating via the direct reaction of catechol and polyethyleneimine for efficient heparin immobilization. Applied Surface Science. 2015;328:163-9.
205.Benvenuto P, Neves MAD, Blaszykowski C, Romaschin A, Chung T, Kim SR, et al. Adlayer-Mediated Antibody Immobilization to Stainless Steel for Potential Application to Endothelial Progenitor Cell Capture. Langmuir. 2015;31(19):5423-31.
206.Lee H, Dellatore SM, Miller WM, Messersmith PB. Mussel-inspired surface chemistry for multifunctional coatings. Science. 2007;318(5849):426-30.
207.Yang Y, Qi P, Ding Y, Maitz MF, Yang Z, Tu Q, et al. A biocompatible and functional adhesive amine-rich coating based on dopamine polymerization. Journal of Materials Chemistry B. 2015;3(1):72-81.
208.Jin W, Yang L, Yang W, Chen B, Chen J. Grafting of HEMA onto dopamine coated stainless steel by Co-60-gamma irradiation method. Radiation Physics and Chemistry. 2014;105:57-62.

209.Liu X, Yue Z, Romeo T, Weber J, Scheuermann T, Moulton S, et al. Biofunctionalized anti-corrosive silane coatings for magnesium alloys. Acta Biomaterialia. 2013;9(10):8671-7.
210.Liu Y, Cao H, Yu Y, Chen S. Corrosion Protection of Silane Coatings Modified by Carbon Nanotubes on Stainless Steel. International Journal of Electrochemical Science. 2015;10(4):3497-509.
211.Jo S, Park K. Surface modification using silanated poly(ethylene glycol)s. Biomaterials. 2000;21(6):605-16.
212.Zhang F, Kang ET, Neoh KG, Wang P, Tan KL. Surface modification of stainless steel by grafting of poly(ethylene glycol) for reduction in protein adsorption. Biomaterials. 2001;22(12):1541-8.
213.Pang LQ, Zhong LJ, Zhou HF, Wu XE, Chen XD. Grafting of ionic liquids on stainless steel surface for antibacterial application. Colloids and Surfaces B-Biointerfaces. 2015;126:162-8.
214.Bastarrachea LJ, Goddard JM. Development of antimicrobial stainless steel via surface modification with N-halamines: Characterization of surface chemistry and N-halamine chlorination. Journal of Applied Polymer Science. 2013;127(1):821-31.
215.Kang C-K, Lee Y-S. The surface modification of stainless steel and the correlation between the surface properties and protein adsorption. Journal of Materials Science-Materials in Medicine. 2007;18(7):1389-98.
216.Jussila P, Ali-Loytty H, Lahtonen K, Hirsimaki M, Vaden M. Effect of surface hydroxyl concentration on the bonding and morphology of aminopropylsilane thin films on austenitic stainless steel. Surface and Interface Analysis. 2010;42(3):157-64.
217.Soya M, Yoshioka T, Shinozaki K, Tanaka J. Effect of Oxide Layers of Ni-Free Stainless-Steel on Silane Coupling Agent Immobilization. Materials Transactions. 2009;50(6):1318-21.
218.Yoshioka T, Tsuru K, Hayakawa S, Osaka A. Preparation of alginic acid layers on stainless-steel substrates for biomedical applications. Biomaterials. 2003;24(17):2889-94.

219.Zhong Q, Yan J, Qian X, Zhang T, Zhang Z, Li A. Atomic layer deposition enhanced grafting of phosphorylcholine on stainless steel for intravascular stents. Colloids and Surfaces B-Biointerfaces. 2014;121:238-47.
220.Hynninen V, Vuori L, Hannula M, Tapio K, Lahtonen K, Isoniemi T, et al. Improved antifouling properties and selective biofunctionalization of stainless steel by employing heterobifunctional silane-polyethylene glycol overlayers and avidin-biotin technology. Scientific Reports. 2016;6.
221.Vuori L, Hannula M, Lahtonen K, Jussila P, Ali-Loytty H, Hirsimaki M, et al. Controlling the synergetic effects in (3-aminopropyl) trimethoxysilane and (3-mercaptopropyl) trimethoxysilane coadsorption on stainless steel surfaces. Applied Surface Science. 2014;317:856-66.
222.Okner R, Domb AJ, Mandler D. Electrochemically deposited poly(ethylene glycol)-based sol-gel thin films on stainless steel stents. New Journal of Chemistry. 2009;33(7):1596-604.
223.Wei J, Ravn DB, Gram L, Kingshott P. Stainless steel modified with poly(ethylene glycol) can prevent protein adsorption but not bacterial adhesion. Colloids and Surfaces B-Biointerfaces. 2003;32(4):275-91.
224.Kaufmann CR, Mani G, Marton D, Johnson DM, Agrawal CM. Long-term stability of self-assembled monolayers on 316L stainless steel. Biomedical Materials. 2010;5(2).
225.Shustak G, Domb AJ, Mandler D. Preparation and characterization of n-alkanoic acid self-assembled monolayers adsorbed on 316L stainless steel. Langmuir. 2004;20(18):7499-506.
226.Mahapatro A, Johnson DM, Patel DN, Feldman MD, Ayon AA, Agrawal CM. The use of alkanethiol self-assembled monolayers on 316L stainless steel for coronary artery stent nanomedicine applications: an oxidative and in vitro stability study. Nanomedicine : nanotechnology, biology, and medicine. 2006;2(3):182-90.
227.Harvey J, Bergdahl A, Dadafarin H, Ling L, Davis EC, Omanovic S. An electrochemical method for functionalization of a 316L stainless steel surface being used as a stent in coronary surgery: irreversible immobilization of fibronectin for the enhancement of endothelial cell attachment. Biotechnology Letters. 2012;34(6):1159-65.

228.Yang Z, Wang J, Luo R, Maitz MF, Jing F, Sun H, et al. The covalent immobilization of heparin to pulsed-plasma polymeric allylamine films on 316L stainless steel and the resulting effects on hemocompatibility. Biomaterials. 2010;31(8):2072-83.
229.Kastellorizios M, Michanetzis GPAK, Pistillo BR, Mourtas S, Klepetsanis P, Favia P, et al. Haemocompatibility improvement of metallic surfaces by covalent immobilization of heparin-liposomes. International Journal of Pharmaceutics. 2012;432(1-2):91-8.
230.Yin Y, Wise SG, Nosworthy NJ, Waterhouse A, Bax DV, Youssef H, et al. Covalent immobilisation of tropoelastin on a plasma deposited interface for enhancement of endothelialisation on metal surfaces. Biomaterials. 2009;30(9):1675-81.
231.Sasaki M, Inoue M, Katada Y, Taguchi T. The effect of VEGF-immobilized nickel-free high-nitrogen stainless steel on viability and proliferation of vascular endothelial cells. Colloids and Surfaces B-Biointerfaces. 2012;92:1-8.
232.Caro A, Humblot V, Methivier C, Minier M, Barbes L, Li J, et al. Bioengineering of stainless steel surface by covalent immobilization of enzymes. Physical characterization and interfacial enzymatic activity. Journal of Colloid and Interface Science. 2010;349(1):13-8.
233.Kruszewski KM, Nistico L, Longwell MJ, Hynes MJ, Maurer JA, Hall-Stoodley L, et al. Reducing Staphylococcus aureus biofilm formation on stainless steel 316L using functionalized self-assembled monolayers. Materials Science & Engineering C-Materials for Biological Applications. 2013;33(4):2059-69.
234.Braceras I, Pacha-Olivenza MA, Calzado-Martin A, Multigner M, Vera C, Labajos-Broncano L, et al. Decrease of Staphylococcal adhesion on surgical stainless steel after Si ion implantation. Applied Surface Science. 2014;310:36-41.
235.Zhao Q, Liu Y, Wang C, Wang S, Peng N, Jeynes C. Bacterial adhesion on ion-implanted stainless steel surfaces. Applied Surface Science. 2007;253(21):8674-81.
236.Navarro M, Michiardi A, Castano O, Planell JA. Biomaterials in orthopaedics. Journal of the Royal Society Interface. 2008;5(27):1137-58.

237.Sutha S, Karunakaran G, Rajendran V. Enhancement of antimicrobial and long-term biostability of the zinc-incorporated hydroxyapatite coated 316L stainless steel implant for biomedical application. Ceramics International. 2013;39(5):5205-12.
238.Gopi D, Ramya S, Rajeswari D, Kavitha L. Corrosion protection performance of porous strontium hydroxyapatite coating on polypyrrole coated 316L stainless steel. Colloids and Surfaces B-Biointerfaces. 2013;107:130-6.
239.Gopi D, Ramya S, Rajeswari D, Surendiran M, Kavitha L. Development of strontium and magnesium substituted porous hydroxyapatite/poly(3,4-ethylenedioxythiophene) coating on surgical grade stainless steel and its bioactivity on osteoblast cells. Colloids and Surfaces B-Biointerfaces. 2014;114:234-40.
240.Agarwal R, Gonzalez-Garcia C, Torstrick B, Guldberg RE, Salmeron-Sanchez M, Garcia AJ. Simple coating with fibronectin fragment enhances stainless steel screw osseointegration in healthy and osteoporotic rats. Biomaterials. 2015;63:137-45.
241.Chen L, Han D, Jiang L. On improving blood compatibility: From bioinspired to synthetic design and fabrication of biointerfacial topography at micro/nano scales. Colloids and Surfaces B-Biointerfaces. 2011;85(1):2-7.
242.Tan QG, Ji J, Barbosa MA, Fonseca C, Shen JC. Constructing thromboresistant surface on biomedical stainless steel via layer-by-layer deposition anticoagulant. Biomaterials. 2003;24(25):4699-705.
243.Joung YK, You SS, Park KM, Go DH, Park KD. In situ forming, metal-adhesive heparin hydrogel surfaces for blood-compatible coating. Colloids and Surfaces B-Biointerfaces. 2012;99:102-7.
244.Li A. Immobilization of hesperidin on stainless steel surfaces and its blood compatibility. Biomedicine and Preventive Nutrition. 2013;3(4).
245.Volny M, Elam WT, Ratner BD, Turecek F. Enhanced in-vitro blood compatibility of 316L stainless steel surfaces by reactive landing of hyaluronan ions. Journal of Biomedical Materials Research Part B-Applied Biomaterials. 2007;80B(2):505-10.
246.Farhatnia Y, Tan A, Motiwala A, Cousins BG, Seifalian AM. Evolution of covered stents in the contemporary era: clinical application, materials and manufacturing strategies using nanotechnology. Biotechnology Advances. 2013;31(5):524-42.

247.Lee JM, Choe W, Kim B-K, Seo W-W, Lim W-H, Kang C-K, et al. Comparison of endothelialization and neointimal formation with stents coated with antibodies against CD34 and vascular endothelial-cadherin. Biomaterials. 2012;33(35):8917-27.
248.Qi P, Yan W, Yang Y, Li Y, Fan Y, Chen J, et al. Immobilization of DNA aptamers via plasma polymerized allylamine film to construct an endothelial progenitor cell-capture surface. Colloids and Surfaces B-Biointerfaces. 2015;126:70-9.
249.Ceylan H, Tekinay AB, Guler MO. Selective adhesion and growth of vascular endothelial cells on bioactive peptide nanofiber functionalized stainless steel surface. Biomaterials. 2011;32(34):8797-805.
250.Huang L-Y, Yang M-C. Surface immobilization of chondroitin 6-sulfate/heparin multilayer on stainless steel for developing drug-eluting coronary stents. Colloids and Surfaces B-Biointerfaces. 2008;61(1):43-52.
251.Huang L-Y, Yang M-C. Behaviors of controlled drug release of magnetic-gelatin hydrogel coated stainless steel for drug-eluting-stents application. Journal of Magnetism and Magnetic Materials. 2007;310(2):2874-6.
252.Hong B, Zu YL. Detecting Circulating Tumor Cells: Current Challenges and New Trends. Theranostics. 2013;3(6):377-94.
253.Saucedo-Zeni N, Mewes S, Niestroj R, Gasiorowski L, Murawa D, Nowaczyk P, et al. A novel method for the in vivo isolation of circulating tumor cells from peripheral blood of cancer patients using a functionalized and structured medical wire. International Journal of Oncology. 2012;41(4):1241-50.
254.Zhang HD, Gong SC, Liu YQ, Liang LJ, He SB, Zhang QX, et al. Enumeration and molecular characterization of circulating tumor cell using an in vivo capture system in squamous cell carcinoma of head and neck. Chinese Journal of Cancer Research. 2017;29(3):196-203.
255.Luecke K, Hoon D, Booth C, Gasiorowski L, Wojciech W. An Effective In Vivo Liquid Biopsy Tool for High-Yield Isolation of Circulating Tumor Cells. Journal of Thoracic Oncology. 2015;10(9):S604-S.
256.Gorges TM, Penkalla N, Schalk T, Joosse SA, Riethdorf S, Tucholski J, et al. Enumeration and Molecular Characterization of Tumor Cells in Lung Cancer Patients

Using a Novel In Vivo Device for Capturing Circulating Tumor Cells. Clinical Cancer Research. 2016;22(9):2197-206.
257.Gallerani G, Cocchi C, Bocchini M, Piccinini F, Fabbri F. Characterization of Tumor Cells Using a Medical Wire for Capturing Circulating Tumor Cells: A 3D Approach Based on Immunofluorescence and DNA FISH. Jove-Journal of Visualized Experiments. 2017(130).
258.Nowaczyk P, Herold S, Kim PS, Schmitz A, Polom K, Murawa P, et al. Functionalized and Structured Medical Wire as a Device for In-vivo Isolation of Circulating Tumor Cells in Breast Cancer Patients. European Journal of Cancer. 2012;48:S58-S9.
259.Herold S, Gasiorowski L, Nowaczyk P, Schumann A, Theil G, Haubold K, et al. An innovative approach for in-vivo isolation of circulating tumor cells (CTCs). European Journal of Cancer. 2013;49:S199-S.
260.Heyden A, Tomasi T, Zeni N, Herold S, Nowaczyk P, Schmitz A, et al. In vivo isolation of circulating tumor cells. European Journal of Cancer. 2011;47:S19-S.
261.Chudak C, Herrmann J, Lesser T. Enumeration and molecular characterization of circulating tumor cells in lung cancer patients using the GILUPI CellCollector. Journal of Thoracic Oncology. 2016;11(4):S104-S5.
262.Dlugaszewska B, Gasiorowski L, Herold S, Nowack B, Dworacki G, Luecke K, et al. An innovative technology for in vivo isolation of circulating tumor cells in non-small cell lung cancer (NSCLC) patients and immunofluorescent detection of ALK protein. Journal of Thoracic Oncology. 2014;9(4):S14-S5.
263.Gasiorowski L, Herold S, Morgenthaler N, Dworacki G, Luecke K, Dyszkiewicz W. A new medical device for in-vivo isolation of circulating tumor cells in non small cell lung cancer (NSCLC) patients. Journal of Thoracic Oncology. 2012;7(6):S32-S.
264.Theil G, Wencker A, Kersten F, Pini G, Luecke K, Fornara P. Verification of a functionalized structured medical wire for the isolation of circulating tumor cells (CTC) in patients with renal cell carcinoma. Journal of Urology. 2013;189(4):E192-E.
265.Theil G, Fischer K, Weber E, Medek R, Hoda R, Lucke K, et al. The Use of a New CellCollector to Isolate Circulating Tumor Cells from the Blood of Patients with

Different Stages of Prostate Cancer and Clinical Outcomes - A Proof-of-Concept Study. Plos One. 2016;11(8).
266.Li J, Geng C, Yan M, Wang Y, Ouyang Q, Yin Y, et al. Circulating tumor cells in patients with breast cancer were detected by a novel device: a multicenter clinical trial in China. National Medical Journal of China. 2017;97(24):1857-61.
267.Markou A, Lazaridou M, Paraskevopoulos P, Chen SK, Swierczewska M, Budna J, et al. Multiplex Gene Expression Profiling of In Vivo Isolated Circulating Tumor Cells in High-Risk Prostate Cancer Patients. Clinical Chemistry. 2018;64(2):297-306.
268.Scherag FD, Niestroj-Pahl R, Krusekopf S, Lucke K, Brandstetter T, Ruhe J. Highly Selective Capture Surfaces on Medical Wires for Fishing Tumor Cells in Whole Blood. Analytical Chemistry. 2017;89(3):1846-54.
269.Weng W-H, Ho I-L, Pang C-C, Pang S-N, Pan T-M, Leung W-H. Real-time circulating tumor cells detection via highly sensitive needle-like cytosensor-demonstrated by a blood flow simulation. Biosensors and bioelectronics. 2018(116):51-9.
270.Amiri A, Ghaemi F. Graphene grown on stainless steel mesh as a highly efficient sorbent for sorptive microextraction of polycyclic aromatic hydrocarbons from water samples. Analytica Chimica Acta. 2017;994:29-37.
271.Rezaei B, Havakeshian E, Ensafi AA. Stainless steel modified with an aminosilane layer and gold nanoparticles as a novel disposable substrate for impedimetric immunosensors. Biosensors & Bioelectronics. 2013;48:61-6.
272.Mehrvar M, Bis C, Scharer JM, Moo-Young M, Luong JH. Fiber-optic biosensors - Trends and advances. Analytical Sciences. 2000;16(7):677-92.
273.Leung A, Shankar PM, Mutharasan R. A review of fiber-optic biosensors. Sensors and Actuators B-Chemical. 2007;125(2):688-703.
274.Correia R, James S, Lee SW, Morgan SP, Korposh S. Biomedical application of optical fibre sensors. Journal of Optics. 2018;20(7).
275.Chryssis AN, Saini SS, Lee SM, Yi HM, Bentley WE, Dagenais M. Detecting hybridization of DNA by highly sensitive evanescent field etched core fiber bragg grating sensors. Ieee Journal of Selected Topics in Quantum Electronics. 2005;11(4):864-72.

276.Marazuela MD, Moreno-Bondi MC. Fiber-optic biosensors - an overview. Analytical and Bioanalytical Chemistry. 2002;372(5-6):664-82.
277.Keiser G. Optical Fibers for Biophotonics Applications. Biophotonics Graduate Texts in Physics: Springer; 2016. p. 53-89.
278.Saini SS, Stanford C, Lee SM, Park J, DeShong R, Bentley WE, et al. Monolayer detection of biochemical agents using etched-core fiber Bragg grating sensors. Ieee Photonics Technology Letters. 2007;19(17-20):1341-3.
279.Mishra V, Singh N, Tiwari U, Kapur P. Fiber grating sensors in medicine: Current and emerging applications. Sensors and Actuators a-Physical. 2011;167(2):279-90.
280.Umesh S, Asokan S. A Brief Overview of the Recent Bio-Medical Applications of Fiber Bragg Grating Sensors. Journal of the Indian Institute of Science. 2014;94(3):319-28.
281.Bal HK, Brodzeli Z, Dragomir NM, Collins SF, Sidiroglou F. Uniformly thinned optical fibers produced via HF etching with spectral and microscopic verification. Applied Optics. 2012;51(13):2282-7.
282.Shu XW, Zhang L, Bennion I. Sensitivity characteristics near the dispersion turning points of long-period fiber gratings in B/Ge codoped fiber. Optics Letters. 2001;26(22):1755-7.
283.Shu XW, Zhang L, Bennion I. Sensitivity characteristics of long-period fiber gratings. Journal of Lightwave Technology. 2002;20(2):255-66.
284.Webb DJ, Hathaway MW, Jackson DA, Jones S, Zhang L, Bennion I. First in-vivo trials of a fiber Bragg grating based temperature profiling system. Journal of Biomedical Optics. 2000;5(1):45-50.
285.Patrick HJ, Kersey AD, Bucholtz F. Analysis of the response of long period fiber gratings to external index of refraction. Journal of Lightwave Technology. 1998;16(9):1606-12.
286.Chen X, Liu C, Hughes M, Nagel D, Hine A, Zhang L. EDC-mediated oligonucleotide immobilization on a long period grafting optical biosensor. J Biosensors and Bioelectronics. 2015;6(2).
287.Chiavaioli F, Baldini F, Tombelli S, Trono C, Giannetti A. Biosensing with optical fiber gratings. Nanophotonics. 2017;6(4):663-79.

288.Chiavaioli F, Gouveia CAJ, Jorge PAS, Baldini F. Towards a Uniform Metrological Assessment of Grating-Based Optical Fiber Sensors: From Refractometers to Biosensors. Biosensors-Basel. 2017;7(2).
289.Iadicicco A, Campopiano S, Cutolo A, Giordano M, Cusano A. Thinned fiber Bragg gratings for sensing applications. Proceedings of WFOPC 2005: 4th IEEE/LEOS Workshop on Fibres and Optical Passive Components. 2005:216-21.
290.Jiao LZ, Dong DM, Zheng WG, Wu WB, Shen CJ, Yan H. Research on fiber-optic etching method for evanescent wave sensors. Optik. 2013;124(8):740-3.
291.Libish T. Design and Development of Fiber Grating Based Chemical and Bio-Sensors. Kerala, India: Cochin University of Science and Technology; 2015.
292.Tao MM, Jin YL, Gu N, Huang L. A method to control the fabrication of etched optical fiber probes with nanometric tips. Journal of Optics. 2010;12(1).
293.Ko S, Lee J, Koo J, Joo BS, Gu M, Lee JH. Chemical Wet Etching of an Optical Fiber Using a Hydrogen Fluoride-Free Solution for a Saturable Absorber Based on the Evanescent Field Interaction. Journal of Lightwave Technology. 2016;34(16):3776-84.
294.Ryu G, Dagenais M, Hurley MT, DeShong P. High Specificity Binding of Lectins to Carbohydrate-Functionalized Fiber Bragg Gratings: A New Model for Biosensing Applications. Ieee Journal of Selected Topics in Quantum Electronics. 2010;16(3):647-53.
295.Puygranier BAF, Dawson P. Chemical etching of optical fibre tips - experiment and model. Ultramicroscopy. 2000;85(4):235-48.
296.Libish TM, Bobby MC, Linslal CL, Mathew S, Pradeep C, Indu S, et al. Etched and DNA coated Fiber Bragg Grating based biosensor for protein concentration measurement. Optoelectronics and Advanced Materials-Rapid Communications. 2015;9(11-12):1401-5.
297.Liu XM, Zhang XM, Cong J, Xu J, Chen KS. Demonstration of etched cladding fiber Bragg grating-based sensors with hydrogel coating. Sensors and Actuators B-Chemical. 2003;96(1-2):468-72.
298.Maguis S, Laffont G, Ferdinand P, Carbonnier B, Kham K, Mekhalif T, et al. Biofunctionalized tilted Fiber Bragg Gratings for label-free immunosensing. Optics Express. 2008;16(23):19049-62.

299.Long F, He MA, Zhu AN, Song BD, Sheng JW, Shi HC. Compact quantitative optic fiber-based immunoarray biosensor for rapid detection of small analytes. Biosensors & Bioelectronics. 2010;26(1):16-22.
300.Albert J, Lepinay S, Caucheteur C, DeRosa MC. High resolution grating-assisted surface plasmon resonance fiber optic aptasensor. Methods. 2013;63(3):239-54.
301.Voisin V, Pilate J, Damman P, Megret P, Caucheteur C. Highly sensitive detection of molecular interactions with plasmonic optical fiber grating sensors. Biosensors & Bioelectronics. 2014;51:249-54.
302.Yildirim N, Long F, He M, Gao C, Shi HC, Gu AZ. A portable DNAzyme-based optical biosensor for highly sensitive and selective detection of lead (II) in water sample. Talanta. 2014;129:617-22.
303.Tang YF, Long F, Gu CM, Wang C, Han ST, He M. Reusable split-aptamer-based biosensor for rapid detection of cocaine in serum by using an all-fiber evanescent wave optical biosensing platform. Analytica Chimica Acta. 2016;933:182-8.
304.Zammatteo N, Jeanmart L, Hamels S, Courtois S, Louette P, Hevesi L, et al. Comparison between different strategies of covalent attachment of DNA to glass surfaces to build DNA microarrays. Analytical Biochemistry. 2000;280(1):143-50.
305.Alzubaidi RMI, Al-Dergazly AA, Candiani A, Cucinotta A, Di Fina E, Selleri S, et al. Biosensor Based on Microstructured Optical Fiber Bragg Grating for DNA Detection. 2014 Fotonica Aeit Italian Conference on Photonics Technologies. 2014.
306.Tedeschi L, Domenici C, Ahluwalia A, Baldini F, Mencaglia A. Antibody immobilisation on fibre optic TIRF sensors. Biosensors & Bioelectronics. 2003;19(2):85-93.
307.Khodakov DA, Thredgold LD, Lenehan CE, Andersson GA, Kobus H, Ellis AV, editors. Surface modification of poly(dimethylsiloxane) (PDMS) microchannels with DNA capture-probes for potential use in microfluidic DNA analysis systems. Conference on Smart Nano-Micro Materials and Devices/SPIE Smart Nano + Micro Materials and Devices Forum; 2011 Dec 05-07; Melbourne, AUSTRALIA2011.
308.Le MH, Jimenez C, Chainet E, Stambouli V. A Label-Free Impedimetric DNA Sensor Based on a Nanoporous SnO2 Film: Fabrication and Detection Performance. Sensors. 2015;15(5):10686-704.

309.Krishan M, Seema S, Tiwari B, Sharma H, Londhe S, Arora V. Surface characterization of nickel titanium orthodontic archwires. Med J Armed Forces india. 2015;71:340-5.
310.Chovelon JM, Aarch LE, Charbonnier M, Romand M. Silanization of stainless steel surfaces: Influence of application parameters. Journal of Adhesion. 1995;50(1):43-58.
311.Minier M, Salmain M, Yacoubi N, Barbes L, Methivier C, Zanna S, et al. Covalent immobilization of lysozyme on stainless steel. Interface spectroscopic characterization and measurement of enzymatic activity. Langmuir. 2005;21(13):5957-65.
312.Latifi A, Imani M, Khorasani MT, Joupari MD. Plasma surface oxidation of 316L stainless steel for improving adhesion strength of silicone rubber coating to metal substrate. Applied Surface Science. 2014;320:471-81.
313.Mahapatro A, Johnson DM, Patel DN, Feldman MD, Ayon AA, Agrawal CM. Surface modification of functional self-assembled monolayers on 316L stainless steel via lipase catalysis. Langmuir. 2006;22(3):901-5.
314.Bohinc K, Drazic G, Abram A, Jevsnik M, Jersek B, Nipic D, et al. Metal surface characteristics dictate bacterial adhesion capacity. International Journal of Adhesion and Adhesives. 2016;68:39-46.
315.Gil A, Fernandez M, Mendizabal I, Korili SA, Soto-Armananzas J, Crespo-Durante A, et al. Fabrication of TiO2 coated metallic wires by the sol-gel technique as a humidity sensor. Ceramics International. 2016;42(7):9292-8.
316.Wei Y, Ji Y, Xiao L-L, Lin Q-k, Xu J-p, Ren K-f, et al. Surface engineering of cardiovascular stent with endothelial cell selectivity for in vivo re-endothelialisation. Biomaterials. 2013;34(11):2588-99.
317.Sun M, Feng JJ, Bu YN, Wang XJ, Duan HM, Luo CN. Palladium-coated stainless-steel wire as a solid-phase microextraction fiber. Journal of Separation Science. 2015;38(9):1584-90.
318.Zhang Z, Zhang W, Bao T, Chen Z. Jacket-free stir bar sorptive extraction with bio-inspired polydopamine-functionalized immobilization of cross-linked polymer on stainless steel wire. Journal of Chromatography A. 2015;1407:1-10.

319.Kheirkhah M, Fathi M, Salimijazi HR, Razavi M. Surface modification of stainless steel implants using nanostructured forsterite (Mg2SiO4) coating for biomaterial applications. Surface & Coatings Technology. 2015;276:580-6.
320.Wang YM, Pang XF, Zhang YY, Wang HZ. Characterization of covalent immobilization on the surface of optical fibers by scanning electron microscopy and energy dispersive X-ray spectrometry. Surface and Interface Analysis. 2009;41(10):775-8.
321.Kyaw HH, Al-Harthi SH, Sellai A, Dutta J. Self-organization of gold nanoparticles on silanated surfaces. Beilstein Journal of Nanotechnology. 2015;6:2345-53.
322.Arghir I, Spasic D, Verlinden BE, Delport F, Lammertyn J. Improved surface plasmon resonance biosensing using silanized optical fibers. Sensors and Actuators B-Chemical. 2015;216:518-26.
323.Sridevi S, Vasu KS, Jayaraman N, Asokan S, Sood AK. Optical bio-sensing devices based on etched fiber Bragg gratings coated with carbon nanotubes and graphene oxide along with a specific dendrimer. Sensors and Actuators B-Chemical. 2014;195:150-5.
324.Sridevi S, Vasu KS, Asokan S, Sood AK. Sensitive detection of C-reactive protein using optical fiber Bragg gratings. Biosensors & Bioelectronics. 2015;65:251-6.
325.Sun DD, Ran Y, Wang GJ. Label-Free Detection of Cancer Biomarkers Using an In-Line Taper Fiber-Optic Interferometer and a Fiber Bragg Grating. Sensors. 2017;17(11).
326.Ribaut C, Loyez M, Larrieu JC, Chevineau S, Lambert P, Remmelink M, et al. Cancer biomarker sensing using packaged plasmonic optical fiber gratings: Towards in vivo diagnosis. Biosensors & Bioelectronics. 2017;92:449-56.
327.François A, Ebendorff-Heidepriem H, Monro T, editors. Comparison of surface functionalization processes for optical fibre biosensing applications. Proc SPIE 7503 20th International Conference on Optical Fibre Sensors; 2009; Edinburgh, UK.
328.Debs JE, Ebendorff-Heidepriem H, Quinton JS, Monro TM. A Fundamental Study Into the Surface Functionalization of Soft Glass Microstructured Optical Fibers via Silane Coupling Agents. Journal of Lightwave Technology. 2009;27(5-8):576-82.

329.Shah S, Hariharan U, Bhargava A. Recent trends in anaesthesia and analgesia for breast cancer surgery. Trends in anasthesia and critical care. 2018;20:11-20.
330.Pavlopoulou A, Oktay Y, Vougas K, Louka M, Vorgias CE, Georgakilas AG. Determinants of resistance to chemotherapy and ionizing radiation in breast cancer stem cells. Cancer Letters. 2016;380(2):485-93.
331.Vorobjev I, Barteneva NS. Temporal Heterogeneity Metrics in Apoptosis Induced by Anticancer Drugs. Journal of Histochemistry & Cytochemistry. 2015;63(7):494-510.
332.Groner B, Vafaizadeh V, Brill B, Klemmt P. Mammary epithelial and breast cancer stem cells. European journal of cancer (Oxford, England : 1990). 2009;45 Suppl 1:186-93.
333.Kim EY, Kim JW, Kim WK, Han BS, Park SG, Chung BH, et al. Selection of Aptamers for Mature White Adipocytes by Cell SELEX Using Flow Cytometry. Plos One. 2014;9(5).
334.Apostolou P, Toloudi M, Papasotiriou I. Identification of genes involved in breast cancer and breast cancer stem cells. Breast Cancer-Targets and Therapy. 2015;7.
335.Kumar D, Gupta D, Shankar S, Srivastava RK. Biomolecular characterization of exosomes released from cancer stem cells: Possible implications for biomarker and treatment of cancer. Oncotarget. 2015;6(5):3280-91.
336.Suman S, Das TP, Damodaran C. Silencing NOTCH signaling causes growth arrest in both breast cancer stem cells and breast cancer cells. British Journal of Cancer. 2013;109(10):2587-96.
337.Pal D, Kolluru V, Chandrasekaran B, Baby BV, Aman M, Suman S, et al. Targeting aberrant expression of Notch-1 in ALDH(+) cancer stem cells in breast cancer. Molecular Carcinogenesis. 2017;56(3):1127-36.
338.Tabarzad M, Kazemi B, Vahidi H, Aboofazeli R, Shahhosseini S, Nafissi-Varcheh N. Challenges to Design and Develop of DNA Aptamers for Protein Targets. I. Optimization of Asymmetric PCR for Generation of a Single Stranded DNA Library. Iranian Journal of Pharmaceutical Research. 2014;13:133-41.
339.Nascimento I, Nery A, Bassaneze V, Krieger J, Ulrich H. Applications of Aptamers in Flow and Imaging Cytometry. In: Mayer G, editor. Nucleic Acid Aptamers:

Selection, Characterization, and Application, Methods in Molecular Biology. New York: Springer; 2016.
340.Beier R, Boschke E, Labudde D. New Strategies for Evaluation and Analysis of SELEX Experiments. Biomed Research International. 2014.
341.Schuetze T, Wilhelm B, Greiner N, Braun H, Peter F, Moerl M, et al. Probing the SELEX Process with Next-Generation Sequencing. Plos One. 2011;6(12).
342.Tolle F, Wilke J, Wengel J, Mayer G. By-Product Formation in Repetitive PCR Amplification of DNA Libraries during SELEX. Plos One. 2014;9(12).
343.Blind M, Blank M. Aptamer Selection Technology and Recent Advances. Molecular Therapy-Nucleic Acids. 2015;4.
344.Dashkova V, Malashenkov D, Poulton N, Vorobjev I, Barteneva NS. Imaging flow cytometry for phytoplankton analysis. Methods. 2017;112:188-200.
345.Rimon N, Schuldiner M. Getting the whole picture: combining throughput with content in microscopy. Journal of Cell Science. 2011;124(22):3743-51.
346.Grimwade LF, Fuller KA, Erber WN. Applications of imaging flow cytometry in the diagnostic assessment of acute leukaemia. Methods. 2017;112:39-45.
347.Viswanath DI, Mace EM, Hsu HT, Orange JS. Quantification of natural killer cell polarization and visualization of synaptic granule externalization by imaging flow cytometry. Clinical Immunology. 2017;177:70-5.
348.McGrath KE. Utilization of imaging flow cytometry to define intermediates of megakaryopoiesis in vivo and in vitro. Journal of Immunological Methods. 2015;423:45-51.
349.Terrazas C, Oghumu S, Varikuti S, Martinez-Saucedo D, Beverley SM, Satoskar AR. Uncovering Leishmania-macrophage interplay using imaging flow cytometry. Journal of Immunological Methods. 2015;423:93-8.
350.Kowalik A, Kowalewska M, Gozdz S. Current approaches for avoiding the limitations of circulating tumor cells detection methods-implications for diagnosis and treatment of patients with solid tumors. Translational Research. 2017;185:58-84.
351.Malheiro VN, Spear RL, Brooks RA, Markaki AE. Osteoblast and monocyte responses to 444 ferritic stainless steel intended for a Magneto-Mechanically Actuated Fibrous Scaffold. Biomaterials. 2011;32(29):6883-92.

352.Nazneen F, Galvin P, Arrigan DWM, Thompson M, Benvenuto P, Herzog G. Electropolishing of medical-grade stainless steel in preparation for surface nano-texturing. Journal of Solid State Electrochemistry. 2012;16(4):1389-97.
353.Okner R, Favaro G, Radko A, Domb AJ, Mandler D. Electrochemical codeposition of sol-gel films on stainless steel: controlling the chemical and physical coating properties of biomedical implants. Physical Chemistry Chemical Physics. 2010;12(46):15265-73.
354.Yang G, Wang B, Tawfiq K, Wei H, Zhou S, Chen G. Electropolishing of surfaces: theory and applications. Surface Engineering. 2017;33(2):149-66.
355.Choi WT, Oh K, Singh PM, Breedveld V, Hess DW. Wettability control of stainless steel surfaces via evolution of intrinsic grain structures. Journal of Materials Science. 2016;51(11):5196-206.
356.Collinson MM, Higgins DA, Kommidi R, Campbell-Rance D. Electrodeposited silicate films: Importance of supporting electrolyte. Analytical Chemistry. 2008;80(3):651-6.
357.Woo H, Reucroft PJ, Jacob RJ. Electrodeposition of organofunctional silanes and its influence on structural adhesive bonding. Journal of Adhesion Science and Technology. 1993;7(7):681-97.
358.Bard A, Faulkner L. Electrochemical methods. Fundamentals and applications. Second ed: Wiley; 2000.
359.Deepa PN, Kanungo M, Claycomb G, Sherwood PMA, Collinson MM. Electrochemically deposited sol-gel-derived silicate films as a viable alternative in thin-film design. Analytical Chemistry. 2003;75(20):5399-405.
360.Isa NNC, Mohd Y, Zaki MHM, Mohamad SAS. Characterization of Copper Coating Electrodeposited on Stainless Steel Substrate. International Journal of Electrochemical Science. 2017;12(7):6010-21.
361.Fayette M, Bertocci U, Stafford GR. In Situ Stress Measurements during Cobalt Electrodeposition on (111)-Textured Au. Journal of the Electrochemical Society. 2016;163(5):D146-D53.

362.Mohd Y, Ibrahim R, Zainal M, editors. Electrodeposition and Characterization of Polyaniline Films. IEEE Symposium on Humanities, Science and Engineering Research; 2012.
363.Libertino S, Giannazzo F, Aiello V, Scandurra A, Sinatra F, Renis M, et al. XPS and AFM characterization of the enzyme glucose oxidase immobilized on SiO2 surfaces. Langmuir. 2008;24(5):1965-72.
364.Moller R, Csaki A, Kohler JM, Fritzsche W. DNA probes on chip surfaces studied by scanning force microscopy using specific binding of colloidal gold. Nucleic Acids Research. 2000;28(20).
365.Gunda NSK, Singh M, Norman L, Kaur K, Mitra SK. Optimization and characterization of biomolecule immobilization on silicon substrates using (3-aminopropyl)triethoxysilane (APTES) and glutaraldehyde linker. Applied Surface Science. 2014;305:522-30.
366.Li GC, Yang P, Qin W, Maitz MF, Zhou S, Huang N. The effect of coimmobilizing heparin and fibronectin on titanium on hemocompatibility and endothelialization. Biomaterials. 2011;32(21):4691-703.
367.Howarter JA, Youngblood JP. Optimization of silica silanization by 3-aminopropyltriethoxysilane. Langmuir. 2006;22(26):11142-7.
368.Siperko LM, Jacquet R, Landis WJ. Modified aminosilane substrates to evaluate osteoblast attachment, growth, and gene expression in vitro. Journal of Biomedical Materials Research Part A. 2006;78A(4):808-22.
369.Kim J, Cho J, Seidler PM, Kurland NE, Yadavalli VK. Investigations of Chemical Modifications of Amino-Terminated Organic Films on Silicon Substrates and Controlled Protein Immobilization. Langmuir. 2010;26(4):2599-608.
370.Ocana C, Hayat A, Mishra RK, Vasilescu A, del Valle M, Marty JL. Label free aptasensor for Lysozyme detection: A comparison of the analytical performance of two aptamers. Bioelectrochemistry. 2015;105:72-7.
371.Walcarius A, Sibottier E. Electrochemically-induced deposition of amine-functionalized silica films on gold electrodes and application to Cu(II) detection in (hydro)alcoholic medium. Electroanalysis. 2005;17(19):1716-26.

372.Sun LB, Li WW, Wang MJ, Ding W, Ji Y. Development of An Electrochemical Impedance Immunosensor for Myoglobin Determination. International Journal of Electrochemical Science. 2017;12(7):6170-9.
373.Mishra SK, Kumar D, Biradar AM, Rajesh. Electrochemical impedance spectroscopy characterization of mercaptopropionic acid capped ZnS nanocrystal based bioelectrode for the detection of the cardiac biomarker-myoglobin. Bioelectrochemistry. 2012;88:118-26.
374.Ooji M, Stacy M, Seth M, Mugada T, Gandhi J, Puomi P. Corrosion Protection Properties of Organofunctional Silanes - An Overview. Tsinghua Science and Technology. 2005;6(6):639-64.
375.Tesoro G, Wu YL. Silane coupling agents - the role of the organofunctional group. Journal of Adhesion Science and Technology. 1991;5(10):771-84.
376.Baumgartel T, von Borczyskowski C, Graaf H. Selective surface modification of lithographic silicon oxide nanostructures by organofunctional silanes. Beilstein Journal of Nanotechnology. 2013;4:218-26.
377.Seguin C, McLachlan JM, Norton PR, Lagugne-Labarthet F. Surface modification of poly(dimethylsiloxane) for microfluidic assay applications. Applied Surface Science. 2010;256(8):2524-31.
378.Xu WJ, Riikonen J, Nissinen T, Suvanto M, Rilla K, Li BJ, et al. Amine Surface Modifications and Fluorescent Labeling of Thermally Stabilized Mesoporous Silicon Nanoparticles. Journal of Physical Chemistry C. 2012;116(42):22307-14.
379.Heller M, Kammerer PW, Al-Nawas B, Luszpinski MA, Forch R, Brieger J. The effect of extracellular matrix proteins on the cellular response of HUVECS and HOBS after covalent immobilization onto titanium. Journal of Biomedical Materials Research Part A. 2015;103(6):2035-44.
380.Aziz MA, Patra S, Yang H. A facile method of achieving low surface coverage of Au nanoparticles on an indium tin oxide electrode and its application to protein detection. Chemical Communications. 2008(38):4607-9.
381.Hosseini F, Sadjadi M, Farhadyar N. Fe3O4 Nanoparticles Modified with APTES as the Carrier for (+)-(S)-2-(6-methoxynaphthalen-2-yl) Propanoic Acid (Naproxen) and

(RS) 2-(3-benzoylphenyl)-propionic Acid (Ketoprofen) Drug. Oriental Journal of Chemistry. 2014;30(4).
382.Tan SW, Wang L, Yu JJ, Hou CR, Jiang R, Li YP, et al. DNA-functionalized silicon nitride nanopores for sequence-specific recognition of DNA biosensor. Nanoscale Research Letters. 2015;10.
383.Lee SH, Yang SW, Park ES, Hwang JY, Lee DS. High-Performance Adhesives Based on Maleic Anhydride-g-EPDM Rubbers and Polybutene for Laminating Cast Polypropylene Film and Aluminum Foil. Coatings. 2019;9(1).
384.Zhang Y, Gao F, Wanjala B, Li ZY, Cernigliaro G, Gu ZY. High efficiency reductive degradation of a wide range of azo dyes by SiO2-Co core-shell nanoparticles. Applied Catalysis B-Environmental. 2016;199:504-13.
385.Jannah F, Kim JH, Lee JW, Kim JM, Lee H. Immobilized Polydiacetylene Lipid Vesicles on Polydimethylsiloxane Micropillars as a Surfactin-Based Label-Free Bacterial Sensor Platform. Frontiers in Materials. 2018;5.
386.Shaimi R, Low SC. Prolonged protein immobilization of biosensor by chemically cross-linked glutaraldehyde on mixed cellulose membrane. Journal of Polymer Engineering. 2016;36(7):655-61.
387.Chuah YJ, Kuddannaya S, Lee MHA, Zhang YL, Kang YJ. The effects of poly(dimethylsiloxane) surface silanization on the mesenchymal stem cell fate. Biomaterials Science. 2015;3(2):383-90.
388.Kemmegne-Mbouguen JC, Ngameni E, Baker PG, Waryo TT, Kgarebe B, Iwuoha EI. Carcinoembryonic Antigen Immunosensor Developed with Organoclay Nanogold Composite Film. International Journal of Electrochemical Science. 2014;9(1):478-92.
389.Arabi L, Badiee A, Mosaffa F, Jaafari MR. Targeting CD44 expressing cancer cells with anti-CD44 monoclonal antibody improves cellular uptake and antitumor efficacy of liposomal doxorubicin. Journal of Controlled Release. 2015;220:275-86.
390.Arya SC, Agarwal N, Agarwal S. Use of polymerase chain reaction to diagnose tubercular arthritis from joint tissues and synovial fluid. Archives of pathology & laboratory medicine. 2004;128(12):1326-7.

391.Shin DS, Kang CK, Kim JK, Chung WJ, Jang KH, Lee YS, et al. Surface modification technology for bio-MEMS. Boston Transducers'03: Digest of Technical Papers, Vols 1 and 2. 2003:1746-9.
392.Lee JM, Kim J, Ryu I, Woo HM, Lee TG, Jung W, et al. An Aptamer-Based Electrochemical Sensor That Can Distinguish Influenza Virus Subtype H1 from H5. Journal of Microbiology and Biotechnology. 2017;27(11):2037-43.
393.Aghajari R, Azadbakht A. Amplified detection of streptomycin using aptamer-conjugated palladium nanoparticles decorated on chitosan-carbon nanotube. Analytical Biochemistry. 2018;547:57-65.
394.Zhen JM, Liu Q, Chen X, Li D, Qiao QQ, Lu YL, et al. An ethanolamine-functionalized fullerene as an efficient electron transport layer for high-efficiency inverted polymer solar cells. Journal of Materials Chemistry A. 2016;4(21):8072-9.
395.Kabala SI, Yagar H, Ozcan HM. A new biosensor for osteoporosis detection. Preparative Biochemistry & Biotechnology. 2019;49(5):511-20.
396.Tsekenis G, Chatzipetrou M, Massaouti M, Zergioti I. Comparative Assessment of Affinity-Based Techniques for Oriented Antibody Immobilization towards Immunosensor Performance Optimization (vol 2019, 6754398, 2019). Journal of Sensors. 2019;2019.
397.Tian L, Heyduk T. Bivalent Ligands with Long Nanometer-Scale Flexible Linkers. Biochemistry. 2009;48(2):264-75.
398.Liu M, Li J, Li BX. A colorimetric aptamer biosensor based on cationic polythiophene derivative as peroxidase mimetics for the ultrasensitive detection of thrombin. Talanta. 2017;175:224-8.
399.Falanga A, Marchetti M. Hemostatic biomarkers in cancer progression. Thrombosis Research. 2018;164:S54-S61.
400.Mani RJ, Dye RG, Snider TA, Wang SP, Clinkenbeard KD. Bi-cell surface plasmon resonance detection of aptamer mediated thrombin capture in serum. Biosensors & Bioelectronics. 2011;26(12):4832-6.
401.Li S, Zhang DM, Zhang Q, Lu YL, Li NT, Chen QW, et al. Electrophoresis-enhanced localized surface plasmon resonance sensing based on nanocup array for thrombin detection. Sensors and Actuators B-Chemical. 2016;232:219-25.

402.Kim H, An Z, Jang C-H. Label-free optical detection of thrombin using a liquid crystal-based aptasensor. 2018;142:71-9.
403.Wang W, Xu DD, Pang DW, Tang HW. Fluorescent sensing of thrombin using a magnetic nano-platform with aptamer-target-aptamer sandwich and fluorescent silica nanoprobe. Journal of Luminescence. 2017;187:9-13.
404.Roxo C, Kotkowiak W, Pasternak A. G-Quadruplex-Forming Aptamers-Characteristics, Applications, and Perspectives. Molecules. 2019;24(20).
405.Lin YN, Li JB, Wang YH, Sun YL, Ding CF, Sun WY, et al. A chemiluminescence biosensor for the detection of thrombin based on the aptamer composites. Spectrochimica Acta Part a-Molecular and Biomolecular Spectroscopy. 2018;192:153-8.
406.Li YJ, Li YQ, Xu N, Pan JH, Chen TF, Chen YW, et al. Dual-signal amplification strategy for electrochemiluminescence sandwich biosensor for detection of thrombin. Sensors and Actuators B-Chemical. 2017;240:742-8.
407.Sun C, Han QR, Wang DY, Xu WM, Wang WJ, Zhao WB, et al. A label-free and high sensitive aptamer biosensor based on hyperbranched polyester microspheres for thrombin detection. Analytica Chimica Acta. 2014;850:33-40.
408.Shevchenko Y, Francis TJ, Blair DAD, Walsh R, DeRosa MC, Albert J. In Situ Biosensing with a Surface Plasmon Resonance Fiber Grating Aptasensor. Analytical Chemistry. 2011;83(18):7027-34.
409.Coelho L, Queiros RB, Santos JL, Martins MCL, Viegas D, Jorge PAS, editors. DNA-Aptamer optical biosensors based on a LPG-SPR optical fiber platform for point-of care diagnostic. Conference on Plasmonics in Biology and Medicine XI; 2014 Feb 01-02; San Francisco, CA2014.
410.Han L, Wu Z, Zhang X, Qiangqiang F, Jian X, Yong T, et al., editors. High sensitive thrombin protein detection by plasmonic tilted fiber grating biosensor. Workshop on Specialty Optical Fibers and their Applications 2015; 2015; Hong Kong, China.
411.Coelho L, de Almeida JMM, Santos JL, Jorge PAD, Martins MCL, Viegas D, et al. Aptamer-based fiber sensor for thrombin detection. Journal of Biomedical Optics. 2016;21(8).

412.Shivananju BN, Renilkumar M, Prashanth GR, Asokan S, Varma MM. Detection Limit of Etched Fiber Bragg Grating Sensors. Journal of Lightwave Technology. 2013;31(14):2441-7.
413.Li XG, Nguyen LV, Zhao Y, Ebendorff-Heidepriem H, Warren-Smith SC. High-sensitivity Sagnac-interferometer biosensor based on exposed core microstructured optical fiber. Sensors and Actuators B-Chemical. 2018;269:103-9.
414.Tsigaridas G, Polyzos D, Loannou A, Fakis M, Persephonis P. Theoretical and experimental study of refractive index sensors based on etched fiber Bragg gratings. Sensors and Actuators a-Physical. 2014;209:9-15.
415.Korganbayev S, Ayupova T, Sypabekova M, Bekmurzayeva A, Shaimerdenova M, Dukenbayev K, et al. Partially etched chirped fiber Bragg grating (pECFBG) for joint temperature, thermal profile, and refractive index detection. Optics Express. 2018;26(14):18708-20.
416.Pham TB, Bui H, Le HT, Pham VH. Characteristics of the Fiber Laser Sensor System Based on Etched-Bragg Grating Sensing Probe for Determination of the Low Nitrate Concentration in Water. Sensors. 2017;17(1).
417.Tyagi D, Mishra SK, Zou B, Lin CC, Hao T, Zhang G, et al. Nano-functionalized long-period fiber grating probe for disease-specific protein detection. Journal of Materials Chemistry B. 2018;6(3):386-92.
418.Tosi D. Review and Analysis of Peak Tracking Techniques for Fiber Bragg Grating Sensors. Sensors. 2017;17(10).
419.Yunus WMB, Rahman AB. Refractive-index of solutions at high-concentrations. Applied Optics. 1988;27(16):3341-3.
420.Lin MC, Chu CJ, Tsai LC, Lin HY, Wu CS, Wu YP, et al. Control and detection of organosilane polarization on nanowire field-effect transistors. Nano Letters. 2007;7(12):3656-61.
421.Wang W, Wang Y, Tu L, Klein T, Feng YL, Wang JP. Surface Modification for Protein and DNA Immobilization onto GMR Biosensor. Ieee Transactions on Magnetics. 2013;49(1):296-9.
422.Zhao Y, Cai L, Hu HF. Fiber-Optic Refractive Index Sensor Based on Multi-Tapered SMS Fiber Structure. Ieee Sensors Journal. 2015;15(11):6348-53.

423.Iadicicco A, Cusano A, Campopiano S, Cutolo A, Giordano M. Thinned fiber Bragg gratings as refractive index sensors. Ieee Sensors Journal. 2005;5(6):1288-95.
424.Tripathi SM, Bock WJ, Mikulic P, Chinnappan R, Ng A, Tolba M, et al. Long period grating based biosensor for the detection of Escherichia coli bacteria. Biosensors & Bioelectronics. 2012;35(1):308-12.
425.Malachovska V, Ribaut C, Voisin V, Surin M, Leclere P, Wattiez R, et al. Fiber-Optic SPR Immunosensors Tailored To Target Epithelial Cells through Membrane Receptors. Analytical Chemistry. 2015;87(12):5957-65.
426.Zhang XJ, Wu Z, Liu F, Fu QQ, Chen XY, Xu J, et al. Hydrogen peroxide and glucose concentration measurement using optical fiber grating sensors with corrodible plasmonic nanocoatings. Biomedical Optics Express. 2018;9(4):1735-44.
427.Hu WJ, Huang YY, Chen CY, Liu YK, Guo TA, Guan BO. Highly sensitive detection of dopamine using a graphene functionalized plasmonic fiber-optic sensor with aptamer conformational amplification. Sensors and Actuators B-Chemical. 2018;264:440-7.
428.Zheng YF, Lang TT, Shen TT, Shen CY. Simple immunoglobulin G sensor based on thin core single-mode fiber. Optical Fiber Technology. 2018;41:104-8.
429.Sai VVR, Kundu T, Mukherji S. Novel U-bent fiber optic probe for localized surface plasmon resonance based biosensor. Biosensors & Bioelectronics. 2009;24(9):2804-9.
430.Zhou WC, Li KW, Wei YL, Hao P, Chi MB, Liu YS, et al. Ultrasensitive label-free optical microfiber coupler biosensor for detection of cardiac troponin I based on interference turning point effect. Biosensors & Bioelectronics. 2018;106:99-104.
431.Nguyen TT, Bea SO, Kim DM, Yoon WJ, Park JW, An SSA, et al. A regenerative label-free fiber optic sensor using surface plasmon resonance for clinical diagnosis of fibrinogen. International Journal of Nanomedicine. 2015;10:155-63.
432.Kim JA, Hwang T, Dugasani SR, Amin R, Kulkarni A, Park SH, et al. Graphene based fiber optic surface plasmon resonance for bio-chemical sensor applications. Sensors and Actuators B-Chemical. 2013;187:426-33.

433.Liu C, Xu BJ, Zhou L, Sun Z, Mao HJ, Zhao JL, et al. Graphene oxide functionalized long period fiber grating for highly sensitive hemoglobin detection. Sensors and Actuators B-Chemical. 2018;261:91-6.
434.Mustapa MA, Abu Bakar MH, Kamil YM, Syahir A, Mahdi MA. Bio-Functionalized Tapered Multimode Fiber Coated With Dengue Virus NS1 Glycoprotein for Label Free Detection of Anti-Dengue Virus NS1 IgG Antibody. Ieee Sensors Journal. 2018;18(10):4066-72.
435.Luo B, Xu Y, Wu S, Zhao M, Jiang P, Shi S, et al. A novel immunosensor based on excessively tilted fiber grating coated with gold nanospheres improves the detection limit of Newcastle disease virus. Biosensors and bioelectronics. 2018;100:169-75.
436.Arcas AD, Dutra FD, Allil R, Werneck MM. Surface Plasmon Resonance and Bending Loss-Based U-Shaped Plastic Optical Fiber Biosensors. Sensors. 2018;18(2).
437.Kaushik S, Tiwari UK, Pal SS, Sinha RK. Rapid detection of Escherichia coli using fiber optic surface plasmon resonance immunosensor based on biofunctionalized Molybdenum disulfide (MoS2) nanosheets. Biosensors & Bioelectronics. 2019;126:501-9.
438.Yang F, Chang TL, Liu TC, Wu D, Du H, Liang JF, et al. Label-free detection of Staphylococcus aureus bacteria using long-period fiber gratings with functional polyelectrolyte coatings. Biosensors & Bioelectronics. 2019;133:147-53.
439.Caucheteur C, Malachovska V, Ribaut C, Wattiez R. INVITED Cell sensing with near-infrared plasmonic optical fiber sensors. Optics and Laser Technology. 2016;78:116-21.
440.Guo T, Liu F, Liu Y, Chen NK, Guan BO, Albert J. In-situ detection of density alteration in non-physiological cells with polarimetric tilted fiber grating sensors. Biosensors & Bioelectronics. 2014;55:452-8.
441.Yanase Y, Araki A, Suzuki H, Tsutsui T, Kimura T, Okamoto K, et al. Development of an optical fiber SPR sensor for living cell activation. Biosensors & Bioelectronics. 2010;25(5):1244-7.
442.Watt D. Fiber Optic Array Biosensors. Biotechniques. 2006;41(5).
443.DeLuna F, Ding XF, Sagredo I, Bustamante G, Sun LZ, Ye JY, editors. Label-free in vitro prostate cancer cell detection via photonic-crystal biosensor. Conference on

Biophysics, Biology and Biophotonics III - The Crossroads; 2018 Jan 28; San Francisco, CA2018.
444.Karimi S, Salahinejad E, Sharifi E, Nourian A, Tayebi L. Bioperformance of chitosan/fluoride-doped diopside nanocomposite coatings deposited on medical stainless steel. Carbohydrate Polymers. 2018;202:600-10.